Hsp70 Chaperone Proteins and their interactions with small molecules as studied by Nuclear Magnetic Resonance.

By

Aikaterini Rousaki

A dissertation submitted in partial fulfillment
of the requirements for the degree of
Doctor of Philosophy
(Biophysics)
in The University of Michigan
2011

Doctoral Committee

        Professor Erik R. P. Zuiderweg Co-Chair
        Professor Hashim M. Al-Hashimi Co-Chair
        Associate Professor Heather A. Carlson
        Associate Professor Zhaohui Xu
        Assistant Professor Jason E. Gestwicki

To my parents Alexander and Charoula

and to my brother Markos

Acknowledgements

First of all I would like to thank my parents for bringing me into this world, my grandparents for bringing my parents into this world, my great-grandparents for bringing my grandparents into this world etc etc etc. So since I have been brought into this world I was taught by my parents as a child the value of education and how it improves and elevates you as a person in all the aspects of your life. I still recall the day of my bachelor's commencement ceremony that my uncle padded me on the shoulder and treated me as an equal by asking me various questions of general interest related to chemistry. Of course I was not expected to get a PhD or a masters by my family. Pursuing a further education as a graduate-student was a personal choice that I think has matured and improved me as a person.

To be more specific, I would like to thank my parents and brother that supported me so much during my PhD years. My father Alexander that always believed in me and encouraged me when I did not believe so solidly in myself. He is a physics teacher in a high school and he always helped my cousin and me when we were children with our physics tasks. He always told me that I'm smarter than my cousin that is currently a professor in civil engineering here in the US and while joking he told me that if he made it I could make it too. I would like to thank my mother Charoula for always being interested to talk to me on the phone, even if it was 3am for her, when I urged to call her and talk to her about my concerns. I would also like to thank her for coming to the US when I had my accident and had to have surgery. Without her I couldn't have made it. I really appreciate that she left her job as a mathematics teacher in the same high school that my father teaches and in

Table of contents

List of Tables

List of Figures

List of appendices

ABSTRACT

Chaperone proteins and their cochaperones are perhaps one of the most intriguing systems for investigation. Ubiquitous in nature, they can be found in every organism and that perhaps is the reason that their sequence shows amazingly high homology and similarity. Allosteric mechanisms govern their functions and that makes them very interesting and hard to investigate at the same time. In medicine, chaperone proteins are of extreme interest since they are related to various diseases including neurodegerative diseases such as Alzheimers disease, Pick's disease and Parkinsons disease. Various forms of cancer also relate to the chaperone proteins. Hence the investigation of various small molecules that could up/down-regulate this system is of great biomedical relevance.

In this dissertation we explored a member of the chaperone family that is constitutively expressed in every mammalian cell, the cognate Hsp70 (Hsc70). More specifically, we investigate the interactions of its ATPase domain with various small molecules that either act as inhibitors or enhancers of the protein's activity. For example, we found that the compound MKT-077 blocks the Hsc70 ATPase activity by binding in a negatively charged cleft with its positive charge. This was identified with the use of chemical shift mapping experiments, NOE experiments and AUTODOCK simulations. MKT-077 binds only to the ADP form of the protein elucidating an amazing mechanism for the inhibition of the protein. Another inhibitor, methylene blue, binds to another locus of the ATPase. Interestingly, both of these molecules reduce the levels of tau in cell-based models of Alzheimers disease. This would suggest that the use of compounds that

bind to Hsc70 at two separate sites could modulate Hsp70 activity in cells in a synergistic fashion.

CHAPTER I An overview of this thesis.

The main focus point of this thesis is the study of the interaction of small chemical inhibitors with Hsc70, a protein-folding chaperone of the Hsp70 class, using NMR spectroscopy. The significance of these investigations lies in the fact that the Hsp70 chaperones, which are the stewards of intra-cellular protein homeostatis, are also implicated in neurogenerative diseases such as Alzheimer's, and in cancer. Hence, inhibition of the chaperones may provide a promising avenue for the treatments of these diseases. We use NMR spectroscopy in solution in conjunction with computer modeling to determine the binding location of the small molecules with the aim to aid in design processes that enhance the efficacy of these compounds. The thesis is laid out to provide a thorough background to the chapters that describe the binding studies in detail (chapters 8 and 9).

Chapter II describes the Hsp70 chaperones

Chapter III describes diseases that are liked to Hsp70 chaperone malfunction

Chapter IV describes existing therapies of these diseases and introduces the small molecule inhibitors of Hsp70 in particular

Chapter V gives details of the NMR methods used

Chapter VI details the assignment of the backbone resonances of HSc70 NBD

Chapter VII gives background on AUTODOCK, the procedure used to help determine the binding site of MKT077

Chapter VIII Gives the details of the interaction of MKT-077 with Hsc70 NBD as determined by NMR and docking calculations

Chapter IX Summarizes the binding experiments carried out with Methylene blue
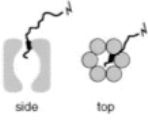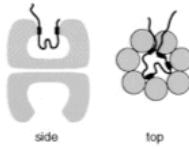
APPENDIX I Summarizes binding experiments with other drugs

APENDIX II Lists the NMR assignments for HSC70 NBD

CHAPTER II. Introduction to molecular chaperones

II.1. Overview.

Molecular chaperones were originally defined as a group of unrelated classes of proteins that mediate the correct assembly of the final functional structures [1, 2]. Examples are chaperones involved in biogenesis of ribosomes [3] and ATPsynthase [4] . Chaperones are also involved in metal transport [5] and in protein transport [6]. In this thesis, however, we will focus on molecular chaperones that are involved in protein folding and refolding, and of those, the subset known as Hsp70 chaperones (see Table II.1).

Table 1. Topology of Polypeptide Binding and Action of Chaperone Families

CHAPERONE	TOPOLOGY OF BINDING	ACTION	REFERENCES
Hsp100	side top	ATP-dependent disaggregation and unfolding for degradation	Schirmer et al., 1996; Levchenko et al., 1997
Hsp90	multiprotein complex	Conformational maturation of steroid hormone receptors and signal transducing kinases	Bohen et al., 1996; Prodromou et al., 1997
Hsp70 (DnaK)		ATP-dependent stabilization of hydrophobic regions in extended polypeptide segments	see text
Hsp60 (GroEL)	side top	ATP-dependent facilitation of folding to the native state	see text
Small Hsps (Hsp25, etc.)		Stabilization against aggregation during heat-shock	Lee et al., 1997; Ehrnsperger et al., 1997
Calnexin/Calreticulin	?	Folding of glucosylated proteins in the ER in cooperation with glucosyltransferase	Sousa and Parodi, 1995; Helenius et al., 1997

Bold lines signify polypeptides, and the thickened segments denote sites that become directly associated with chaperone, typically hydrophobic in character. Structures are not drawn to scale.

Table II.1. The protein folding chaperones. [7]

The Hsp70 chaperones were discovered as 70 kDa heatshock proteins in the 60s and 70s [8]. Later on it was realized that several of the heatschock proteins of the Hsp70 class are also constitutively expressed, and hence the name Hsp is a bit of a misnomer

Table II.2: Names, properties and homologies of human Hsp70s					
Protein name	Old names	Location	# res.	Id. to HSPA8	Id. to HSPA9
HSPA1A/B	HSP70-1; HSP72; HSPA1; HSP70-2	cytosol	641	86%	52%
HSPA1L	hum70t; hum70t; Hsp-hom	cytosol	641	84%	52%
HSPA2	Heat-shock 70kD protein-2	cytosol	639	88%	49%
HSPA5	BIP; GRP78; MIF2	ER, constitutive	654	66%	50%
HSPA6	Heat shock 70kD protein 6 (HSP70B′)	cytosol	643	80%	50%
HSPA7	Heat shock 70kD protein 7	cytosol	367	77%	49%
HSPA8	HSC70; HSC71; HSP71; HSP73	Cytosol, constitutive	646		53%
HSPA9	GRP75; HSPA9B; MOT; MOT2; PBP74; mot-2, mortalin	Mitochondrion, constitutive	679	53%	
HSPA12A	FLJ13874; KIAA0417	cytosol	675	25%	24%
HSPA12B	RP23-32L15.1; 2700081N06Rik	cytosol	687	21%	25%
HSPA13	Stch, (Microsomal stress 70 protein ATPase core)	ER	471	39%	36%
HSPA14	HSP70-4; HSP70L1; MGC131990	cytosol	509	34%	31%
DnaK	DnaK-Ecoli	-	638	52%	60%
The last two columns give the amino acid identity as obtained from BLAST-2.					

In 1977, Georgopoulos[9] reported a mutation groPC756 later termed as dnaK756 which conferred resistance to E.coli against lytic infection by bacteriophage λ [10, 11]. Molecular chaperones were originally defined as a group of unrelated classes of proteins that mediate the correct assembly of the final functional structures [1, 2]. This was the first discovery of the first member of the HSP70 family DnaK [2, 7]. Their highly conserved structure suggests that they play a role in fundamental cellular processes. As

their name suggests they are induced in cells exposed to heat shock. They occur ubiquitously and many of them are classified as stress proteins, although they have essential functions under non-stress conditions. Induction of HSPs can occur as a result of heat shock as already mentioned but also from a significant number of other factors that include: exposure of cells in amino acid analogs [12, 13], glucose analogs [14], heavy metals [15], protein kinase C (PKC) stimulators [16], ischemia, sodium arsenite , microbial infections, nitric oxide, hormones and antibiotics also induce the expression of HSPs. Furthermore, tumor cells are invariably shown to express excess Hsp70 chaperones, likely because the tumor microenvironment resembles a stress condition (low pH) [17]. Hsp70s is one class of HSPs that is highly conserved and demonstrates a 60-78% base identity among eukaryotic cells and a 40-60% identity between eukaryotic HSP70 and bacterial DnaK [18-21].

HSP70s are proteins that bind to and stabilize an otherwise unstable conformer of another protein-and by controlling binding and release, facilitate its correct fate in vivo, be it folding of newly synthesized proteins or denatured proteins that were the result of heat shock, oligomeric assembly, transport to a particular subcellular compartment, or disposal by degradation [22, 23]. Other functions include clathrin vesicle un-coating, dissociating protein aggregates, facilitating protein translocation, chaperoning protein folding in various cellular compartments, disassembling oligomeric protein structures, facilitating proteolytic degradation of unstable proteins, controlling the activation of regulatory proteins including transcription factors. A number of investigators have suggested that Hsp70 itself serves as a type of thermometer by which the cell senses a particular metabolic insult[23].

In all these proposed roles, the HSP70s bind directly to unfolded or partially folded polypeptide chains. Because of their suggested roles in protein folding, Hsp70 have been classified as molecular chaperones [24]. More specifically we can say that Hsp70s together with their Hsp40 co-chaperones prevent the aggregation of non-native proteins through association with hydrophobic patches of substrate molecules, which yields from intermolecular interactions ('holdase' activity). Hsp70 chaperone systems also assist non-native folding intermediates to fold to their native state ('foldase' activity). They also have a disaggregation role.

II.2. Molecular architecture

The HSP70s are structurally subdivided into an N-terminal ATPase domain of ~45K which is followed by an ~18K part containing the substrate binding site, followed by a more variable ~10K flexible lid. A scheme representing these domains as well as the domains of the cochaperones is shown in figure II.1.

Figure II.1: Domains of the bacterial Hsp70 and its co-chaperones.[7]
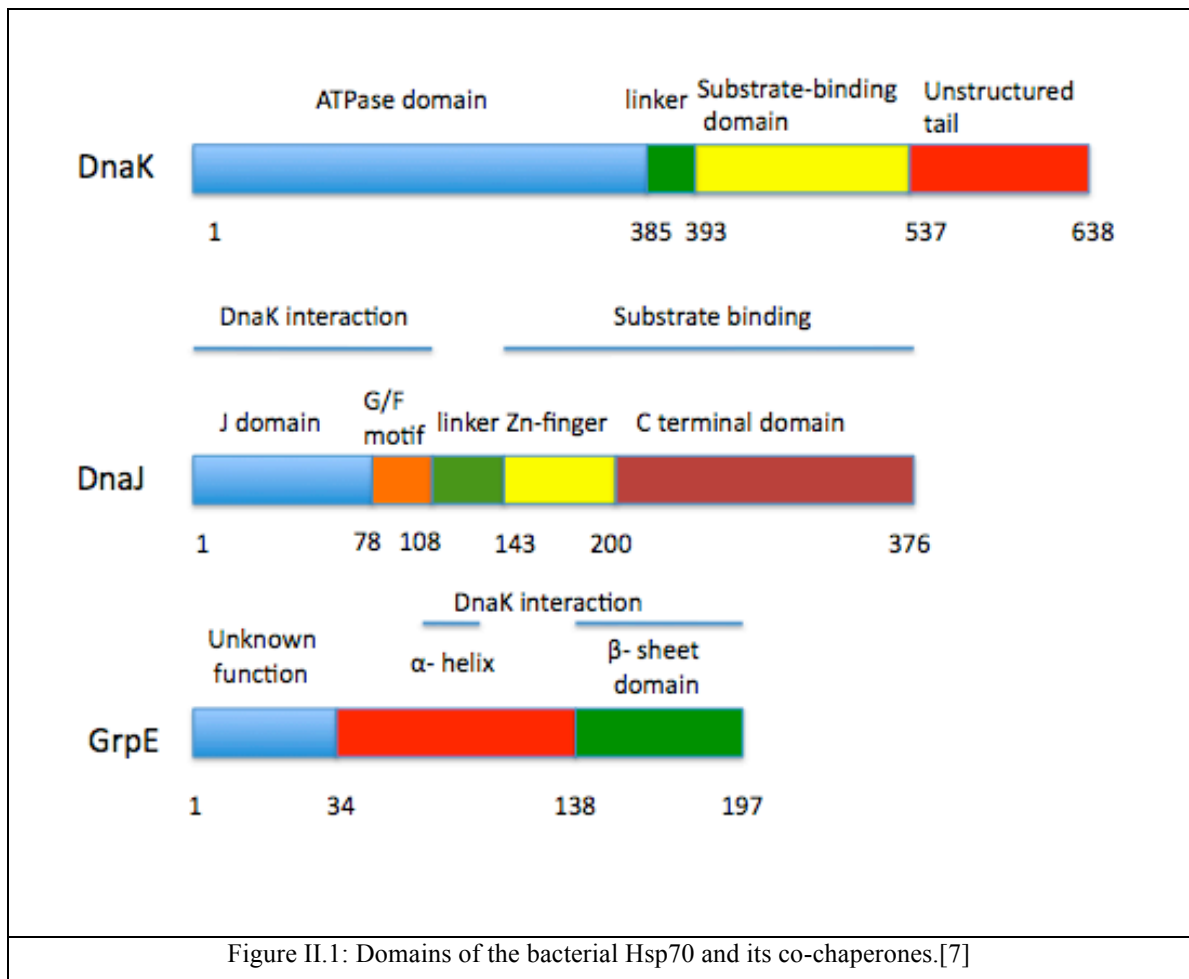
DnaK was characterized by SAXS (Small Angle X-ray Scattering) and it was found to be 112 A long in the ADP state and have the shape of a dumbbell [25]. These

characteristics have later been confirmed with a solution structure of DnaK as determined by NMR [26].

II.2.1 Hsp70 ATPase domain

The biggest HSP70 domain that hydrolyzes ATP to ADP is the ATPase domain (Fig II.4). The ATPase domain from sugar kinases, actin and Hsp70s is very similar structurally even though they have very contradictory sequence homology [27]. Essential amino acids for the ATPse activity of DnaK are threonine 199 and lysine 70. As we will see in the results section shifts around amino acids 220 and on are related to the ADP to ATP exchange mechanism. The crystal structure of the ATPAse domain of DnaK was determined in complex with the nucleotide exchange factor GrpE [28]. The crystal structure of the NBD of the human chaperone Hsc70 was determined in 1990 by the group of McKay [29]. In follow-up studies crystal structures of mutants were obtained in order to determine the residues of importance for ATP hydrolysis.

II.2.2. Hsp70 Substrate binding domain

The substrate-binding domain (Fig II.3) shows high sequence conservation within the Hsp70 family, although differences of unclear functional relevance exist. Detailed structural information about this domain exists for the E.coli DnaK. An X-ray structure of this domain was solved in complex with a heptameric peptide substrate NRLLLTG at 2Å resolution [30]. The peptide-binding cavity (residues 389-607) forms a sandwich of 2 four-stranded β-sheets with four upwards-protruding loops (two inner and two outer loops) and two helices A and B which are packed against the inner loops. The substrate-binding cavity is formed by the β-sheets 1 and 2 and the inner loops. The cavity is lined with hydrophobic residues and contains one particularly deep hydrophobic pocket, in which a Leu side-chain of the substrate is buried. The main chain of the residues of the substrate form hydrogen bonds with the residues of the substrate-binding-domain. The mutation V436F, which closes the Leu-specific-pocket attenuates the peptide binding ability of DnaK by just a factor of 10 [31, 32], suggesting that the domain contains some plasticity. Helix B constitutes a lid, which closes the cavity through a salt bridge and two hydrogen bonds to the outer loops. ATP binding must at least open this lid to allow substrate release. The X-ray study of the substrate-binding domain of DnaK (res 389-

607) suggested that the a-helical domain could be the key for the allosteric control of substrate binding. However, a later study showed that DnaK constructs from which the entire alpha-helical domain was deleted (from the N-terminus of helix A onwards) were fully allosterically active in–vitro and still conferred resistance to E.coli against lytic infection by bacteriophage λ in–vivo [33]. Kinetic measurements showed that the presence of the LID reduces on and off rates of substrate equally in both ADP and ATP states, hence not affecting allostery[34]. This does not mean that the LID is not important: protein refolding in the cell is not only a matter of binding and release, but also a matter of timing of binding and release.

The presence of bound substrate protein increases the thermostability of Hsp70 molecular chaperones. The beta-domain has a unique architecture [35], and is stable in the absence of the entire helical LID [36]. The isolated beta domain becomes rather unstable in the absence of peptide and shows a widespread conformational change as compared to the peptide-bound form [33] and supports the notion of plasticity.

	Bacteria	Compartment	Eukaryotic homologues	
Hsp70 system			Yeast	Higher eukaryotes
Hsp70				
∼70K ATPases, bind extended peptides, interact with DnaJ homologues and GrpE		Cytosol	SSA1-4; heat-inducible and constitutive forms SSB1,2: bind to polysomes	Hsp72: stress-inducible Hsc73: constitutive; binds to nascent chains
		Mitochondria	SSC1: required for protein import and folding	mHsp70
	DnaK	ER lumen	Kar2/BiP: required for post-translational protein import and folding	BiP: abundant, binds unfolded ER proteins
Hsp40				
∼40K proteins, bind unfolded proteins, interact with matching Hsp70s and stimulate ATP hydrolysis		Cytosol	YDJ1: interacts with Hsp70 SSA1; involved in protein transport across membranes SIS1: similarity to mammalian Hsp40	Hsp40: binds nascent polypeptides Hdj1: human Hsp40 homologue
		Mitochondria	MDJ1: required for folding of newly imported proteins	
	DnaJ	ER	SCJ1 (lumen), Sec63 (membrane)	
GrpE				
∼20K nucleotide-exchange factor for Hsp70		Mitochondria	MGE1: interacts with Hsp70 SSC1	
	GrpE			

Table II.3: Hsp70s and their co-chaperones from various organisms [37]

Hsp40 and NEF function as regulators of this system by stimulating Hsp70's ATP hydrolysis activity and subsequent nucleotide exchange[38-41]. We listed Hsp70s, Hsp40s and NEFs from various organisms in Table II.3.

II.3 The cochaperones

II.3.1 Hsp40.

Hsp40 co-chaperones are a heterogeneous class of multi-domain proteins, which share a conserved stretch of approximately 70 residues, called the J-domain, often located at the N-terminus as seen in Figure II.2 . Cells encode a wide spectrum of J domain proteins which differ in their domain composition and cellular functions [42, 43]. Six JDPs (J domain proteins) exist in E.coli, 20 in *Saccharomyces cerevisiae*, 33 in *Caenorhabditis elegans*, 34 in *Drosophila melanogaster* and presumably 44 in human cells. DnaJ the basic bacterial Hsp40 protein is composed of 376 amino acids and is a chaperone with thioldisulfide reductase activity. Apart from its co- chaperone activity in conjunction with the DnaK chaperone, Dna J has other functions such as binding to unfolded proteins and preventing them to aggregate[44, 45], protein translocation [46], protein degradation [46] and a thioldisulfide oxidoreductase activity [47]. It can be found in various compartments of the cell, such as auxilin in clathrin coated vesicles [48, 49], cysteine string protein in neurosecretory vesicles[50]. It has been shown to exist as a homodimer of two 41 K subunits by size exclusion chromatography.

There are three classes of J-Domain proteins as seen in Figure II.2

Figure II.2 : The 3 classes of the J domain cochaperones [51]
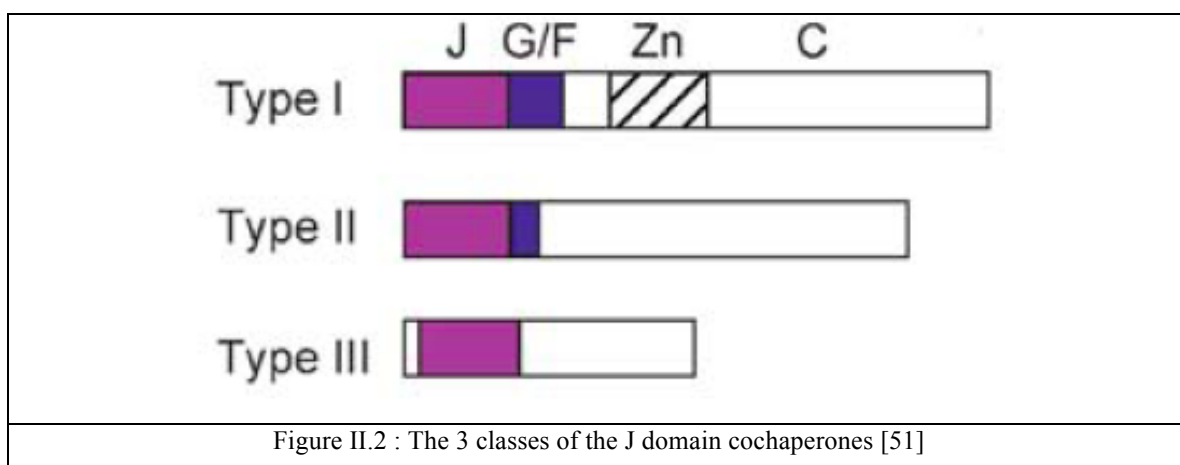
Class I share all 4 domains characteristic for the prototype for all JPD E.coli DnaJ. DnaJ is composed of the N-terminal J domain, follow by a glycine/phenylalanine

rich region, a Zn binding domain and a C terminal domain. Class II JPDs lack the Zn binding domain. Class III proteins share with DnaJ only the J domain , that is not necessarily located at the N terminus as in the two above mentioned classes. The Zn binding domain (zinc finger) is necessary for the autonomous chaperone activity in cooperation with the C-terminal domain of the protein [52]. The G/F rich region is critical for the chaperone's function and it is related to the mechanism that the substrate binds to the SBD of the protein. The $_{61}$QKRAA$_{65}$ motif was proposed to be the binding site of DnaJ to DnaK . NMR chemical shift mapping suggested that the ATPase domain binds to the J-domain helix II of DnaJ and the flanking loops.

| Figure II.3 J-domain | The peptide-binding domain of Hsp40 (residues 162-335) [53] |
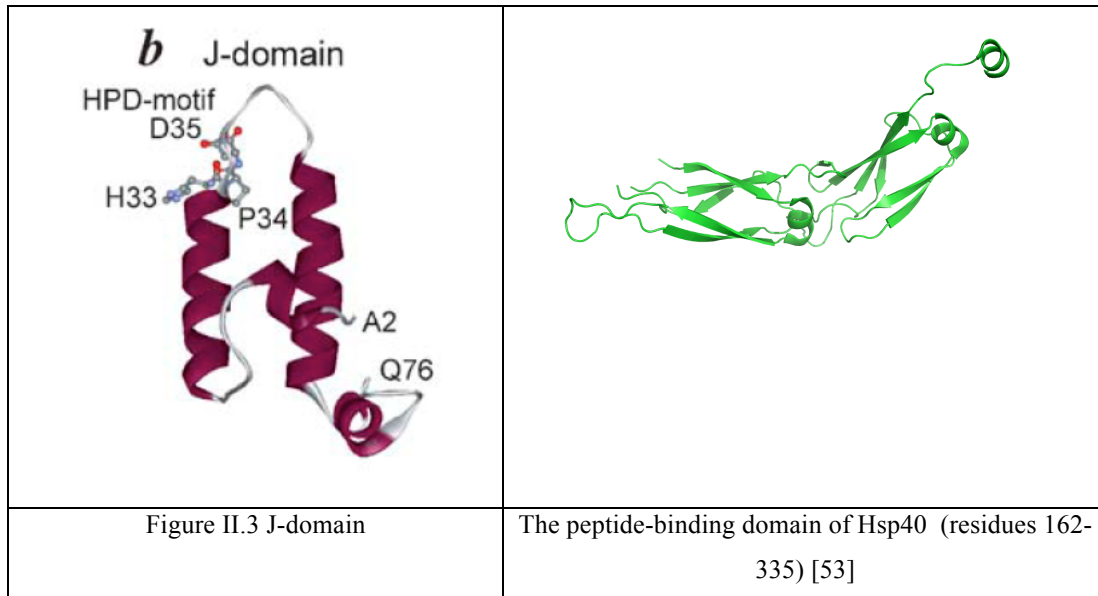
The solution structure of the E.coli J-domain has been revealed by NMR by the Nobel Prize Wüthrich group and is shown in Figure II.3 [54]. Other sections of the J-proteins have been crystallized as well [53].

There is a crystal structure of a J-domain cross-linked by enginneered disulfides to the ATP-domain of Hsc70[55]. In this structure, residues in helix II of the J-domain that are essential for interaction with the Hsp70 ATPase domain, as determined by mutagenesis [56] and NMR[57], are exposed to solvent and are not even in proximity of the ATPase domain. We conclude that this crystal structure of an artificial adduct cannot disclose any relevant interactions between the proteins.

The efficiency with which DnaJ stimulates the ATPase activity of DnaK is increased in the presence of polypeptide substrates. E.coli DnaJ and polypeptide substrates synergistically stimulate the rate of ATP hydrolysis by >1000 fold [38, 41, 58]. The action of DnaJ requires both binding of protein substrates to the central hydrophobic pocket of DnaK's substrate binding cavity and structural coupling between DnaK's ATPase and SBD domains, which transmit the substrate binding event to the catalytic center [41]. DnaJ's coupling activity requires the ability to interact with DnaK through its J domain [58, 59] and with substrates through its C-terminal substrate-binding domain. On the basis of the available data a model of DnaJs action has been proposed [58]. DnaJ

starts the functional cycle of the DnaK system by rapid association with the substrate, then the substrate is transferred to DnaK in a two step process a) DnaJ J domain interacts with DnaK ATP and it associates with the open SBD of DnaK then b) allostery comes into play and the association of the substrate-DnaJ lowers the activation energy barrier for the hydrolysis of ATP by the ATPase domain of DnaK. T-antigens also act as the Hsp40 molecular chaperone[60].

II.3.2 NEF (Nucleotide Exchange Factors)

NEFs are critical for the functional cycle of HSP70s because they promote the release of ADP and rebinding of ATP that triggers unloading of the bound polypeptide substrate [61]. They also play the role of a thermo sensor for the chaperone system [62]. Proteins of the BAG family are said to play a general facilitator role in signal transduction pathways involved in the regulation of the cell survival [63]. There are two temperature transitions of GrpE that take place upon increased temperatures, the first one is reversible while the second one is not. A disulfide bond between the two GrpE monomers is believed to enhance the stability of the ADP state. Mt-GrpE is related to the mitochondrion viability [64]. Well-known NEFs are the E.Coli GrpE and the heterogenous and diverse family of the BAG proteins, which are the NEFs for the cytosolic HSP70 in eukaryotic cells. The NEFs or GrpEs were first observed to exhibit an increased expression in cells starved from glucose, and therefore were called the glucose regulated proteins (grps) [14]. The bacterial and eukaryotic NEFs have relatively low sequence homology compared to the homology found in other chaperone families such as the HSP70s.

The availability of crystal structures for five NEFs- GrpE [28], Bag-1, HspBP1 [65], Bag-2 [66] and Hsp110[67] in complex with the NBD domain of their partner chaperones provides an impressive demonstration of the NEFs mechanistic and structural diversity that overall leads to the same Hsp70 ATP structure, by exchanging ADP to ATP through an opening of the nucleotide binding cleft and opening the lid for the release of the polypeptide from the SBD of the chaperone.

The ATPase domain of E.Coli DnaK interacts with GrpE[28, 68] even though that crystal structure has been in question as seen in the referred paper [28]. Figure II.4 shows the interaction of the GrpE dimer with the DnaK ATPase domain. A GrpE mutant (G122D) seems to have impaired interaction with the chaperone DnaK [69] since that residue is at the interaction site of the two proteins as it seems in the crystal structure. The GrpE tail (amino acids 88-197) was shown to be able to displace bound substrate from DnaK[70].

Figure II.4 : Crystal structure of DnaK complexed with the GrpE dimer. [1DKG.pdb]
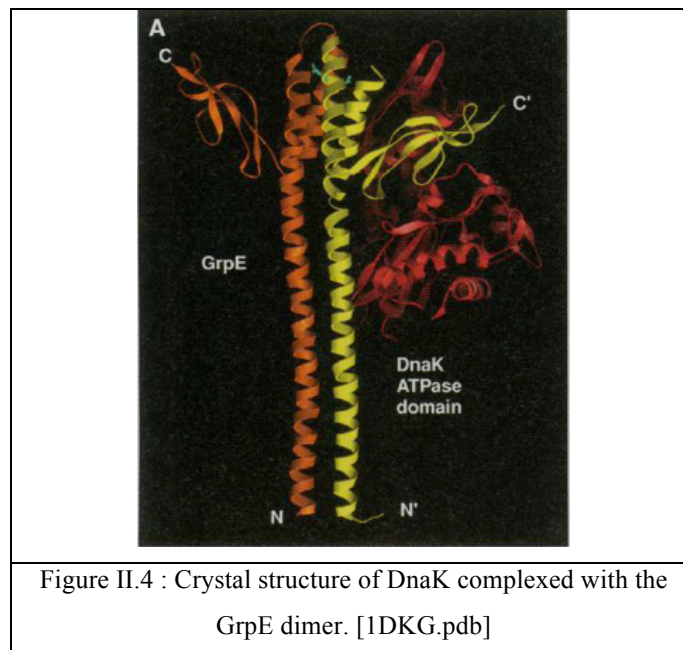
GrpE binds to the ADP bound and nucleotide free states of DnaK with high affinity (K_d=1nM). Addition of ATP leads to the dissociation of the complex. The dissociation of bound nucleotides requires the opening of the SBD cleft. When NEFs are bound to the chaperone the lid of the SBD cleft opens in order for the polypeptide to be able to be released. Apart from the opening of the SBD lid GrpE also stabilizes the open conformation of the nucleotide-binding pocket, which facilitates the rapid binding of ATP to the nucleotide free state of DnaK[71, 72].

The Hsc70 GrpE analogs are the Bag co-chaperones. In humans 6 Bag homologs exist. They all contain one Bag domain except Bag 5, which contains 5 Bag domains. Bag proteins 3, 4 and 5 seem to be shorter by three to four turns of each of the helices,

which compose the three-helix bundle, but all of the Hsp70 interacting residues seem to be in these shorter Bag family members. These proteins comprise a family of NEFs that is heterogenous and their main characteristic is that they all share a Bag domain located at their C-termini [73]. This domain interacts with the Hsc70 chaperones and stimulates their nucleotide exchange. Bag-1 may only bind and stimulate the open state of the Hsc70 ATPase domain and is thus specific for that state. It has been shown that Bag-1 inhibits in-vitro polypeptide refolding while Bag 1 mutants that do not bind to Hsc70 do not affect the chaperone activity of the protein. The mammalian Bag domains form a three helix bundle [74-76] that associates as a monomer with the subdomains IB and IIB of the Hsc70 ATPase domain, through electrostatic interactions involving the conserved residues Glu 212, Asp222, Arg237, Gln245. Mutations on the DnaK residues 32, 455 and 468 affect the GrpE stimulated ATPase activity [77]. Other NEF for Hsc70 exist in the cytosol too. One of them is HspBP1 [78, 79]. In the mammalian cytosol several nucleotide exchange factors coexist including the Bag family proteins with is composed of six family members one of which is the four variants of HspBP1. The physiological role of this diversity remains a mystery.

II.4 Hsp70 protein (re)folding Cycle
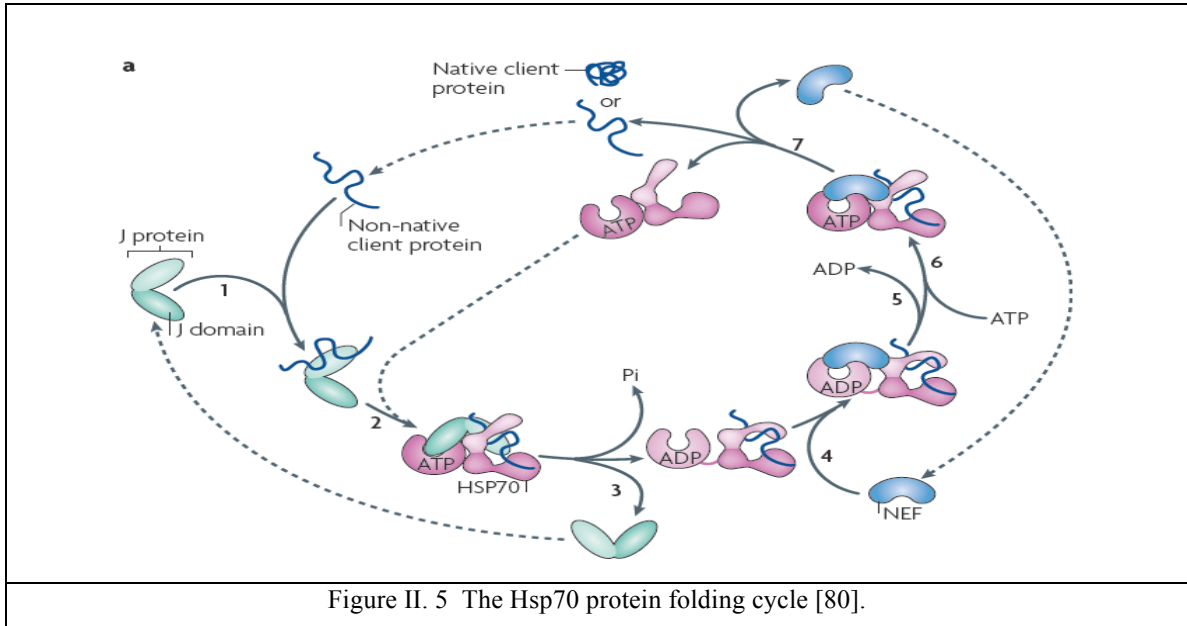
Figure II. 5 The Hsp70 protein folding cycle [80].

The chaperone folding cycle in bacteria that is shown in Fig II.5 was suggested in which the bacterial cochaperones play a central role [81]. Based on results from various laboratories the cycle mechanism that was proposed is the following [39, 41, 58, 81]. In this proposed cycle a misfolded protein substrate first associates with DnaJ, which will present it to DnaK-ATP and induce the formation of a trimeric DnaK-ATP-DnaJ-substrate complex. DnaJ and substrate synergistically stimulate the ATP hydrolysis by DnaK and thus trigger the transition of the DnaK ATP state (low substrate affinity- T state) to the DnaK ADP state (high affinity efficiency- R state). Then GrpE comes into play by binding to the DnaK ADP complex and catalyzing the ADP release and exchange for ATP that is abundant in the cell. ATP binding induces conformational changes to the protein that lead to a rapid dissociation of GrpE and substrate from the complex. How DnaK (re)folds mis-or unfolded substrate is still enigmatic. A model regarding the disaggregation of aggregated proteins was proposed [82]. The Brownian power stroke model suggests that the relatively small Hsp70 molecule retains when bound to the bigger aggregate a higher thermal motility as compared to the aggregate. This difference in thermal motility creates a force that leads to the solubilisation of the aggregated protein.

The mechanism of action of Hsp70 was proposed and is based on the hydrophobic interactions between the Hsp70 and the unfolded protein that has its hydrophobic amino acids exposed to its surface and is thus able to interact with the SBD of the chaperone .By binding to the exposed hydrophobic surfaces Hsp70s promote disaggregation of the aggregated proteins. Then it used the ATP energy to release itself from the substrate while undergoing an allosteric conformational change.

In eukaryotic cells the cycle is essentially the same and it is represented in FigureII.6

Figure II.6 The chaperone cycle in eukaryotic cells. Hdj refers to the J domain protein and Bag is the nucleotide exchange factor. [83].
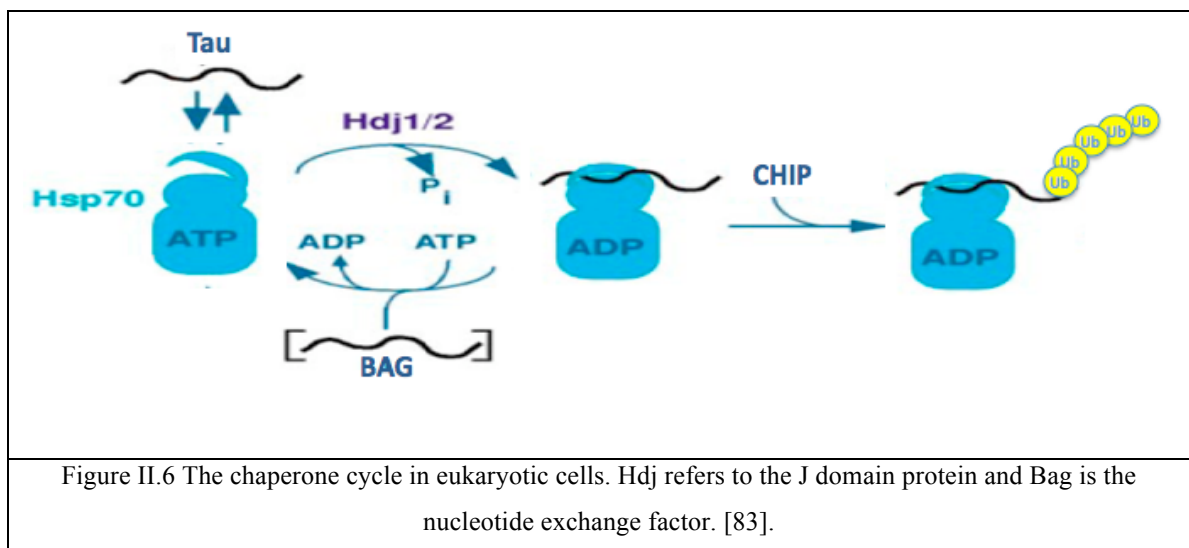
In bacterial cells the rate-limiting step appears to be the ADP release while in the eukaryotic cells the rate-limiting step is the ATP hydrolysis. Mammalian cells contain a 48K protein termed as Hip that bind to the ATPase domain of the chaperone and prevents ADP release[84]. Bag 1 appears to promote release of the bound ADP from the chaperone that results in the release of the substrate. Hop has also been proposed to stimulate nucleotide exchange for the Hsp70s[85].

II.5. Allostery of the Hsp70 chaperones

II.5.1 Introduction

Hsp70s are allosteric proteins, in which ATP binding at the NBD causes substrate release at the SBD, and in which substrate binding causes hydrolysis of ATP, and where hydrolysis of ATP enhances substrate binding. In the ADP-state substrate binding is tight; in the ATP-state, the substrate binding affinity is reduced by one-to-two orders of magnitude (depending on substrate and species)[86].

Our discussion here will focus exclusively on allosterics as observed in DnaK of E.coli. This is because much of the early Hsp70 work was carried out for DnaK, and that the majority of the structural information has been collected on DnaK.

As of this writing we are not aware of any structural/kinetic/thermodynamic findings that are fundamentally different for the mammalian Hsp70's.

The DnaK ATP-ADP difference in affinity corresponds to a free energy of allostery of only 2 Kcal/Mole, less than a typical H-bond. However, the substrate off-rate is different by three-orders of magnitude between the ADP and ATP state, which corresponds to a respectable change of 4-5 Kcal/M in the free-energy of the dissociation barrier.

DnaK's allostery can be measured in indirect ways as well. Enhancement of ATP-hydrolysis upon substrate binding [39] can be monitored by detecting the release of γ-PO4 by radio isotopic, colorimetric assay or 31P NMR spectroscopy. In addition, DnaK E coli, substrate binding causes a change in the fluorescence wavelength of Trp102, which is located in the NBD[87]. Functional assays include, for DnaK, its ability to stimulate lambda-phage growth in in E.coli [9]. A more stringent test is the refolding of mutated or heat-denatured luciferase, which will only occur in the presence of ATP and co-chaperones of the DnaJ and NEF class[81]. Recently, the suspicions that all of these functional / biophysical assays may not perfectly correlate with each other have been confirmed [88].

II.5.2 Structures.

Much about allosteric mechanisms of proteins can usually be learned from the comparison of the structures of different allosteric states of the proteins. The classical example is the comparison of the X-ray structures of oxy and deoxy hemoglobin. The major conformational changes seen immediately provided strong clues about the allosteric mechanism, which were eventually verified with biochemical and genetic experiments.

At least four different allosteric states can be distinguished for the Hsp70s: NBD(ATP)-SBD(apo); NBD(ATP)-SBD(sub); NBD(ADP)-SBD(sub) and NBD(ADP)-SBD(apo). Nucleotide-free NBD can exist only transiently during the ADP <> ATP exchange process facilitated by NEFs and should not be considered to be a naturally occurring state. However, biochemical evidence suggests that its properties are not unlike the ADP-bound state.

The NBD (ATP)-SBD(sub) state is short lived. This leaves three other relevant states to be studied by physical methods. The NBD(ADP)-SBD(sub) state is completely stable in the absence of NEFS and so is the NBD(ADP)-SBD(apo) state. The NBD(ATP)-SBD(apo) is stable enough for most biophysical experiments (ATP hydrolysis rate is $5 \times 10\text{-}4 \text{ s}^{-1}$), but not for NMR or X-ray structure determination.

Figure II.51 The DnaK full length structure
Top: The relative orientation of the SBD (left) and NBD (right) for wt-DnaK in the ADP – NRLLTG state in solution [26]. Color coding: NBD domain IA: yellow, IB: blue, IIA, green, IIB, red, linker: white, beta domain: cyan, LID-helix-A: magenta, lid_helix_b, pink, Lid, orange: Residues rendered in spacefil are important for the NBD-SBD allosteric communication as determined by mutagenesis studies from several other workers as discussed in the text.
Bottom: dynamical properties of protein backbone as determined from the NMR data[26]. Here: High intensity indicates high mobility, low intensity indicates low mobility. Colors: NBD: red, Linker: black, SBD: green, LID: blue.
From Zuiderweg, Allostery in the Hsp70 Chaperones, review, in preparation

Only one of these allosterically relevant structures is available to date: it is the NBD(ADP)-SBD(sub) state, determined in solution for wt-DnaK in the presence of ADP, Phosphate and the peptide NRLLLTG (KD=1 uM) [26]. (Figure II.5.1) In this structure, the LID domain is docked to the SBD, but the SBD-LID unit moves rather unrestricted with respect to the NBD[26]. This detailed study of wt-protein confirmed earlier NMR data that noted that the NBD and SBD move relatively independently in the

ADP state[89, 90]. This is the only wild-type structure available for any of the Hsp70 chaperones. In this state, there is no (permanent) communication between the NBD and the SBD, which makes it difficult to explain the allostery between the two domains. Hence, one expects that the two domains interact in the ATP state.

A crystal structure of a two-domain construct of bovine Hsc70 truncated at residue 554 was reported in which interdomain docking was observed [91]. The protein in the crystal is nucleotide-free, and the truncated C-terminus is bound to its own substrate-binding cleft. Hence, the construct should reflect the NBD (ADP)-SBD(sub) state, and should be comparable to the solution structure of DnaK in the same state, in which no docking takes place. The crystal structure shows extensive hydrophobic packing between NBD and SBD. The deletion construct contained the mutations E213A and D214A, which in the crystal structure are found to be on the interface between NBD, SBD and LID and seem to mediate the docking. This crystal structure is likely not a representation of any of the allosteric states of the Hsp70s, and is unlikely to exist in wild-type protein, not even transiently.

A crystal structure of Hsp110 from *S. cerevisiae* has appeared[92]. Hsp110's are homologous to Hsp70s when they are locked in the ATP state. The structure shows a docked NBD and SBD, in agreement with the expectation for the ATP state Hsp70. The linker is docked, as expected, and is found to be engaged as an additional strand of the two-stranded beta sheet in NBD domain IIB. This docking would explain the solution NMR chemical shift changes upon ATP/ADP exchange seen for residues in these strands [93-95]. The LID in Hsp110 has moved away from the SBD, as expected for the ATP state, and is docked against domain IA. This docking would explain the fact that the fluorescence of Trp102 in domain IA of DnaK is affected by the ATP-ADP conformational change, but not in the absence of the LID [87]. Despite all of these expected features, there is still doubt as of the validity of Hsp110 as a model for the Hsp70 ATP-apo state: the amino acid homology between Hsp70 and Hsp110 is a quite modest 44%, and the severe lack of homology for the NBD-SBD linker is of great concern. The linker plays a key role in the allosteric function of the Hsp70s (see below).

II.5.3 Global characteristics of the allosteric change

Mutations of surface residues that yield Hsp70 constructs that still can hydrolyze ATP and bind substrate, but which lack allosteric coupling are: Y145A, N147A and D148A [96]; P143G and R151A [97]; K155D and R167D [98]. Mutagenesis of any residues of the NBD-SBD linker leads to loss of allosteric communication [99] [98] . On the SBD, mutations K414I [100] and P419A [101, 102] have been identified that eliminate allostery. N415G and D326V attenuate allostery[103]. All mutation positions are shown on Fig II.5.1 as spheres . The NBD mutations all occur in sub-domain IA facing the SBD in the solution structure except for D326V on domain IIB, rendered in a different shade of green in figure II.5.1. The SBD mutations occur on the solvent exposed loops that face the NBD in the solution structure of the ADP-state. These areas are potentially in contact in the ATP state. Recent work showed that these areas contain co-evolutionary mutagenesis[103], further bolstering the observation that they could be in contact in the ATP allosteric state.

SAXS experiments showed that considerable changes in overall molecular shape take place between the ATP and ADP form of the protein [25, 104]. The ADP form is extended and monomeric, while the ATP state has a more globular shape. Both hydrogen exchange and limited proteolytic digestion studies of DnaK show that ATP binding stabilizes the NBD, while simultaneously destabilizing most of the SBD[105] [87].

The determinants for the allosteric communication are solely embedded in the NDB and the B-basket domain of the SBD and the NBD-SBD linker. Apparently, the LID domain, which certainly has to move away from the beta-basket domain to allow substrate binding and release, does not directly drive the allostery. Mutant DnaK in which the complete LID was deleted (1-507) showed wild-type activity in the ATP-hydrolysis and ligand fluorescence assays [33] [34, 106-110]. It seems prudent to conclude that the conformational changes of the LID domain are rather a result than a cause of the Hsp70 allostery.

TROSY NMR spectra of the isolated NBD and isolated SBD superposed well on

the TROSY NMR spectrum for DnaK in the ADP state, but not for DnaK in the ATP state [90] [89]. This data suggested that NBD and SBD do not interact in the ADP state, but do interact in the ATP state. These findings of major differences between the ADP and ATP states are surprising in the light that there is only a small free energy of allostery.

II.5.3 The key role of the NBD-SBD linker

The ten-residue linker between NBD and SBD is mostly hydropobic and strongly conserved between Hsp70s. This linker is more exposed in the ADP than ATP state according to proteolysis assays [111] and hydrogen exchange [105]. Combined with the knowledge that mutations in the linker are detrimental to the allosteric coupling [41] [99], these results infer a significant role for the linker in allosteric signal transduction between the NBD and SBD.

Hydrogen exchange [98] and NMR data [89] demonstrated that the linker itself is sufficient for allosteric control of the NBD. NMR experiments suggest that the linker binds in a hydrophobic cleft between NBD domains IA and IIA, but only in the ATP state [89].

II.5.4. Allosteric changes in the NBD.

If the linker interacts with the NBD differently in the ATP than in the ADP state, one expects significant differences in the structures of these domains between these states. Remarkably, no differences were observed between ADP and ATP states of the (isolated) NBD by X-ray crystallography, making it difficult to explain how the linker docks in on estate, but not the other. However, NMR spectra showed distinct differences in chemical shifts between the ADP and ATP states in Hsc70 [93] and in DnaK-T.Th. [95, 112], suggesting that conformational changes do occur in solution.
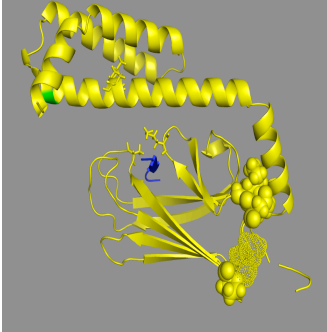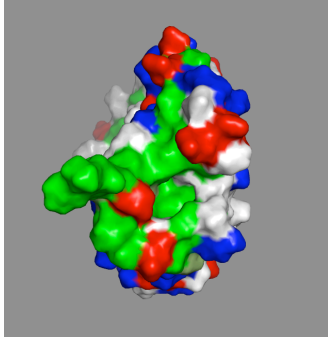
Using NMR methods it was possible to detect 9 degrees rotation between the different domains for the isolated NBD of DnaK Thermos thermophilus when comparing

the ADP and AMPPNP states [95]. In particular, the hydrophobic cleft between subdomains IA and IIA is different between the AMPPNP state and the ADP state (See Figure II.5.2)

The NMR data show that the nucleotide-binding cleft is "closed" in the ATP state and is "open" in the ADP-state. From these studies it could also be deduced that the crystal structures of the isolated NBD all correspond to the "closed" ATP state, irrespective of the bound ligand.

II.5.4. Allosteric changes in the SBD.

The SBD has been extensively investigated. Its topology is unique in the PDB [113]. A crystal structure of an SBD-LID construct of DnaK showed that a cleft is lined with hydrophobic residues to which a hydrophobic substrate (NRLLLTG) binds [30]. The cleft shows one particularly deep pocket that accommodates the sidechain of Leu4 of the substrate. In the substrate-bound form, the lid is closed. The isolated domain DnaK (387-552, L542Y, L543E) with and without bound substrate NRLLLTG was studied by NMR [114]. Analysis of NOEs and hydrogen bonding showed very little and certainly no widespread conformational change upon ligand binding. These studies present a conundrum: if no changes occur in the SBD structure upon substate binding, how does substrate binding get transmitted to the NBD?

Subunit rotations for DnaK-TTh NBD in the ADP state (blue) and AMPPNP state (yellow)	DnaK(389-605).NRLLLTG. The ligand is in blue. Residue 552 is in green. L542Y, L543E on the LID are in sticks. K414, N415 and P419 are in spacefill, T417 and I418 are in dots.	The N-terminal "face" of DnaK(389-605).NRLLLTG. Phobics are in green, positives in blue, negatives in red, polars white. The structure protruding at 3 o'clock is the residual NBD-SBD linker, with Asp393 (red) close to the SBD core.

Figure II.5.2 Allosterics in NBD and SBD. From Zuiderweg, Allostery in the Hsp70 Chaperones, review, in preparation

These results are at variance with the results of an earlier NMR investigation, in which a construct, DnaK 393-507, that lacked the lid, was investigated. In that case, the properties of substrate-bound and substrate free protein differed greatly. The apo protein was dynamically unstable: resonances for the loops 3,4 and 5,6 were broadened away beyond detection by milli-microsecond conformational change processes, suggesting a dynamical collapse, or melting, of the substrate binding cleft. Significant dynamics was observed for residues that form the latter half of the edge strand of the "lower" beta sheet. Broadening was also observed for the amide protons in a loop in which mutations that abolish allosteric communications have been found. Hence the "lidless" construct behaves very differently than the construct with lid. It is possible that DnaK 393-507 is representative of the SBD in NBD (ATP)-SBD(apo) and NBD(ATP)-SBD(sub) states, while Dnak(387-552, L542Y, L543E) is representative of the SBD in NBD(ADP)-SBD(sub) and NBD(ADP)-SBD(apo) states. Mayer and co-workers mapped the differences in amide proton exchange of DnaK (T199A) between ADP and ATP state

using proteolysis and mass spectrometry. The NBD is generally protected in the ATP state, while the SBD is dramatically destabilized in that state. Noteworthy is that the area which contains the mutations K414I [100] and P419A [101, 102] and N415G [103] which abolish or attenuate allosteric communications becomes seriously deprotected in the ATP state (see Figure II.5.2).

Taken together, the majority of data do suggest that major conformational changes beyond lid opening do occur in the SBD between the different allosteric states. The "melting" of the substrare binding cleft as seen in apo DnaK(387-507) suggest general flexibility that may be helpful for the interaction of the Hsp70s with so many different substrates.

II.5.5. SBD interaction with the SBD in the ATP state

This question is still not answered. There have been suggestions that the hydrophobic linker may interact with a hydrophobic patch that "faces" the NBD as seen in Figure II.5.1 and in Figure II.5.2. In this way, the NBD and SBD never interact directly and the linker mediates the interaction. It was also noted that LID helix A is docked to the same hydrophobic patch. Perhaps the NBD-SBD linker can displace the LID in the ATP form.

II.5.6. Conclusion

Due to efforts of several groups, the following properties can be listed for the two "end-point" allosteric states.

Table II.51 Summary of allosteric changes							
	Nucleotide binding cleft	IA-IIA cleft	NBD dynamics	Linker	SBD	SBD dynamics	LID
NBD(ATP)-SBD(apo)	closed	open	rigid	docked	docked	floppy	released
NBD(ADP)-SBD(sub)	open	closed	floppy	mobile	Not docked	rigid	docked

Some, but not all aspects of this table can be represented in a cartoon as shown in Figure II.5.3.

Figure II.5.3. Cartoon representation of the allosteric changes between the ADP.sub state (top) and ATP-apo state (bottom). Color coding is (as in Fig II.5.1): NBD domain IA, yellow; IB, blue; IIA, green; IIB, red; linker, gray; beta domain, cyan; LID-helix-A, magenta; Lid, orange. Relative domain orientations of NBD, SBD and LID in the top cartoon are represenative of reality (see Fig II.5.1). The relative domain orientations of those domains is based on the hypotheses reviewed herein (bottom cartoon). From Zuiderweg, Allostery in the Hsp70 Chaperones, review, in preparation

II.6 The constitutively expressed chaperone Hsc70

II.6.1 Architecture.

The member of the chaperone family that we focus on studying this thesis is the constitutively expressed chaperone Hsc70 (heat shock cognate). In contrast to the heat and stress induced HSPs, Hsc70 is expressed under normal cytosolic conditions and folds and repairs proteins that are newly synthesized. Molecular chaperones were originally defined as a group of unrelated classes of proteins that mediate the correct assembly of the final functional structures[1], and Hsc70 fits this definition perfectly. Like all HSP70s, it is composed of a 44K nucleotide binding domain and a 15K substrate-binding domain[113, 115] , with a 10K helical lid, linked by a flexible hydrophobic linker. The nearly identical ATPase domains of DnaK and Hsc70 consist of two large globular sub domains (I and II) separated by a deep central cleft and connected by two crossed alpha helices. Both sub domains and the connecting helices contribute to forming the binding pocket for nucleotide and the required Mg^{2+} and K^+ ions at the bottom of the cleft [116]. Figure II.6.1 represents the structure of Hsc70.
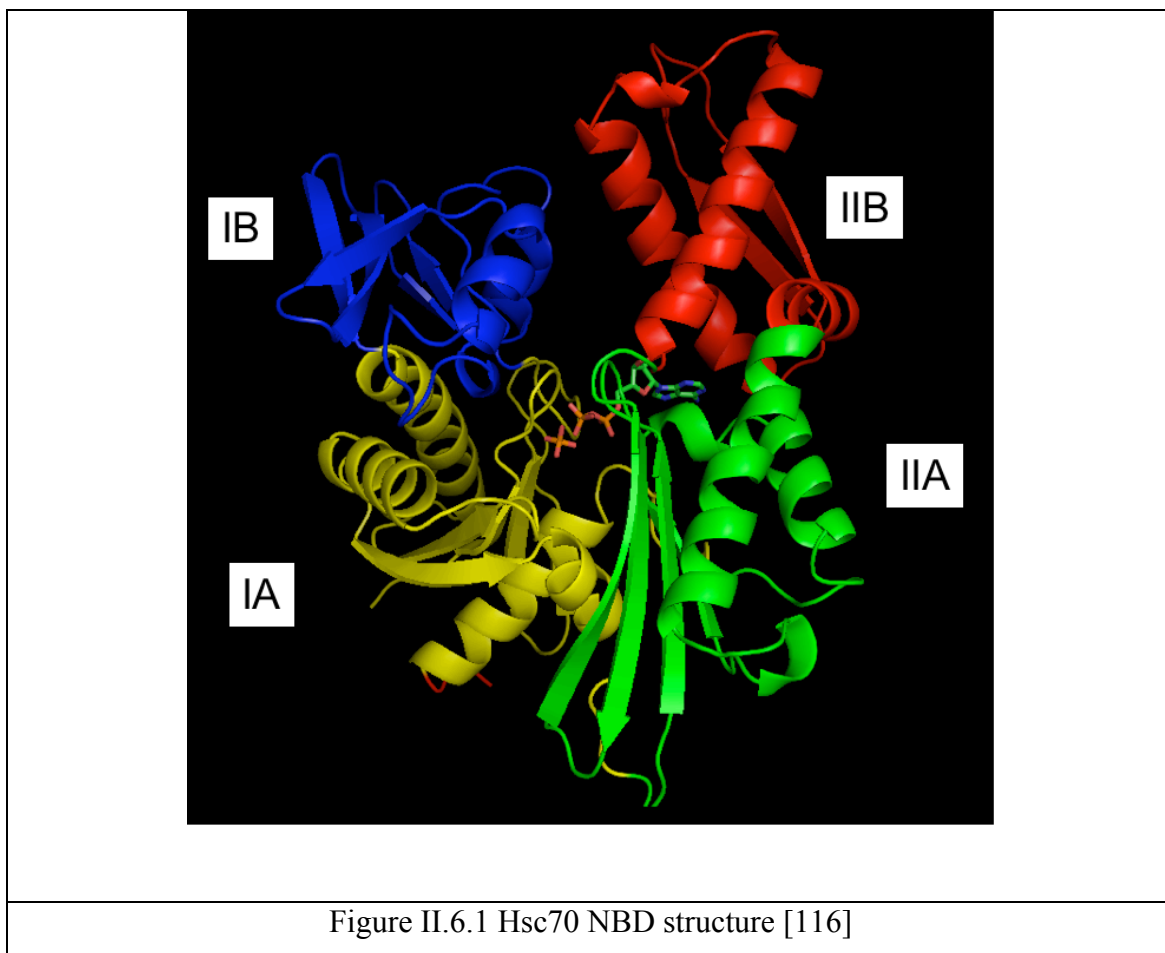
Figure II.6.1 Hsc70 NBD structure [116]

The crystal structure of Hsc70 has been solved and it shows threonine 204 in close proximity to the γ-phosphate of the ATP, in a position that it might be related to the hydrolysis mechanism [117]. The differences in chemical shifts that were observed for Hsc70 NBD in the ADP and ATP states are in agreement with the above mentioned observation as seen in Figure II.6.2 [95].

Figure II.6.2: Chemical shift differences as obtained from chemical shift mapping NMR experiments for the ATP and ADP state of the protein [95].
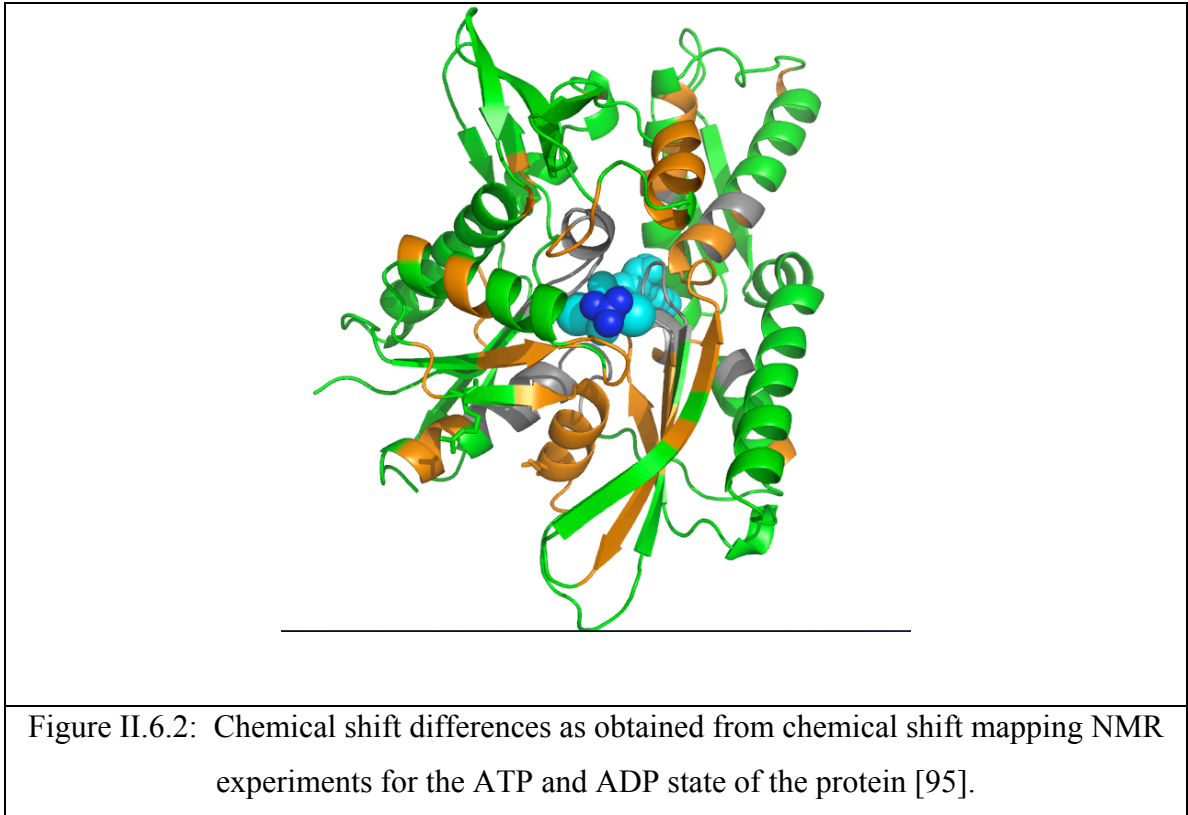
The substrate-binding domain has an unusual secondary structural topology[113]. It consists of two four-stranded antiparallel β sheets and a single α helix [68].

In the cytosol the cognate Hsp70 is expressed constitutively and it has its co-chaperones that fine-tune the Hsc70 cycle. These are mainly HDJ and NEF proteins of the BAG family. Mammalian Hsc70 homologs have intermediate dissociation rates and thus posses chaperone activity without an exchange factor. Hsc70 has many partner proteins and co chaperones, which are CHIP and proteins of the BAG family which bind to it in the proteosome [2]. CHIP in association with Hsc70 target CFTR for proteosome mediated degradation while Bag1 facilitates CFTR degradation by stimulating the Hsc70-CHIP complex [118, 119]. Hsc70 participates in a ternary complex consisting of Hsc70, Hop and Hsp90. This complex is essential in the chaperoning of transcription factors. The many functions of Hsc70 place it as a central player in intra-cellular protein homeostasis: unfolded proteins are folded; misfolded proteins are refolded; terminally misfolded proteins are escorted to the proteosome; apoptosis of terminally ill cells is induced through the BAG-Bcl2 pathway.

II.6.2 Comparison of DnaK and Hsc70

All HSP70 are highly homologous but it is worth noting the following variations between Hsc70 and DnaK. Variations exist in the interface of the nucleotide-binding cleft. DnaK proteins contain a hydrophobic patch (L257-V59 of DnaK) at the top of the cleft and two putative salt bridges (E264-R56, upper, E267-K55, lower) that are mainly responsible for the polarity of the interface. In constrast, Hsc70 proteins lack the DnaK hydrophobic patch and the upper salt bridge. The loop and the salt bridges constitute a device that allows rapid dissociation of ATP and formation of ADP+P_i. The salt bridges together with the hydrophobic contact probably function in a mousetrap like fashion to allow tight closure of the nucleotide-binding cleft. The role of the loop is not that obvious. It is presumed that it could reach subdomain IB of the ATPase domain of DnaK , thereby acting as a latch [72].

While in the DnaK case the NEF is necessary for the chaperone activity and cycle in the Hsc70 case due to the fact that the Hsc70 dissociation rates are intermediate the NEF is not necessary for the chaperone to be active. The NEFs for DnaK and Hsc70 are GrpE and Bag1 respectively. They have entirely different structures and mechanisms although they generate the same conformational open state of their target chaperone[28, 75]. These proteins may thus be generated by convergent functional evolution.

CHAPTER III. Chaperonopathies

III.1. AD (Alzheimers disease)

III.1.1. Tau tangles

Tau proteins stabilize microtubules, which serve as structural components within cells and which are involved in mitosis. Tau is abundant in neurons in the central nervous system. When tau proteins are defective, and no longer stabilize microtubules properly, they can cause dementias, such as Alzheimer's disease. Alzheimer's disease and other tau-related diseases in general are characterized by progressive memory loss and is a common cause of dementia among people of an older age. It affects 10% of the population that is older than 65 years of age. [120]. Memory loss is the first sign of cognitive impairment, followed by aphasia, agnosia, apraxia and behavioral disturbances. It leads to the death of the patient approximately after 9 years of its initial diagnosis. Those tauopathies affect over 27 million people worldwide and their number is expected to increase to 100 million by 2050 [121]. Therefore an effective treatment is a necessity since it will improve the quality of living of many individuals.

Understanding the mechanism of degeneration of the nerve cells is the key concept that relates to the solution of this disease. Post-mortem examination of patient brains with AD reveals the presence of neurofibrillary lesions and neuritic plaques. The amyloid cascade hypothesis holds that the plaques that are formed by $A\beta$ protein are neurotoxic and cause to the formation of neurofibrillary tangles and cell death. Although these deposits have been known to exist since they were first detected in 1907 by Alois Alzheimer, their chemical composition was determined

not before 1984 by Glenner et al [122, 123]. Extracellular plaques were found to consist of beta amyloid protein Aβ, which is a fragment of the larger amyloid precursor protein APP - this is the so-called amylodiasis.

Neufibrillary lesions form within nerve cells of the cerebral cortex, the hippocampal formation and some subcortical nuclei. The nerve cells eventually degenerate and die because of the presence of these lesions. These lesions consist of paired helical filaments and straight filaments. They are found in nerve cell bodies and apical dendrites as neufibrillary tangles, in distal dendrites as neurophil threads and in the abnormal dendrites that are associated with the plaques. The paired helical filaments were named as such because of their appearance as a twisted ribbon under the electronic microscope [124, 125]. Their ultrastructure has been intensely investigated by electron microscopy and atomic force microscopy [124-128]. These studies show a helical pitch of typically ~80nm with widths of 10 and 22nm in the narrow and wide points, respectively. According to X-ray studies, no regular structure exists in these filaments [129]. According to other studies, they were found to have alpha-helical structure with a persistence length of ~530nm [130]. Straight filaments seem to have the same periodicity as are paired helical filaments but with a smaller modulation in width [131].

The filaments are made of the hyper-phosphorylated protein tau that is associated with microtubules. Unlike normal tau, which contains two or three phosphate groups, the cytosolic hyper-phosphorylated tau from the AD brain (AD P-tau) contains 5-9 mol of phosphate/mol of the protein [132]. The mechanism of neurofibrillary lesions in AD is now beginning to be understood. Tau becomes hyper-phosphorylated, detaches from the microtubules, accumulates in the cytoplasm. Subsequently dimers and polymers form. The polymers assemble into globular particles. As the concentration of the globular particles increases, tau fibrils, paired helical filaments and straight filaments are formed. While globular particles are found in the non-AD brain, their concentration is lower and they do not form filaments. This suggests that the difference of an non-AD and an AD brain are those filaments and the globular particles that they are composed of [133]. The dimerization process is aided by the presence of polyanions [134]. Figure III.1.1 represents the dimerization process.
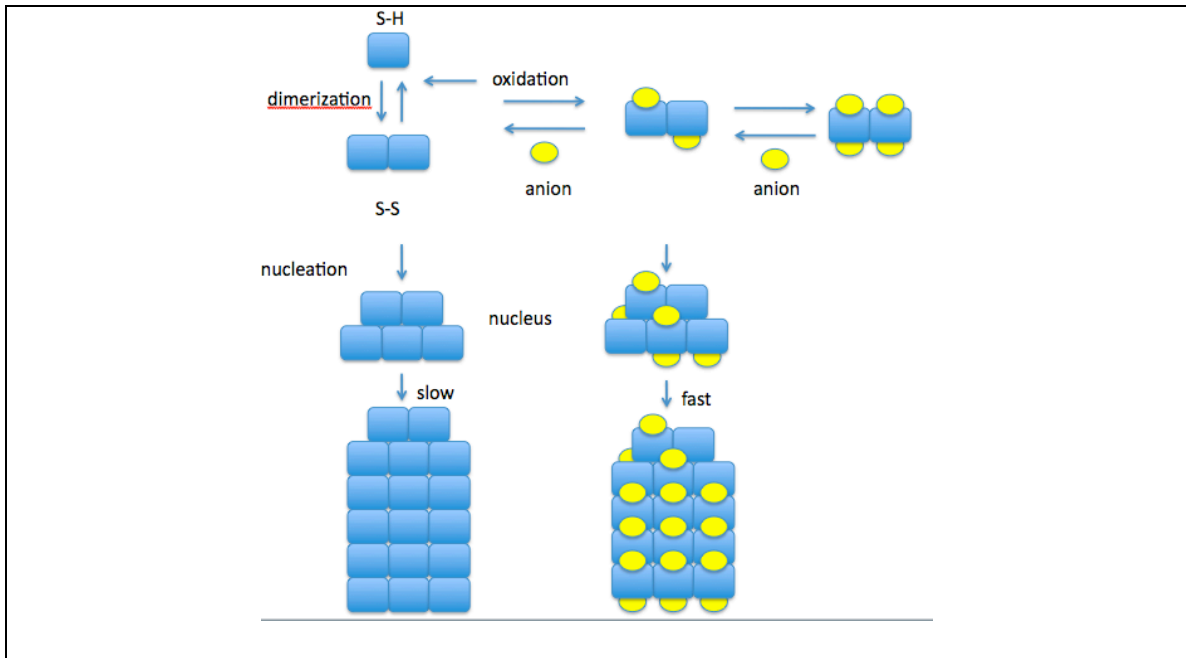
Figure III.1.1 : Diagram of tau dimerization and paired helical filaments formation and assembly. Either covalent bonds are formed when a redox reaction takes place that results in disulfide bridges or non covalent bonds are formed. In the precence of polyanions nucleation takes place fast. [134]

III.1.2 Stages of AD

There is a specific pattern regarding the progression of AD [135, 136]. Six AD progression stages have been defined determined by the distribution and severity of the neurofibrillary tangles. Stage I: It shows neurofibrillary tangles and neurophil threads confined to pre-a neurons of the transentorhinal cortex. Stage II: It shows a more remarkable involvement of this area and a mild involvement of the pre-a neurons in the entirhinal cortex. Stages I and II are also called the transentorhinal stages. Stage III: AD brains have severe neurofibrillary lesions in the above-mentioned region and extracellular tangles emerge. Stage IV: Extensive neurofibrillary lesions are found in the deeper layers of entorhinal and transentorhinal cortex. Stages III and IV are also characterized by neurofibrillary pathology in layer I of Ammons's horn in the hippocampus and in subcortical nuclei and are called called the limbic stages. Stages V and VI: Increasingly abundant lesions are present in isocortical association cortex. Stages V and VI are also

named the isocortical stages. Subjects with stages V and VI meet the neuropathological criteria for the diagnosis of AD and are severely demented at the time of death. The brain and its various subdomains can be seen in Figure III.1.2.

Figure III.1.2: The brain and its various functional domains.
(http://www.miniscience.com/projects/modelbrain/)
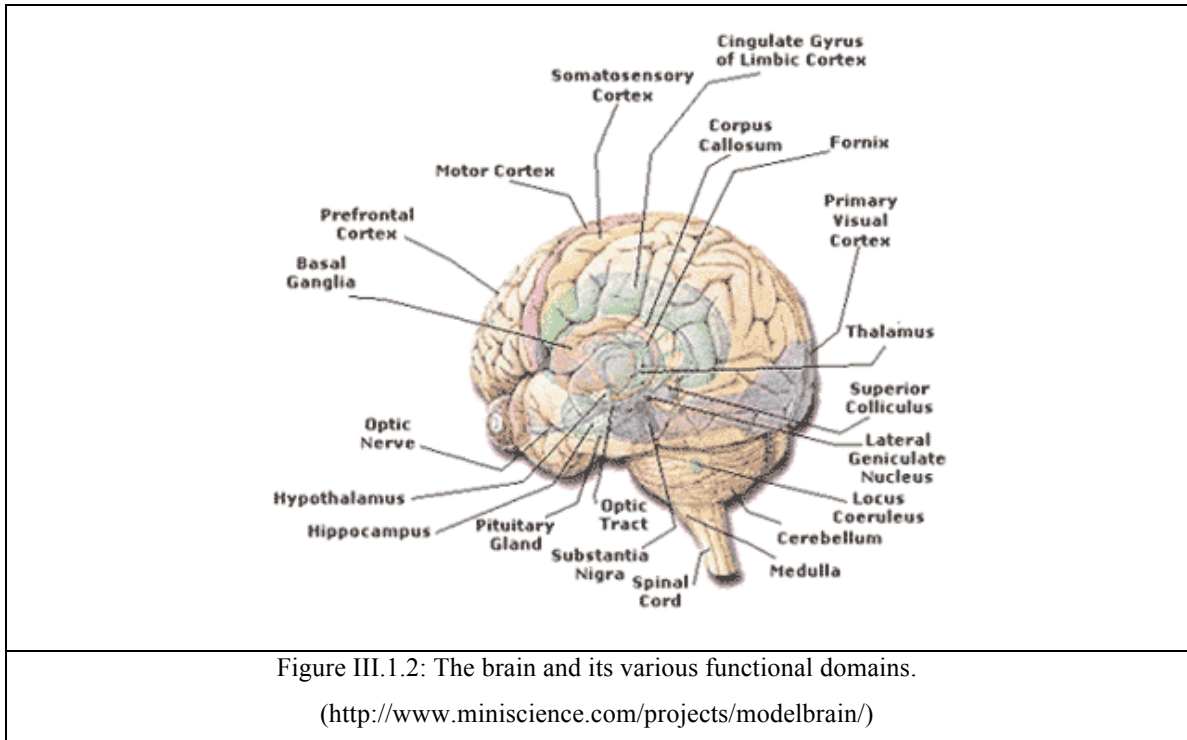
III.1.3 Tau and diseases

Tau is related to various neuronal diseases such as AD (Alzheimer's disease), progressive suprenuclear palsy, Pick disease, cortiocobasal degeneration and other tauopathies [137]. A table of various tau related diseases is shown in Figure III.1.1 [133].

•AD
•Pick's
•Parkinsons
•Down's syndrome
•Argyrophilic grain disease
•Tangle only dementia
•Corticobasal degeneration
•Progressive supranuclear palsy
•Amyotropic lateral sclerosis
•Niemann-Pick disease type C
•Subacute sclerosing panencephalitis
•Postencephalitic parkinsonism
•Dementia pugilistica
•Myotonic dystrophy
•Gestmann-Straussler-Scheinker disease with tangles
•Prion protein amyloid angiopathy
•Presenile dementia with tangles and calcifications
•Hallervorden-Spatz disease
•Cancer
Table III.1.1: Tauopathies [133]

Alzheimers Disease has two characteristic pathological features. The first one is the appearance of senile plaques composed mainly of Aβ and the appearance of neurofibrillary tangles and neurophil threads. Although the tauopathies are often sporadic, they are linked to tau mutations that have as a result the diverse clinical phenotypes. They are linked to the chromosome 17 [138] since all the tau proteins are translated from a single gene of the chromosome 17 [139]. Most studies usually focus on AD since it's the most common tauopathy and it is used as a tauopathy to compare the rest of the tauopathies [140].

It is assumed by some scientists that the formation of tau aggregates is the result of a protective mechanism against the toxic tau oligomers. Another point of view is that not the loss of function of tau but the formation of tau oligomers is the physical barrier against axonal transport or is toxic to the cells. In such a scenario tau aggregation might be a gain of function rather than a loss of function during the disease as seen in Figure III.1.3.

Tau binding to microtubules is disrupted by changes in phosphorylation or by mutations in the tau gene. Loss of tau binding may result in the loss of microtubule function. On the other hand, decreased tau binding to microtubules might result in increased hyperphosphorylated free tau. This may cause aggregation of tau into neurofibrillary tangles and neuronal death. Another possibility is that hyperphosphorylated tau itself is toxic to neurons as a result of structural changes induced by phosphorylation.
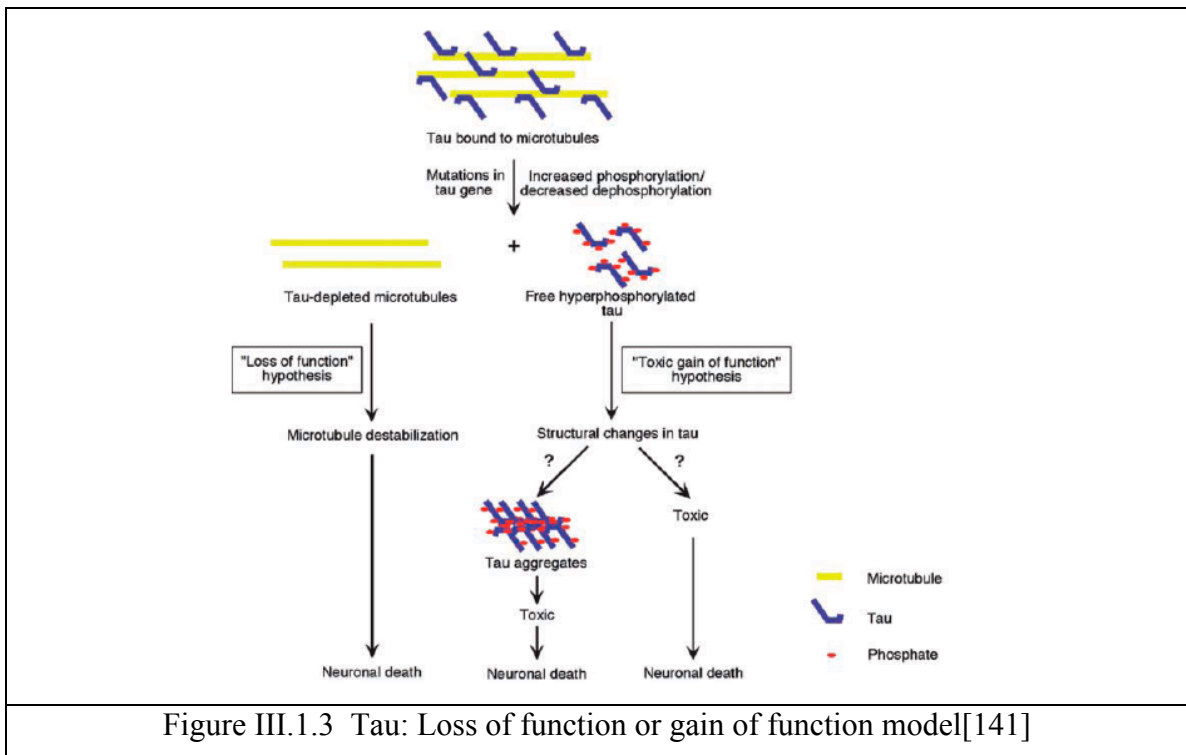
Figure III.1.3 Tau: Loss of function or gain of function model[141]

Hyperphosphorylated aggregated tau is the pathological form of the tau protein that causes the tauopathies. It has been mentioned [142] that hyperphosphorylated tau can

cause neuronal cell death. The result of the hyperphosphorylation is the abnormal folding of this normally linear protein and its aggregation and the formation of tangles. Kinases are proteins that interact with tau and they have been linked with tauopathies too. Two distinct phosphorylation motifs are present within the tau protein, proline-directed serine/threonine sites and KXGS motifs within the four microtubule binding repeat domains of tau (serine residues at 262,293,324 and 356). These KXGS sites have been identified as substrates for the microtubule affinity regulating kinase (MARK), which plays a normal role in the regulation of tau function, causing tau to be released from the microtubules. Evidence suggest that prior phosphorylation by MARK (the PAR-1 drosophila analog) is required to initiate the pathogenic cascade of hyperphosphorylation by other kinases that are associated with the formation of neurofibrillary tau lesions in taupathies [143]. Along with hyperphosphorylation, an early event in the process of tau aggregation is a conformational change that occurs, allowing the N-terminus of tau to interact with its microtubule-binding region [138]. Tau in this folded state can be detected with the MC-1 antibody that recognizes amino acids 7 -9 and 312-342 only when these residues are adjacent to each other[138]. Together those studies suggest that dephosphorylation of the tau protein is crucial for the therapy of AD.

III.1.4. Normal tau function

Tau protein was discovered almost simultaneously in the United States and Europe as a protein that lowered the concentration at which tubulin polymerizes into microtubules in the brain [136, 144-146]. It is a microtubule-associated protein expressed mainly in neurons where it has a role in the assembly and stability of the microtubule network. It localizes mainly in the axon. It has been found to have a rod like shape[147]. The structure of tau is mentioned to have the structure of a random coil with beta structure in the second and third microtubule repeats[141, 148]. Its amino acid sequence is shown in Figure III.1.4.

```
        10          20          30          40          50          60
MAEPRQEFDV MEDHAQGDYT LQDQEGDMDP GLKESPLQTP ADDGSEEPGS ETSDAKSTPT

        70          80          90         100         110         120
AEDATAPLVD EGAPGEQAAA QAPAEIPEGT AAEEAGIGDT SNLEDQAAGH VTQARMVSKG

       130         140         150         160         170         180
KDGTGPDDKK TKGADGKPGT KIATPRGAAP PGQKGQANAT RIPAKTTPTP KTSPATMQVQ

       190         200         210         220         230         240
KKPPPAGAKS ERGESGKSGD RSGYSSPGSP GTPGSRSRTP SLPTPPTREP KKVAVVRTPP

       250         260         270         280         290         300
KSPSAAKSRL QAAPGPMPDL KNVKSKIGST ENLKHQPGGG KVQIINKKLD LSNVQSKCGS

       310         320         330         340         350         360
KDNIKHVPGG GSVQIVYKPV DLSKVTSKCG SLGNIHHKPG GGQVEVKSEK LDFKDRVQSK

       370         380         390         400         410         420
IGSLDNITHV PGGGNKKIET HKLTFRENAK AKTDHGAEIV YKSPVVSGDT SPRHLSNVSS

       430         440
TGSIDMVDSP QLATLADEVS ASLAKQGL
```

Figure III.1.4: Amino acid sequence of bovine tau.[149]

Tau is a highly soluble phosphoprotein and its biological activity is regulated by phosphorylation [150]. Fetal tau is phosphorylated to a higher degree than adult tau and the degree of phosphorylation of the tau protein decreases with age. The phosphorylation sites are clustered at regions flanking to the microtubule binding regions. Phosphorylation of specific sites seems to affect negatively the binding of tau to the microtubules [151-160]. These sites are mentioned to be Serine-262 and 396. These sites are phosphorylated in fetal tau and in hyperphosphorylated adult tau in AD patients. While older studies focused on the phosphorylation of serine and threonine residues [161-163]more recent studies have also focused on the phosphorylation of the tyrosine residue [164]. There are 79 serine and threonine phosphorylation sites on the longest tau isoform that contains 441 amino acids. These sites have been divided into two main groups: those that can be modified by proline directed kinases like tau protein kinase I (glycogen synthase kinase 3, GSK3), tau protein kinase II (cdk5), MAP kinase (p38), JNK and other stress kinases or cdc2 and those that can be modified by non proline directed kinases like protein kinase A (PKA), protein kinase C (PKC), calmodulin (CaM) kinase II, MARK

kinases [161, 165-171], or CKII that modifies residues close to acidic residues mainly in axons 2 and 3 [165]. GSK-3 is the kinase that plays the major role in phosphorylating tau both in physiological and pathological conditions. Regulation of the kinase activity is done by the phosphatases that dephosphorylate tau. Several phosphatases like phosphatase (PP) 1, PP2A, PP2B, (calcineurin), and PP2C have been implicated in reversing the phosphorylation of tau [172-175]. Only PP1,PP2A and PP2B [176, 177] have been shown to dephosphorylate hyperphosphorylated tau. Figure III.1.5 is representative of the phosphorylation sites of tau in the various tau isoforms and is indicative of the variety of phosphorylated tau present in healthy and unhealthy neurons.
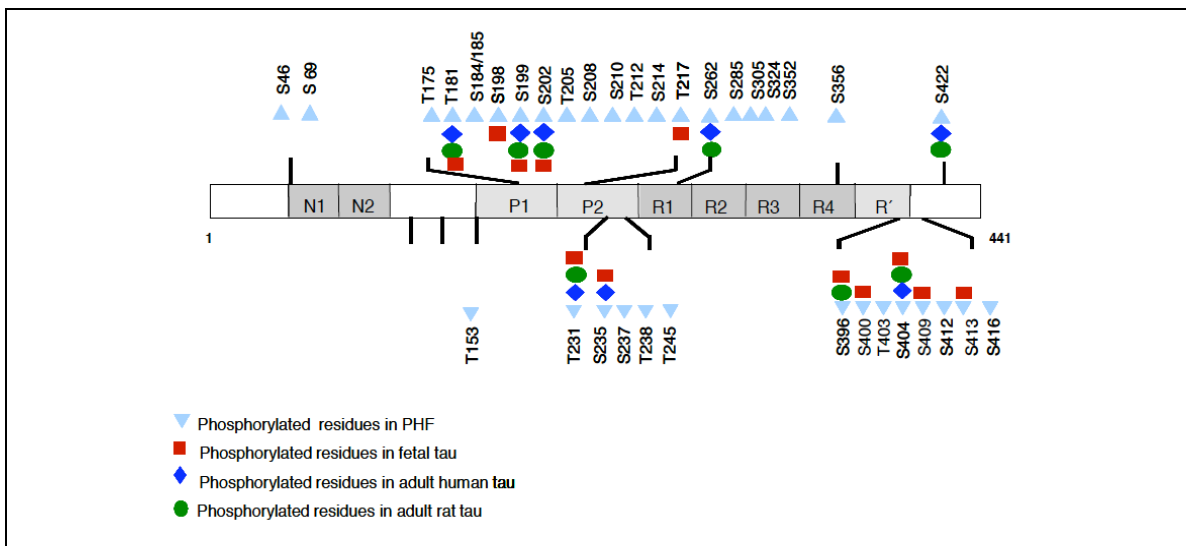
Figure III.1.5 Phosphorylation sites of various tau isoforms. (Bratisl Lek Listy 2006 .107 (9-10) :346-353 Post-translational modifications of tau protein Pevalova M. , Filipcik P, Novak M, Avila J, Iqbal K.)

Phosphorylated tau is long and stiff while dephosphorylated tau is more elastic. Its shape is rod like and its length is approximately 50nm with tubulin binding domains clustered at one end of the molecule. This explains the stiffness of the phosphorylated version of tau [178]. When dephosphorylated it is presumed that it is flaccid. That suggests that tau may regulate the viscosity of the axonal cytoplasm [147].

Tau has multiple functions, one of which is the stabilization of the axonal mictotubules [179, 180]. Other functions include a role in signal transduction [181, 182], interaction with the actin cytoskeleton [183], neurite outgrowth [182, 184], interactions with the plasma membrane [185, 186], anchoring of enzymes such as protein kinases and

phospatases [32-35], and the regulation of intracellular vesicle transport [187].Relevant reviews exist in the literature [188].

III.1.5. Tau and microtubules

The morphology of the neuron is determined by its cytoskeletal scaffolding. Proteins associated with the principal cytoskeletal components such as the microtubules have a strong influence on both the morphology and physiology of the neurons. Tau is one of these proteins. Tau is categorized as a MAP (microtubule assembly protein) because it was found to bind to microtubules and stimulate microtubule assembly in cell-free reactions[136, 146]. Thus tau is capable of promoting microtubule nucleation, growth and bundling [189, 190]. It also stabilizes the microtubules [157, 180, 191-193]. The repeat region of tau is the basic microtubule interacting unit, however flanking regions to the repeat proline rich increase the binding of tau to microtubules [189, 194, 195]. Tau has been reported to bind to microtubules in two ways. When binding was tested on previously assembled and closed microtubules , tau bound to the outer surface [196, 197] as seen in Figure III.1.7 . When tau was mixed with tubulin and then assembled, tau binds to the inside of the microtubule [198].

Figure III.1.6 Tau is a microtubule-associated protein. A view of the binding of tau (red) to the tubulin dimer is indicated.	Figure III.1.7 : The binding of tau to the microtubules A) Tau with its four repeats bound to the microtubule surface B) Tau bound to the microtubule only though repeat I C) Tau bound to the microtubule through repeats I and IV. [149]
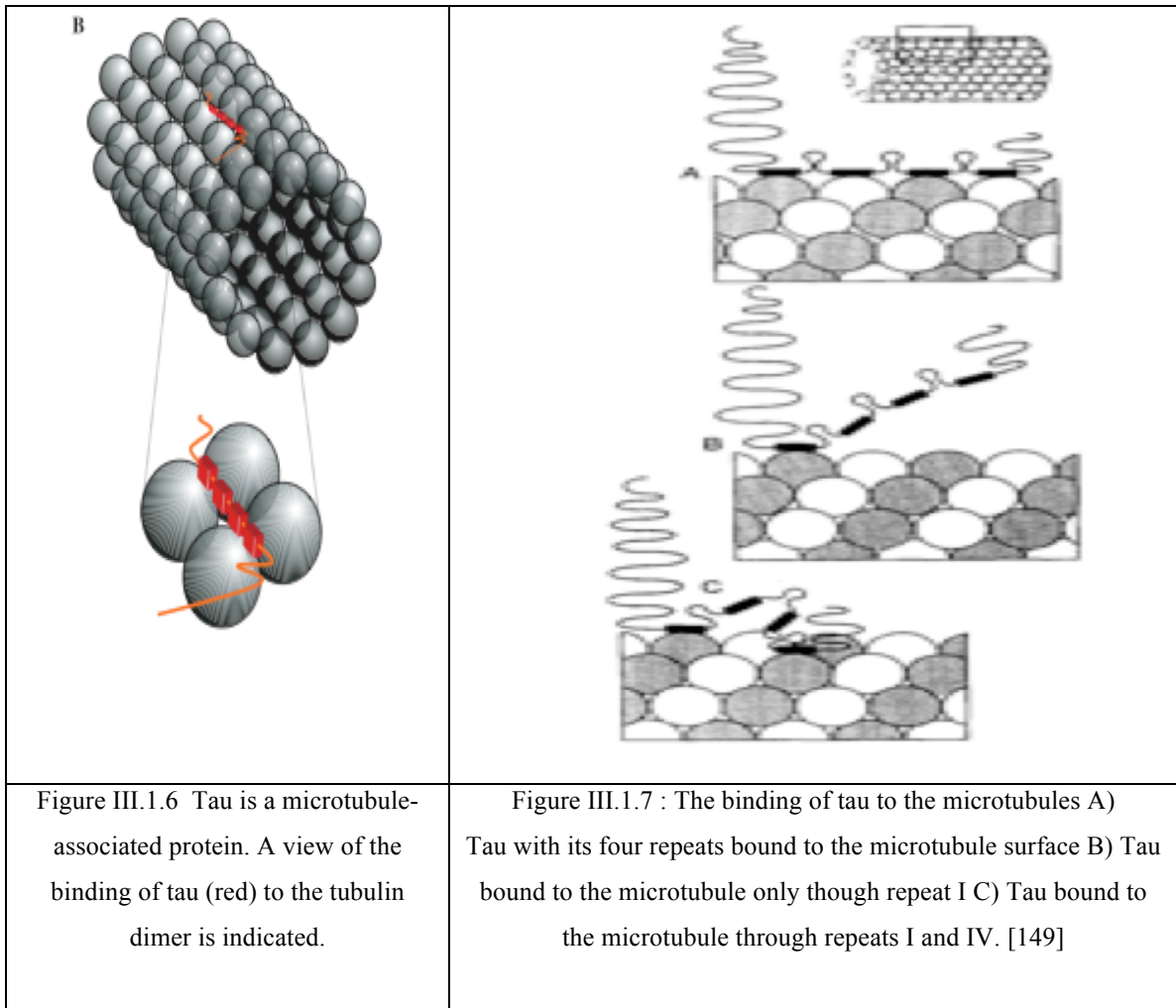
In the figure III.1.6 tau is shown to bind to microtubules. The first repeat of tau has higher affinity to the microtubules. It binds 75 to 200 times tighter than the other repeats [149].

Phosphorylation of tau is related to the binding of tau to microtubules. For example, Phosphorylation of serine 262 completely abolishes the binding of tau to microtubules [199]. Phosphorylation of sites within the proline-rich region reduces the capacity of tau to promote de novo nucleation of microtubules in cell free assembly reactions. This suggests that the role of tau is temporarily and spatially regulating neuronal microtubule assembly is modulated by its phosphorylation state.

Other functions of tau include its fundamental role in neurite outgrowth and stabilization, its interaction with the actin cytoskeleton and its role in the PLC-γ signaling pathway. The N-terminal part of the protein is crucial for the stabilization and

organization of certain types of axons. Tau protein binds to spectrin and actin filaments[200-204] Through these interactions, tau proteins probably allow microtubules to interact with other components of the cytoskeleton such as neurofilaments [205-207] and may restrict the flexibility of the microtubules [208]. There is also evidence that tau proteins interact with other organelles of the cytoplasm. Such interactions probably allow the binding between microtubules and mitochondria [209]. The tau N-terminal projection domain also permits interactions with the neuronal plasma membrane [185]. Thus tau may interact as a mediator between the mictotubules and the plasma membrane.

Figure III.1.8 represents the tau protein in terms of its various domains.

Figure III.1.8 : Functional domains of the longest tau isoform.
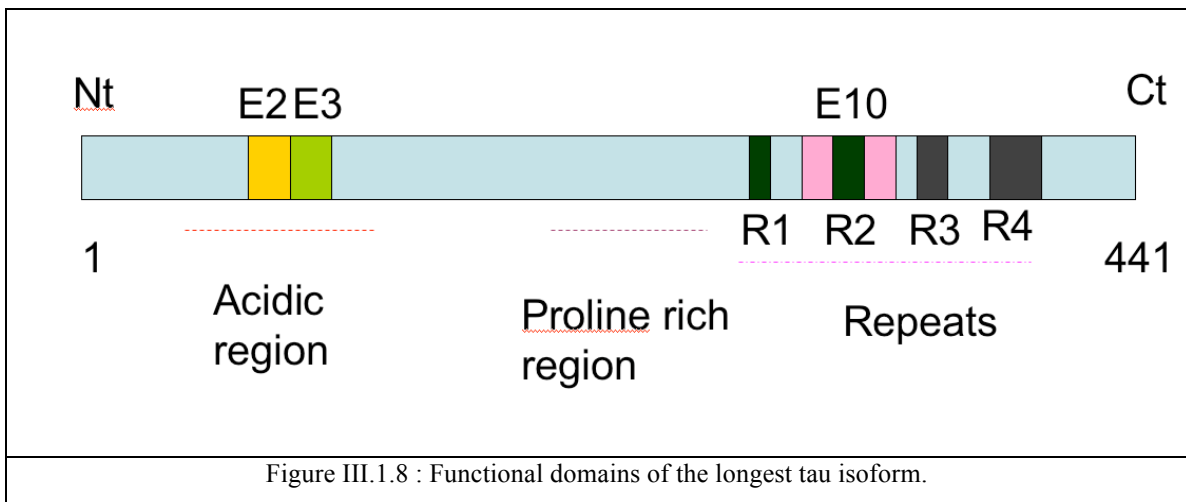
III.1.6 Tau and Hsp70 chaperones

Alzheimer's disease, Parkinson's disease and amyotrophic lateral sclerosis have been termed protein misfolding disorders[210]. Alzheimer's disease is the most common of all. Heat shock proteins provide a line of defense against aggregated misfolded proteins. Analysis of constitutively expressed heat shock proteins revealed variable levels of Hsc70 and Hsp27 in different classes of neurons in the adult rat brain [211]. Neurons are postmitotic and cannot dilute toxic species such as tau oligomers though cell division, hence misfolded proteins accumulate in neurons during aging [210].

The heat shock proteins Hsp70 and Hsp90 bind to tau, and as a consequence of this interaction, the association of tau protein with microtubules increases, decreasing the self association and hence the formation of tangles [212]. The Cochaperone BAG-2

dissociates tau from the microtubules [66] and thus we could inhibit the BAG- Hsc70 interaction by the binding of small molecules that will lead to the inhibition of the Hsc70 cycle and will affect to the binding of tau to the microtubules. Recent work has shown that tau phosphorylation at substrate sites for the kinases Cdk5 and GSK3-beta can trigger the binding of tau to chaperones Hsc70 and Hsp27. The binding of phosphorylated tau to CHIP-Hsc70 ubiquitinates the phosphorylated tau and enhances the cell survival [213]. The binding to chaperones was also presumed to be part of the protective mechanism against tau oligomer toxicity.

Oligomeric tau is a toxic molecule, especially those forms of tau that have been phosphorylated by the kinases glycogen synthase kinase 3β and Cdk5. Alzheimer's tau bind to Hsc70 and its phosphorylation is a recognition requirement for its ubiquitination by the E3 Ub ligase CHIP and the E2 conjungating enzyme UbeH5B [213]. A model for this procedure has been proposed and it is shown in figure III.1.9 .
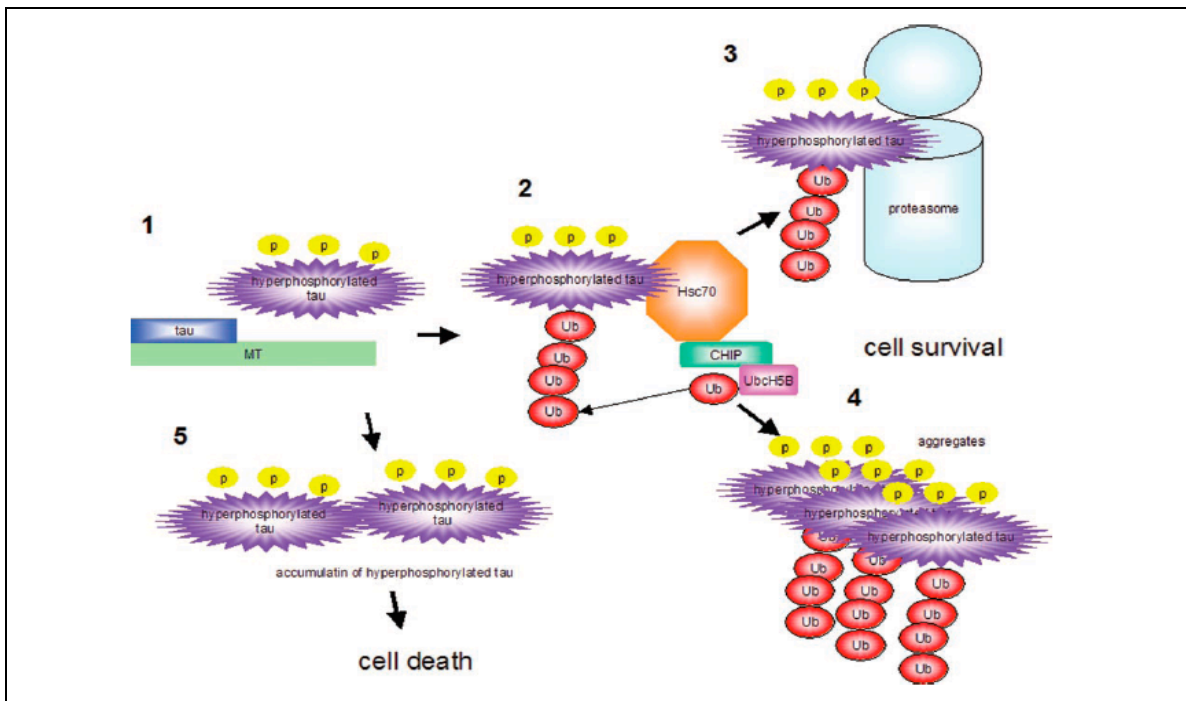
Figure III.1.9 : Model according to which the CHIP-Hsc70 complex decreases the toxicity of hyperphosphorylated tau by either leading it to the proteosome for degradation or by the formation of non toxic tangles. Step1, tau is phosphorylated by GSK-3β, Cdk5, and other kinases and is released from the microtubules Step2, hyperphosphorylated tau is ubiquitinated by the CHIP-Hsc70 complex for degradation in the proteosome (step 3) or the formation of aggregates (step4) Step 5, interference with step 2 leads to the accumulation of hyperphosphorylated tau [213]

Hsc70 binds to the microtubule binding domain of tau without an absolute requirement for tau to be phosphorylated [214]. Hsc70 binds to tau at two sites that are involved in tau aggregation. The C-terminus of Hsc70 and especially amino acids 360-646 is involved in this binding. That is the so-called substrate binding domain of Hsc70 and the unstructured tail that is linked to that domain. It has been shown that heat shock 70 proteins can bind 5-7mer sequences rich in hydrophobic amino acids [215-217] and a site represented as ΦQΦΦ where Φ is a hydrophobic amino acid mediates tau binding to Hsc70/Hsp70 [214]. Such motifs exist in tau and were reported to be VQII and VQIV [214]. The Hsc70-tau binding constant was found to be two orders of magnitude lower than the tau-tau binding constant (46μM) and thus it probably competes the tau-tau interaction and aggregation. The location of the Hsc70-tau binding also suggests that it competes with tau binding to microtubules. On the other hand other studies suggest that chaperones promote the partitioning of tau into microtubules [212].

Another mechanism for the degradation of tau that involves CHIP, includes Hsp90 and AKT and is shown in Figure .The activity of AKT is involved in the degradation pathway of tau. Under normal conditions (left), stress or Hsp90 inhibition stimulates the CHIP/Hsp90 complex to recognize both Akt and phosphorylated tau targeting them for proteosome- mediated degradation by the ubiquitin pathway. As Akt levels increase (right) with age or disease, the CHIP/Hsp90 complex either targets Akt over phosho-tau or alters CHIP activity.

Figure III.1.10 :Proposed mechanism for the ubiquitination of tau by the CHIP/Hsp90 complex. [218]
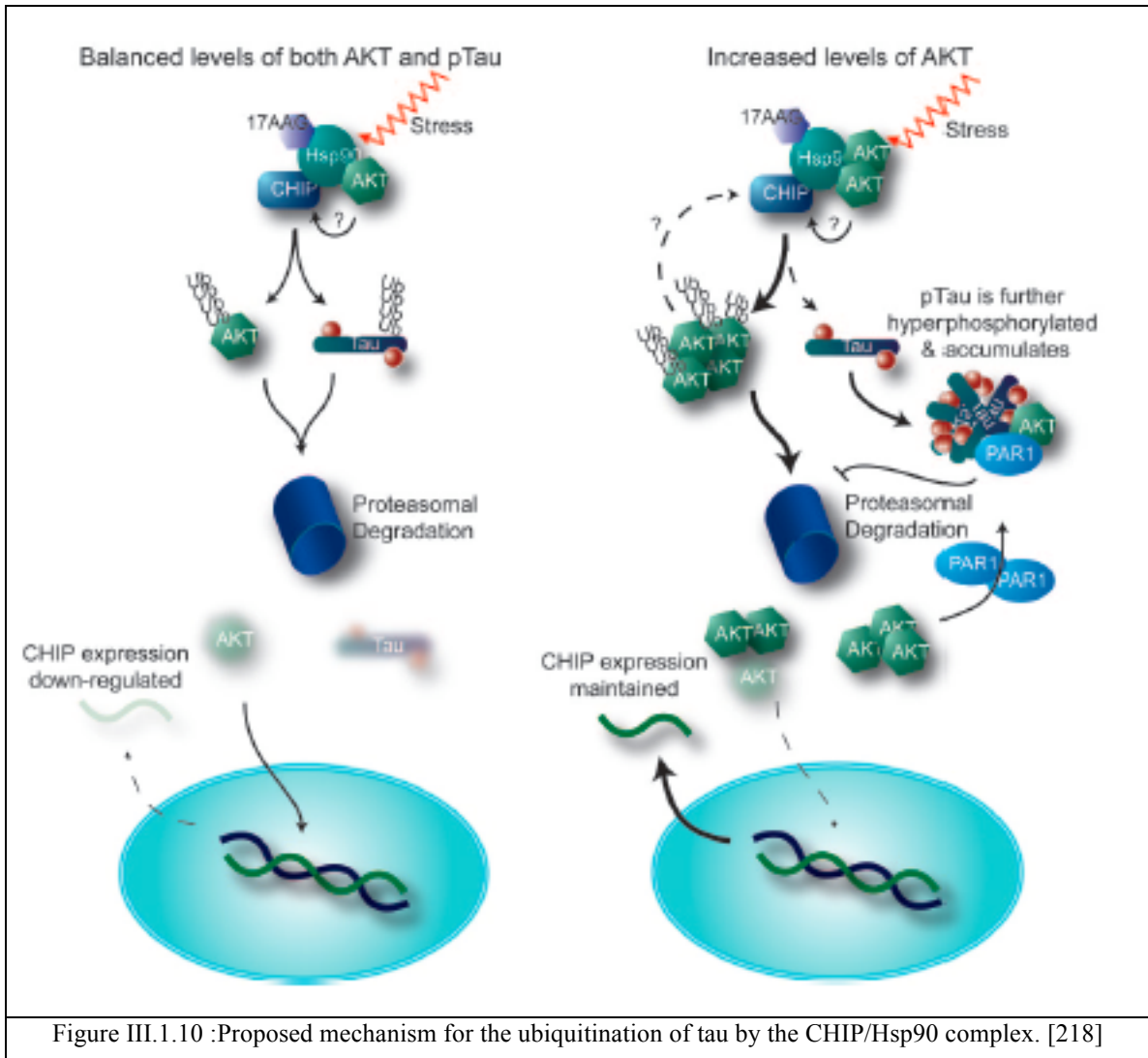
Another mechanism regarding the Hsc70-tau interaction has been recently suggested [219]. When tau is hyperphosporylated it is stiff and nonfunctional. The protein Hsc70 instead of allowing it to ubiquitinate and enter the apoptosis pathway it prolongs its life scan allowing it to return to the microtubules, aggregate and remain there as tangles.

Figure III.1.11: Model for the early stage of tau disfunction.[219]
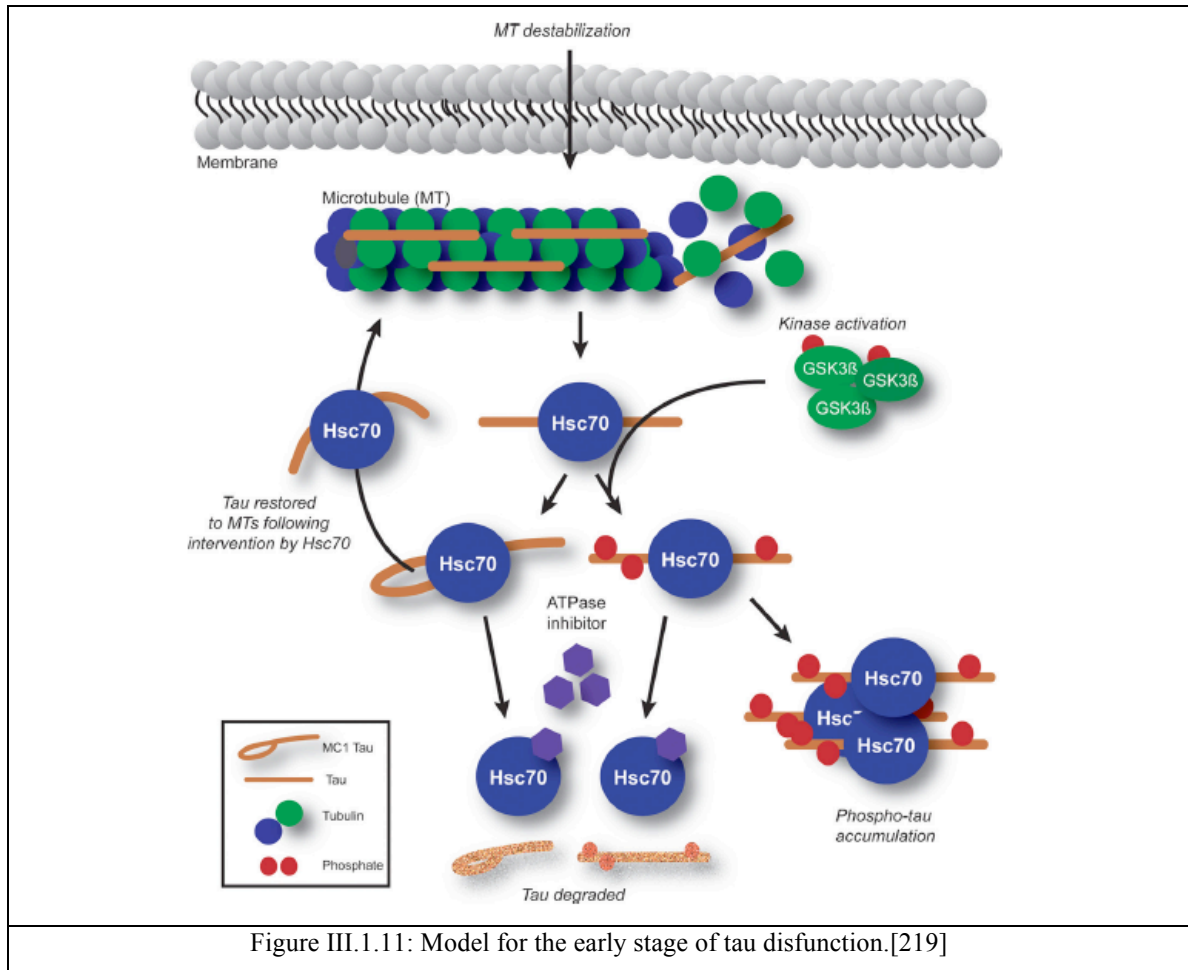
III.1.7. Tau isoforms

In human brain six isoforms of the tau protein are expressed. They differ by the presence of three or four tandem repeats of 31 or 32 amino acids each located in the carboxy-terminal region in conjuction with 0, 29 or 58 amino acid inserts located in the amino terminus. The repeat sequences of tau consist the microtubule-binding domain of the protein. Only three isoforms of tau are expressed in rodents. The ones with the four repeats and the 0, 29 and 58 amino acid amino terminal inserts [220-223]. In humans the three repeat isoforms are more abundant than the four repeat ones. Tau isoforms with three repeats assemble into paired filaments in AD brains whereas tau isoforms with four repeats assemble into straight filaments. The longest isoform has four repeats and 441 residues, the shortest isoform (fetal) has 352 residues and three repeats. The 'big' tau isoform contains ~ 300 extra residues. The abundance and variety of tau isoforms in

humans is related to the developmental stages of their life. Fetal tau is the shortest of all. The other isoforms are expressed during childhood [224, 225]. Tau contains either one or two cysteins, depending on the isoform. These are Cys 291 (repeat 2) and Cys 322 (repeat 3-always present). This difference affects the assembly of the paired helical filaments. The amino acid composition of tau is dominated by charged residues, in an acidic stretch near the N-terminus that is followed by mostly basic domains. The repeat region is flanked upstream by a basic proline rich region (~25% proline) and downstream by another basic stretch also containing several prolines. Many of these occur in Ser-Pro or Thr-Pro motifs whose phosphorylation is diagnostic of AD disease. The C-terminal half of the tau protein constitutes the microtubule binding domain [195, 226]. In AD, paired helical filaments and straight filaments have been shown to contain all six isoforms [227] in a hyperphosphorylated and abnormally phosphorylated state compared to tau from normal adult brain [228-230].

III.2. Cancer relevance

All known tumors express excess Hsp70; in fact, Hsp70 is required for the survival of cancer cells[231], [232, 233]. Immunoelectron microscopy revealed that endosomal and lysosomal membranes of tumor cells contained Hsp70s. Various drugs such as MAL3-101 bind to chaperones and are also cytotoxic to carcinoma cells. Heat shock and radiation in human prostate carcinoma cells had positive results on the patients treated. Hsp70 depletion triggers massive caspase independent tumor cell death. Hsp70s are present on the surface of cancer cells, which is not the case for non-cancer cell lines. It is assumed that they might be involved in their protection from apoptosis. Enhanced Hsp70 is emerging as an important predictor of resistance to chemotherapy, radiation and hyperthermia therapy in breast cancer[234],[17]. Suppression of Hsp70 chaperone expression in tumor cell lines by anti-sense RNA[235],[236] or by direct inhibition by small compounds[237] is lethal to these cell lines. One hypothesis for the enhanced Hsp70 expression holds that the physiopathological features of the tumor microenvironment (low glucose, pH, and oxygen) mimic stress conditions[238, 239]. Alternatively, conformationally unstable oncoproteins such as mutated p53 may elicit an Hsp response[240-244].

Hsp70s promote cancer-cell survival by inhibiting cell death pathways[239, 245-249]. At the pre-mitochondrial level Hsp70 can inhibit receptor-mediated activation of JNK[250], activation of caspases-3, -8, and -9 and Bid cleavage into tBid[251]. In addition, Hsp70 may prevent translocation of the apoptotic enhancer BAX from the cytosol to the mitochondria[252]. Hsp70 can also stabilize lysosomal membranes to inhibit the release of cathepsins and other enzymes which can induce cell death[253]. At the post-mitochondrial stage, Hsp70 antagonizes the release of apoptogenic factors including cytochrome c and AIF[252]. Furthermore, Hsp70 can bind to and block the activity of APAF1 to avert the formation of the apoptosome and subsequent activation of caspase enzymes[254].

Hsp70 may also directly participate in oncogenesis, since overexpression of heat shock proteins can increase the tumorigenic potential of cells[239]. One of the responsible mechanisms may be the interaction of Hsp70 (especially mt-Hsp70) with mutant and wild-type tumor suppressor proteins   p53 [242-244, 255]'[256, 257] and Rb107[258]. In particular, wild-type p53 and the non-truncated mt-Hsp70 proteins co-localize in the cytoplasm in several human cancers (undifferentiated neuroblastoma, retinoblastoma, colorectal and hepatocellular carcinomas, and glioblastoma).[244]

Due to its general cytoprotective properties, Hsp70 over expression in tumor cells leads to resistance to chemotherapy [247]. As a particularly cynical twist, Hsp70s were found to be induced in colon and ovarian cancer cell lines exposed to Hsp90 inhibitors[259]'[260], reducing the efficacy of the Hsp90-targeted cancer therapies.

Mortalin is the mitochondrial Hsp70 that is highly homologous to DnaK and it is said that this is due to the prokaryotic origin of the mitochondria as an individual cell. It has been mentioned[261] that it is directly related to cancer.

III.3. Hsps in disease: Microbial Pathogenesis

The prokaryotic Hsp70, DnaK, promotes bacterial survival under stress[262]. Consistent with these roles, DnaK knockouts in *E. coli* or *S. aureus* DnaK are sensitized to antibiotics[263]'[264] . Knockouts of the co-chaperone DnaJ also show growth defects under stress conditions[263]. Together, these observations have led to the exciting

hypothesis that inhibitors of DnaK and its co-chaperones could have antibiotic applications[265].

CHAPTER IV. Small molecule modulators of tauopathies.

IV.1. Tau-directed therapies

Various drugs have been screened for chaperone inhibition/activation since that pathway is so crucial [266-269]. One example is Geldanamycin (GA), which is an Hsp90 inhibitor [270]. It proved to be hepatotoxic and various analogs of this drug were generated. Other drugs include acetylcholinesterase inhibitors to improve cognitive functions and other drugs to improve mood changes, agitation and psychosis that often occur in the later stages of the disease. Memantine has also been used. A good approach is to prevent tau from phoshorylation and thus block the kinases that phosphorylate tau. GSK-3β is the kinase that appears to have a critical role in AD pathogenesis [271] and lithium is a good GSK-3β inhibitor [272]. Other GSK-3β inhibitors are aloisines, flavopiridol, hymenialdisine, paullones and staurosporine[273, 274]. Another kinase that is a good target for inhibition is cyclin-dependent protein kinase 5 (Cdk5). Roscovitine, inhibits 50% of cdk5/p25 at a concentration of 0.16μmol/L [275, 276], has useful selectivity for cdk5 over other kinases and can pass through the blood-brain burrier [277]. Other cdk5 inhibitors include olomoucine, flavopiridol, aloisines and inirubins [274]. Inhibition of cdk5 though has been proven to upregulate GSK-3β so cdk5 does not seem to be the proper kinase for tau phosphorylation inhibition [278].

One other pathway is tau dephosphorylation with upregulation of the phosphatases that dephosphorylate tau. PP2A in the major tau phosphatase in the brain and that is a good target for upregulation [279-283]. Two inhibitors of PP2A exist in the brain I_1^{PP2A} and I_2^{PP2A}. They are disregulated in the AD brain [284, 285]. Targeting these inhibitors could be another way of upregulating PP2A.

Modifying tau itself so that it can no longer be hyperphosphorylated could be

another way to AD treatment. Besides phosphorylation the serine/threonine residues of tau are also modified by a monosaccharide called β-N-acetylglucosamine (GlcNAc) via a glycosidic bond, and this modification is called O-GlcNAcylation [286-288]. In AD brain impaired glucose metabolism may cause decreased tau O-GlcNA-cylation, which in turn facilitates hyperphosphorylation of tau contributing to neurofibrillary degradation. So restoring glucose metabolism in the brain can help restore hyperphosphorylated tau downregulation. Rosigliazone is a well known insulin sensitizer that has been shown to reduce tau phosphorylation in cultured cells [289]. Tau O-GlcNAcylation is regulated by O-GlcNAc transferase and β-N-acetylglucosaminidase (O-GlcNAcase). Thiamet-G is a O-GlcNAcase inhibitor and it has been shown to decrease tau phosphorylation at pathologically relevant sites in the PC12 cell line and in rat brains [290].

Drugs that act against tau fibril formation were found after library screening to be daunorubicin and adriamycin [291, 292]. One more pathway regarding an AD cure would be increasing the clearance of tau, that can be done either by macroautophagy (encapsulation by an autophagosome and fusion with a hydrolase-containing lysosome[293])or by the ubiquitin proteosome system (the misfolded proteins are ubiquitinated and degraded by the proteasome complex). Inhibition of Hsp90 seems to promote tau clearance too. Hsp90 prevents protein degradation and thus inhibition of Hsp90 promotes tau clearance. A drug that induces macroautophagy is rapamycin but its side effect is that it is immunosuppresant. Lithium also seems to upregulate macroautophagy and increase clearance of a-synuclein that forms intracellular inclusions in the Parkinson's disease brain [294].

Tau vaccination is another approach that has the potential for success. Mice vaccinated with tau showed improved behavioral performance. Using antibodies against misfolded tau to clear the pathological tau has also been proposed[295].

It is noteworthy at this point to mention drugs that have a positive effect against AD and other tauopathies do exist but some people see the formation of tangles and aggregation from abnormal tau as neuroprotective since tangle bearing neurons survive for many years [296]. Also in human transgenic mice, while there was widespread neurodegeneration, the PHF-containing neurons appeared 'healthy' in terms of nuclear

morphology[297]. That also suggests the neuroprotection mechanism. Without being pessimistic it would be noteworthy to say that we do not know what would be the side effects on the longevity and structure of the neurons in the absence of these tangles. Elderly people develop AD and delay a process that would be fatal for their neurons. The AD (delay) proves to be fatal for them finally. An insight into the mechanism of AD and the time-long side effects that a drug that treats AD would have, would be necessary. We need to see the advantages and disadvantages of those treatments.

All those treatments have been proven very modest in humans and their results do not last over a year. Our goal is to stop the chaperone pathway with the use of various drugs on the cognate Hsp70.

IV.2. Chaperone-directed therapies

IV.2.1. General

Chemical modulators of Hsp70 might find use in a wide variety of conditions. Especially the down-regulation or selective inhibition of Hsp70 constitutes a valuable strategy for the treatment of AD. Several major medicinal chemistry groups (Peter Wipf, Jeff Brodsky, Jason Gestwicki) and a few major institutions, such as the Sloan Kettering Cancer institute, are pursuing the inhibition of Hsp70.

Arimoclomol is a drug that acts as a coinducer of the heat shock response and increases Hsp70 expression in spinal cord motor neurons. It improves the behavioral phenotype and prevents neuronal loss while extending the survival rate in transgenic mice [298]. Other drugs that are Heat shock response activators are shown in Table IV.1.1.

Compound	Effective concentration
Activators	
Protein synthesis inhibitors	
Puromycin	36μM
Azetidine	5mM
Proteasome inhibitors	
MG132	10μM
Lactacystin	10-20μM
Serine protease inhibitors	
DCIC	5μM
TPCK	50μM
TLCK	75μM
Hsp90 inhibitors	
Radicinol	1-10μM
Geldanamycin	0.1-1μM
17-AAG	0.1-1μM
Inflammatory mediators	
Cyclopentenone prostaglandins	12μM
Arachidonate	20μM
Phospholipase A2	2μM
Triterpenoids	
Celastrol	1-10μM
Co-inducers	
NSAIDS:	
Sodium salicylate	20mM
Indomethacin	1mM
Hydroxylamine derivatives:	
Bimoclomol	1-10μM
Arimoclomol	10mg/Kg
Inhibitors	
Flavonoids:	
Quercetin	100μM
Benzylidene lactam compound	
KNK437	100μM

Table IV.1.1 : Small molecules that act as heat shock response activators.[299]

It has been mentioned [300] that Hsp27 binds selectively to hyperphosphorylated tau. It facilitates the degradation of hyperphosphorylated tau without ubiquitination. The mechanism remains unknown but assumptions have been made such as the non-ubiquitin mechanism that has been already mentioned or an ubiquitin dependent pathway mediated by the carboxyl terminus of Hsc70[213]. Figure IV.1.1 represents these two tau

degradation pathways. The cognate Hsp70 and molecular chaperones in general appear to be involved in the removal of the disease associated hyperphosphorylated tau, a primary component of neurofibrillary tangles. The Hsp70 cochaperone CHIP (carboxyl terminus of the Hsc70 interacting protein) appears to be a critical ligase required for ubiquitin dependent tau degradation.

Figure IV.1.1 : Phosphorylated tau degradation mechanisms.left: a ubiquitin independent pathway that can be facilitated by Hsp27 and a ubiquitin dependent pathway mediated by the CHIP-Hsc70 complex. [301]
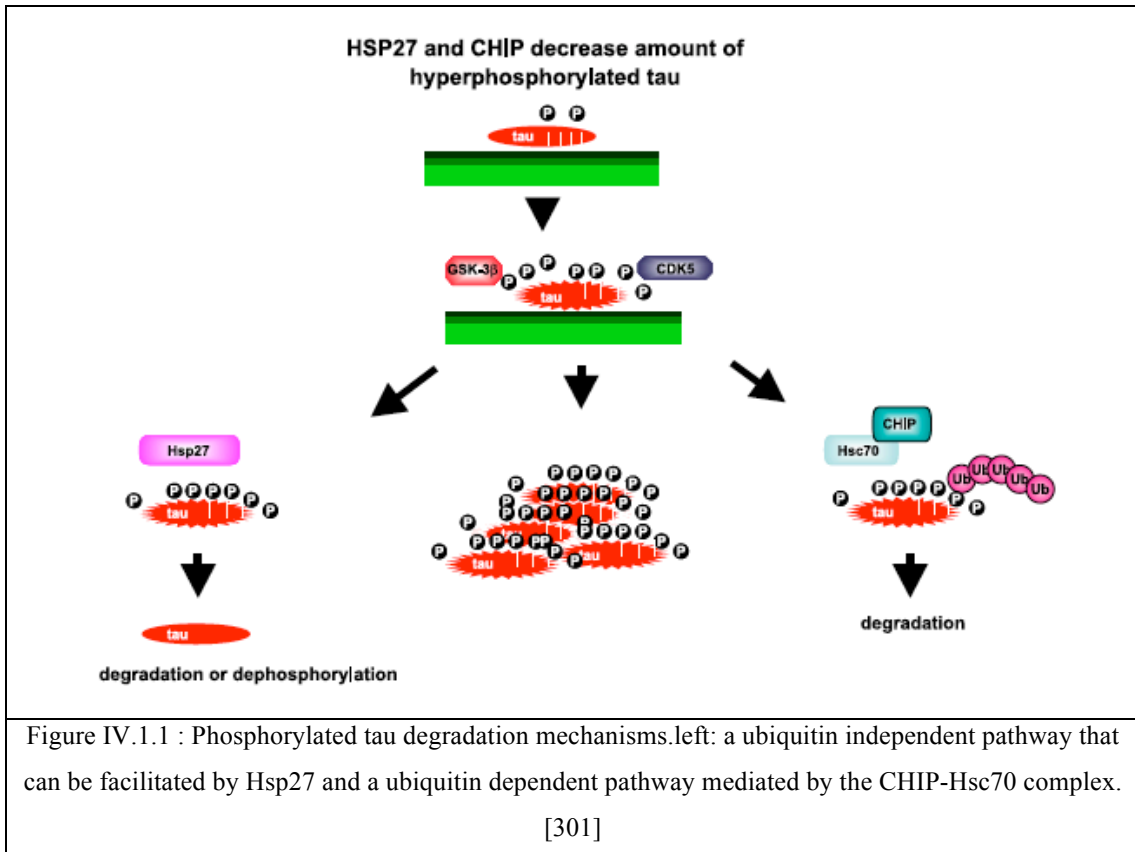
The phosphorylarion of tau may promote a conformational change that can be functionally reversed in the presence of trimethylamine N-oxide (TMAO), a natural occurring osmolyte[302]. This conformational change can also be reversed by the chaperone protein Pin-1[303] , a molecule that upon tau binding facilitates the posterior action of PP2A in dephosphorylating the protein [304]. It is presumed that tau phosphorylation occurs before its assembly [305]. Indeed, strong evidence exists that the phosphorylation of tau promotes its self-assembly [306].

IV.2.2. Methylene blue

Methylene blue is inexpensive and available in hospitals pharmacies. It was FDA approved in 2003 and it is generally used to treat emoglobinemia. It has been proposed that it destabilizes tau binding to the microtubules and the formation of a Hsc70-tau complex is favored[219].Brunden et al [307] has an interesting review on various drugs that prevent tau polymerization; methylene blue, N774, daunorubicin, phenylthiazolyl-hyrazides, N-phenylamines, rhodanines, exifore, quanoxalines and aminothienopyridazines seem to have positive impact on AD patients. Among all the previous compounds methylene blue seems the most promising one (Figure IV.2.1). It has been shown to alter the structure of existing paired helical filaments isolated from the AD brain[308].
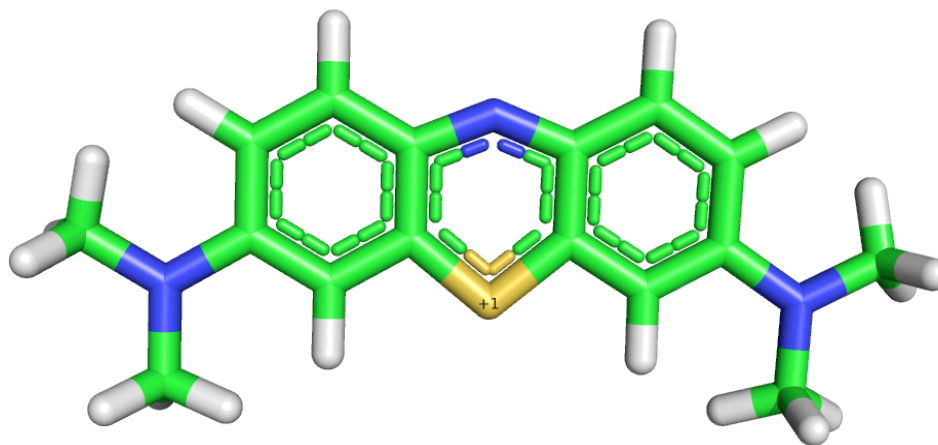
Figure IV.2.1 Structure of methylene blue (Nitrogen blue, sulfur yellow).

A recent phase II clinical trial for AD indicated a positive therapeutic effect of this compound. The rate of decline of the patient's cognitive functions is lower when the patients take methylene blue orally. A larger phase III study is necessary to prove its efficacy. Along with this success, methylene blue has also been examined as an anticancer drug. Photodynamic therapy sensitized by intratumor administration of

methylene blue was able to treat superficial tumors of the bladder [309], esophageal carcinomas [310], melanoma [311], and Kaposi's sarcoma[311] with no reported toxicities. The mechanism underlying its success against cancer is related with the compound's complex redox chemistry.

$$2MB \xleftrightarrow{K_D} (MB)_2 \xrightarrow{K_1} MB\bullet + MB\bullet^{2+}$$
$$MB\bullet + O_2 \xrightarrow{K_2} O_2^- + MB$$
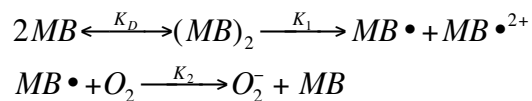
The monomers and the dimmers are in equilibrium with K_D the dissociation constant. Then MB radicals are formed which a rate constant K_1 proportional to the laser excitation with MB$\bullet$ and MB$\bullet^{2+}$ representing the semi reduced and semi oxidized radical forms. The last equation represents the formation of superoxide and ground state MB monomer with rate K_2.
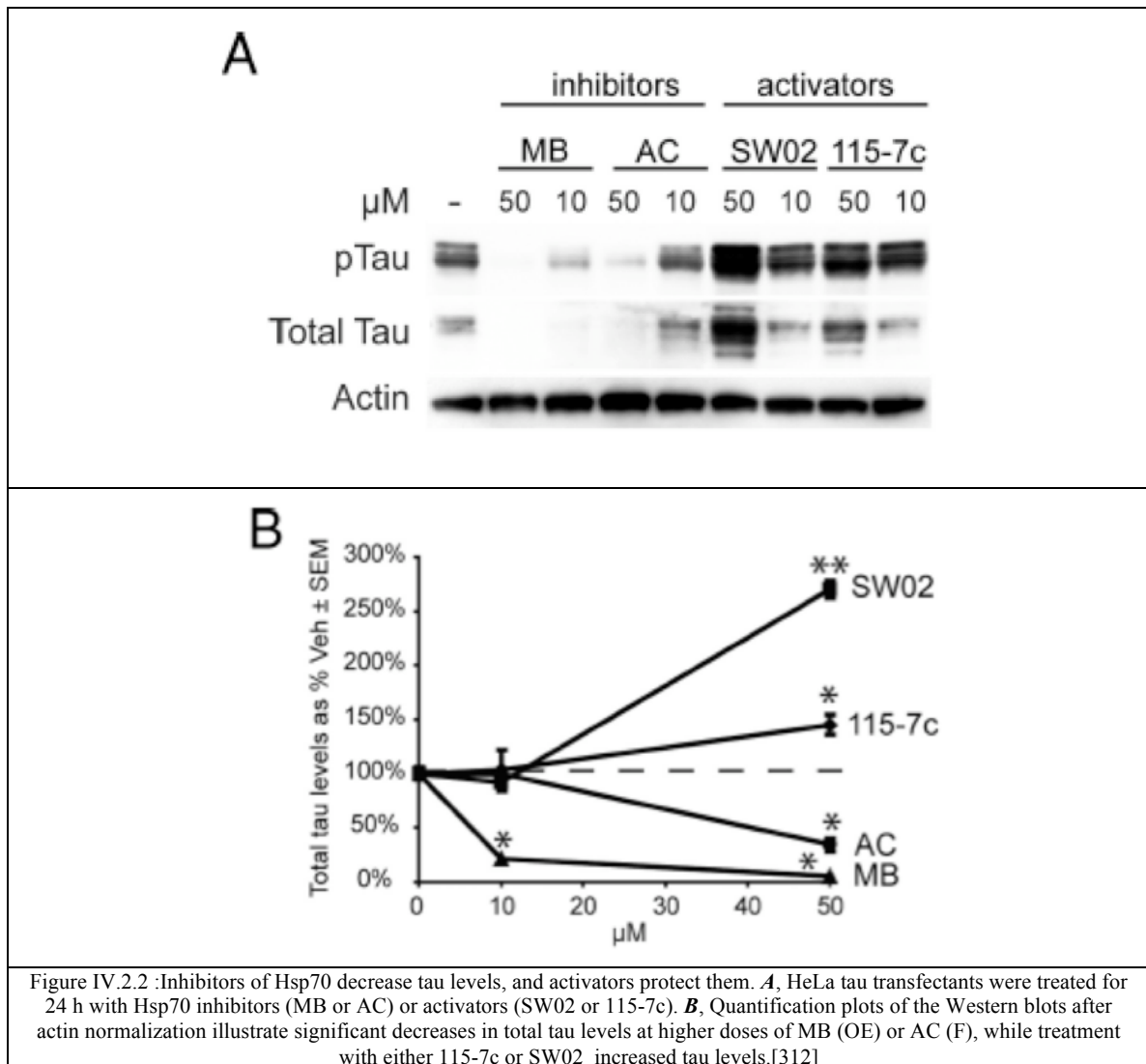
Figure IV.2.2 :Inhibitors of Hsp70 decrease tau levels, and activators protect them. *A*, HeLa tau transfectants were treated for 24 h with Hsp70 inhibitors (MB or AC) or activators (SW02 or 115-7c). *B*, Quantification plots of the Western blots after actin normalization illustrate significant decreases in total tau levels at higher doses of MB (OE) or AC (F), while treatment with either 115-7c or SW02 increased tau levels.[312]

Our collaborators Gestwicki and Dickey have established that Methylene blue is an Hsc70 inhibitor using ATP hydrolysis assays, and showed that Methylene blue causes reduction in tau levels in Hela transfectant cells (see Figure IV.2.2) . We have investigated the interaction of methylene blue and Hsc70 by NMR. We have found that MB binds to this protein, substantiating the linkage between Methylene blue – Hsc70 – tau. This study will be decribed in Chapter IX

IV.2.3. MKT-077
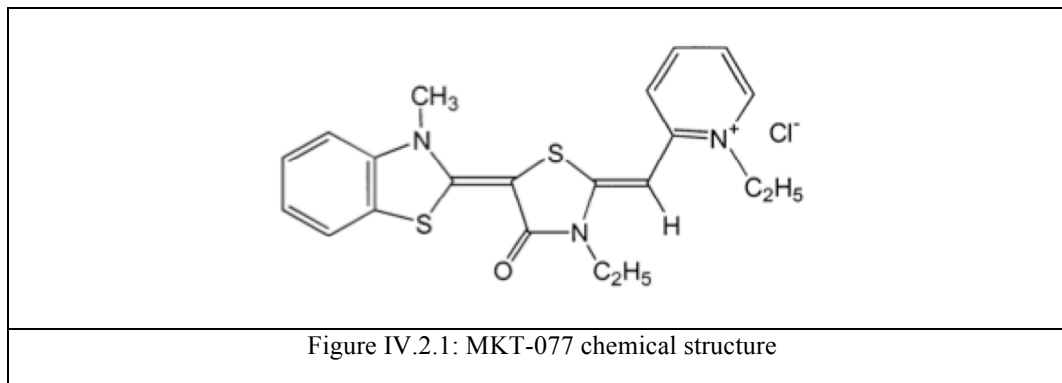
Figure IV.2.1: MKT-077 chemical structure

MKT-077 (1-ethyl-2[[3-ethyl-5-(3-methylbenzothiazolin-2-yliden)]-4-oxothiazolidin-2-ylidenemethyl]pyridium chloride) is a Fuji photo film paraproduct that was initially named as FJ-776. Its structure is shown in Figure IV.2.1. It is orange in color (maximum absorbance at 495nm) and highly soluble in water (>200mg/ml). This organic molecule has a positively charged pyridine but is also lipophilic. The compound has been investigated for cancer therapy [313, 314]. In preclinical trials using nude mice, it was found to have lower toxicity than other cytostatic agents and efficacy against a range of tumors including renal, pancreatic and prostate tumors. More specifically it inhibits the growth of the following lines: human renal carcinoma A498 and human prostate carcinoma DU145 and prolongs the survival of mice bearing human melanoma LOX. In culture it inhibits the growth of five human cancer cell lines (colon carcinoma CX-1, breast carcinoma MCF-7, pancreatic carcinoma CRL1420, bladder transitional cell carcinoma EJ and melanoma LOX) but not monkey kidney CV-1, an indicator cell line for normal epithelial cells. As shown in Figure IV.2.2 panels A,B,C,D the potency and selectivity of MKT-077 as an anticancer drug is much higher than conventional cancer treatments.
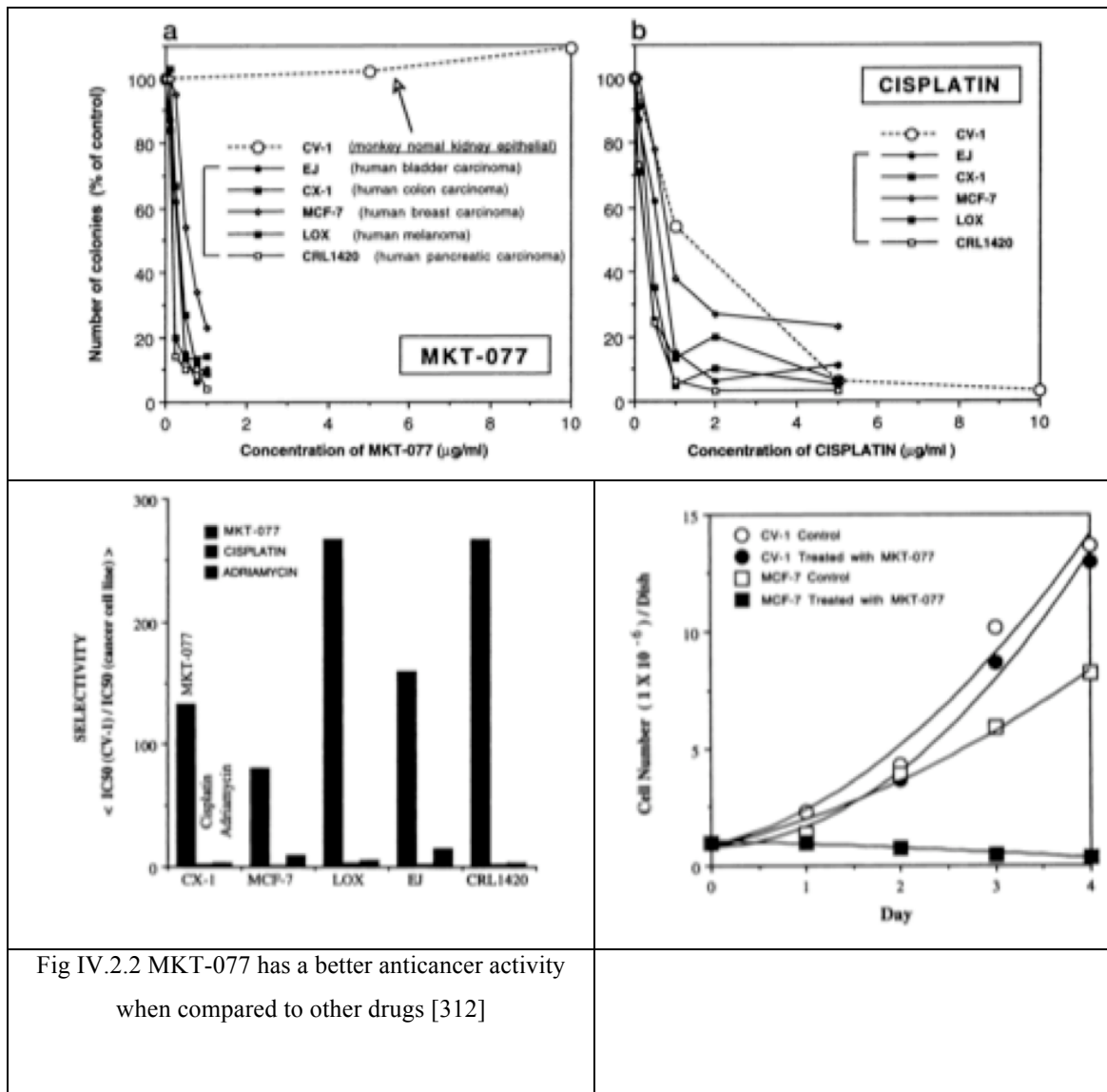
Fig IV.2.2 MKT-077 has a better anticancer activity when compared to other drugs [312]

MKT-077 shows preferential accumulation in the mitochondria of cancer cells compared to normal cells. It is one of the very few drugs that can enter the mitochondria and interact with proteins that can be found there such as mortalin. The reasoning for that is that mitochondria have high negative membrane electrical potential. [315]. A previous study has demonstrated that MKT-077 binds 250 times more effectively to cancer cells compared to normal cells[316, 317]. The reason for that is that the cancer cell mitochondrial membrane shows elevated membrane potential compared to normal

cell membrane potential and that is the reason for the cancer cell mitochondrial membrane preference of lipophillic cations such as MKT-077 [318, 319]. Such an agent is known to enter cells via by potential driven simple diffusion [315].

Further research revealed that it inhibits preferentially the growth of cancer cells in vitro. The former fact when coupled to the high aqueous stability of the drug and the lesser light sensitivity when compared to other rhodacyanite analogs makes it a potent anticancer drug.

MKT-077 has been under phase I studies but was regretfully found to be nephrotoxic in 6% of the patients involved. The trial was terminated.

Several lines of evidence show that MKT077 (also) interacts with Hsp70 proteins, and with mitochondrial-Hsp70 in particular. Hence the hypothesis that the binding [314] of MKT-077 to mt-Hsp70 in the mitochondrion is related to the annihilation of cancer. According to previous publications [313] the binding site of MKT-077 to mt-Hsp70 was deduced to be residues 252-310.

Because of the high homology between mt-Hsp70 and Hsc70, our collaborators Dickey and Gestwicki wondered whether MKT-077 would mimick methylene blue, an Hsc70 binder, in stimulating the clearance tau proteins. They showed this indeed to be the case (see Figure IV.2.3).

Figure IV.2.3 :MKT077 enhances tau clearance in transfected Hela cells.
Gestwicki and Dickey, to be published
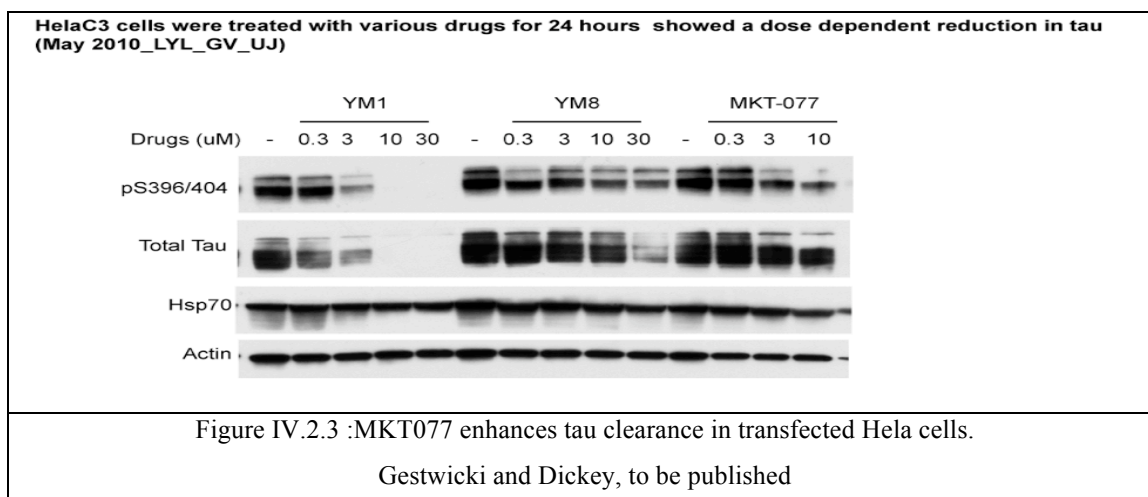
We decided to study the interaction of MKT077 with human Hsc70 in detail by NMR, in order to establish the binding site, and perhaps suggest chemical modifications

of MKT 077 that would retain binding, but would reduce the toxicity associated with the compound. This study is presented in chapter IX.

CHAPTER V. NMR methods used in this study

V.1. HSQC

There are three two-dimensional heteronuclear correlation experiments in common use: The heteronuclear multiple quantum coherence (HMQC) experiment [320] , the heteronuclear single quantum coherence (HSQC) experiment [321] , and the refocused-HSQC experiment [322]. There are advantages and disadvantages in all the above mentioned experiments. We will focus our analysis on the HSQC experiment and the refocused HSQC experiment that have the magnetization during the t1 labeling period evolve as anti-phase single quantum 2IzSy (singly excited state and thus Heteronuclear single quantum coherence-HSQC in contrast to HMQC that is represented by 2IxSx which is double quantum coherence) and pure in phase Sx magnetization respectively. Even though the HMQC experiment has the fewest number of pulses and thus is the most sensitive of all its use is not widespread because of line-broading effects in the t1 direction caused by the proton T_2 decay.

The HSQC experiment (Fig V.1) will be discussed extensively using the product operator formalism. In the following analysis the common notation of I, S spins will be used. The I spin will represent the proton and the S spin will represent the heteronucleus (nitrogen or carbon).

The HSQC pulse sequence is shown in Figure V.1
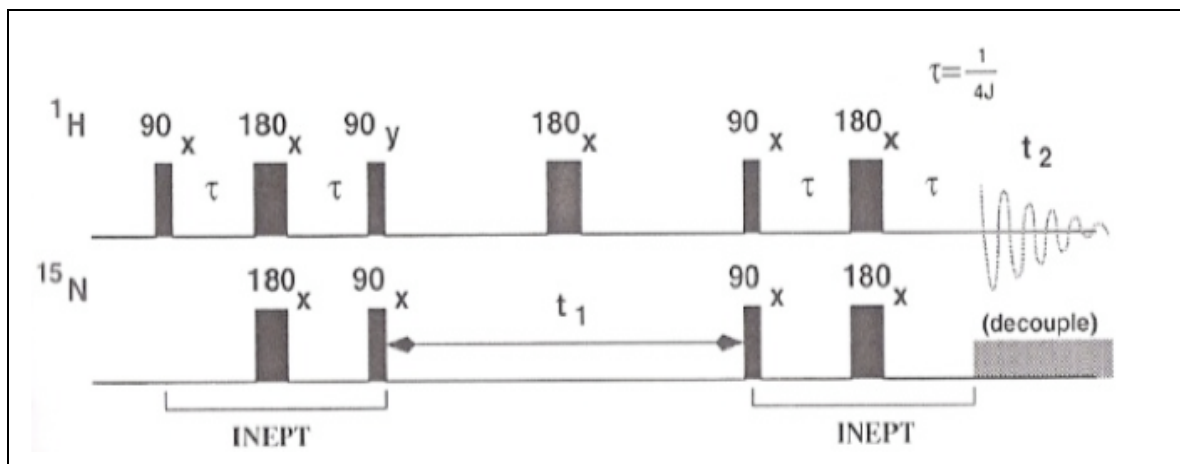
Figure V.1 The pulse sequence of HSQC without solvent suppression (from [323])

First INEPT (Insensitive Nuclei Enhanced by Polarization Transfer). The first 90 proton pulse converts Iz to –Iy. The proton chemical shift does not evolve during the INEPT time period due to the 180 chemical shift evolution refocusing pulse. So only the J-coupling evolves. The 180 pulses in the middle of the INEPT period are usually applied to both the proton and the heteronucleus simultaneously but in the following analysis they are considered to occur sequentially.

$$-Iy \xrightarrow{J} -[Iy\cos(\varphi) - 2IxSz\sin(\varphi)]$$
$$\xrightarrow{180_I^x} -[-Iy\cos(\varphi) - 2IxSz\sin(\varphi)] \xrightarrow{180_S^x} -[-Iy\cos(\varphi) + 2IxSz\sin(\varphi)]$$
$$\xrightarrow{J} \cos(\varphi)[Iy\cos(\varphi) - 2IxSz\sin(\varphi)] - \sin(\varphi)[2IxSz\cos(\varphi) + Iy\sin(\varphi)]$$
$$= Iy[\cos^2(\varphi) - \sin^2(\varphi)] - 2IxSz[2\sin(\varphi)\cos(\varphi)] = Iy\cos(2\varphi) - 2IxSz\sin(2\varphi)$$

Here, $\phi = \pi J\tau$. The delay τ is set to be equal to 1/4J giving sin(2ϕ)=sin(2πJ/4J)=sin(π/2)=1 and cos(π/2)=0 and thus the magnetization after the first INEPT is -2IxSz. The effect of the INEPT magnetization transfer is the conversion of the in phase proton magnetization –Iy to anti-phase magnetization -2IxSz. The 90 y proton pulse and x heteronuleus pulse convert this to -2IzSy.

Evolution during t1. The 180 pulse in the middle of the evolution period refocuses the J coupling, there is no chemical shift evolution for the protons since the proton state is Iz and thus we only have heteronucleus chemical shift evolution.

$$2IzSy \xrightarrow{\omega_S t_1} 2Iz[Sy\cos(\omega_S t_1) - Sx\sin(\omega_S t_1)]$$
$$= 2IzSy\cos(\omega_S t_1) - 2IzSx\sin(\omega_S t_1)$$

Polarization transfer back to protons- The Reverse INEPT . The two 90 x pulses on both the heteronucleus and the proton interchange the state of the heteronucleus and the proton spins.

$$2IzSy\cos(\omega_S t_1) \rightarrow 2IySz\cos(\omega_S t_1)$$
$$2IzSx\sin(\omega_S t_1) \rightarrow -2IySx\sin(\omega_S t_1)$$

The term $-2IySx\sin(\omega_S t_1)$ represents double quantum magnetization that cannot be detected during the t_2 period and thus will be ignored. The reverse INEPT will refocus the $2IySz\cos(\omega_S t_1)$ to Ix $\cos(\omega_S t_1)$..

The final two-dimensional time-domain signal is $\cos(\omega_S t_1)\{$ Ix $\cos(\omega_I t_2)+$ Ix $\sin(\omega_I t_2))$. A second experiment is collected in which the first hetronucleus pulse is applied with y-phase, resulting in a final signal modulated as $\sin(\omega_S t_1)\{$ Ix $\cos(\omega_I t_2)+$ Ix $\sin(\omega_I t_2))$. The two signals are interleaved to allow a two-dimensional phase-sensitive Fourier transformation.

Minimum phase cycle. x, -x on the first 1H 90 pulse, x,x,-x,-x (or y,y,-y,-y) on the first X 90 pulse, with receiver +,-,-,+. This cycle selects for protons that are coupled to X nuclei and X-nuclei that are coupled to protons.

Figure V.2 Fast HSQC optimized for solvent suppression, carbon decoupling and phasing as used in our lab. Phasecycle: x,-x (or y,-y) on the N 90 pulse prior to t1, with receiver +,-. Adapted from Ref. [324]
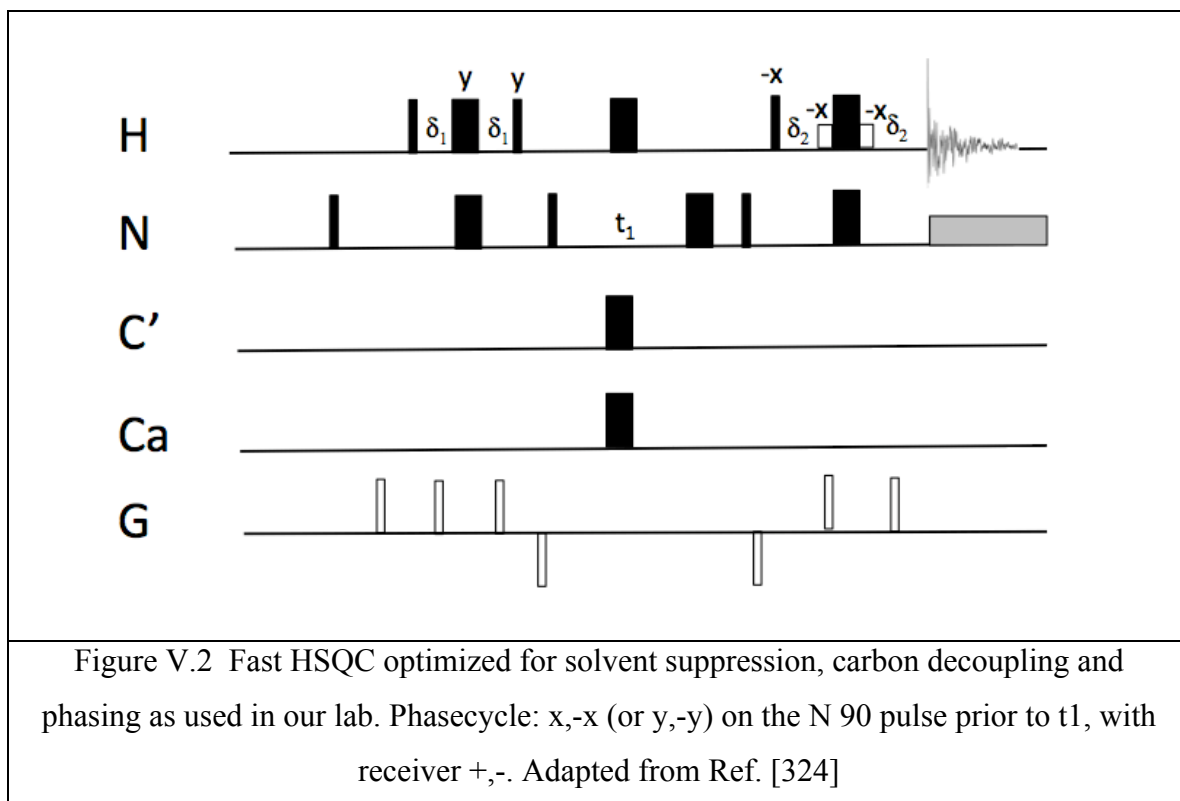
V.2. TROSY

TROSY (Transverse relaxation-optimized spectroscopy) is a technique that increases the resolution and sensitivity of heteronuclear NMR experiments on larger proteins at high magnetic field strengths. This technique has been applied to two dimensional proton nitrogen [325] (optimal at 800-900 MHz for amide protons) and proton carbon [326, 327] (optimal at 500-700 MHz for CH groups) spectroscopy as well as to a large number of triple resonance experiments, such as the HNCA experiment [327]. Several comprehensive reviews are available[328].

The TROSY technique works by taking advantage of the interference between dipolar coupling and chemical shift anisotropy in the relaxation of coupled heteronuclear spins to produce a quartet of peaks with different half height widths due to the different transverse relaxation rates for each peak. We select the narrowest of those peaks, which is considerably narrower than the corresponding decoupled peak in HSQC. Hence one gains in terms of resolution as compared to the HSQC.

The TROSY effect is also exploited to make sensitivity gains in triple resonance protein assignment experiments. These experiments have all in common that the coherence resides for a long time on the 15N transition; selecting for the narrow, and therefore long-lived TROSY component of that transition, enhances sensitivity of these experiments dramatically, even for small proteins at moderate fields. One may say that the biggest impact of TROSY was to extend the feasibility of protein triple-resonance assignment from 20 kDa to 100 kDa.

More specifically we can say that the magnetic field fluctuations that drive the relaxation of the proton or heteronuclear spin are generated by the chemical shift anisotropy of the relaxing spin and the field generated from the dipolar coupled spin.

The correlated motion of the spin and its dipolar coupled partner cause these two fields to either cancel or add depending on the spin state (α or β) of the coupled spin. When there is destructive interference between these two relaxation mechanisms the oscillating field becomes small and the relaxation rate of the spin decreases, leading to longer spin-spin relaxation times and narrower resonance lines for that component of the doublet. The exact opposite case occurs in the case of constructive interference. This will be discussed in more detail below.

Figure V.3 : Decreased linewidth in two-dimensional spectra due to the TROSY effect.
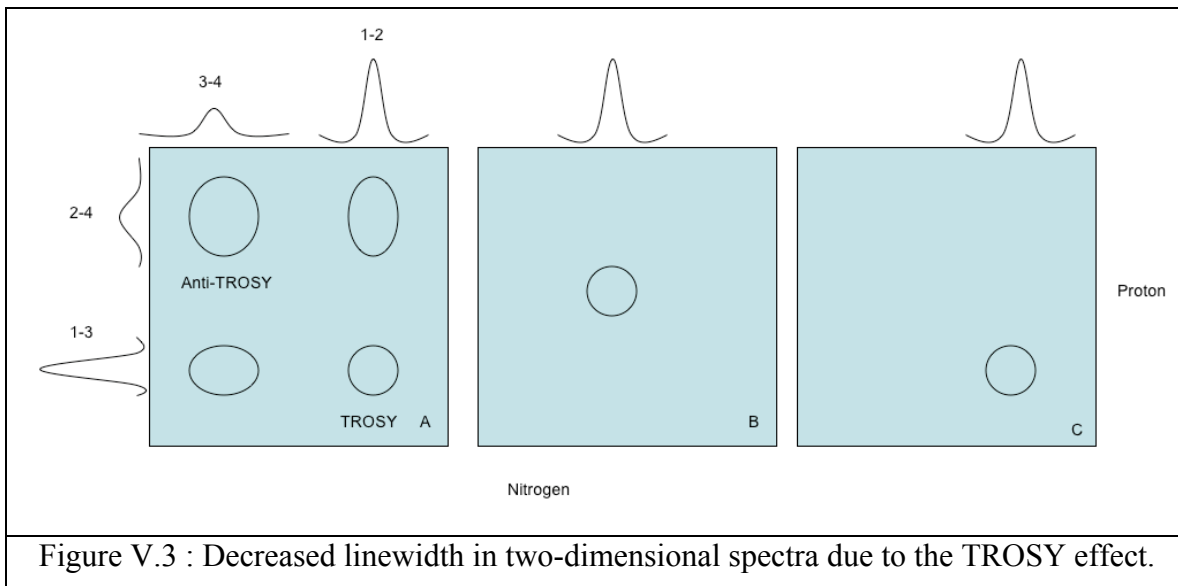
To illustrate schematically the TROSY-effect consider Figure V.3 . In a proton-nitrogen coupled two dimensional experiment shown if decoupling during t_1 and t_2 does not occur then a quartet will be found for each NH group, as illustrated in Panel A of figure x . Each peak in the quartet arises from a distinct pair of single quantum nitrogen- proton transitions as shown in Figure V.4.

Figure V.4. Transitions in the 15N-1H spin system. The red arrows represent transitions with narrower lines.
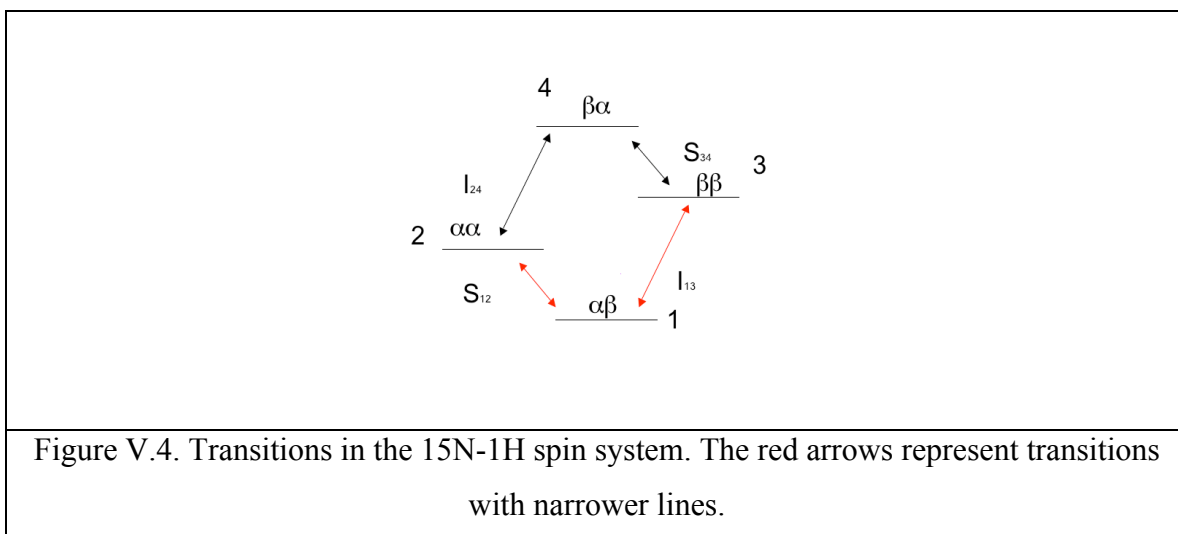
The frequency and relaxation rate of each of them is given in Table V.1.

Table V.1 : TROSY relaxation rates . From [325]		
Transition	Frequencies	Rate
1-3	$\omega_H - \pi J$	$4J(0)[(p+\delta_H)^2]$
2-4	$\omega_H + \pi J$	$4J(0)[(p-\delta_H)^2]$
1-2	$\omega_N + \pi J$	$4J(0)[(p+\delta_N)^2]$
3-4	$\omega_N - \pi J$	$4J(0)[(p-\delta_N)^2]$

The expressions for the relaxation rates were obtained from [325] and assume that the protein is large such that $J(0) >> J(\omega)$, and that the chemical shift tensor is aligned along the NH bond vector.

$J(0)$ is the spectral density at $\omega=0$ and is defined here as:

$$J(\omega)=(2/5)[\tau_c/(1+\omega^2\tau_c^2)] \sim (2/5)\tau_c.$$

p and $\delta_{H,N}$ represent the contribution to dipolar coupling and chemical shift anisotropy to relaxation respectively:

$$p = \frac{1}{2\sqrt{2}} \frac{\gamma_H \gamma_N \hbar}{r^3}$$

$$\delta_{H,N} = \frac{1}{3\sqrt{2}} \gamma_{H,N} B_o \Delta\sigma_{H,N}$$

where B_o is the static magnetic field, and $\Delta\sigma_{H,N}$ is the chemical shift anisotropy for either the proton or the nitrogen.

The four components of the quartet have different linewidths due to different relaxation rates that occur due to the cross relaxation among the different states of the spins that are shown in table V.1. Theoretically since the CSA for the amide proton is negative, the 2 to 4 transition have the smallest relaxation rate for the two proton transitions. Also the nitrogen CSA is negative and thus the 3 to 4 transition would have in theory the narrowest line. That is not the case though because we didn't take into consideration the negative gyromagnetic ratio of the nitrogen which reverses the α and β spins. The peak down and right in Figure V.3 measures the nitrogen 1-2 transition during t_1 and the proton 1-3 transition during t_2. Since both of these transitions have slow relaxation rates, the component of the multiplet is narrow in both dimensions.

If proton decoupling during t_1 and nitrogen decoupling during t_2 is applied, then the spin states are exchanged and we do not observe a quartet any more but a singlet in the center of the quartet that represents the average of the relaxation rates (Panel B Figure V.3). For example the proton relaxation rate during t_2 would be the average for the 1-3 and 2-4 transition, or $p^2+\delta^2_H$. The peak obtained from the TROSY experiment is shown in Figure V.3 Panel C. That is the narrowest peak in both dimensions and represents the 1-3, 1-2 transitions during proton and nitrogen evolution respectively. The remaining 3 components of the quartet have been removed by phase cycling.

Since we only get one out of four peaks that should have been obtained, one expects that the sensitivity of the experiment would be decreased by a factor of four. However, more detailed analysis shows it to be just a factor of two. Nevertheless, for larger proteins one gains though in signal to noise level since we obtain narrower peaks in our spectrum.

A basic pulse sequence of a TROSY experiment is shown in Figure V.5.

Fig V.5. The basic pulse sequence of sensitivity-enhanced [329] TROSY
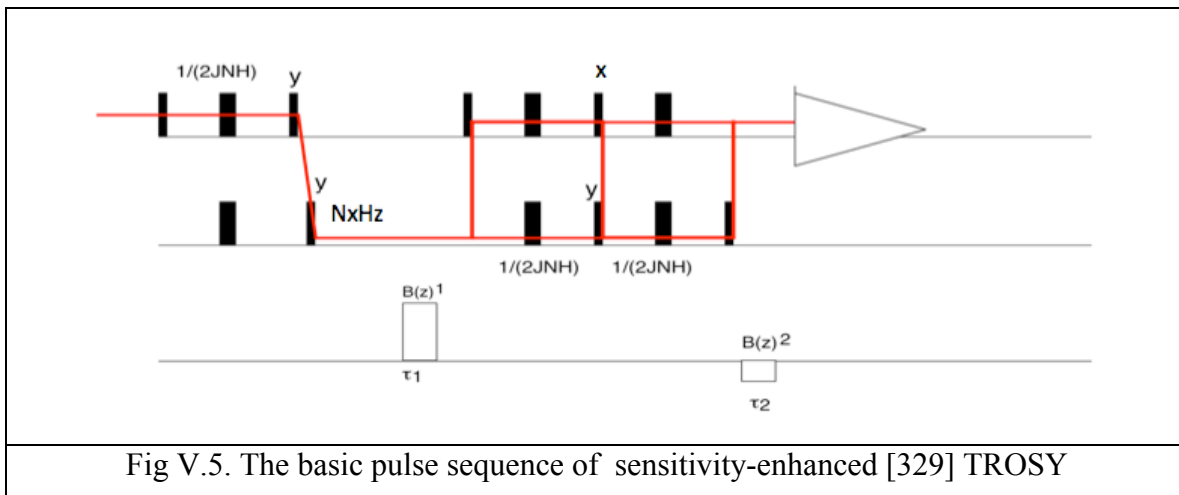
We will describe the physics of the TROSY selection using Cartesian product operators [330] [331] (the literature uses either cartesian single transitions or shift single transition operators).

Fig V.6. Decomposition of 15N coherence in TROSY and anti-TROSY components
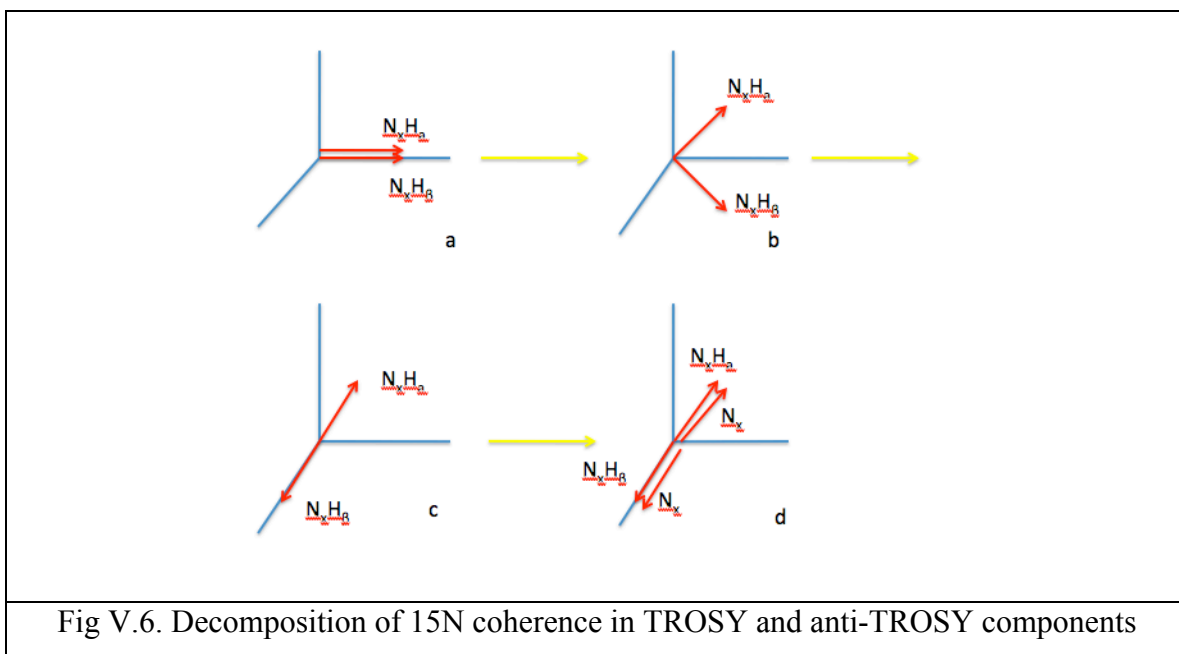
We consider the $2N_xH_z$ magnetization after the first INEPT transfer as follows:

In Figure V.6. Panel a, the magnetization $2N_xH_z$ is decomposed into its two components $N_xH_z{}^\alpha$ and $N_xH_z{}^\beta$ that evolve in the first evolution period as seen in Figure V.6 panel b. The magnetization becomes antiphase as seen in Figure V.6 Panel c. At this point in order to understand the trosy and the antitrosy components we add and substract N_x. So we have:

$$2N_xH_z = \left(2N_xH_z + N_x \quad + \quad 2N_xH_z - N_x\right)/2$$

i.e. the sum of a ^{15}N TROSY and anti-TROSY term

Developing the ^{15}N TROSY term: $2N_xH_z + N_x$: (without chemical shift)

$$2N_xH_z + N_x \xrightarrow{\text{Gradient @ location } z} \left(2N_xH_z + N_x\right)\cos\gamma_N B_{z,1}\tau_1 - \left(2N_yH_z + N_y\right)\sin\gamma_N B_{z,1}\tau_1$$

$$\xrightarrow{90_y^H} \left(2N_xH_x + N_x\right)\cos\gamma_N B_{z,1}\tau_1 - \left(2N_yH_x + N_y\right)\sin\gamma_N B_{z,1}\tau_1$$

$$\xrightarrow{JNH} \left(2N_xH_x + 2N_yH_z\right)\cos\gamma_N B_{z,1}\tau_1 - \left(2N_yH_x - 2N_xH_z\right)\sin\gamma_N B_{z,1}\tau_1$$

$$\xrightarrow{90_x^H} \left(2N_xH_x - 2N_yH_y\right)\cos\gamma_N B_{z,1}\tau_1 - \left(2N_yH_x + 2N_xH_y\right)\sin\gamma_N B_{z,1}\tau_1$$

$$\xrightarrow{90_y^N} \left(-2N_zH_x - 2N_yH_y\right)\cos\gamma_N B_{z,1}\tau_1 - \left(2N_yH_x - 2N_zH_y\right)\sin\gamma_N B_{z,1}\tau_1$$

$$\xrightarrow{JNH} \left(-H_y - 2N_yH_y\right)\cos\gamma_N B_{z,1}\tau_1 - \left(2N_yH_x + H_x\right)\sin\gamma_N B_{z,1}\tau_1$$

$$\xrightarrow{90_x^N} \left(-H_y - 2N_yH_z\right)\cos\gamma_N B_{z,1}\tau_1 - \left(2N_zH_x + H_x\right)\sin\gamma_N B_{z,1}\tau_1$$

$$\xrightarrow{\text{Gradient @ location } z}$$

$$\left(-H_y - 2N_yH_z\right)\cos\gamma_N B_{z,1}\tau_1 \cos\gamma_H B_{z,2}\tau_2 + \left(H_x + 2N_xH_z\right)\cos\gamma_N B_{z,1}\tau_1 \sin\gamma_H B_{z,2}\tau_2$$
$$-\left(2N_zH_x + H_x\right)\sin\gamma_N B_{z,1}\tau_1 \cos\gamma_H B_{z,2}\tau_2 - \left(2N_zH_y + H_y\right)\sin\gamma_N B_{z,1}\tau_1 \sin\gamma_H B_{z,2}\tau_2$$

if $\quad \gamma_N B_{z,1}\tau_1 = \gamma_H B_{z,2}\tau_2 = \varphi$

$$\longrightarrow$$

$$\left(-H_y - 2N_yH_z\right)\left(\cos\varphi\cos\varphi + \sin\varphi\sin\varphi\right) = -\left(H_y + 2N_yH_z\right)$$

i.e. the ^{15}N TROSY term refocuses into the ^{1}H TROSY term Developing the ^{15}N Anti-TROSY term $2N_xH_z - N_x$: (without chemical shift)

$$2N_xH_z - N_x \xrightarrow{\text{Gradient @location z}} \left(2N_xH_z - N_x\right)\cos\gamma_N B_{z,1}\tau_1 - \left(2N_yH_z - N_y\right)\sin\gamma_N B_{z,1}\tau_1$$

$$\xrightarrow{90^H_y} \left(2N_xH_x - N_x\right)\cos\gamma_N B_{z,1}\tau_1 - \left(2N_yH_x - N_y\right)\sin\gamma_N B_{z,1}\tau_1$$

$$\xrightarrow{JNH} \left(2N_xH_x - 2N_yH_z\right)\cos\gamma_N B_{z,1}\tau_1 - \left(2N_yH_x + 2N_xH_z\right)\sin\gamma_N B_{z,1}\tau_1$$

$$\xrightarrow{90^H_x} \left(2N_xH_x + 2N_yH_y\right)\cos\gamma_N B_{z,1}\tau_1 - \left(2N_yH_x - 2N_xH_y\right)\sin\gamma_N B_{z,1}\tau_1$$

$$\xrightarrow{90^N_y} \left(-2N_zH_x + 2N_yH_y\right)\cos\gamma_N B_{z,1}\tau_1 - \left(2N_yH_x + 2N_zH_y\right)\sin\gamma_N B_{z,1}\tau_1$$

$$\xrightarrow{JNH} \left(-H_y + 2N_yH_y\right)\cos\gamma_N B_{z,1}\tau_1 - \left(2N_yH_x - H_x\right)\sin\gamma_N B_{z,1}\tau_1$$

$$\xrightarrow{90^N_x} \left(-H_y + 2N_yH_z\right)\cos\gamma_N B_{z,1}\tau_1 - \left(2N_zH_x - H_x\right)\sin\gamma_N B_{z,1}\tau_1$$

$$\xrightarrow{\text{Gradient @location z}}$$

$$\left(-H_y + 2N_yH_z\right)\cos\gamma_N B_{z,1}\tau_1 \cos\gamma_H B_{z,2}\tau_2 + \left(H_x - 2N_xH_z\right)\sin\gamma_N B_{z,1}\tau_1 \sin\gamma_H B_{z,2}\tau_2$$

$$-\left(2N_zH_x - H_x\right)\sin\gamma_N B_{z,1}\tau_1 \cos\gamma_H B_{z,2}\tau_2 - \left(2N_zH_y - H_y\right)\sin\gamma_N B_{z,1}\tau_1 \sin\gamma_H B_{z,2}\tau_2$$

if $\gamma_N B_{z,1}\tau_1 = \gamma_H B_{z,2}\tau_2 = \varphi$

$$\left(-H_y + 2N_yH_z\right)\left(\cos\varphi\cos\varphi - \sin\varphi\sin\varphi\right) + \left(H_x - 2N_xH_z\right)\left(\cos\varphi\sin\varphi + \sin\varphi\cos\varphi\right)$$

$$= \left(-H_y + 2N_yH_z\right)\cos 2\varphi + \left(H_x - 2N_xH_z\right)\sin 2\varphi$$

i.e. the ^{15}N anti-TROSY term and all that develops from it, is suppressed

(Note, though, if $\gamma_N B_{z,1}\tau_1 = -\gamma_H B_{z,2}\tau_2$, that the anti-TROSY term does comes through as the ^{1}H anti-TROSY term.)

While retaining the basic set-up, the pulse sequence actually used in this work has been optimized for solvent suppression, 13C decoupling and phasing behavior. The sequence is shown in Figure V.7.
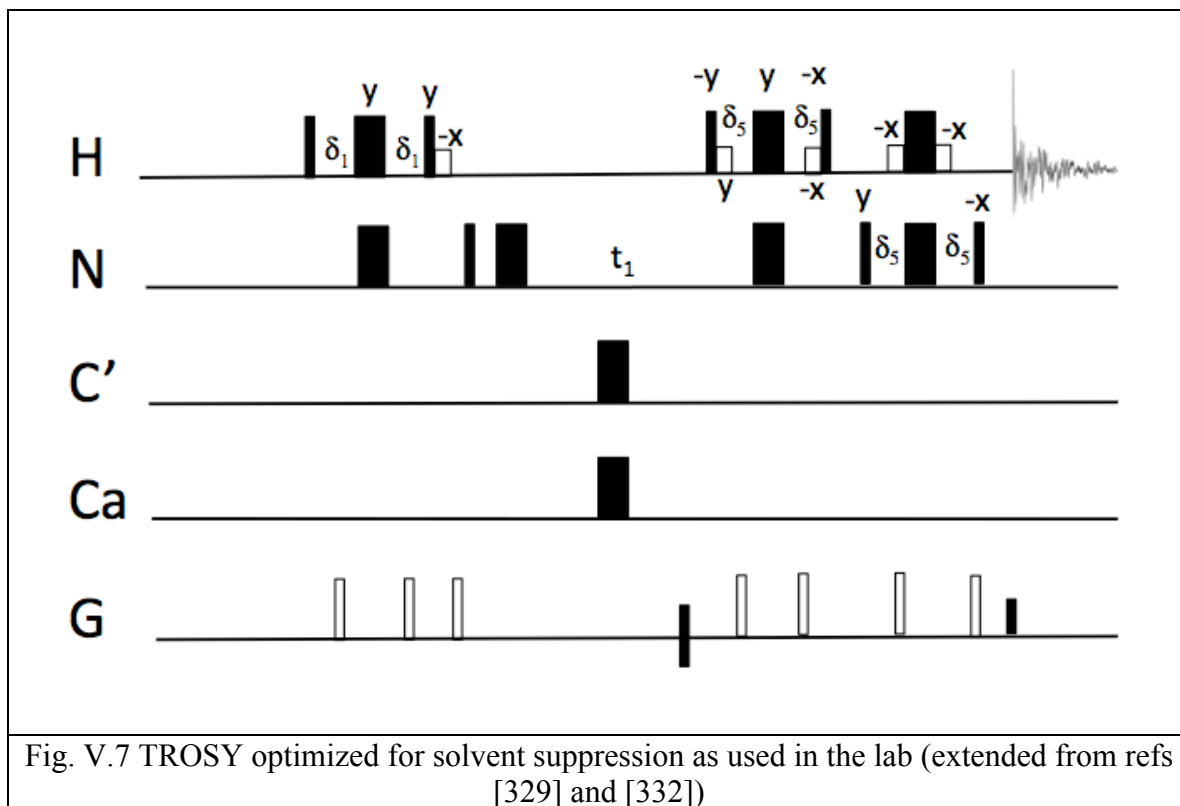
Fig. V.7 TROSY optimized for solvent suppression as used in the lab (extended from refs [329] and [332])

Now that we have explained the experiment in terms of Cartesian product operators we will try to give an overview of the parameters that cause the difference in the relaxation rates of the quartet and these are as already mentioned the dipole-dipole/CSA cross correlation and the dipole-dipole/dipole-dipole cross correlation.

As seen TROSY gives us a quartet with various linewidths of which the narrowest linewidth peak in both dimensions is selected. This is the effect of dipole-dipole/CSA cross correlation and dipole-dipole/dipole-dipole cross correlation. The question that arises now is how the different linewidths of the peaks were created? We will give an insight in the CSA and dipole-dipole relaxation mechanisms and try to understand the phenomenon.

Let's consider the N-H bond in an ^{15}N labeled protein. If the N-H bond is parallel to the external magnetic field B_o, the induced currents in the electron cloud set up a local magnetic field at the N nucleus parallel to the external field as seen in Figure V.8. If the

N-H bond is perpendicular to the external field the induced currents in the electron cloud set up a local magnetic field at the N nucleus antiparallel to the external field as seen in Figure V.9. As the molecule freely rotates in solution, the induced field at the N nucleus is modulated in accordance to the position of the N-H bond to the B_o field and thus the CSA induced field is modulated too which leads to relaxation.

Figure: V.8.Induced field around the N site when the NH bond is parallel and perpendicular to the external field.
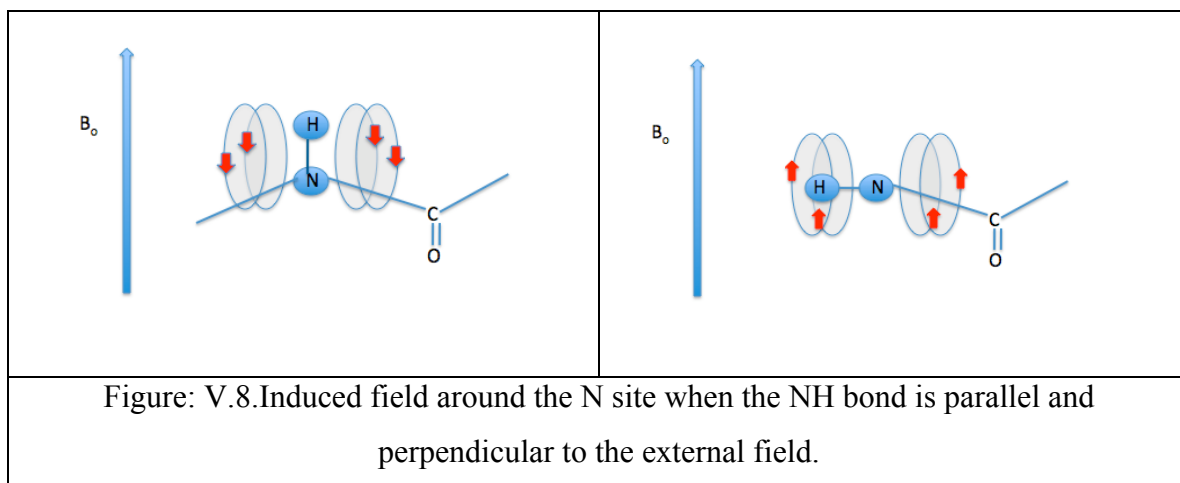
Let's see now the CSA relaxation mechanism from the H_β point of view.

Figure V.9: Local field generated when H_β-N is parallel and perpendicular to the external magnetic field.
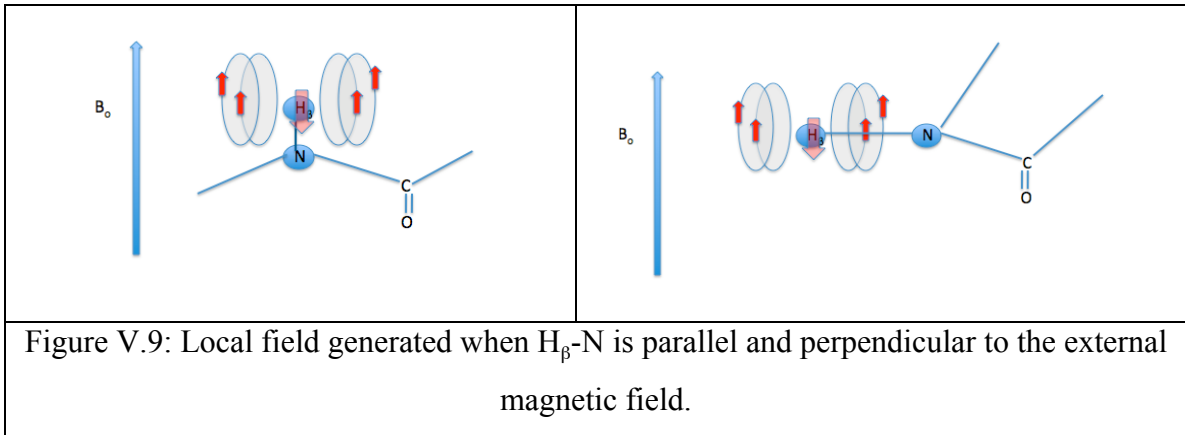
If we consider H_β the NH vector is parallel to the external field and the local field is antiparallel to the external field. The same holds for the case that the NH vector is perpendicular to the external field as seen in Figure V.9. We can say that the N local field is reduced by the CSA and dipolar interactions in the case of the H_β state. When we have the H_α state the opposite holds. So the peaks narrow due to the CSA/dipole-dipole cross correlation when we have the H_β state and they broaden when we have the H_α state. The CSA interaction is proportional to the external field and thus at a specific external field magnitude the CSA and dipole-dipole interactions tend to cancel each other.

The extent of cancellation is dependent on the magnitude and orientation of the CSA tensor, the relevant resonance frequency, and the magnitude of the dipolar relaxation.

For the amide 1H – 15N system in proteins a particulary fortunate coincidence occurs. The 15N TROSY line is narrowest around 21 Tesla (corresponding to 900 MHz 15N, see Figure V.10), while the 1H TROSY line is also narrowest around the same magnetic field strength (900 MHz 1H, see Fig V.10).

These optimal effects can be achieved only in isolated 1H-15N spinsystems. Presence of other protons in the protein almost completely spoils the 1H- TROSY effect, while it also broadens the 15N TROSY lines. For best results, therefore, the protein is best perdeuterated, with amide protons back-exchanged in.
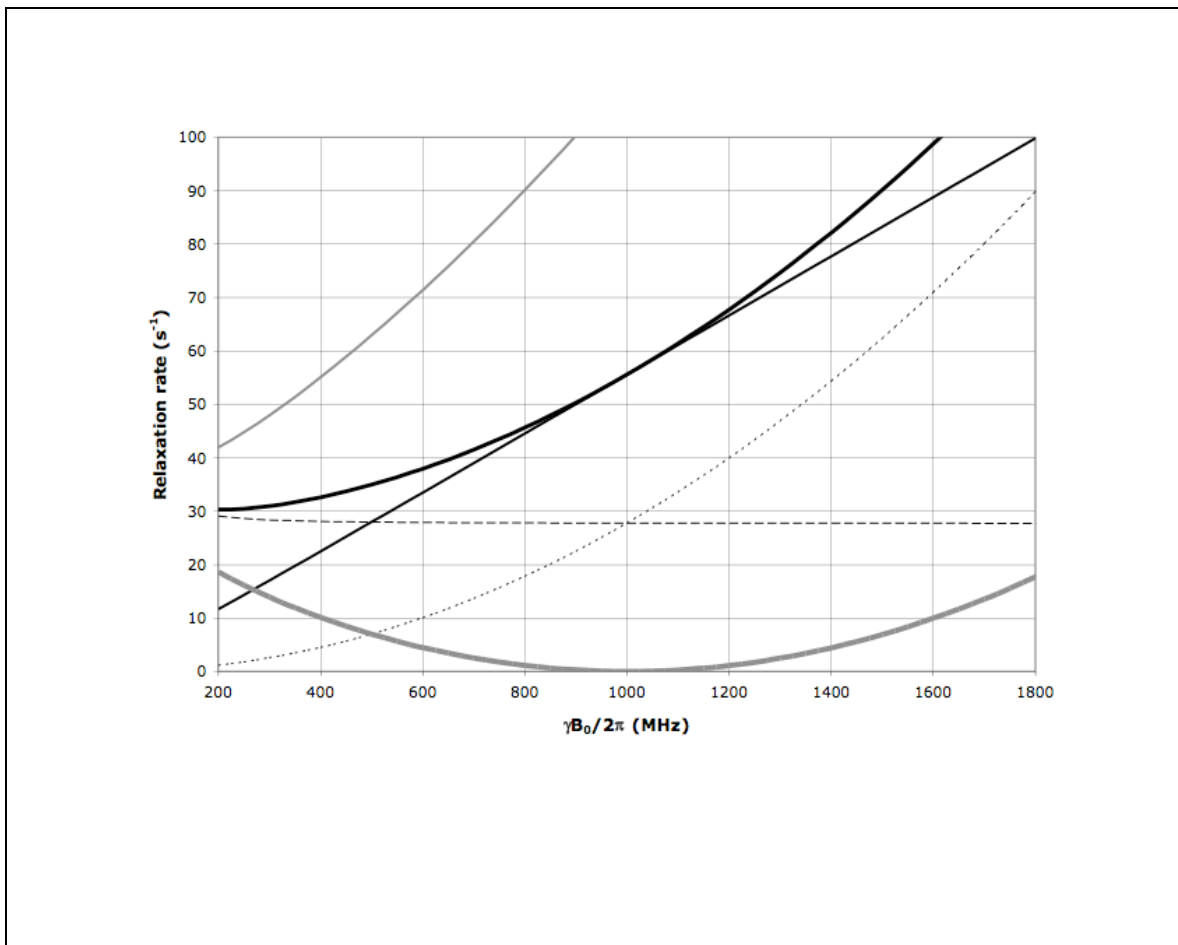
Fig V.10. The "classical" field dependence of the protein ^{15}N TROSY effect calculated using an axial CSA tensor of 160 ppm alligned with the NH-bond of 1.04 Å. Thick solid line: total ^{15}N R_2 as encountered in a HSQC or HMQC; Thick dashed line: ^{15}N R_2 due to ^{15}N-^{1}H dipolar relaxation; Thin dashed line: ^{15}N R_2 due to ^{15}N CSA relaxation; Thin grey line: the ^{15}N R_2 ^{15}N-^{1}H dipolar / ^{15}N CSA cross correlated relaxation rate; Thick grey

line: ^{15}N R_2 as encountered in a TROSY (i.e. total ^{15}N R_2 minus ^{15}N R_2 ^{15}N-^{1}H dipolar / ^{15}N CSA cross correlation). Thin grey line: ^{15}N R_2 of the anti-TROSY line (i.e. total ^{15}N R_2 plus ^{15}N R_2 ^{15}N-^{1}H dipolar / ^{15}N CSA cross correlated relaxation rate).

From Zuiderweg and Case, NMR in Biophysical Chemistry, in preparation.
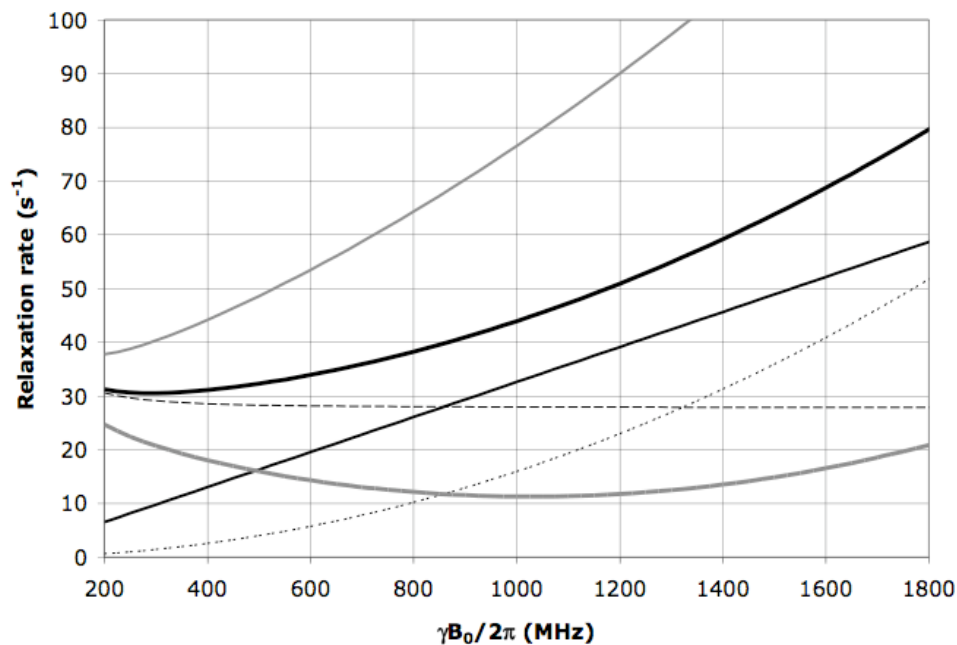
Fig V.11. The field dependence of the peptide ^{1}H TROSY effect for t_c=30 ns calculated using a rhombic ^{1}H CSA tensor with s_{11}=3, s_{22}=8 and s_{33}=17 ppm, with s_{11} alligned with the NH-bond of 1.04 Å.

Thick solid line: total ^{1}H R_2 as encountered in a HSQC or HMQC; Thick dashed line: ^{1}H R_2 due to ^{15}N-^{1}H dipolar relaxation; Thin dashed line: ^{1}H R_2 due to ^{1}H CSA relaxation; Thin grey line: the ^{1}H R_2 ^{15}N-^{1}H dipolar / ^{1}H CSA cross correlated relaxation rate; Thick grey line: ^{1}H R_2 as encountered in a TROSY (i.e. total ^{1}H R_2 minus ^{1}H R_2 ^{15}N-^{1}H dipolar / ^{1}H CSA cross correlation). Thin grey line: ^{1}H R_2 of the anti-TROSY line (i.e. total ^{1}H R_2 plus ^{1}H R_2 ^{15}N-^{1}H dipolar / ^{1}H CSA cross correlation).

From Zuiderweg and Case, NMR in Biophysical Chemistry, in preparation.

V.3. COSY

The idea of two dimensional NMR was introduced by Jeener and Ernst [333] . The pulse sequence is simple and can be described as: 90x-t_1-90x-t_2. The first pulse brings the magnetization to the transverse plane, then during the evolution period t_1 the magnetization is labeled by the chemical shift and the J coupling. Then during the second 90° pulse, coherence transfer takes place and at last the FID acquisition takes place and the magnetization is labeled by t_2. When we vary the values of t_1 the signal oscillates sinusoidally during t_1 in similar to its oscillation during t_2. Fourier transformation on both dimensions t_1 and t_2 gives us cross and diagonal peaks in f_1 and f_2 (at the corresponding frequencies for t_1 and t_2).

Using the product operator formalism we can describe the system as follows:

$$I_z \text{ and } S_z \xrightarrow{(\frac{\pi}{2})_x} -I_y \text{ and } -S_y \xrightarrow{\omega_I t_1 \text{ and } \omega_S t_1} -I_y \cos(\omega_I t_1) + I_x \sin(\omega_I t_1) - S_y \cos(\omega_S t_1) + S_x \sin(\omega_S t_1)$$

$$\xrightarrow{J_{IS}\pi t_1} -I_y \cos(\omega_I t_1)\cos(\pi J_{IS}t_1) + 2I_x S_z \cos(\omega_I t_1)\sin(\pi J_{IS}t_1) + I_x \sin(\omega_I t_1)\cos(\pi J_{IS}t_1) + 2I_y S_z \sin(\omega_I t_1)\sin(\pi J_{IS}t_1)$$

$$-S_y \cos(\omega_S t_1)\cos(\pi J_{IS}t_1) + 2S_x I_z \cos(\omega_I t_1)\sin(\pi J_{IS}t_1) + S_x \sin(\omega_S t_1)\cos(\pi J_{IS}t_1) + 2S_y I_z \sin(\omega_I t_1)\sin(\pi J_{IS}t_1)$$

$$\xrightarrow{(\frac{\pi}{2})_x} -I_z \cos(\omega_I t_1)\cos(\pi J_{IS}t_1) - 2I_x S_y \cos(\omega_I t_1)\sin(\pi J_{IS}t_1) + I_x \sin(\omega_I t_1)\cos(\pi J_{IS}t_1) - 2I_z S_y \sin(\omega_I t_1)\sin(\pi J_{IS}t_1)$$

$$-S_y \cos(\omega_S t_1)\cos(\pi J_{IS}t_1) - 2S_x I_y \cos(\omega_I t_1)\sin(\pi J_{IS}t_1) + S_x \sin(\omega_S t_1)\cos(\pi J_{IS}t_1) - 2S_z I_y \sin(\omega_I t_1)\sin(\pi J_{IS}t_1)$$

At this point we will consider only the observable magnetization terms I_x, S_x, $2I_yS_z$, $2I_zS_y$. Thus the observable magnetization labeled by t_2 is :

$$I_x \sin(\omega_I t_1)\cos(\pi J_{IS}t_1) - 2I_z S_y \sin(\omega_I t_1)\sin(\pi J_{IS}t_1) + S_x \sin(\omega_S t_1)\cos(\pi J_{IS}t_1) - 2S_z I_y \sin(\omega_I t_1)\sin(\pi J_{IS}t_1)$$

$$\xrightarrow{\pi J t_2}$$

$$I_x \sin(\omega_I t_1)\cos(\pi J_{IS}t_1)\cos(\pi J_{IS}t_2) + I_y S_z \sin(\omega_I t_1)\cos(\pi J_{IS}t_1)\sin(\pi J_{IS}t_2)$$

$$-2I_z S_y \sin(\omega_I t_1)\sin(\pi J_{IS}t_1)\cos(\pi J_{IS}t_2) + S_x \sin(\omega_I t_1)\sin(\pi J_{IS}t_1)\sin(\pi J_{IS}t_2)$$

$$+S_x \sin(\omega_S t_1)\cos(\pi J_{IS}t_1)\cos(\pi J_{IS}t_2) + S_y I_z \sin(\omega_S t_1)\cos(\pi J_{IS}t_1)\sin(\pi J_{IS}t_2)$$

$$-S_z I_y \sin(\omega_I t_1)\sin(\pi J_{IS}t_1)\cos(\pi J_{IS}t_2) + I_x \sin(\omega_I t_1)\sin(\pi J_{IS}t_1)\sin(\pi J_{IS}t_2)$$

The cross peaks will be detectable as a result of the I_x and S_x product operators of the second and forth term of the above equation. The diagonal peaks will be detectable due to the I_x and S_x product operators of the first and third term of the above equation. Thus we will consider only these terms when we consider the chemical shift evolution during the FID acquisition period t_2.

$$I_x \sin(\omega_I t_1)\cos(\pi J_{IS} t_1) - 2I_z S_y \sin(\omega_I t_1)\sin(\pi J_{IS} t_1) + S_x \sin(\omega_S t_1)\cos(\pi J_{IS} t_1) - 2S_z I_y \sin(\omega_I t_1)\sin(\pi J_{IS} t_1)$$

$$\xrightarrow{\pi J t_2}$$

$$I_x \sin(\omega_I t_1)\cos(\pi J_{IS} t_1)\cos(\pi J_{IS} t_2) + I_y S_z \sin(\omega_I t_1)\cos(\pi J_{IS} t_1)\sin(\pi J_{IS} t_2)$$

$$-2I_z S_y \sin(\omega_I t_1)\sin(\pi J_{IS} t_1)\cos(\pi J_{IS} t_2) + S_x \sin(\omega_I t_1)\sin(\pi J_{IS} t_1)\sin(\pi J_{IS} t_2)$$

$$+S_x \sin(\omega_S t_1)\cos(\pi J_{IS} t_1)\cos(\pi J_{IS} t_2) + S_y I_z \sin(\omega_S t_1)\cos(\pi J_{IS} t_1)\sin(\pi J_{IS} t_2)$$

$$-S_z I_y \sin(\omega_I t_1)\sin(\pi J_{IS} t_1)\cos(\pi J_{IS} t_2) + I_x \sin(\omega_I t_1)\sin(\pi J_{IS} t_1)\sin(\pi J_{IS} t_2)$$

$$\xrightarrow{\omega_S t_2}$$

$$I_x \sin(\omega_I t_1)\cos(\pi J_{IS} t_1)\cos(\pi J_{IS} t_2)\cos(\omega_I t_2) + I_y \sin(\omega_I t_1)\cos(\pi J_{IS} t_1)\cos(\pi J_{IS} t_2)\sin(\omega_I t_2)\,diagonal$$

$$+S_x \sin(\omega_I t_1)\sin(\pi J_{IS} t_1)\sin(\pi J_{IS} t_2)\cos(\omega_S t_2) + S_y \sin(\omega_I t_1)\sin(\pi J_{IS} t_1)\sin(\pi J_{IS} t_2)\sin(\omega_S t_2)\,cross$$

$$+S_x \sin(\omega_S t_1)\cos(\pi J_{IS} t_1)\cos(\pi J_{IS} t_2)\cos(\omega_S t_2) + S_y \sin(\omega_S t_1)\cos(\pi J_{IS} t_1)\cos(\pi J_{IS} t_2)\cos(\omega_S t_2)\sin(\omega_S t_2)\,diagonal$$

$$+I_x \sin(\omega_I t_1)\sin(\pi J_{IS} t_1)\sin(\pi J_{IS} t_2)\cos(\omega_S t_2) + I_y \sin(\omega_I t_1)\sin(\pi J_{IS} t_1)\sin(\pi J_{IS} t_2)\sin(\omega_S t_2)\,cross$$

Now we assume that we detect only the y-magnetization, and obtain, finally,

$$+I_y \sin(\omega_I t_1)\cos(\pi J_{IS} t_1)\cos(\pi J_{IS} t_2)\sin(\omega_I t_2)\,diagonal$$

$$+S_y \sin(\omega_I t_1)\sin(\pi J_{IS} t_1)\sin(\pi J_{IS} t_2)\sin(\omega_S t_2)\,cross$$

$$S_y \sin(\omega_S t_1)\cos(\pi J_{IS} t_1)\cos(\pi J_{IS} t_2)\cos(\omega_S t_2)\sin(\omega_S t_2)\,diagonal$$

$$I_y \sin(\omega_I t_1)\sin(\pi J_{IS} t_1)\sin(\pi J_{IS} t_2)\sin(\omega_S t_2)\,cross$$

We can also treat the COSY experiment using a density matrix representation for the coherence (following and expanding the notations in class notes of Erik Zuiderweg and the book of Frank Van de Ven Multimensional NMR in liquids).

Considering

$$I_y S_Z = \frac{1}{2}\begin{bmatrix} 0 & 0 & -i & 0 \\ 0 & 0 & 0 & i \\ i & 0 & 0 & 0 \\ 0 & -i & 0 & 0 \end{bmatrix}$$

$$2I_y S_z \sin(\omega_I t_1)\sin(\pi J t_1) =$$

$$\begin{bmatrix} 0 & 0 & -i\sin\omega_I t_1 \sin\pi J t_1 & 0 \\ 0 & 0 & 0 & i\sin\omega_I t_1 \sin\pi J t_1 \\ i\sin\omega_I t_1 \sin\pi J t_1 & 0 & 0 & 0 \\ 0 & -i\sin\omega_I t_1 \sin\pi J t_1 & 0 & 0 \end{bmatrix}$$

We apply a 90° pulse to the above matrix.

The operator for a 90° rotation is known to be:

$$\begin{bmatrix} \cos 90 & -\sin 90 \\ \sin 90 & \cos 90 \end{bmatrix} = \begin{bmatrix} 0 & -1 \\ 1 & 0 \end{bmatrix}$$

The matrix representation of the operators in a two-spin system can be calculated from the direct product of the one spin operator with the identity operator and results to the following rotation matrix.

$$\begin{bmatrix} 0 & 0 & 0 & -1 \\ 0 & 0 & -1 & 0 \\ 0 & 1 & 0 & 0 \\ 1 & 0 & 0 & 0 \end{bmatrix}$$

Multiplication of the matrix of interest with the rotation matrix gives the following:

$2I_y S_z \sin(\omega_I t_1)\sin(\pi J t_1) =$

$$
\begin{bmatrix}
0 & 0 & -i\sin\omega_I t_1 \sin\pi J t_1 & 0 \\
0 & 0 & 0 & i\sin\omega_I t_1 \sin\pi J t_1 \\
i\sin\omega_I t_1 \sin\pi J t_1 & 0 & 0 & 0 \\
0 & -i\sin\omega_I t_1 \sin\pi J t_1 & 0 & 0
\end{bmatrix}
\begin{bmatrix}
0 & 0 & 0 & -1 \\
0 & 0 & -1 & 0 \\
0 & 1 & 0 & 0 \\
1 & 0 & 0 & 0
\end{bmatrix}
=
$$

$$
\begin{bmatrix}
0 & -i\sin\omega_I t_1 \sin\pi J t_1 & 0 & 0 \\
i\sin\omega_I t_1 \sin\pi J t_1 & 0 & 0 & 0 \\
0 & 0 & 0 & -i\sin\omega_I t_1 \sin\pi J t_1 \\
0 & 0 & i\sin\omega_I t_1 \sin\pi J t_1 & 0
\end{bmatrix}
= S_y \sin(\omega_I t_1)\sin(\pi J t_1)
$$

We can clearly see by the use of the matrix representation that the elements that evolve with the frequency of spin I have been moved to elements to the new matrix that evolve with the frequency of the S spin.

We calculated that the diagonal peaks will be represented as:

$$I_x \sin(\omega_I t_1)\cos(\pi J_{IS} t_1)\cos(\pi J_{IS} t_2)\cos(\omega_I t_2) + I_y \sin(\omega_I t_1)\cos(\pi J_{IS} t_1)\cos(\pi J_{IS} t_2)\sin(\omega_I t_2)$$

substitution with

$$I_x = \frac{1}{2}\left[I^+ + I^-\right] \text{ and } I_y = \frac{1}{2i}\left[I^+ - I^-\right] \text{ gives:}$$

$$\frac{1}{2}(\sin\omega_I t_1)\cos(\pi J_{IS}t_1)\cos(\pi J_{IS}t_2)\left[(I^+ + I^-)\cos(\omega_I t_2) + \frac{1}{i}(I^+ - I^-)\sin(\omega_I t_2)\right] =$$

$$\frac{1}{2}(\sin\omega_I t_1)\cos(\pi J_{IS}t_1)\cos(\pi J_{IS}t_2)\left[I^+\cos(\omega_I t_2) - iI^+\sin(\omega_I t_2) + I^-\cos(\omega_I t_2) + iI^-\sin(\omega_I t_2)\right] =$$

$$\frac{1}{2}(\sin\omega_I t_1)\cos(\pi J_{IS}t_1)\cos(\pi J_{IS}t_2)\left[I^+e^{-i\omega_I t_2} + I^-e^{i\omega_I t_2}\right]$$

since

$$\cos\vartheta + i\sin\vartheta = \frac{e^{i\theta} + e^{-i\theta}}{2} + i\frac{e^{i\theta} - e^{-i\theta}}{2i} = e^{i\vartheta}$$

$$\cos\vartheta - i\sin\vartheta = \frac{e^{i\theta} + e^{-i\theta}}{2} - i\frac{e^{i\theta} - e^{-i\theta}}{2i} = e^{-i\vartheta}$$

Following the same thinking for the cross peaks we get:

$$I_x \sin(\omega_I t_1)\sin(\pi J_{IS}t_1)\sin(\pi J_{IS}t_2)\cos(\omega_s t_2) + I_y \sin(\omega_I t_1)\sin(\pi J_{IS}t_1)\sin(\pi J_{IS}t_2)\sin(\omega_s t_2) =$$

$$\frac{1}{2}\sin(\omega_I t_1)\sin(\pi J_{IS}t_1)\sin(\pi J_{IS}t_2)\left[I^+e^{-i\omega_s t_2} + I^-e^{i\omega_s t_2}\right]$$

The position of the diagonal and cross peaks in the two dimensional spectrum is defined by the terms that contain chemical shift information. Thus the diagonal peaks will be defined from $(\omega_I,\omega_I) and (\omega_S,\omega_S)$ and the cross peaks will be defined by $(\omega_S,\omega_I) and (\omega_I,\omega_S)$. The additional terms in the above equations are responsible for the J coupling splitting of the peaks.

The diagonal and the cross peaks are 90° out of phase with respect to each other. Since the cross peaks are the peaks of our interest, they are phased to have absorption line-shape, thus the diagonal peaks have dispersive line-shape.
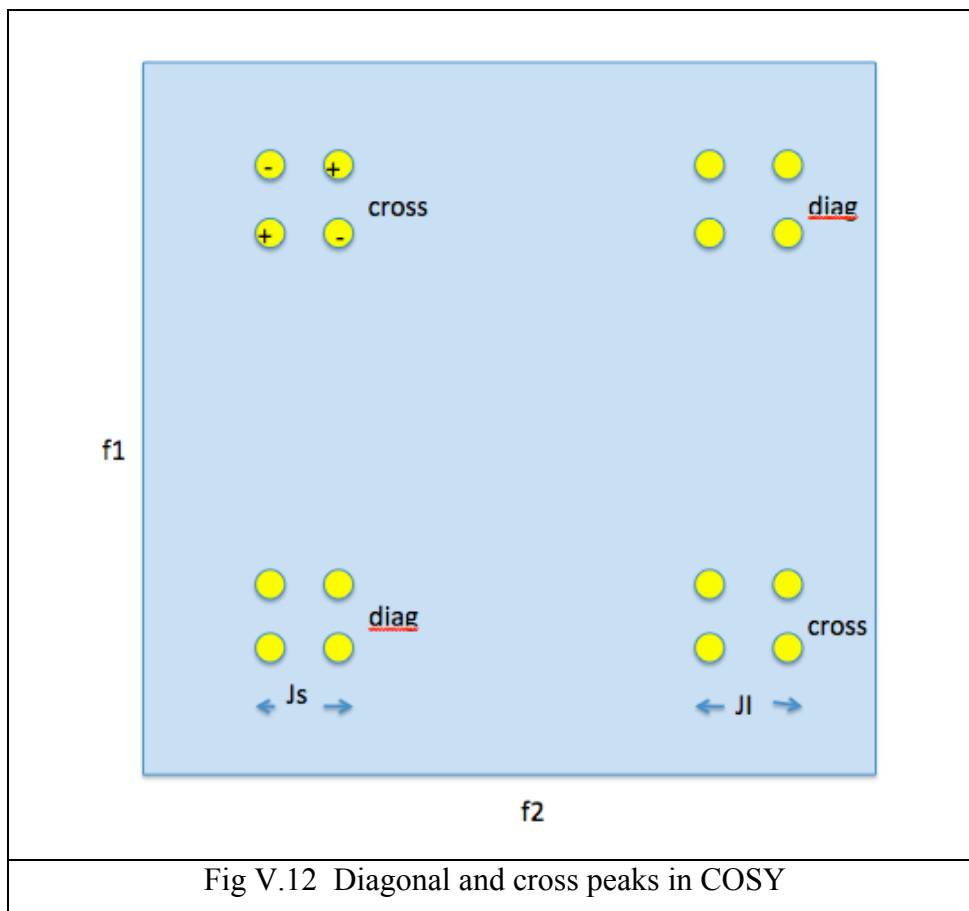
Fig V.12 Diagonal and cross peaks in COSY

V.4. DQF COSY

Although very useful, the COSY spectrum has some drawbacks. The cross and diagonal peaks are 90° out of phase and that causes various problems such as poor resolution of the peaks that are in close proximity to the diagonal peaks. The water peak is not suppressed by the COSY experiment and due to the high intensity of the water peak present in water solutions compared to the protein peaks a big dynamic range problem is caused.

The DQF-COSY (double quantum filtered COSY) experiment is an improved version of the COSY experiment and does not suffer from the above- mentioned deficiencies [334]. In the DQF-COSY experiment the water signal is suppressed since non-coupled spins do not give rise to peaks. The water protons are equivalent and they

behave as non-coupled spins that do not give rise to a signal. Another benefit from this experiment is that the diagonal and cross peaks have the same phase and thus we can both phase them in absorption mode, giving rise to a less crowded spectrum and to a better resolution of the peaks that are close to the diagonal.

The pulse sequence of the DQF-COSY experiment is similar to the pulse sequence of the COSY experiment. The second 90° pulse of the COSY experiment, has been substituted by two 90° pulses, that serve as mixing pulses. The first pulse converts the single quantum magnetization into double quantum magnetization and the second pulse converts the double quantum magnetization into detectable single quantum magnetization.
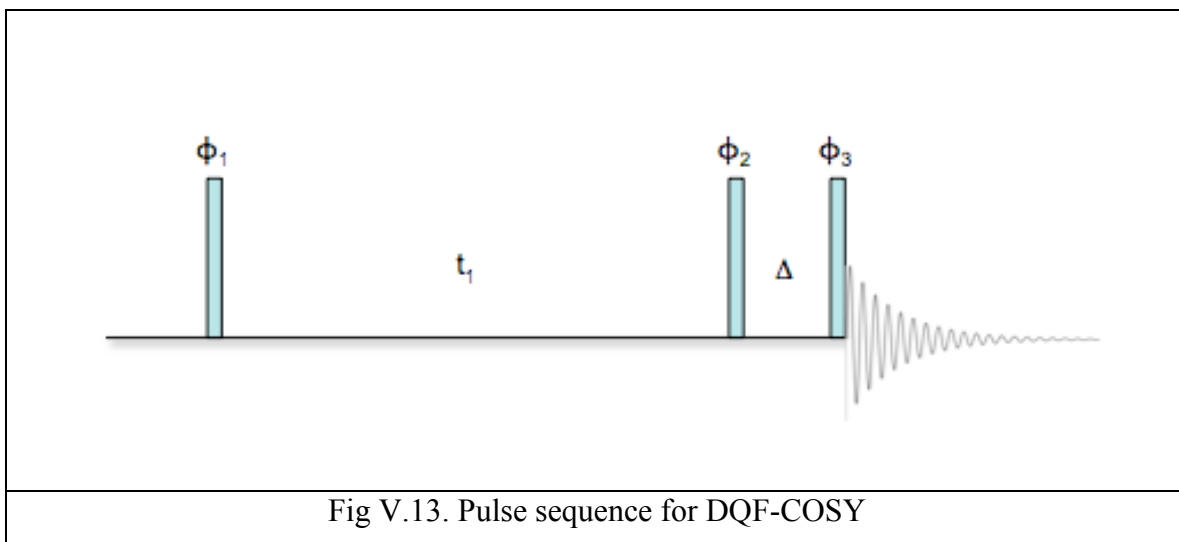
Fig V.13. Pulse sequence for DQF-COSY

The matrix algebra of the DQF-COSY experiment before the last 90° pulse is the same as in the case of the COSY experiment since these two pulse sequences resemble so much one another.

The phase cycle is the one shown in the following table:

Table V.2 DQF COSY Phase Cycling			
φ_1	φ_2	φ_3	ψ
x	x	x	x
x	x	y	-y
x	x	-x	-x
x	x	-y	y

$$I_z \, and \, S_z \xrightarrow{(\frac{\pi}{2})_x} -I_y \, and - S_y \xrightarrow{\omega_I t_1 \, and \, \omega_S t_1} -I_y \cos(\omega_I t_1) + I_x \sin(\omega_I t_1) - S_y \cos(\omega_S t_1) + S_x \sin(\omega_S t_1)$$

$$\xrightarrow{J_{IS}\pi t_1} -I_y \cos(\omega_I t_1)\cos(\pi J_{IS} t_1) + 2I_x S_z \cos(\omega_I t_1)\sin(\pi J_{IS} t_1) + I_x \sin(\omega_I t_1)\cos(\pi J_{IS} t_1) + 2I_y S_z \sin(\omega_I t_1)\sin(\pi J_{IS} t_1)$$

$$-S_y \cos(\omega_S t_1)\cos(\pi J_{IS} t_1) + 2S_x I_z \cos(\omega_I t_1)\sin(\pi J_{IS} t_1) + S_x \sin(\omega_S t_1)\cos(\pi J_{IS} t_1) + 2S_y I_z \sin(\omega_I t_1)\sin(\pi J_{IS} t_1)$$

$$\xrightarrow{(\frac{\pi}{2})_x} -I_z \cos(\omega_I t_1)\cos(\pi J_{IS} t_1) - 2I_x S_y \cos(\omega_I t_1)\sin(\pi J_{IS} t_1) + I_x \sin(\omega_I t_1)\cos(\pi J_{IS} t_1) - 2I_z S_y \sin(\omega_I t_1)\sin(\pi J_{IS} t_1)$$

$$-S_y \cos(\omega_S t_1)\cos(\pi J_{IS} t_1) - 2S_x I_y \cos(\omega_I t_1)\sin(\pi J_{IS} t_1) + S_x \sin(\omega_S t_1)\cos(\pi J_{IS} t_1) - 2S_z I_y \sin(\omega_I t_1)\sin(\pi J_{IS} t_1)$$

In DQF-COSY we preserve only the double quantum terms $I_x S_y$ and $S_x I_y$. Therefore we are left with:

$$-2I_x S_y \cos(\omega_I t_1)\sin(\pi J_{IS} t_1) - 2S_x I_y \cos(\omega_I t_1)\sin(\pi J_{IS} t_1)$$

The last 90° pulse gives us:

$$-2I_z S_y \cos(\omega_I t_1)\sin(\pi J_{IS} t_1) - 2S_z I_y \cos(\omega_I t_1)\sin(\pi J_{IS} t_1) \xrightarrow{\pi J_{IS} t_2}$$

$$-2I_z S_y \cos(\omega_I t_1)\sin(\pi J_{IS} t_1)\cos(\pi J_{IS} t_2) - S_x \cos(\omega_I t_1)\sin(\pi J_{IS} t_1)\sin(\pi J_{IS} t_2)$$

$$-2S_z I_y \cos(\omega_I t_1)\sin(\pi J_{IS} t_1)\cos(\pi J_{IS} t_2) - I_x \cos(\omega_I t_1)\sin(\pi J_{IS} t_1)\sin(\pi J_{IS} t_2)$$

The detectable single quantum terms evolve with their respective chemical shifts and thus we get:

$$-S_x\cos(\omega_I t_1)\sin(\pi J_{IS} t_1)\sin(\pi J_{IS} t_2)\cos(\omega_S t_2)-S_y\cos(\omega_I t_1)\sin(\pi J_{IS} t_1)\sin(\pi J_{IS} t_2)\sin(\omega_S t_2) cross$$

$$-I_x\cos(\omega_I t_1)\sin(\pi J_{IS} t_1)\sin(\pi J_{IS} t_2)\cos(\omega_I t_2)-I_y\cos(\omega_I t_1)\sin(\pi J_{IS} t_1)\sin(\pi J_{IS} t_2)\sin(\omega_I t_2) diagonal$$

The first of these peaks is a cross peak and the second one is a diagonal peak as seen from the frequencies (ω_I,ω_S) for the cross peaks and (ω_I,ω_I) and (ω_S,ω_S) for the diagonal peaks. Across the diagonal will be the second cross peak with frequencies (ω_S,ω_I). The cross and diagonal peaks have the same evolution with respect to the J coupling and thus will have the same phase. This is the major advantage of the DQF-COSY spectrum. We can phase both cross and diagonal peak in absorption mode and we can have better resolution for the peaks that are in close proximity to the diagonal. This is shown in Figure V.14.
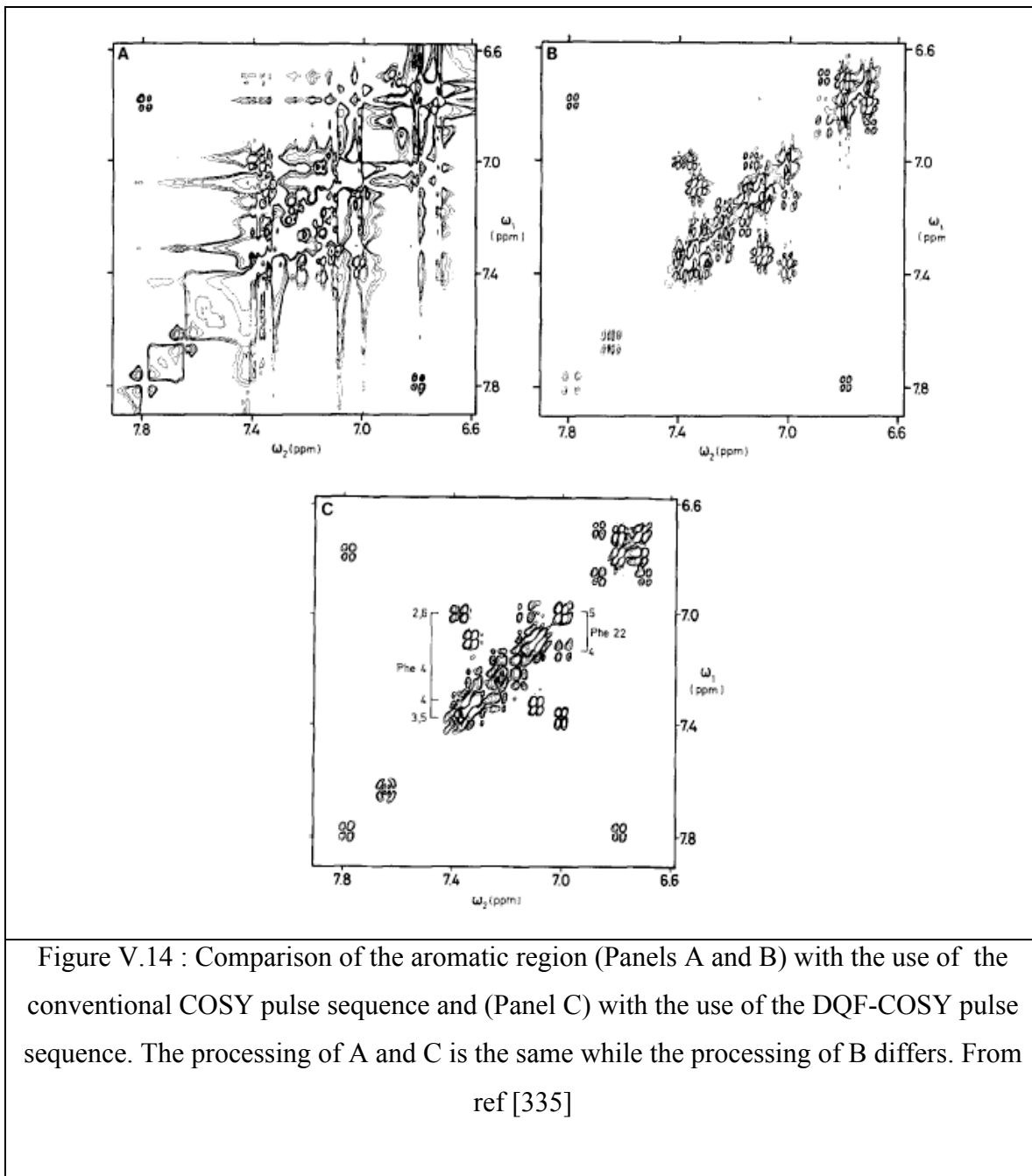
Figure V.14 : Comparison of the aromatic region (Panels A and B) with the use of the conventional COSY pulse sequence and (Panel C) with the use of the DQF-COSY pulse sequence. The processing of A and C is the same while the processing of B differs. From ref [335]

A better suppression of the of the spurious magnetization due to the pulse imperfections and to inequalities of the radiofrequency filters in the quadrature detection, is achieved with the use of a 16 step phase cycle which is achieved by incremented the

phases of each pulse and the receiver phase by 90° each time. We finally get selectively the double quantum term of the magnetization for detection in the receiver. That results in losing half of the magnetization and thus half of the peak intensity for the gain of better resolution especially of the cross peaks close to the diagonal and absorptive line-shapes of all the peaks cross and diagonal.

V.5 NOE-TROSY

The nuclear Overhauser effect (NOE) is a manifestation of cross relaxation between two nuclear spins, which are close to each other (usually <5A) in space. It is a powerful tool for the identification of structural features of organic compounds as well for the determination of secondary and tertiary structures of biological macromolecules. It is also used to assign spectra and to analyze conformational changes. The NOE phenomenon is the result of dipole-dipole interactions between nuclear spins [336].

The NOE phenomenon. Considering the case of nuclear dipoles (I=1/2) at thermal equilibrium, this ensemble exists as a Bolzmann distribution of spins aligned with (the α state) or against (the β state) the applied magnetic field. The strength of the dipolar interaction is dependent upon internuclear distance $1/r^6$ and thus the NOE effect, which is a result of that interaction is dependent on $1/r^6$ too. Since the energy difference between the α and the β states is small (<<kT) the population difference between the two states in the ensemble is also small. This small population difference is essential for the detection of the NMR signal that arises from the α to β transition, which is related to the populations of the spins in the states α and β and thus any change in these populations will affect the NMR signal. One source of a population change is the NOE effect of the NOE partner nuclei that occurs due to the cross relaxation rate change. The classical method of detecting NOE is to observe a change in signal intensity[331] at one nucleus upon perturbation of the second nucleus with a selective weak RF pulse. (Figure V.15)
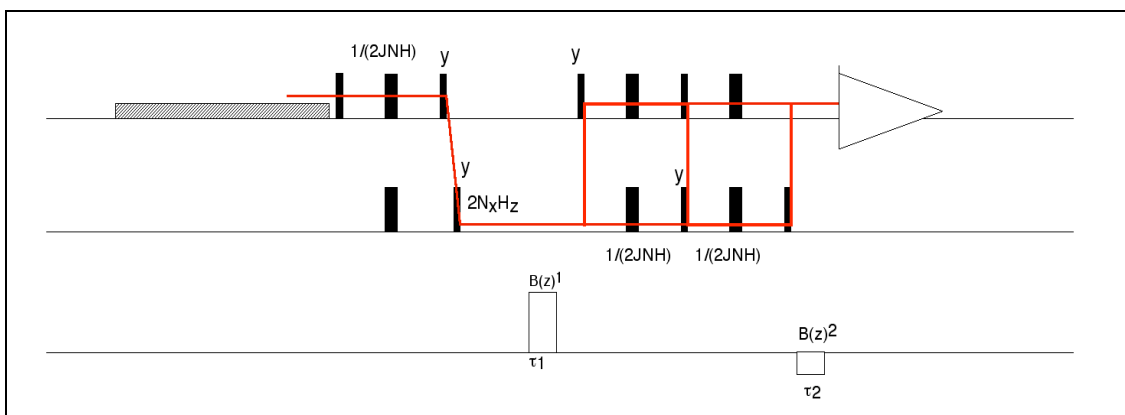
Fig V.15. A NOE-TROSY sequence used in conjunction with a perdeuterated protein and a protonated ligand. The initial 1H irradiation selectively saturates the methyl signals of the ligand.

The NOE is typically expressed as a fractional change in signal intensity S $_{perturbed}$ upon saturation of I relative to the signal in the absence of such perturbation S_0

$$NOE = f_S\{I\} = \frac{S_{perturbed} - S_0}{S_0}$$

This experiment is usually abbreviated as S{I} NOE, that is nucleus S is observed while nucleus I is irradiated.

Steady state NOE . In our case we used the so-called steady state NOE. We selectively irradiated the resonances of the 2 methyl groups of the MKT077 drug by a low power RF pulse and then used a TROSY as a read out pulse sequence (Figure V.15) . This results in the establishment of steady state spin populations which differ from the equilibrium populations for nuclei near the irradiated nucleus. The change in signal intensity is obtained by recording a reference spectrum under identical conditions to those under which the NOE containing spectrum was obtained, but with the saturating RF pulse set to an empty region of the spectrum. Subtraction of the two spectra gives us the difference spectrum, which reveals the amino acids that are affected by the saturation pulse and thus are in close space proximity to the methyl groups of the drug. The drug MKT077 has three methyl groups but we only irradiated two of them because the third methyl

frequency was not well resolved due to the fact that the water resonance was in that regime of the spectrum. The steady state experiment is appropriate only in the extreme narrowing limit, for large or small molecules in viscous solvents where correlation times are very long, NOEs are negative, which means that saturation of the irradiated spin leads to saturation near neighbors, followed by saturation transfer to spins further away (spin diffusion), which implies loss of distance information.

In two dimensional cross relaxation experiments such NOESY [337] or ROESY [338, 339], perturbations are usually non selective and the two dimensional spectra resulting from such experiments are essentially cross relaxation maps of the spin system under investigation.

An overview of the NOE cross relaxation pathways. Lets consider a two spin-1/2 nuclei system I and S that have different chemical shifts and have energy levels as the ones represented in Figure Panel A. Let's assume that the S single transitions gives one peak for the protein and the I single transitions gives one peak for the drug.
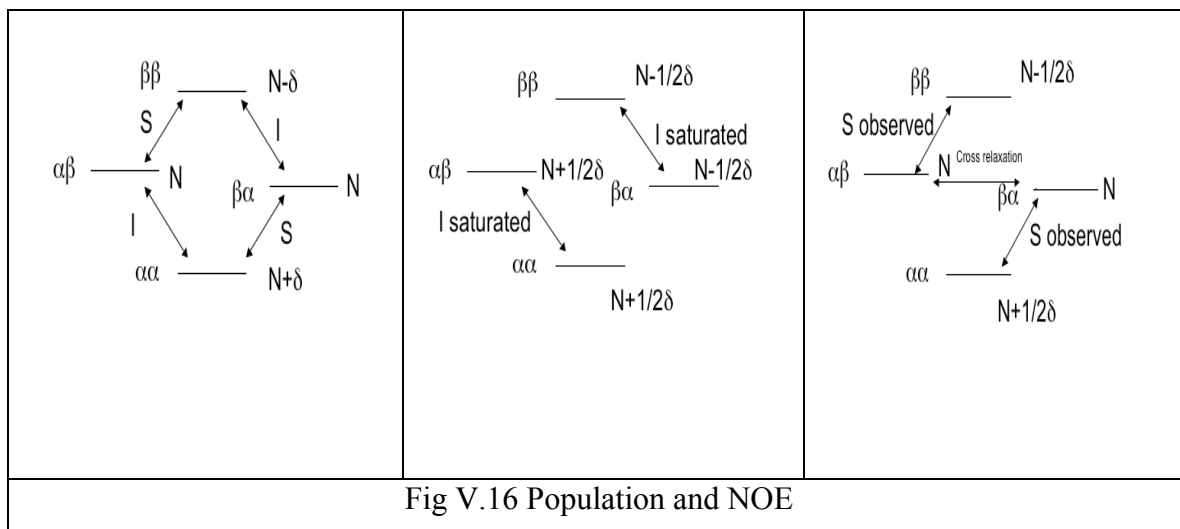
Fig V.16 Population and NOE

If only single transitions existed (W_1 - $\alpha\beta$ to $\beta\beta$, $\beta\alpha$ to $\beta\beta$, $\alpha\alpha$ to $\alpha\beta$ and $\alpha\alpha$ to $\beta\alpha$) we would not be able to observe NOE. It is the double (W_2 - $\alpha\alpha$ to $\beta\beta$) and zero quantum (W_0 -$\alpha\beta$ to $\beta\alpha$) terms that give rise to the NOE phenomenon. In Figure V.16

Panel A We see the populations of the four energy levels in equilibrium. Two lines are present, one for the S single transitions and one for the I single transitions. The N denotes the populations of the states. We saturate the I spin (the drug methyl group) meaning that the populations for the I transitions are equal and thus we will see no peak for the I spin (figure V.16 Panel B) and we observe the effect on the protein after the cross relaxation effect takes place. That is the zero quantum transition populations equalize as we see in Figure V.16 Panel C. The intensity of the S spin peak is small due to the fact the population difference is smaller.

CHAPTER VI. Expanding and correcting the assignment of the bckbone resonances of Hsc70-NBD

VI.1 Method

A key step for every protein under investigation is the so-called assignment of the backbone ^{13}C, ^{1}H and ^{15}N resonances, a laborious but necessary step for the investigation of every kind of interaction with small molecules or proteins and/or dymamics and structural measurements. The so-called 3 dimensional experiments are the key to assigning a protein. The key ideas for the suite of experiments was originally created in the early 1990, mostly in the group of Dr. A. Bax[340]. Since that time many improvements have come about. A reasonably up-to-date account is found in [341]. Sometimes 4 dimensional experiments, such as the 4D-HNCACB [342] are used, but for the assignment of Hsc70 NBD we only used the 3D experiments as described in Table VI.1.

Table VI.1 Three-dimensional Assignment Experiments	
Sequential	Intraresidue
HNCO	HN(CA)CO
HN(CO)CA	HNCA
HN(CO)CACB	HNCACB

Three Dimensional spectroscopy. In order to assign our protein we used three-dimensional experiments. More specifically we incremented the values of two pulse-sequence delays, t_1 and t_2, and we acquired the third signal as a cosine modulation of t_3. The data are represented as a data -cube that is Fourier transformed in all three dimensions and gives us a three dimensional cube of peaks that are represented with frequencies ω_1, ω_2 and ω_3.

The following cube represents the Hsc70 NBD HNCO three-dimensional spectrum-peaks after Fourier transformation of the FIDs. The three dimensions represent the amide proton, nitrogen and CO frequencies of the Hsc70 NBD.

Figure VI.1: 3D HNCO of Hsc70 NBD
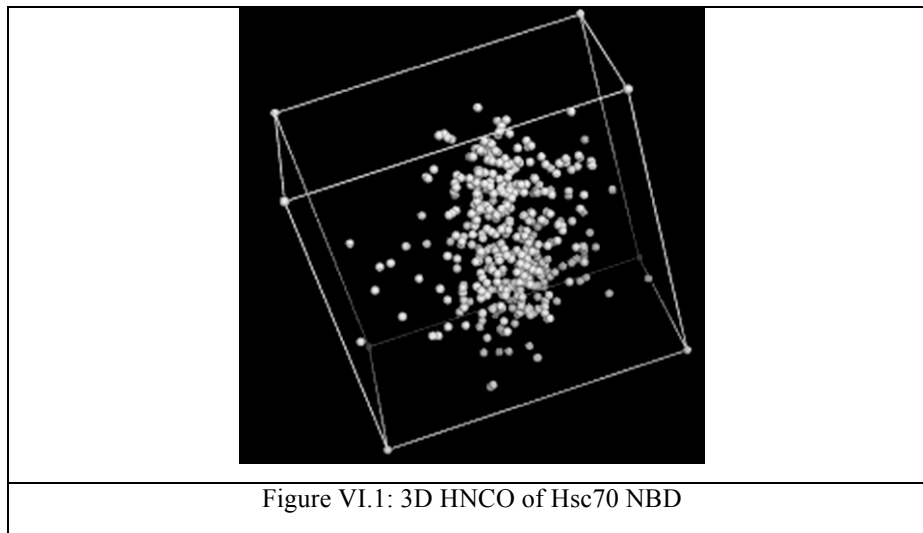
Every protein is composed of amino acids; these amino acids have specific H, N, Ca, Cb, CO etc. frequencies that are dependent on the position of each amino acid in the tertiary structure of the protein. When we run an NMR experiment, magnetization is transferred over the peptide bond to various parts of the peptide. We see those parts of each peptide resonating at specific frequencies. The assignment process is the process that determines which amino acid resonates in which frequencies in the NMR spectrum via the usage of various intra-residue and sequential experiments. Figure VI.2 indicates schematically that every amino acid has a specific pair (in a two dimensional experiment) of frequencies and that is called the assignment of the protein.

Figure VI.2 Symbolic representation of the NMR assignment process
(from Zuiderweg's classnotes)
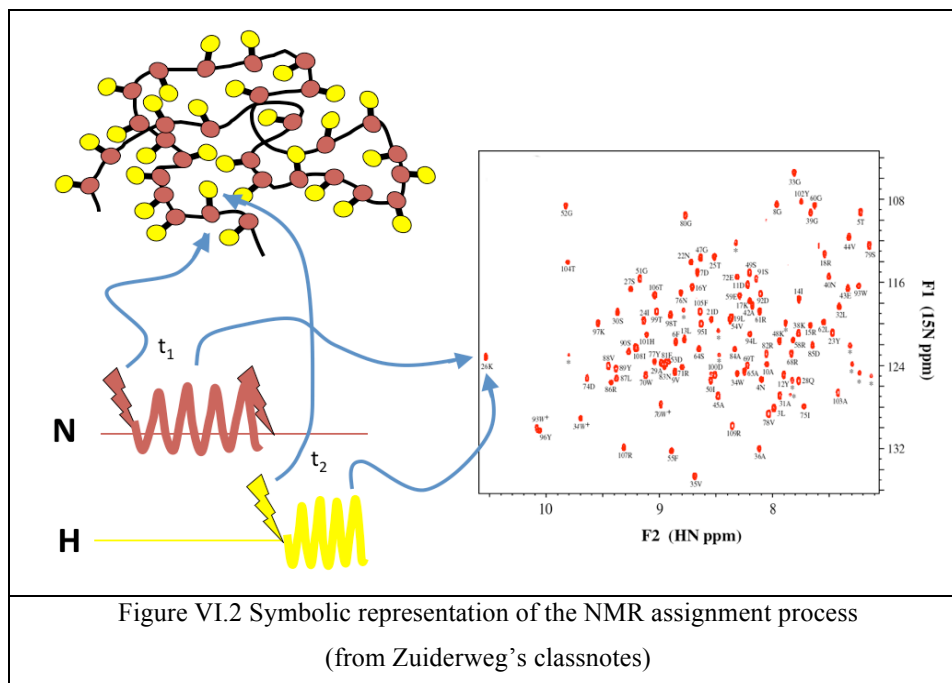
For the assignment of the bovine Hsc70 nucleotide-binding domain we run various experiments. The experiments we run have already been mentioned in Table VI.1. We will analyze the experiments used one by one and give a detailed description on how the assignment was done.

HNCO. The HNCO experiment correlates the amide proton and nitrogen shifts with the CO resonance of the i-1 residue. Figure VI.3 shows the pulse scheme used for this experiment. Using the INEPT pulse scheme, magnetization is transferred from the amide proton to nitrogen. Then it with the use of another INEPT it is transferred to the CO where it is t_1 labeled. Then it is transferred back to the nitrogen that it is t_2 labeled and then back to the amide protons and the FID is recorded (t_3 labeling).

Figure VI.3: The HNCO-TROSY pulse sequence as used in our lab.

A basic phase cycle with $\phi 1 = x, -x$ with $\psi = +, -$ is used.

States-TPPI Quadrature detection in t1 is achieved by $\phi 1 = x,y,-x,-y$ with $\psi = +,+,-,-$;

Rance-Kay-TPPI Quadrature detection in t2 is achieved by $\phi 2 = y,y,-y,-y$, $\phi 3 = -y,y$ $\phi 4 = -x,x$ with

inversion of G1 and $\psi = +,+,-,-$. The experiment combines elements from references [343], [344], [332]
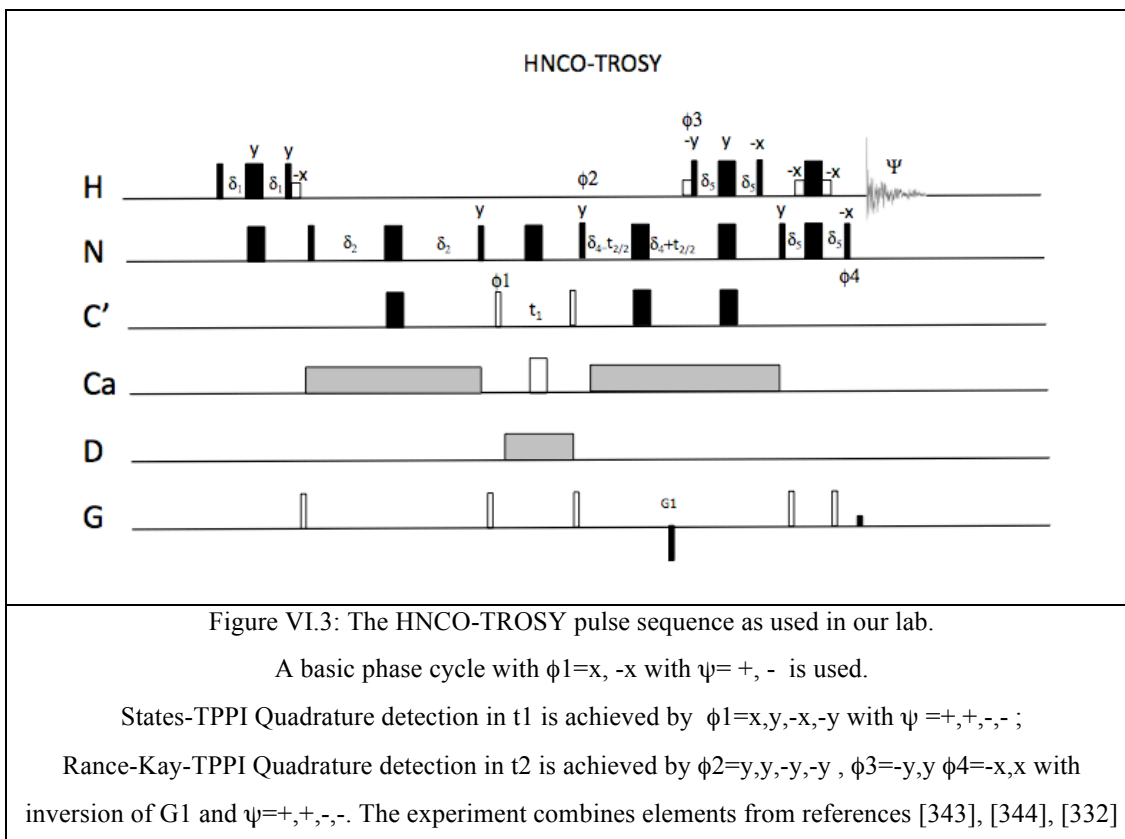
The HNCO experiment yields only the i-1 peaks of the residues and thus in order to sequentially assign the protein we need a complementary experiment to the HNCO experiment that gives us both the i and the i-1 frequencies of a specific amino acid. That is the HN(CA)CO experiment. The magnetization pathways that both experiments follow are shown in Figure VI.4. In Figure the HN(CA)CO experiment is shown in green and the HNCO experiment is shown is red. For the HNCO experiment the magnetization is transferred from H to N and to CO_{i-1} while the magnetization for the HN(CA)CO is transferred to both the H, N, CO_{i-1} and to the H,N,CO_{i}. The combination (overlay) with the HNCO spectrum allows us to identify which residue is the i and which is the i-1 residue.
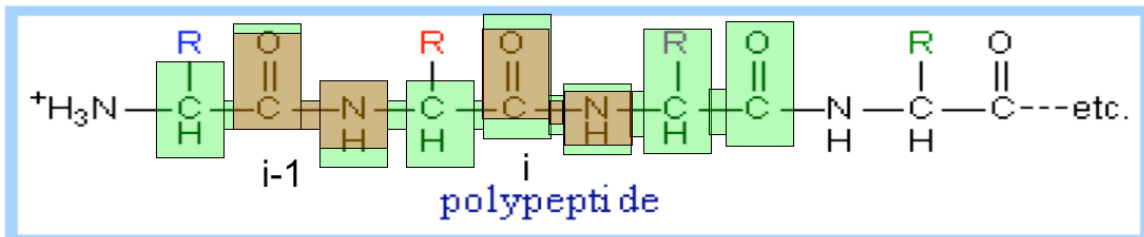
Figure VI.4: Coherence pathways in HNCO and HN(CA)CO

HN(CA)CO: The HN(CA)CO experiment is shown in Figure VI.5. This experiment gives us the i-1 peak exactly as the HNCO experiment does, but it also gives us the i peak and thus enables us to sequentially connect the amino acids of a protein and thus get the assigned spectrum of that protein.

Figure VI.5: Pulse sequence for the HN(CA)CO experiment. Open boxes indicate pulses selective for the 13CO and 13CA frequency ranges. The phase cycling and quadrature detection is similar to the HNCO.
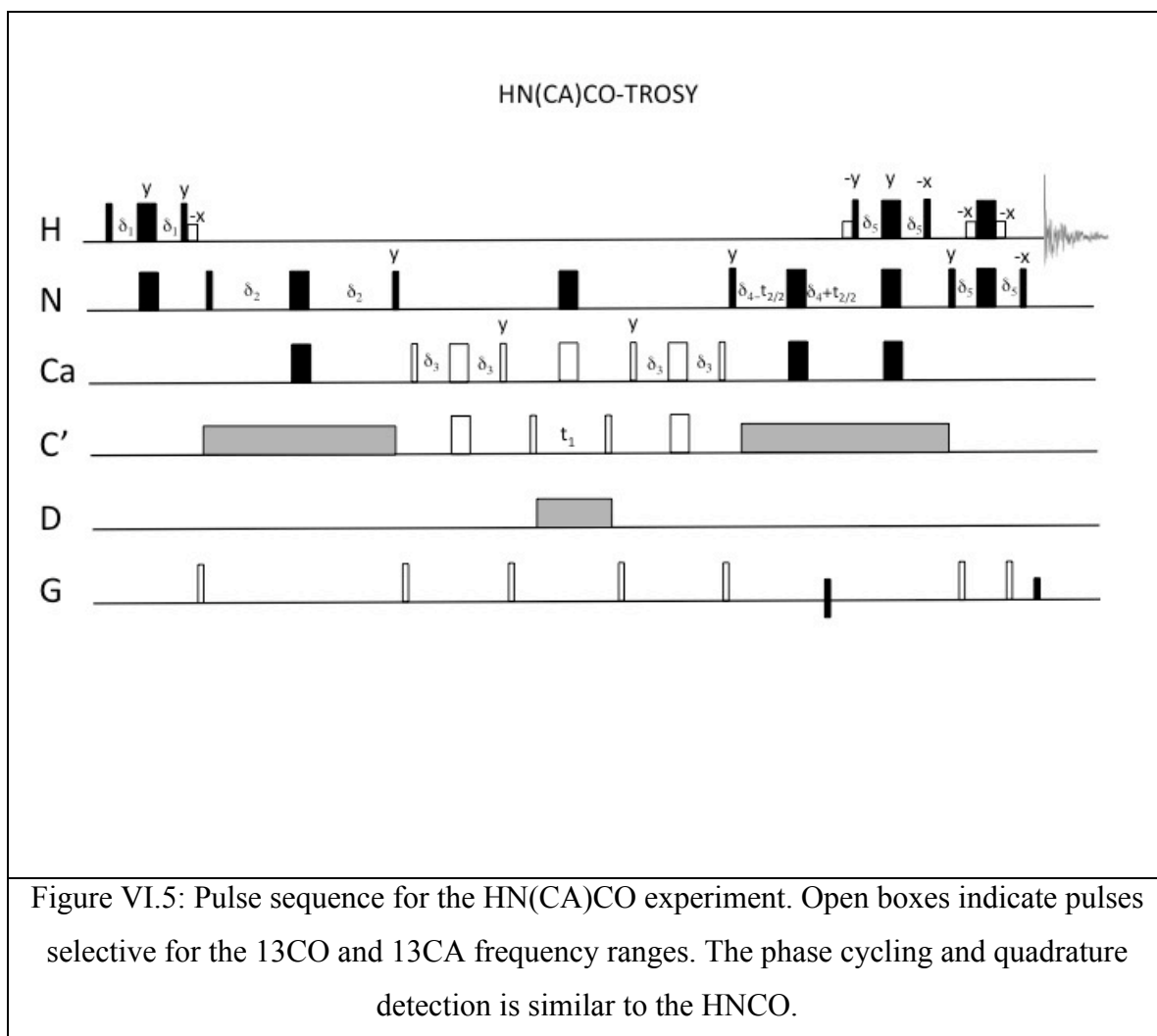
The HN(CA)CO sequence begins with an INEPT transfer to the nitrogen. It is transferred to the Ca and then to the CO that is t_1 labeled. Then the magnetization is transferred back to the nitrogen where is t_2 labeled and then to the hydrogens for detection with the use of reverse steps.
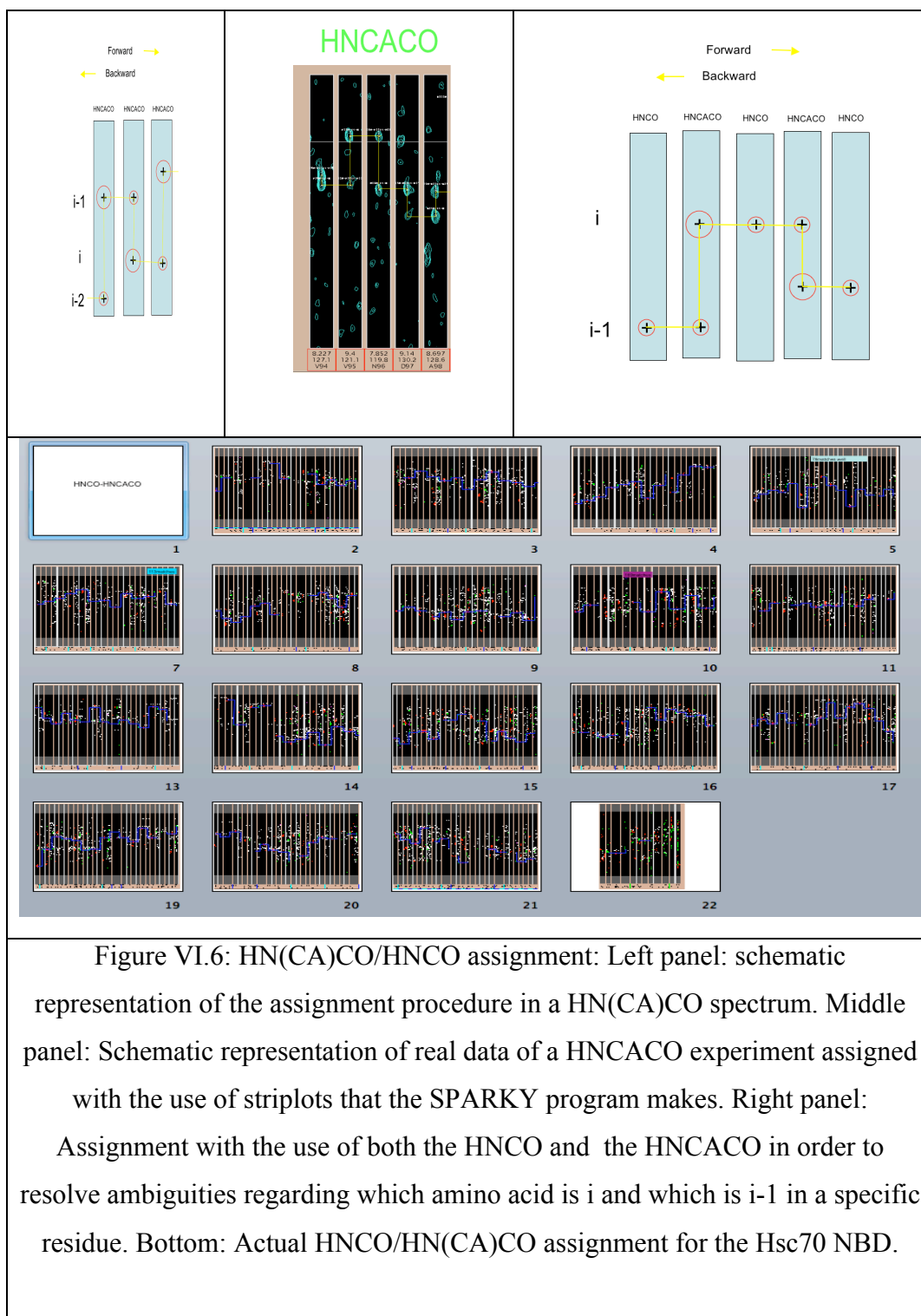
Figure VI.6: HN(CA)CO/HNCO assignment: Left panel: schematic representation of the assignment procedure in a HN(CA)CO spectrum. Middle panel: Schematic representation of real data of a HNCACO experiment assigned with the use of striplots that the SPARKY program makes. Right panel: Assignment with the use of both the HNCO and the HNCACO in order to resolve ambiguities regarding which amino acid is i and which is i-1 in a specific residue. Bottom: Actual HNCO/HN(CA)CO assignment for the Hsc70 NBD.

Practically in order to assign our data we sequentially follow the backbone amino acids with the HN(CA)CO experiment and link them with the use of the common peak for the i-1 amino acid of a specific residue as shown in Figure VI.6 left and middle panel.

The magnetization begins at amino acid i-1 that has two peaks the i-2 and i-1 peak. This allows us to link the i-2 and i-1 amino acids. Then we search all the nitrogen planes to find the proper strip that has the same CO and H frequency as the i-1 amino acid that will be linked in that specific strip plot with the i amino acid etc till the whole backbone of the protein is assigned or till a proline interferes with the backbone and stops the assignment procedure. The use of an HNCO spectrum is needed when ambiguities arise as shown in Figure VI.6, right panel.

In principle, the HNCO HN(CA)CO combination would be sufficient to assign all HN, N and CO resonances is a protein, and hence yield the sought-after assignments for the 2D HSQC or TROSY spectrum. However, in practice, the NMR data are incomplete (dynamic processes can broaden resonances away) so that one typically does not know where the fragment of linked resonances is placed on the amino acid sequence. In addition, there are often several residues that have (within the linewidth) identical CO frequencies , so that unique connections can often not be made.
Hence, the assignment process is also carried out with CA, and also CB connectivities coming from HNCA-HN(CO)CA ad HNCACB-HN(CO)CACB combinations.

HNCA. The HNCA experiment has three frequency axis 1H, nitrogen-15 and Ca carbon-13. It correlates the i amide proton to the i Ca atom with a big intense intraresidue peak. It also correlates the i amide proton to the i-1 Ca atom with a smaller interesidue peak. The intensity difference of the peaks is due to less bonds being in between the amide proton and Ca atom in the latter case. The blue lines in Figure VI.7 indicate the paths that the magnetization follows. Following those magnetization paths we can 'walk' through the backbone of the protein step by step from amino- acid i-1 to amino-acid i, i+1, i+2 etc. Proline residues do not have an amide proton and thus interrupt our backbone walk. This is a three dimensional experiment with it's pulse sequence given in Figure VI.8.

Figure VI.7: Coherence pathoways for the HNCA and the HN(CO)CA experiments

Top: Coherence pathways for the I and I-1 peaks in the HNCA experiment.

Top: Coherence pathways for the I-1 peaks in the HN(CO)CA experiment.
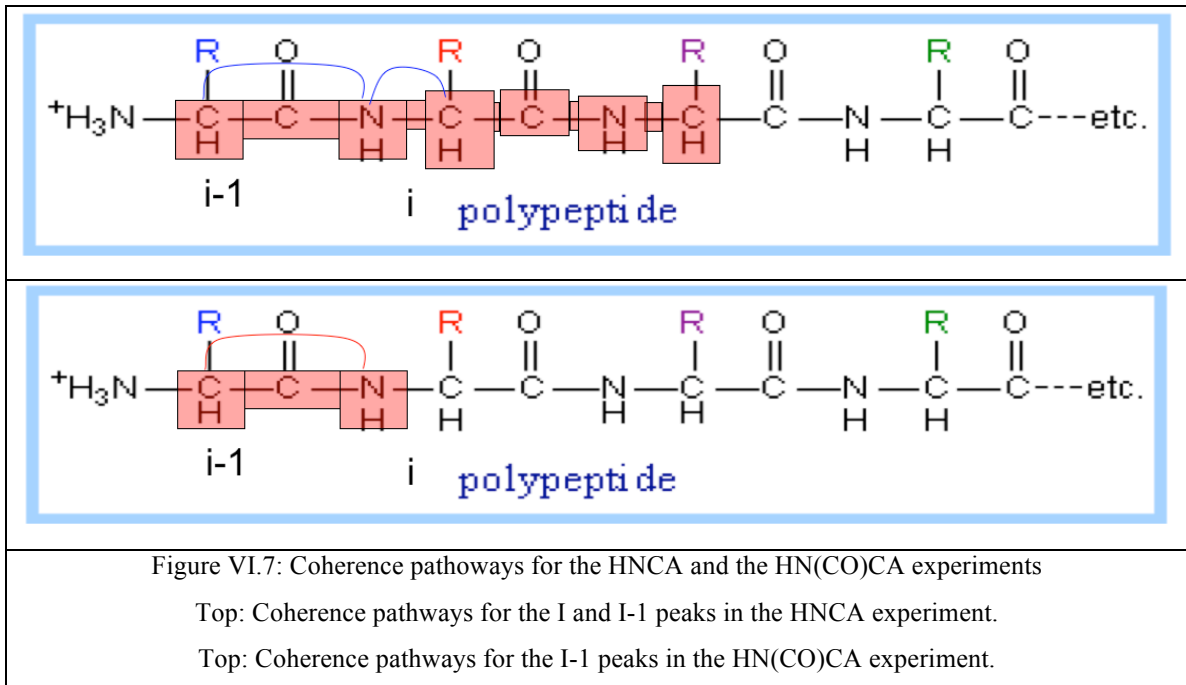
Considering the backbone of the protein the HNCA experiment gives us as already mentioned two peaks the i and the i-1 peak of a specific residue. The i peak is shown with the indication i in Figure VI.7 and the i-1 peak due to the CO bond in between gives us a smaller peak in intensity (more J couplings) and is indicated as i-1 in figure. The blue lines in Figure indicate the two pathways that give the i and i-1 peaks.

Figure VI.8: Pulse sequence for the HNCA experiment. The phase cycling and quadrature detection is similar to the HNCO.
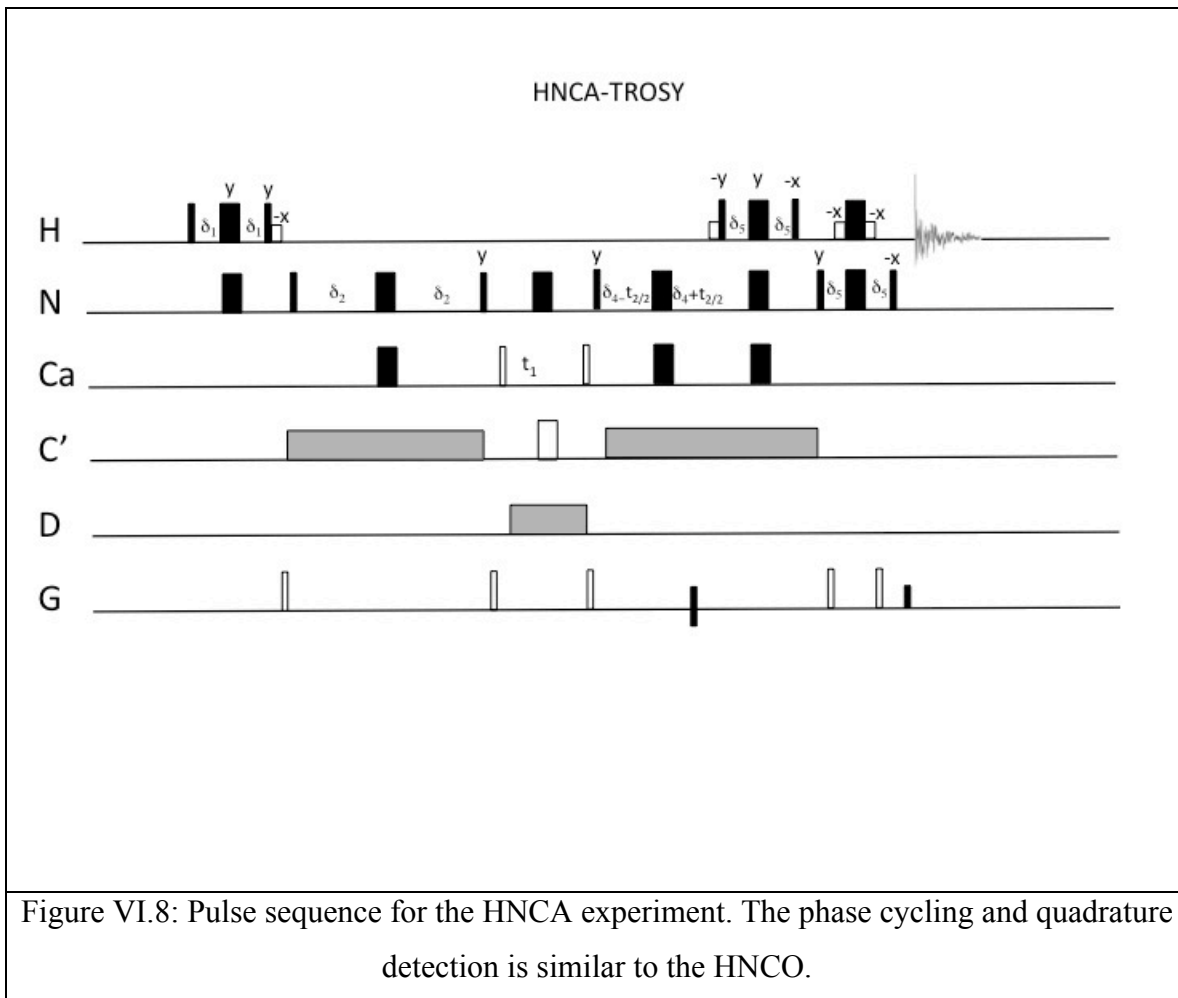
The assignment is much easier if we know which peak is peak i and which is peak i-1 as we walk through the backbone. As already mentioned the intensities of the peaks are often ambiguous and that is why we need to know the i and i-1 peaks via another more reliable method. We thus use another experiment. The so-called HN(CO)CA experiment that only gives us the i-1 peak and not the i peak. Overlapping the HNCA and HN(CO)CA experiments makes it possible to distinguish the i and i-1 peaks. Figure gives a representation of the HNCOCA and the HNCA experiments. As seen the HNCOCA spectrum gives only one peak for a specific amino acid while the HNCA gives two peaks. That enables us to resolve which is the I and which is the i-1 peak in a specific amino acid.

Figure VI.9 : Slices of a three dimensional cube for an HNCOCA and an HNCA
spectrum. (From Protein NMR spectroscopy principles and practice. Cavanagh J.,
Fairbrother W., Palmer A.G., Skelton N.J.)
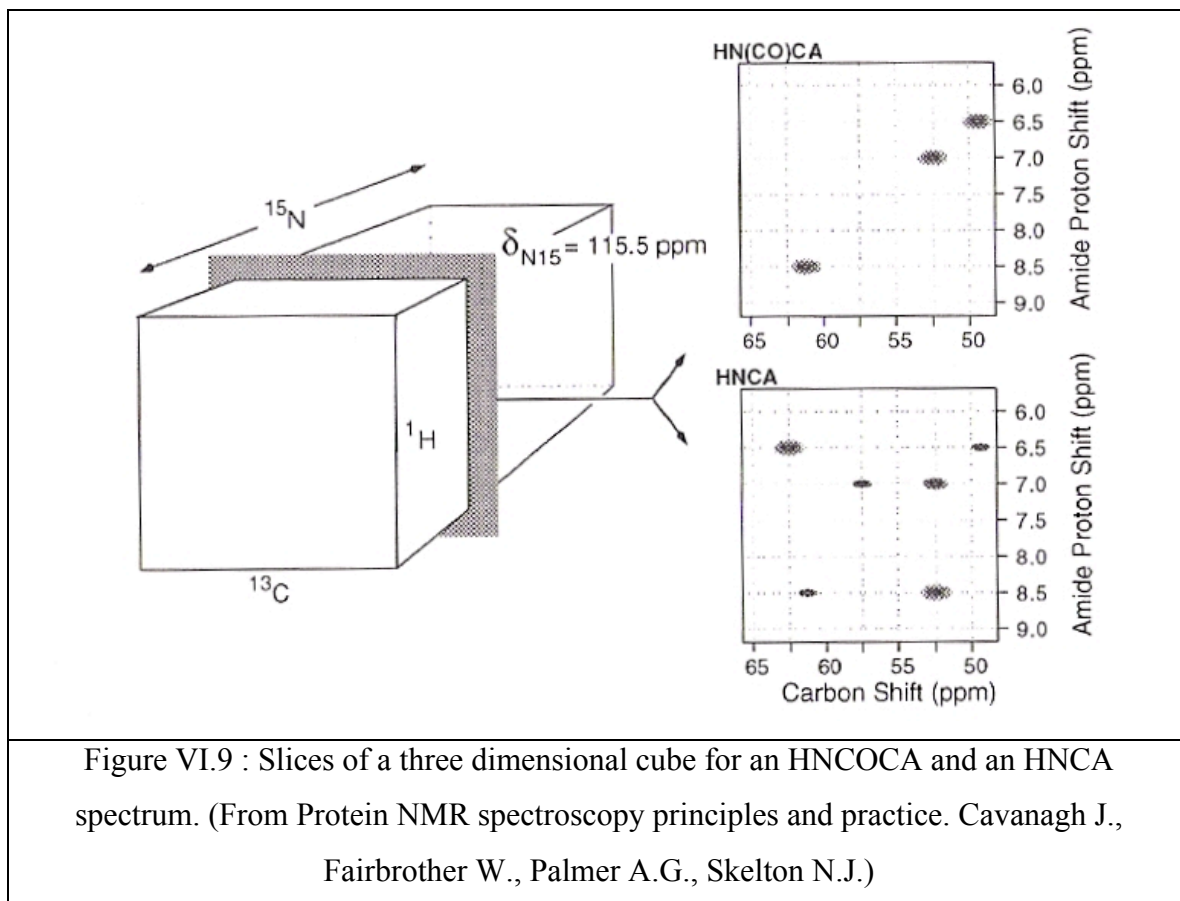
HN(CO)CA. The HN(CO)CA experiment has three frequency axis 1H, nitrogen-15 and
carbon-15. It correlates the i amide proton with the i-1 Ca atom. The red boxes in figure
VI.7 indicate the path that the magnetization follows and gives us only the i-1 peak. The
HN(CO)CA experiment is a complimentary experiment to the HNCA experiment since it
distinguishes the i from the i-1 peaks and resolves which amino acid is i and which is i-1.
The pulse sequence of the HN(CO)CA experiment is given in Figure VI.10.

HN(CO)CA-TROSY

Figure VI.10: The HN(CO)CA pulse sequence. The phase cycling and quadrature detection is similar to the HNCO.
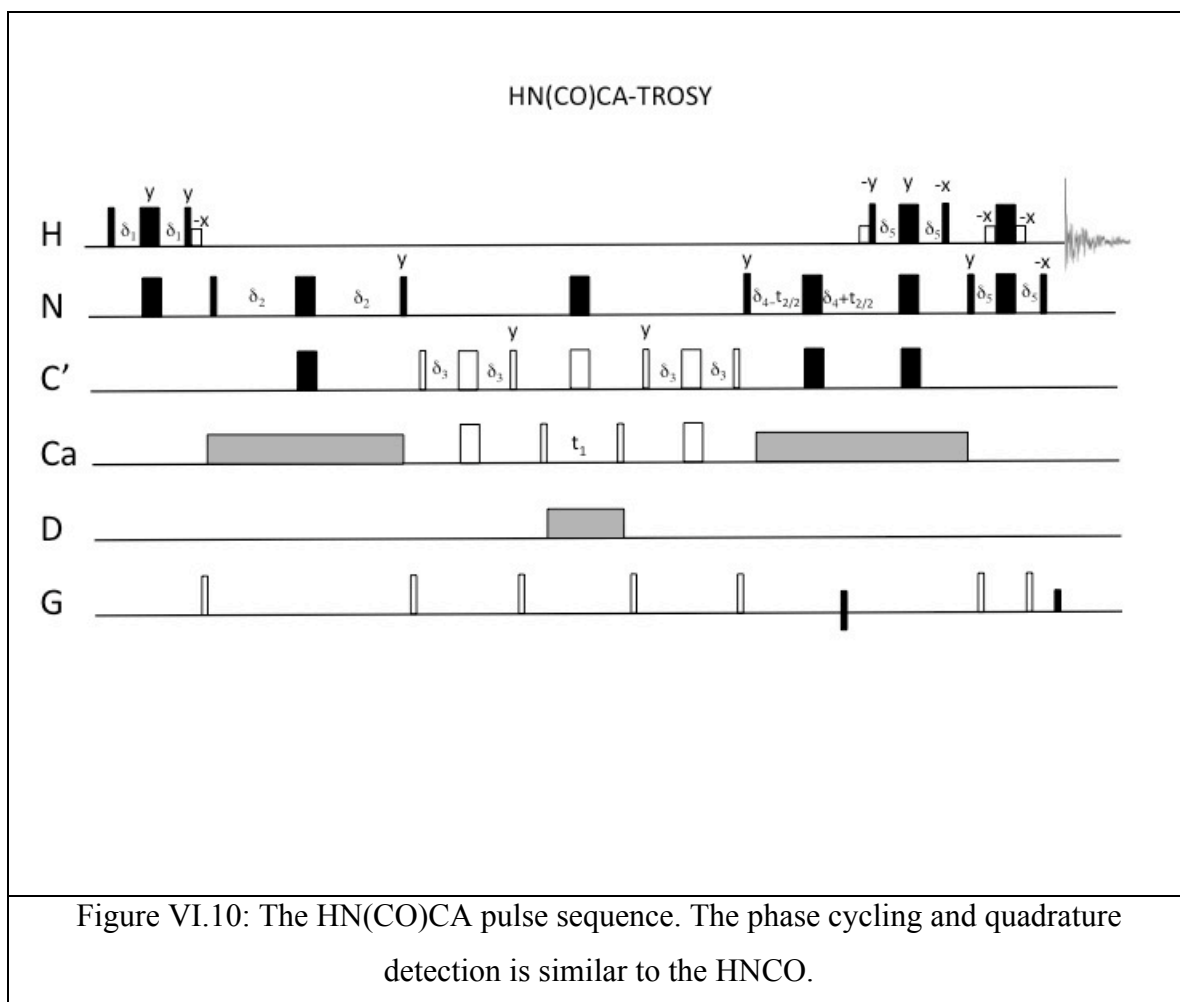
The HNCACB and the HN(CO)CACB experiments are essentially the same experiments as the HNCA and HN(CO)CA with the only difference that the magnetization does not only go the alpha carbon but it also goes to the beta carbon. Short descriptions of these experiments follow. We will not be very detailed since we have already described the HNCA and the HNCOCA experiments.

HNCACB: The HNCACB is a three dimensional experiment. It correlates the i amide proton to the i Ca atom and to the i Cb atom with two intense peaks. It also correlates the i amide proton to the i-1 Ca atom and to the i-1 Cb atom with two less intense peaks that have the opposite sign. The opposite signs are due to the pulse sequence that is shown in Figure VI.11.

Figure VI.11.: The HNCACB pulse sequence.
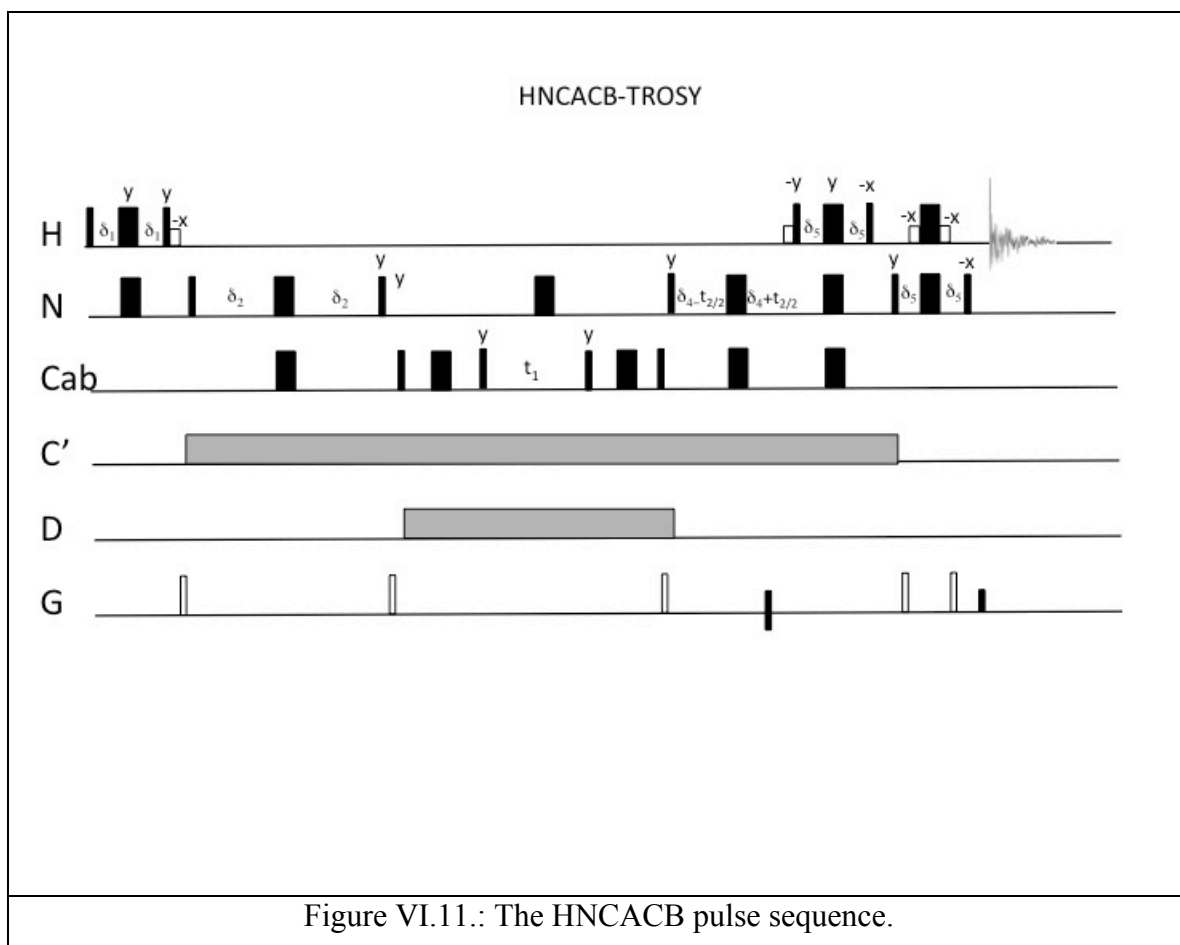
The pulse sequence resembles the HNCA pulse sequence with the difference that in the carbon channel we do not only obtain the C_a frequency but the C_β frequency as well. We get the C_β frequency in the expense of the C_a signal to noise and the magnetization is transferred from the Ca to the Cb , while they both share the same channel, in an INEPT like manner. A 180 like pulse scheme is used in order to have opposite signs for the C_a and C_β spins.

Figure VI.12 panels left and right show how the assignment was done with the use of the HNCACB experiment. The HNCA and HNCOCA experiments were also used since the signal to noise is much better in these experiments but the information that an HNCA experiment gives is contained in the HNCACB experiment and the information that an HNCOCACB experiment gives is contained in an HNCOCA experiment.

Figure VI.12. Left: schematic assignment pathways. Right actual assignment for residues 94-98 in Hsc70. Bottom Actual assignments for the whole protein
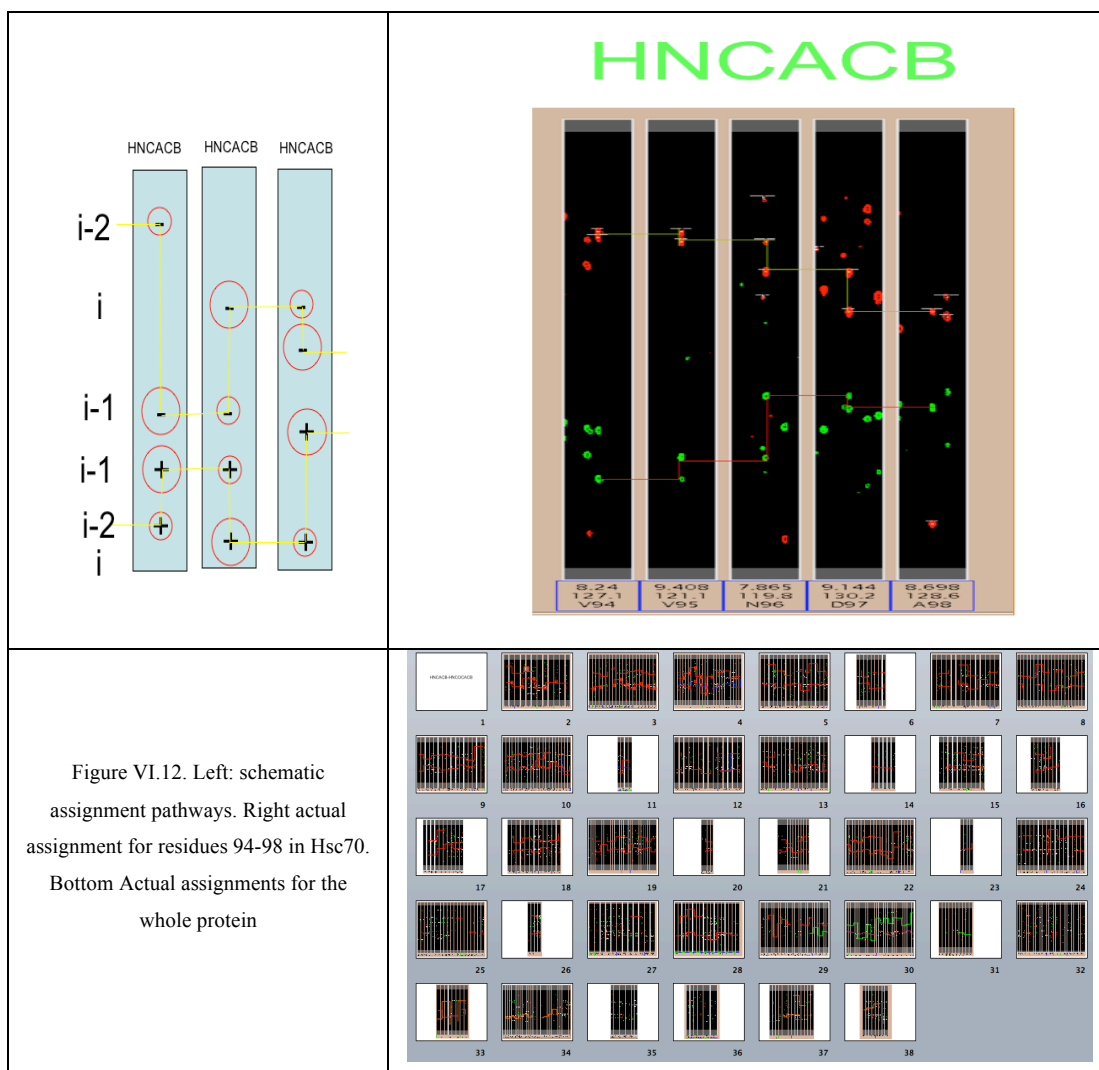
Following Figure VI.12 left panel, the magnetization begins from i-2 residue that has the same H and N frequency with the i-1 residue in the same amino acid. Then we search all the nitrogen planes and find the proper strip that has the same CA and CB frequences as the i-1 amino acid then we find to which amino acid that is linked in that strip and that is going to be amino acid i and so on till the amino acid sequence stops or till a proline stops the assignment.

As already mentioned, the HNCACB, HNCA, HNCOCACB and HNCOCA experiments all overlap and resolve ambiguities of one another as seen in Figure. In red is shown the HNCA experiment, in blue the HNCOCA that only gives the 'back' peak and in green the HNCACB experiment. The HN(CO)CACB was not included in the scheme

because there would be too much color overlap but we can clearly see that it would follow the HNCOCA pattern that would be extended also to the CB spins and would thus gives two 'back' peaks one for the CA and one for the CB.

Figure VI.13. Backbone assignment with the use of HNCACB, HNCOCA and HNCA experiments.
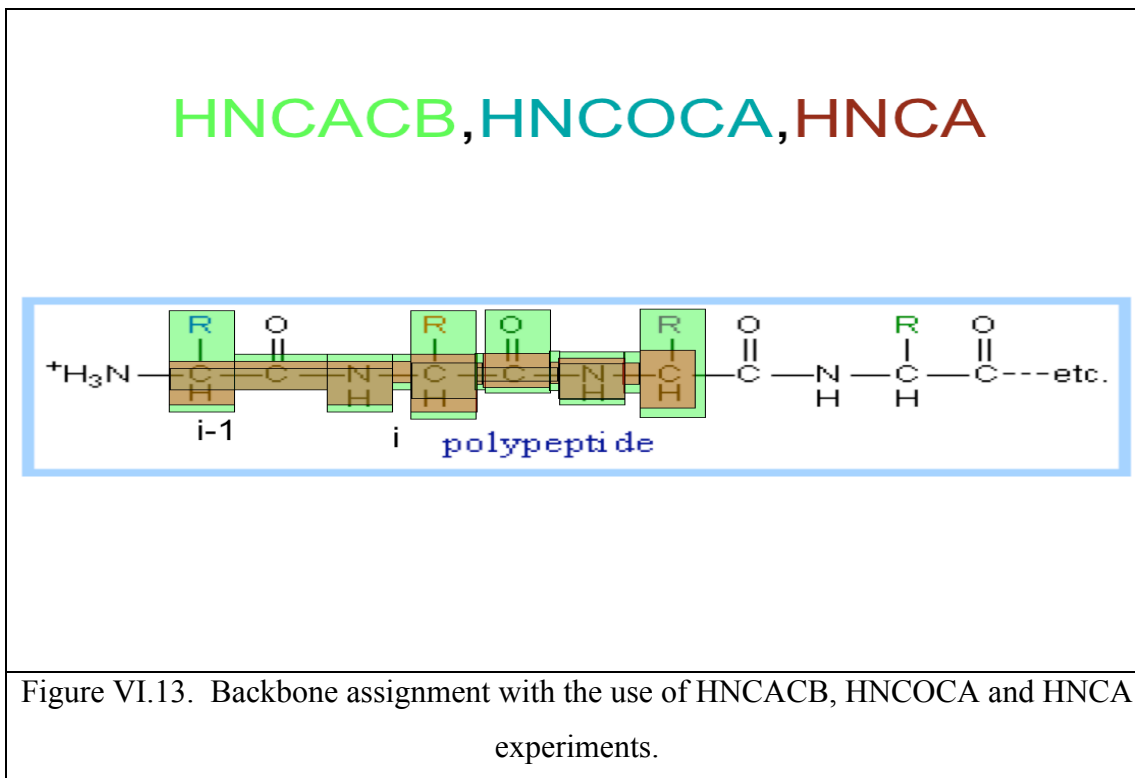
HN(CO)CACB. The HN(CO)CACB experiment is complimentary to the HNCACB experiment. As in the case of the HN(CO)CA experiment that complimented the HNCA experiment, the HN(CO)CACB experiment gives us exclusively the i-1 peaks for the C_a and C_β spins. It is thus used to interpret the HNCACB spectrum. However, due to the longer pulse sequence and the need to use selective pulses, the S/N of the HN(CO)CACB is quite limited, and can sometimes be impossible to record.

The pulse sequence used is given in Figure VI.14.

Figure VI.14. HN(CO)CACB.
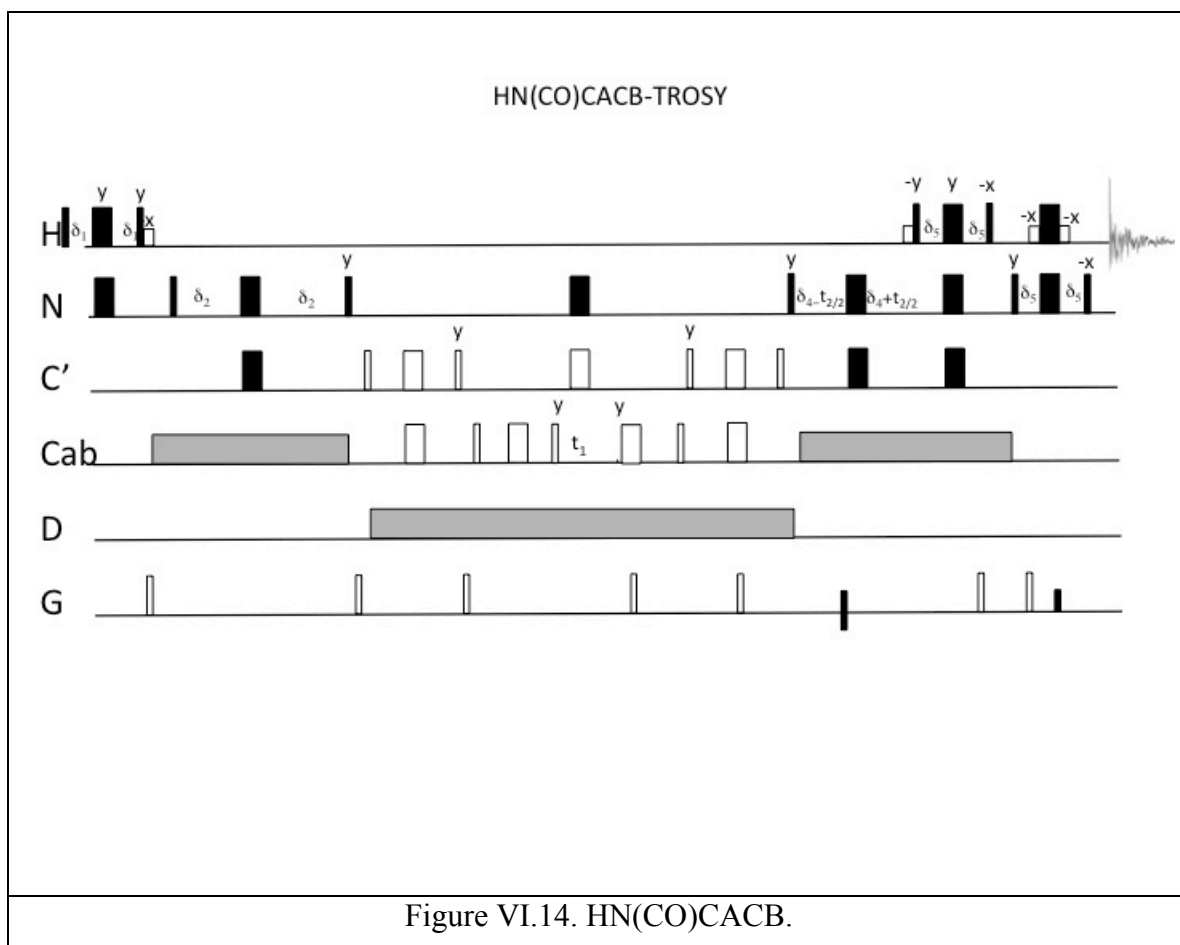
As already mentioned the HNCOCACB experiment resembles the HNCOCA experiment and we thus not give any more details about it.

Assignment of resonances to individual amino acids is also based on the criterion that the 13C resonance frequencies (and lesser so, 15N frequencies) match a data-base statistics of the frequencies of the residue type. Figure VI.15 shows these statistics.
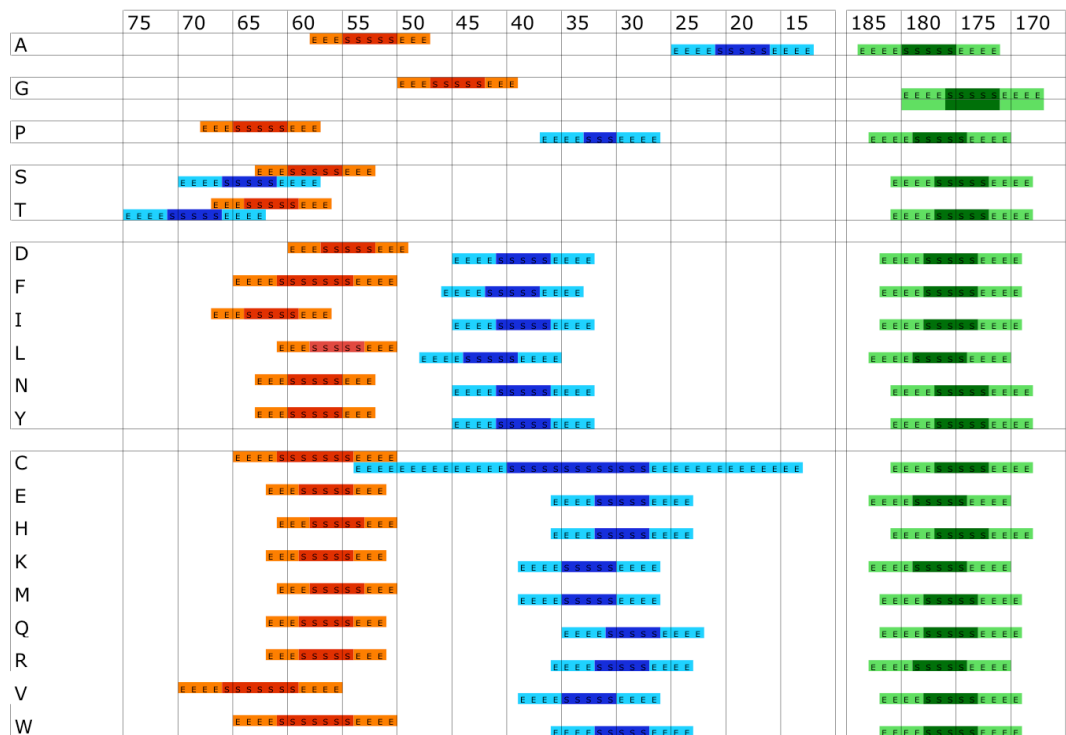
Figure VI.15. BMRB statistics for the Ca, CB and CO resonances of proteins. The dark colored ranges are 1 standard deviation, the lighter ranges three standard deviations as used in the SAGA program (see below). From Ref [345]

VI.2 Experimental.

We used a 300 uM sample of 15N,13C,2H labeled Hsc70NBD that had already been prepared by Dr. Daniel Weaver in our lab. The six experiments were recorded on a 800 MHz Varian Inova equipped with cryo-probe. The experimental parameters were as given in Table VI.2.

Table VI.2 Acquisition parameters of the Hsc70-NBD assignment experiments										
Experiment	NT	1H			13C			15N		
		Offset (ppm)	SW (Hz)	Complex points	Offset (ppm)	SW (Hz)	Complex points	Offset (ppm)	SW (Hz)	Complex points
HNCO	2	4.754	12001.20	2048	176.549	2750.086	60	118.774	2500.00	40
HN(CA)CO	1	4.725	12001.20	2048	176.549	2749.991	60	118.743	2500.00	40
HNCA	24	4.80	12001.20	832	55.15	5500.172	60	120.1	2500.00	40
HN(CO)CA	32	4.80	12001.20	832	55.15	5500.172	40	120.1	2500.00	32
HNCACB	8	4.754	12001.20	2048	46.071	15000.938	150	118.774	2500.00	40
HN(CO)CACB	8	4.754	12001.20	2048	46.071	15000.938	150	118.774	2500.00	37

The spectra were processed in NMRPipe [346], and converted to Sparky[347]. The ambiguous assignments available for this domain from Zhang and Zuiderweg [93] were loaded in the Sparky project. These assignments were checked using strip plots in Sparky, using the Sparky search routine, as well as an in-house-written search program called Sparky-helper, that can search on Ca, CB and CO frequencies simultaneously, and which checks if the 13C resonance frequencies are consistent with the amino acid residues they are assigned to.

The Sparky-assisted manual re-assignment corrected several assignments, mostly by deleting assignments of stretches of less than 3 connected residues and adding extra unassigned residues.

VI.3. SAGA program

SAGA is a new algorithm for the automatic determination of the mainchain sequential assignments of the NMR spectra of a protein written by Profs. Crippen and Zuiderweg [345]. Using the experiments shown in Table VI.1 we can obtain the assignment of various size proteins , even when their size is relatively big and the signal to noise of the data gives the potential to only half of the residues to be assigned.

SAGA is the program used in our second attempt to assign Hsc70 NBD with the use of better signal to noise data. It used the nomenclature of the Autoassign program[348] and the basic steps that it follows in order to assign the protein are the following: First the peaks are assembled from the above mentioned triple resonance experiments and they are groups into generic spin systems (GSs) that specify the chemical shifts of various nuclei of a particular residue and the sequentially previous residue. We thus end with a group of chemical shifts for this specific residue that represents the –CO-, -CA- and -CB- frequencies for the i and i-1 residues of a specific amino acid. Next the GSs are arranged into sequentially ordered groups (segments) where there is a unique match of chemical shifts between successive GSs in a segment. Those segments are placed in the amino acid sequence of the protein in a way that satisfies a scoring function for the chemical shifts of each amino acid based on the chemical shift statistics of this specific amino acids that are are taken from various previously assigned proteins. The challenges are two: a) the formation of the GSs that can be attempted with the use of various papers as mentioned in [348] and in the current version of the SAGA program is done automatically and the validity of the judgment criteria of the position of the amino acid in the sequence that are based on chemical shift statistics. For the first problem we hand peak picked and formed the GSs by hand even though in the current version of the program that does the formation of the GSs automatically only a check of the results is needed. Regarding the second problem we already had hand-assigned the protein as described in the previous paragraphs and we use the greedy algorithm to obtain more assignments from the leftover data. What we did is that we locked the hand-assigned amino acids in specific positions and the leftover peaks were optimized by the

use of the greedy for 2 hours. We obtained a higher percentage of assigned protein than the one we already had as seen in Figure VI.16 . The final assignments for Hsc70 NBD are listed in Appendix II to this thesis.

Figure VI.16. Improvement of the assignment of the Hsc70 NBD with the use of the SAGA program. White areas in the first colums identify regions for which peaks were assigned, and to which these assignents were constrained. The dark areas were not assigned. Assignments found by CASA are in the right column, together with the fraction of assignments that all agreed, and the rank number of the assignment. (From [345])

CHAPTER VII. Drug-Protein Docking

VII.1. AUTODOCK

Molecular docking is a computational procedure that attempts to predict non-covalent bonding of macromolecules or more frequently a macromolecule (receptor) and a small molecule (ligand) efficiently, starting with their unbound crystal or NMR structures, structures obtained from MD simulations, homology modeling etc. The goal is to predict the bound conformations and the binding affinity. In this thesis we attempt to dock Hsc70 NBD with the drug MKT077 using AUTODOCK 4, since it has been successfully used in a variety of protein-ligand [349, 350], protein-protein[351, 352] and DNA-ligand [350] docking studies and is currently the most cited docking program [353].

The purpose of AUTODOCK is to predict the interaction of ligands with biomacromolecular targets, which is highly needed in the discipline of computer-aided drug design [354, 355]. It is used as a test tool in order to rank trial drug geometries perhaps based on modifications of an existing lead compound or to screen entire databases of available molecules searching for novel compounds. It is composed of a suite of C programs and it is highly valuable in the field of computer aided drug design. It works with AUTOGRID and it employs a graphical user interface AutoDockTools. AutoDockTools facilitates formatting input molecule files, with a set of methods that guide the user through protonation, calculating charges, and specifying rotatable bonds in the ligand and the protein. More specifically, it allows the user to identify the active site and determine visually the volume of space searched in the docking simulation. This feature is attractive, since it allows AUTODOCK to take into account other information, such as NMR chemical shift mapping. Finally, AutoDockTools includes visual methods for clustering the results and displaying and analyzing the results of docking experiments.

More specifically the steps that AUTODOCK follows in order to perform a docking simulation are the following: a)it assigns torsional motions and docking parameters of a ligand, b) it precalculates 3D grids of interaction energy of the input ligand in the binding site and c) It performs the actual docking simulation. It can also be a valuable tool in X-ray determination process itself: given the electron density of a ligand and it can help narrow down the structural possibilities and help identify the conformation of the ligand that fits best.

Procedure. The researcher specifies a rectangular volume around the entire or part of the protein, the rotatable bonds for the substrate, and an arbitrary or random starting configuration, and the procedure produced a relatively unbiased docking.

In order to minimize the calculation time the affinity potentials for each atom type are precalculated as described by Goodford [355]. This has the advantage that the interaction energies do not have to be calculated at each step of the docking process but need only to be looked up in the respective grid map. In the autogrid procedure the protein is embedded in a three dimensional grid and a probe atom is placed at each grid point. Grid maps are being constructed. A grid map consists of a three dimensional lattice of regularly spaced points, surrounding and centered on some region of interest of the macromolecule. These grid maps are one for each atom type being probed and include the dispersion/repulsion and hydrogen bonding energies, which are only calculated for atoms within 8A from each grid point. The energy of interaction of this single atom with the protein is assigned to the grid point. This energy is determined by a set of parameters supplied for that particular atom type and is the summation over all the atoms of the macromolecule. Typical grid point spacing varies from 0.1 A to 1 A and the number of grid points is even since AUTODOCK add one more point at the center of the grid and the necessary number of points for AUTODOCK to function is an odd number. The default value is 0.375 A (a quarter of the length of the carbon-carbon single bond). Our calculations were done with grid point spacing of 0.2 A. A typical grip map is shown in Figure VII.1
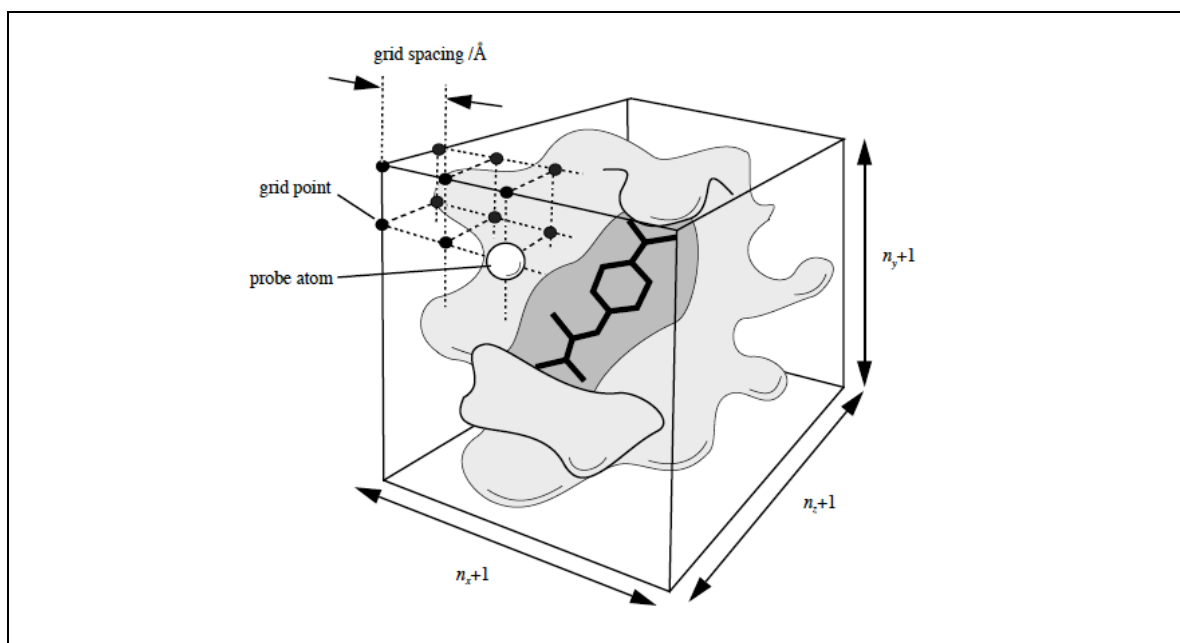
Figure VII.1 Pictorial representation of a typical grid map. The ligand can be seen in the center of the grid map, buried inside the active site of the protein. In this case the grid map encompasses the whole protein. The grid spacing is the same in all three dimensions. From [356]

Since a grid map represents the interaction energy as a function of the coordinates, their visual inspection may reveal potential unsaturated hydrogen acceptors or donors or unfavorable overlaps between the ligand and the receptor.

The docking simulation is carried out using one of a number of possible search methods. In any simulation the computational time is always an issue. The ideal simulation would be able to explore all the available degrees of freedom for the system but that would require substantial time that is not always available. The original version of AUTODOCK used a Monte Carlo simulated annealing technique for configurational exploration with rapid energy evaluation using grid based molecular affinity potentials. That is a powerful approach to the problem of docking a flexible ligand into the binding site of a static protein.

Monte Carlo simulated annealing The original search method was the metropolis algorithm also known as Monte Carlo simulated annealing [357]. The protein is

considered static and the flexible ligand performs a random walk in the space around the protein. At each step in the simulation one degree of freedom of the ligand is being changed. This results in a new configuration whose energy is evaluated by looking up the precalculated grid interaction energies. The new energy is compared to the energy of the preceding step. If it is lower it is accepted, if it is higher then it is either accepted or rejected based on a probability expression dependent on a user-defined temperature:

$$p = e^{\frac{-\Delta E}{kT}}$$

where ΔE is the size of the energy gain and k is the Boltzmann constant. In the beginning of the optimization the temperature is high and a global search is achieved since high temperature allows transitions from on energy barrier to the next. Once the global minimal barrier has been found the temperature is lowered so that the probability of transition to another well is lowered and a more refined search is achieved.

Simulated annealing allows an efficient exploration of the complex configurational space with multiple minima that is typical of a docking problem. It has been to various applications [358].

Genetic algorithms Evolutionary algorithms have been incorporated into AUTODOCK and have been applied to standard test problems [354]. Genetic algorithms represent a family of mathematical functions derived from concepts based on the language of molecular genetics. By the use of biological concepts adapted to the mathematical functions, the docking simulation mathematical background is made easy for the non-math-oriented scientific disciplines. The ligand's chromosome is defined to have seven standard genes accounting for the ligands Cartesian coordinates and four coordinates specifying its orientation. These define the well-known degrees of freedom of the ligand. The three translation genes (x,y,z) are given a random value between the minimum and maximum of the search area, the four genes describing the orientation are given a random quartenion of a unit vector and a rotation angle and the torsion angle genes are given random values between -180 and 180. The assessment is defined by the following

mathematical criterion. If $p = e^{\frac{-\Delta E}{kT}}$ is satisfied the individual survives, if it is not

fulfilled the individual becomes extinct and does not carry its genes to the next

generation.

$$n_0 = \frac{f_w - f_i}{f_w - <f>} fw \neq <f>$$

when n_o is the number of offspring to be allocated to the individual, f_i is the fitness of the

individual (energy of the ligand), f_w is the fitness of the worst individual (highest energy

individual) and $<f>$ is the mean fitness of the population. Once reproducing individuals

have been selected the next generation is created by two functions imitating biological

crossover (linear combination of functions) and mutation (variation of a parameter of the

related function) events. In the crossover event equivalent genes are swapped between a

small set of randomly picked chromosomes. Once this has been achieved a random

mutation generates mutations on genes randomly picked from a chromosome pool. While

crossover directs search between fit candidates, mutation plays a role on jumping out of

local minima. Each generation has a specific number of individuals that are being

evaluated according to eq (the above) and either survive or become extinct.

Lamarkian genetic algorithm In AUTODOCK version 3 and its further versions a new

hybrid search technique that implements an adaptive global optimizer with local search

[354] was added. This local optimization has been shown to significantly improve the

performance of the algorithm [354]. The global search method is a C++ implementation

of a modified genetic algorithm (GA), with 2-point crossover and random mutation. The

Lamarkian (discredited) part of the name of this algorithm implies that the adaptation of

an individual to its environment can be inherited by its offspring. Translational step sizes

of 0.2A along with orientation and torsional step sizes of 5° are being applied to a user

defined proportion of each new generation, followed by an energy evaluation of the new

conformation. If the new conformation is of lower energy then the procedure is repeated

until the energy increases or the specified number of steps has been performed as seen in

Fig. VII.2.
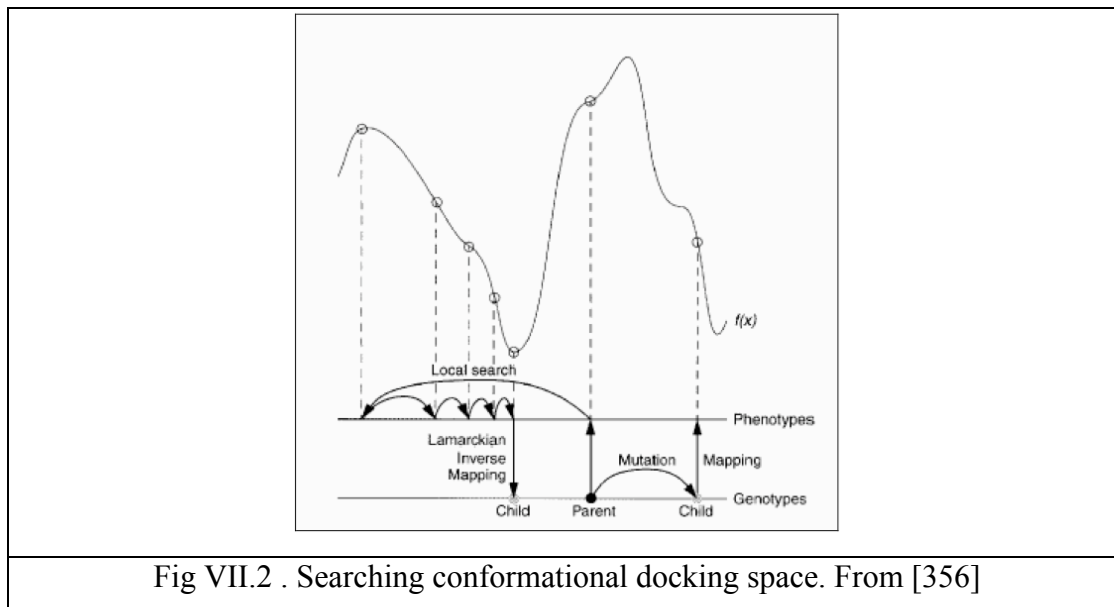
Fig VII.2 . Searching conformational docking space. From [356]

Energy assessment within AUTODOCK. AUTODOCK uses a variation of the AMBER95 force field with terms empirically determined by linear regression analysis from a set of protein-ligand complexes with known binding constants. The Gibbs free energy is determined by

$$\Delta G = \Delta G_{vdv} + \Delta G_{hbond} + \Delta G_{elec} + \Delta G_{conf} + \Delta G_{tor} + \Delta G_{sol}$$

These sub terms represent the dispersion/repulsion, hydrogen bonding, electrostatic interactions, deviation from covalent geometry, internal ligand-torsional constraints and de-solvation effects. The standard Lennard-Jones 12-6 potential is used for the Van der Waals forces. The conf term measures the unfavorable entropy of a ligand binding due to the restriction of conformational degrees of freedom, using a measure that is proportional to the number of sp^3 bonds in the ligand.

The method has been calibrated on a set of 188 diverse protein-ligand complexes of known structure and binding energy, showing a standard error of 2-3 Kcal/mol in prediction of the binding free energy in cross validation studies. Energy evaluations are performed as already mentioned inside the grid box.

VII.2 AUTODOCK and NMR

Even though programs specific for NMR chemical shift perturbations such as LIGDOCK and HADDOCK [359] exist in the literature, papers that combine NMR chemical shift perturbations and AUTODOCK also exist [360]. AUTODOCK as seen in the literature [361] is the best program for docking simulations of a single ligand and as seen in our results the experiments are in agreement with the simulations. It is mentioned that it outperforms DOCK, FlexX and GOLD in predicting the correct binding modes that appear in the X-Ray structures of protein ligand complexes [362]. The drawback of AUTODOCK's high precision in calculating docked structures and the cost the scoring function's high accuracy is the actual simulation total time but that was not an issue for us. AUTODOCK's Lamarckian genetic algorithm together with an empirical free energy correlation calibrated with known binding constants makes AUTODOCK a good toolbox for docking.

There are many versions of AUTODOCK but we chose to use AUTODOCK4 [360]. The advantage of this version is that it is able to incorporate a couple of degrees of freedom flexibility to the receptor. In our case we chose the grid-based method in conjunction with various AMBER structures of the receptor while keeping the ligand flexible because as mentioned in the literature [363] the success of the flexible sidechain method with small molecules is lower when compared to the grid based method (It failed more than half of the cases). The literature [363] also mentions that AUTODOCK4 has a very high rate of success for complexes with 10 or fewer degrees of freedom and that is our case.

CHAPTER VIII.

Allosteric drugs: the interaction of anti-tumor compound MKT-077 with human Hsp70 chaperones

Aikaterini Rousaki, Yoshi Miyata, Umesh K. Jinwal, Chad A. Dickey,

Jason E. Gestwicki and Erik R.P. Zuiderweg

Submitted to J. Mol. Biol.

VIII.1 Abstract

The Hsp70 chaperones (Heat shock protein 70 kDa) are key to cellular protein homeostatis. However, they also have the ability to inhibit tumor apoptosis, and contribute to aberrant accumulation of hyperphosphorylated tau in neuronal cells affected by tauopathies, including Alzheimer's disease. Hence, Hsp70 are increasingly been identified as targets for therapeutic intervention in these widely abundant diseases. Hsp70 proteins are allosteric machines and offer besides classical active site targets, also opportunities to target the mechanism of allostery. In this work, it is demonstrated that the action of the potent anti-cancer compound MKT-077, is through differential interaction with the Hsp70 allosteric states. MKT-077 (1-ethyl-2-[[3-ethyl-5-(3-methylbenzothiazolin-2-yliden)]-4- oxothiazolidin-2-ylidenemethyl] pyridinium chloride) is therefore an "allosteric drug". Using NMR spectroscopy, the compound's binding site on human HSPA8 (Hsc70) is identified. The binding pose is obtained from NMR-restrained docking calculations, subsequently scored by molecular dynamics-based energy and solvation computations. Suggestions for improvement of the compound's properties are made on the basis of the binding location and pose.

VIII.2 Introduction

The Hsp70 chaperones (Heat shock protein 70 kDa, systematic name: HSPA) assist in protein folding, protein refolding, protein transport and protein targetting[7]. The human genome contains 13 HSPA genes which encode 12 distinct proteins[364]. HspA5 (Bip), HSPA8 (Hsc70) and HSPA9 (mt-Hsp70 or Mortalin) are expressed constitutively. They are resident in the ER, cytosol and mitochondria, respectively. Cells respond to stress such as, but not limited to, elevated temperature, by upregulating the expression of the other HSPAs, which help reverse the stress-induced protein misfolding. The chaperones carry this out by unfolding the misfolded proteins in ATP-driven cycles of binding and release[81].

HSPAs are significantly up-regulated in tumors[365], and are required for the survival of these cells[231]'[232, 233]. Knockdown of HSPA2 by siRNA inhibits human tumor growth in nude mice[366]. Selective HSPA1 knockdown induces apoptosis in pancreatic cancer cells[367]. Enhanced expression of HSPAs in tumor cells is likely caused by conditions which mimic stress[238, 239]. The HSPAs are thought to attempt to neutralize the conformational changes in mutated proteins[368]'[369] which are common in tumorogenic cells. In addition, HSPAs are found to specifically inhibit cell death pathways[239, 245-249]. Lastly, HSPA9 may directly inactivate p53 tumor suppressor protein[244, 370]. Hence, inhibition of HSPA has been recognized as a promising avenue for the prevention or therapy of a wide variety of cancers.

HSPAs are also involved in several CNS disorders. Diseases such as Alzheimer's, Pick's disease, progressive supranuclear palsy, corticobasal degeneration and argyrophilic grain disease are characterized by the aberrant accumulation of hyperphosphorylated tau, called tau-tangles[137, 142, 160, 371]. HSPAs participate in the clearance of tau-tangles through a mechanism that is not well understood as of yet[372]. Recently, we found that inhibitors of HSPA8 led to a rapid increase in tau ubiquitination and proteasome-dependent degradation, in tau-overexpressing HeLa cells[373]. Clearance of tau-tangles is being recognized as therapeutic to Alzheimer-affected neuronal cells[374]. Hence, inhibition of HSPA is also a promising avenue for the prevention or therapy of CNS disorders[148].

HSPA proteins are becoming recognized as very druggable[375] because they offer so many opportunities for interference. HSPA proteins consist of a nucleotide-binding domain[376] (NBD) which competitively binds ATP and ADP[39], and substrate-binding domain (SBD) which harbors the hydrophobic substrate-binding cleft[30]. Compounds that compete for binding in either of these sites would modulate HSPA function. Examples of such compounds are adenosine analogs dibenzyl-8-aminoadenosine[377, 378] and VER-155008[377], which compete for the ATP binding site. Compounds that modulate HSPAs by competing with substrate binding

such as Gentamycin[379], geranylgeranylacetone[380] and several peptidomimetics[381] have been described as well.

In addition, HSPA are regulated by the DnaJ co-chaperone family and by a diverse set of nucleotide exchange factors[382]. They also interact with HIP[84], HOP[383] and CHIP[118], and some specialized factors such as ZIM (for HSPA9)[384]. Competing with or enhancing the interaction of these ancillary proteins with HSPA may also be an avenue for HSPA modulation. One of the first HSPA inhibitors, 15-deoxyspergualin, was long known to bind to the C-terminal EEVD sequence[385, 386]. This C-terminus is now also known to be the CHIP-HSPA interaction site[387], so likely 15-deoxyspergualin functions by competition with CHIP. Recently, we discovered an inhibitor of the bacterial HSPA orthologue DnaK, that most likely functions by competing with the J-HSPA protein interaction[388] .

Finally, HSPA are allosteric proteins. Substrate binding enhances ATP hydrolysis while ATP binding stimulates substrate release. Recently, much insight in the allosteric mechanism has been gained from comparing the structural properties of HSPA in the ADP-state, bound to substrate (referred to as HSPA-ADP-SUB), and in the HSPA-ATP-APO state. HSPA-ADP-SUB is best described as a dynamic ensemble in which NBD and SBD are loosely tethered[26, 89], while the NBD and SBD in HSPA-ATP-APO are docked[89]. In the HSPA-ADP-SUB state, a protective LID docks to the SBD[41], while the LID releases in the HSPA-ATP-APO state. The subdomains of the NBD rearrange and reorient between ADP and ATP state[27]. A surface cleft on the NBD opens and closes between these states[40,][27]. Compounds that can recognize such allosteric differences and perturb the allosteric equilibrium between the states should also modulate HSPA function.
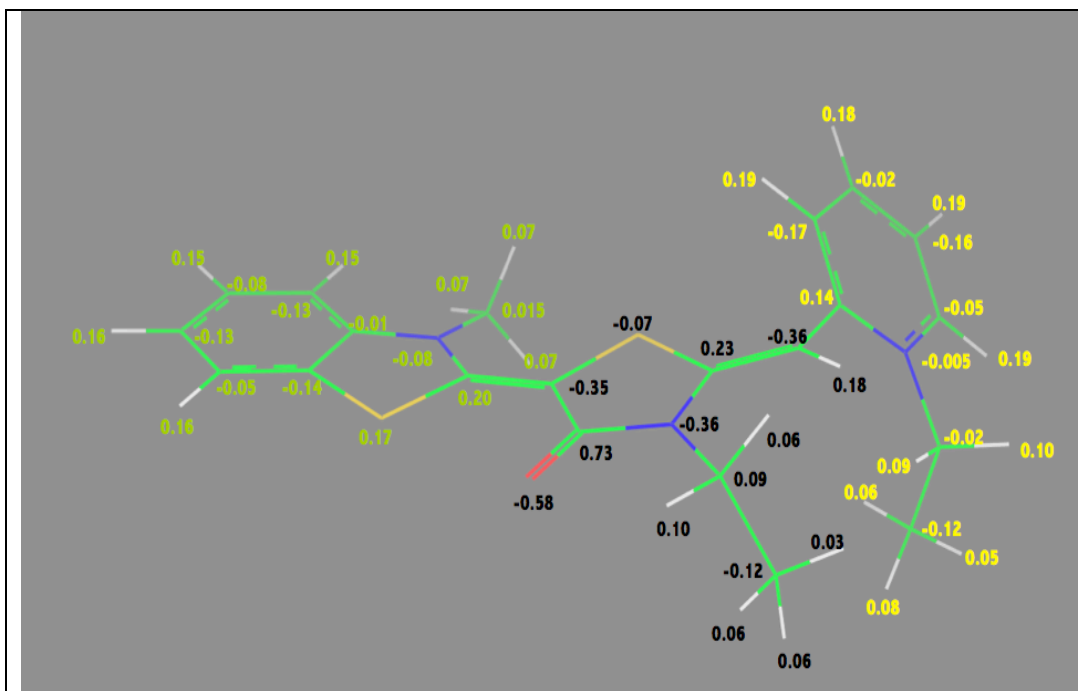
Figure VIII.1. The quantum-mechanically optimized structure of MKT-077. Nitrogen is in blue, sulfur in yellow, oxygen in red. Double-bond assignments were made based on quantum mechanical calculations. AM1-BCC charges[389] are shown. $\sum Q_{green}$=+0.56; $\sum Q_{black}$=-0.29; $\sum Q_{yellow}$=+0.73

(see Methods for details)

Recently, we identified a flavonoid called myricetin, which binds to the Hsp70 of *E. coli*, DnaK, at an non-canonical site on he nucleotide binding domain. This compound blocks the binding of DnaK to DnaJ.[390] It is the first example of an allosteric HSPA drug.

Taken together, there are many opportunities for the manipulation of HSPA function. In principle, the protein could be targeted by a combination of compounds that are individually not very potent, but act in synergy. In analogy to tumor irradiation therapy, using several low-intensity beams reinforcing each other at the target, a molecular target-specific combination therapy may also have reduced toxicity. In addition, the potential of addressing several different HSPA functions with small compounds may provide an avenue to HSPA-directed personalized medicine.

In the current work, we investigate the interaction of a well-known HSPA interacting compound, MKT-077. MKT-077 is known to interact with HSPA9[313] and HSPA8[391]. We show here that MKT-077 affects HSPA8 function through differential interaction with HSPA's different allosteric states. Hence, MKT-077 is found to be an "allosteric drug". MKT-077 is a

Fuji dye compound with the systematic name (1-ethyl-2-[[3-ethyl-5-(3-methylbenzothiazolin-2-yliden)]-4-oxothiazolidin-2-ylidenemethyl] pyridinium chloride) (see Figure VIII.1). MKT-077 has an IC_{50} of 0.35-1.2 μM against several human cancer cell lines[392]. The IC_{50} of MKT-077 towards these tumor cell lines is more than 100 times lower than the IC_{50} against healthy cell lines. Because of these very favorable properties, MKT-077 has been evaluated as cancer chemotherapeutic in a Phase I trial [393]. The trial was aborted because of renal toxicity of MKT-077. Despite this finding, interest in MKT-077 and its derivatives have remained strong [394] [395, 396].

As mentioned above, we recently found that inhibitors of HSPA8 also lead to a rapid increase in tau ubiquitination and proteasome-dependent degradation, in tau-overexpressing HeLa cells[373]. We show here that MKT-077 also enhances tau clearance, which makes the compound also of interest for therapy of CNS disorders such as Alzheimer's. We determine by NMR the binding site of MKT-077 to the ADP-state of HSPA8 (Hsc70). The drug locates itself in a negatively charged pocket close to, but not identical to, the nucleotide binding site. The identification of its binding pocket and binding pose should allow for the design of more potent, more selective, and less toxic MKT-077 derivatives.

VIII.3 Results.

Inhibition of the HSPA8 by small molecules such as methylene blue or azure c causes clearance of tau-tangles in transfected HeLa cells[373]. It was hypothesized that the compounds interfere with the dissociation of HSPA8-tau complexes, leading to clearance through the ubiquitin-proteasome system[373]. Based on this, we wondered whether the known HSPA9[313] and HSPA8[391] inhibitor, MKT-077, would also lead to clearance of hyper-phosphorylated tau. Figure VIII.2 shows that such indeed is the case, suggesting that MKT-077 also interacts and interferes with the function of HSPA8 in these cells. Inhibition of HSPA8 with MKT-077 therefore is a potential avenue for therapeutic intervention with tauopathic diseases such as Alzheimer's.

Figure VIII.2. MKT-077 promotes the clearance of hyperphosphorylated tau (top line) in engineered HeLaC3 cells in a dose-dependent way (24-hour incubations).
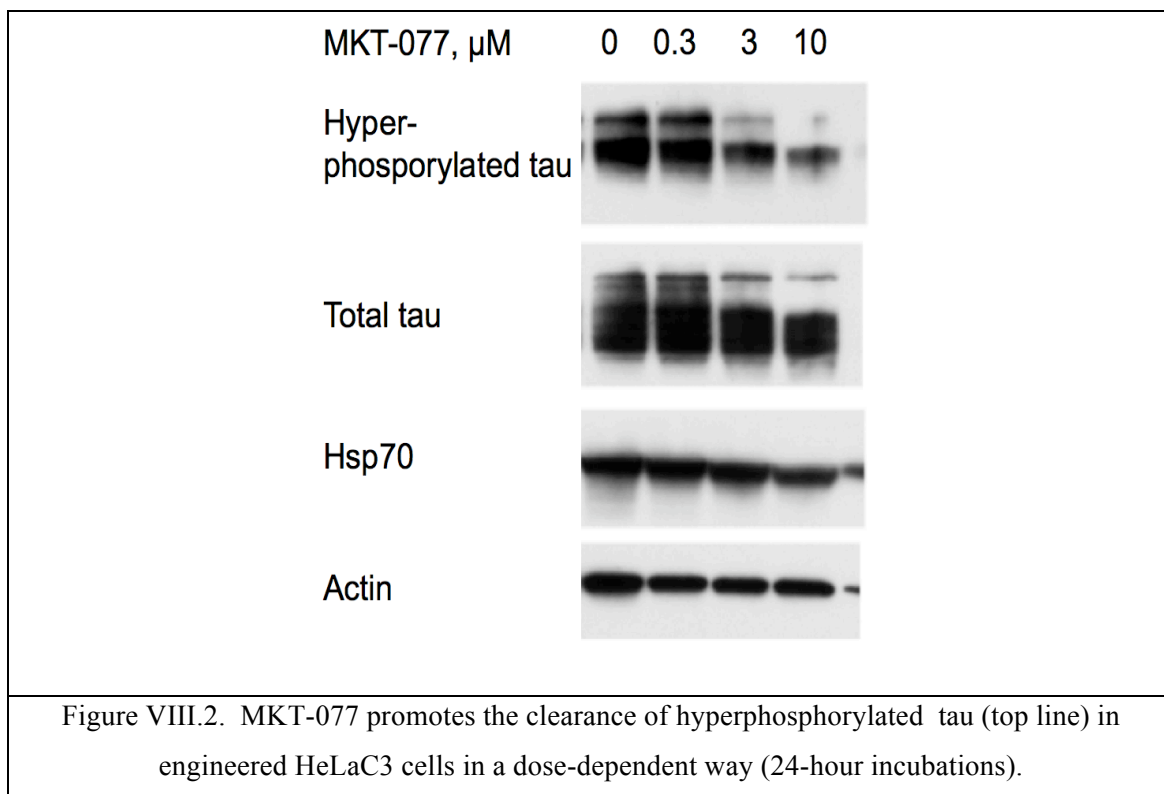
In recent work, we have used NMR spectroscopy to locate the binding sites of several compounds to the bacterial Hsp70 chaperone, DnaK[388, 390, 397]. Here we use the same approach, combined with extensive computer modeling and molecular dynamics calculations, to decipher the binding location, pose and mechanism of MKT-077 with the nucleotide-binding domain (NBD) of human HSPA8.

The ^{15}N-^{1}H TROSY NMR spectrum of HSPA8 NBD in the ADP state is shown in the supplemental material. Many of the resonances in the spectrum of this 383-residue protein have been assigned by hand[93] and double-checked by a computer algorithm[345]. Enlargements of the sections of the spectrum are shown in Figure VIII.3. A select number of resonances show gradual chemical shift changes upon addition of MKT-077 up to a molar ratio of 1:1 (using a concentrated sample of ^{2}H,^{15}N,^{13}C–labeled HSPA8-NBD) after which the chemical shifts do no change any more (using a more dilute sample of ^{15}N–labeled HSPA8-NBD). The observed changes in chemical shifts for these two experiments are shown on the amino-acid sequence in the supplemental material.

Figures VIII.4a and VIII.4b show the composite chemical shifts observed depicted on a surface rendition of HSPA8 NBD. The majority of the shift changes take place in an area which turns out to be an otherwise unoccupied negatively charged pocket located on the interface of subdomains IA and IIA. As outlined in the introduction, HSPAs are allosteric proteins, which show global conformational and dynamical changes on the NBD between the ADP and ATP state[93, 95]. Hence, we wondered if MKT-077 would also bind to the ATP-state of the NBD. Figures VIII.4c and d shows a similar display of changes in the TROSY spectrum of HSPA8 NBD in the AMP-PNP state. Significantly, none of the residues affected by MKT-077 binding in the ADP state are affected in AMPPNP state. We conclude that MKT-077 does not bind to Hsc70 NBD in the AMP-PNP state. We also monitored MKT-077 binding to HSPA8 NBD in the true ATP state. No chemical shift changes in the (largely unassigned) NMR spectrum could be discerned, indicating that MKT-077 does not bind to the ATP-state (not shown), indicating that the results for the AMP-PNP state are representative for the ATP state. We also monitored MKT-077 binding to HSPA8 NBD in the apo state. Many changes occurred in the NMR spectrum (not shown) but those were largely uninterpretable because a lack of NMR assignments for this state. Nevertheless, we may conclude that MKT-077 also binds to the apo-state.

The MKT-077-induced changes to the spectrum of HSPA8 NBD in the ADP state are in the fast-exchange limit (see Figure 3), with little or no line broadening. The largest shifts in the spectrum are approximately 20 Hz, which sets a lower limit of 100 s^{-1} for MKT-077's off-rate. This sets the limit $K_D > 1$ μM, when assuming an upper limit on the diffusion-controlled on-rate of 10^8 M^{-1}s^{-1}. The shifts are linear over the titration interval (see Figure VIII.5), and saturate abruptly at equivalence (see Figure VIII.3a and VIII.3c). This is compatible with a K_D that is at least order of magnitude smaller than the protein concentration; with Hsc70 concentration of 200 uM, we obtain $K_D < 10$ uM. In combination, thus, we estimate from the NMR titration

$1 \mu M < K_D < 10 \mu M$. Attempts to determine the binding affinity of MKT-077 to Hsc70 by ITC have not been successful.

Figure VIII.3. Details of some the chemical shift changes in the TROSY spectrum of HSPA8 NBD upon addition of MKT-077. Panels a and c: Blue, no MKT-077; Red, MKT-077: HSPA8 =1:1; Black, MKT-077: HSPA8=2:1 using a sample of 80 uM ^{15}N-labeled HSPA8-NBD in the ADP state.

Ratios MKT-077/HSPA8 for all other panels: Blue, no MKT-077; Green, 0.25:1; Yellow, 0.5:1; Red, 0.75:1; Black, 1:1. For these, a sample of 260 uM ^{15}N, ^{2}H-labeled HSPA8-NBD in the ADP state was used.

HSPA8 NBD is a flexible molecule, which can rotate its subunits with respect to each other, especially in the ADP and apo states[93, 95]. Hence, chemical shift changes at the interface between sub-domains should be eyed with some skepticism. Indeed, there is an area of chemical shift changes (residues 140-144; see Fig VIII.2 of supplemental material) which is not contiguous with the primary shift area shown in Figure VIII.4a. The former area is completely buried, and the shifts must be caused by conformational changes due to MKT-077 binding at the primary and solvent-accessible pocket comprised by the residues shown in figure VIII.5.

Figure VIII.4. Mapping of the chemical shift changes of MKT-077 on the structure of HSPA8 NBD (3HSC.pdb). Panels a and b: ADP state. Left and right images are rotated 180 degrees along the vertical axis with respect to each other. Color coding: Red, sites detected using 250 uM ^{15}N-^{2}H labeled HSPA8-NBD; Green, no changes; grey, no assignments and cannot be decided. Cyan, approximate position of MKT-077 as determined using AUTODOCK. Panels c and d: AMPPNP state. Panels and color scheme as above.. Pymol was used[398].

The entrance to pocket located on the interface of subdomains IA and IIA is hydrophobic, while the interior is negatively charged due to the presence of the sidechains of Glu175, Asp199 and Asp206. As matter of fact, the electrostatic potential of the entire binding area is strongly negative (see Figure VIII.6). Hence, the chemistry of the binding area complements the chemical properties of MKT-077, which is positively charged, very well (see Fig VIII.1). In support of the hypothesis that electrostatics is a important contributor to the binding energy of MKT-077 is the fact that an uncharged MKT-077 derivative does not perturb the NMR spectrum of HSPA8 (results not shown).

Together, the evidence strongly suggests that MKT-077 binds preferentially to the ADP- and not the ATP-bound state of HSPA8. To test whether this compound could *stabilize* the ADP-like conformation, we performed limited proteolysis experiments. It has been previously shown that trypsin treatment of human Hsc70 yields digestion patterns diagnostic of the chaperone's nucleotide state[87]. Consistent with those reports, we confirmed that Hsc70 saturated with ATP was primarily cleaved into three high molecular weight bands, including prominent bands at approximately 69 kDa (band 1) and 66 kDa (band 2) (Figure VIII.7). Conversely, treatment with ADP strongly favors band 2. Addition of the J-domain of prokaryotic DnaJ, which stimulates ATP turnover in Hsc70, converted the ATP-like pattern to an ADP-like pattern. Next, we tested whether MKT-077 could stabilize the ADP-like configuration. Addition of MKT-077 (200 μM) largely blocked formation of band 1, consistent with the NMR data that this compound binds preferentially to the ADP-bound state of Hsc70.

Figure VIII.5. Fractional shifts upon addition of MKT-077 in the ^{15}N-^{2}H-labeled HSPA8. Cyan: T222; Red: A223; Blue: D225; Green H227; Purple, L228; Black, Average. For each resonance, the shift at molar ratio 0.5 was defined as 50% completed.
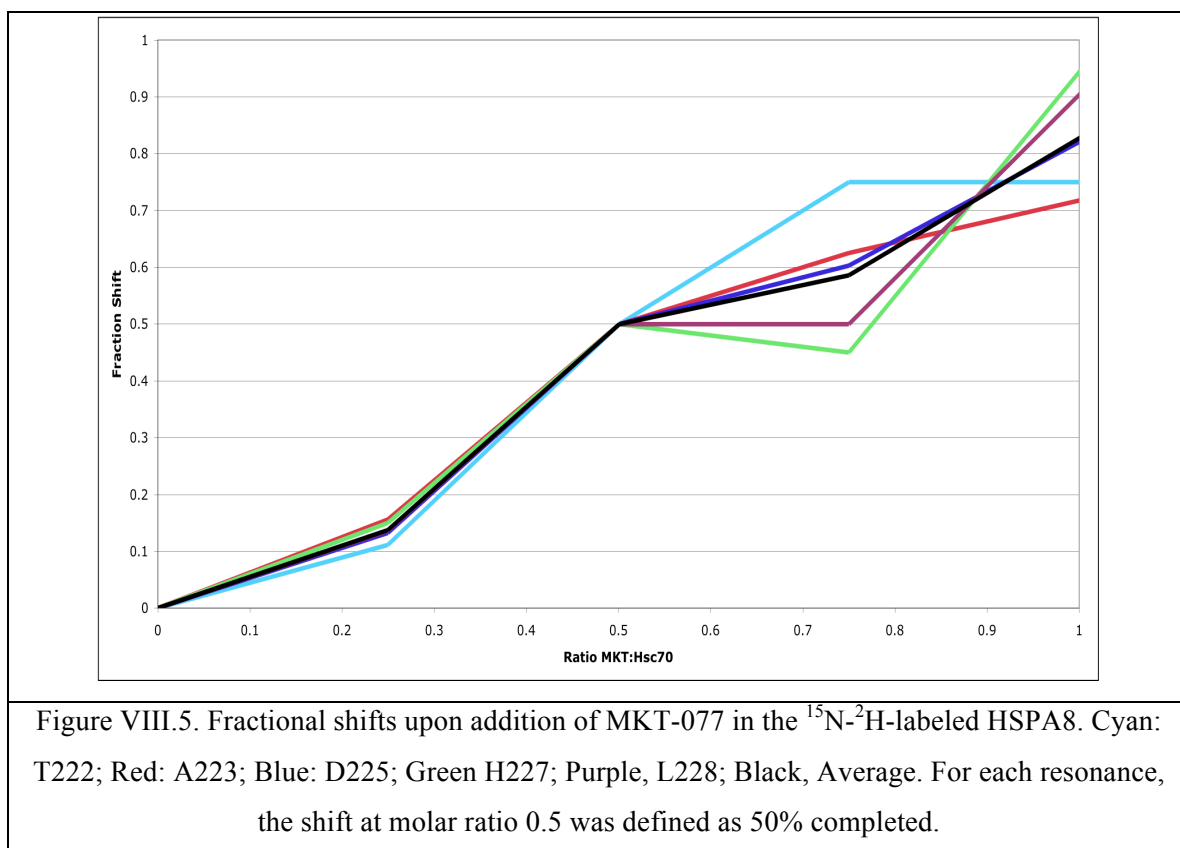
VIII.4 Discussion.

Our key finding is that MKT-077 binds to the ADP state of HSPA8, but not to the ATP state, which are the two most extreme allosteric states that an HSPA can adopt. The compound does not bind to the natural ATP binding site. This qualifies MKT-077 as an allosteric effector, acting not unlike 2,3-DPG that modulates hemoglobin function by binding to a non-heme site that is exposed in the T-state and closed in the R-state[399]. Based on these properties, MKT-077 must be characterized as an allosteric drug. We find that the compound binds to an area which is at the interface of the four HSPA NBD

Figure VIII.6 Energy diagram of Hsc70 NBD as computed by PYMOL.
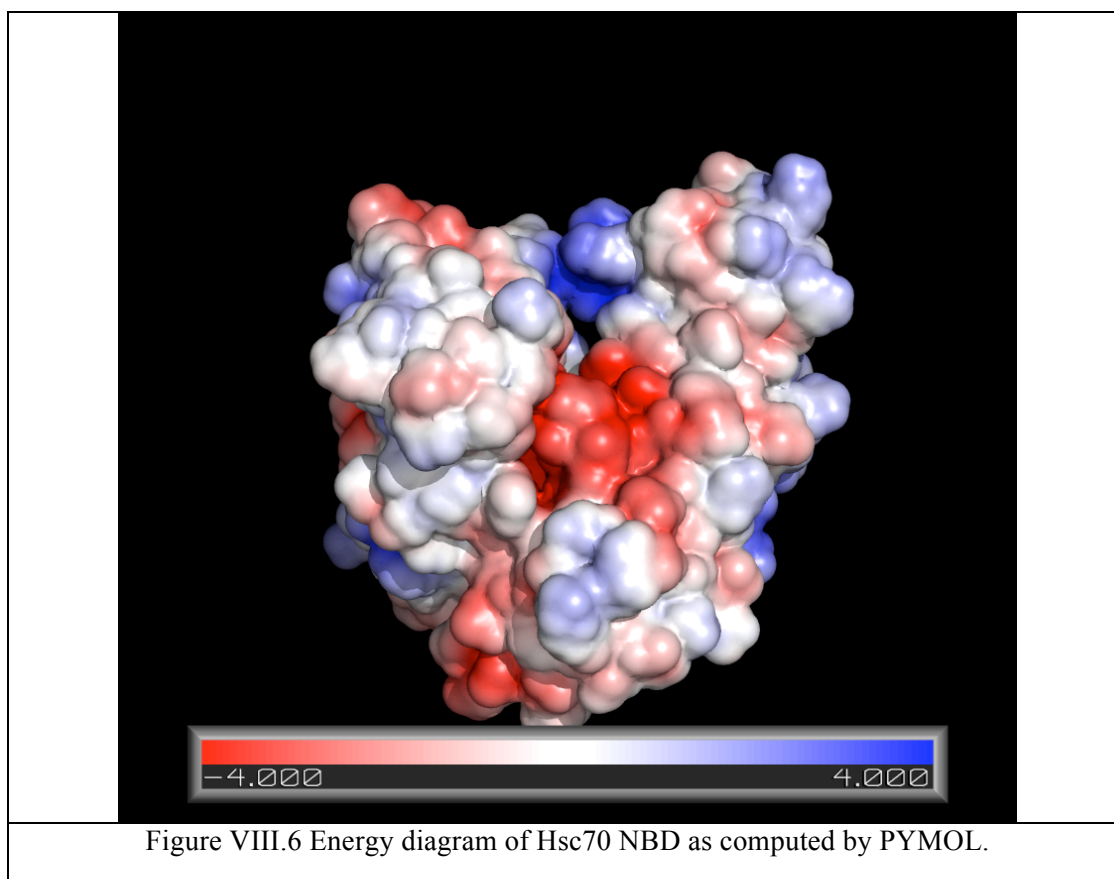
subdomains. We have recently identified that the HSPA NBD subdomains change their relative orientations between the different allosteric states[95] (see Fig VIII.8). In detail, it was found (a) that the relative orientations of the subdomains of the HSPA ortholog DnaK of *Thermos thermophilus* in the ADP state resemble, in solution, those of HSPA8 complexed with nucleotide exchange factor as seen in a crystal, and (b) that the relative orientations of the subdomains of the HSPA ortholog DnaK of *Thermos thermophilus* in the AMP-PnP state resemble, in solution, those of HSPA8s NBD in a crystal, *irrespective* of the latter's nucleotide state. We defined the

130

ATP state as the "closed" state and the ADP state as the "open" state. In this context, the binding of MKT-077 to the ADP (open) state and not to the ATP (closed) state makes perfect sense: the binding pocket is (more) accessible in the ADP state but (less) not in the ATP state (see Figure VIII.8).
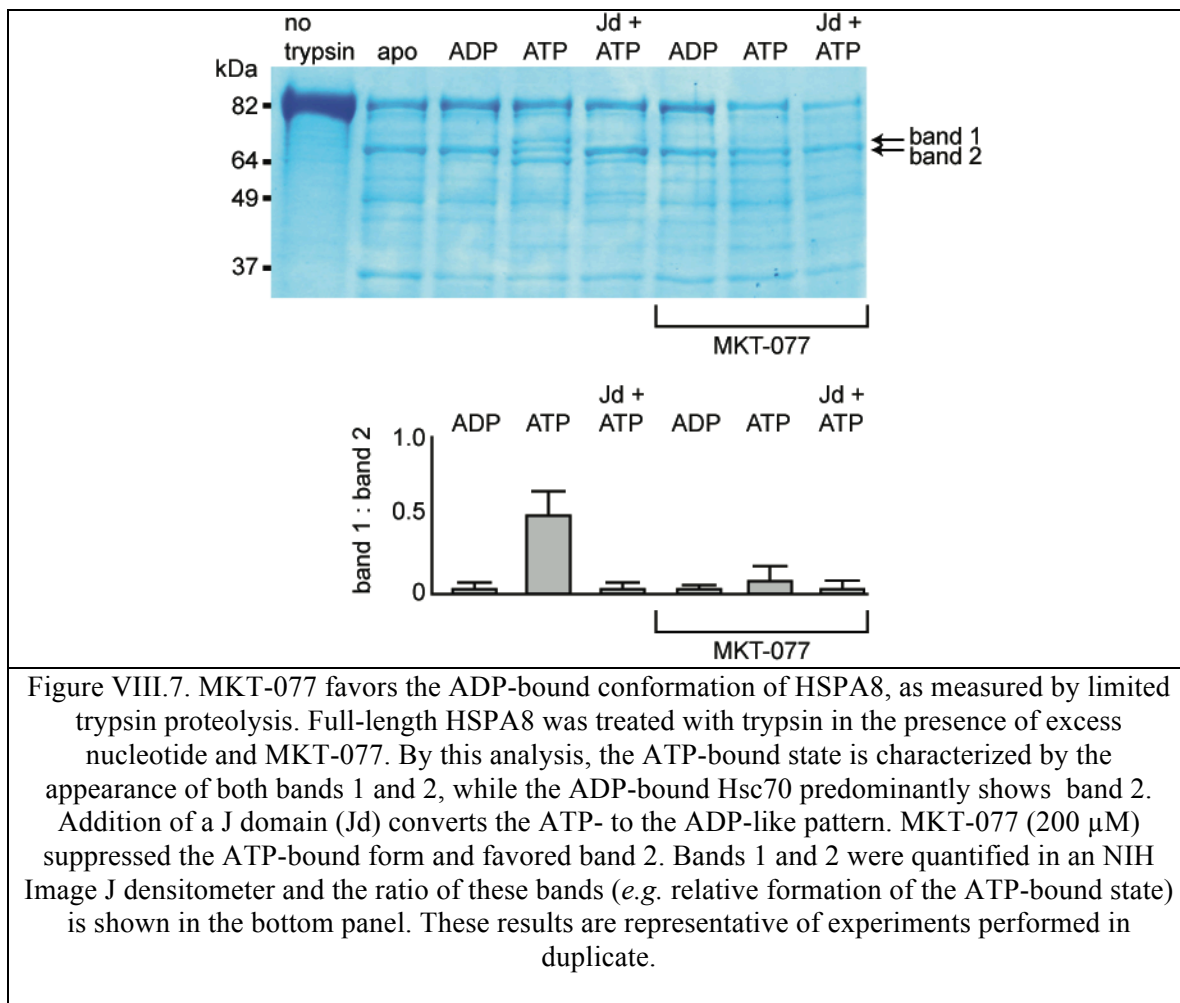
Figure VIII.7. MKT-077 favors the ADP-bound conformation of HSPA8, as measured by limited trypsin proteolysis. Full-length HSPA8 was treated with trypsin in the presence of excess nucleotide and MKT-077. By this analysis, the ATP-bound state is characterized by the appearance of both bands 1 and 2, while the ADP-bound Hsc70 predominantly shows band 2. Addition of a J domain (Jd) converts the ATP- to the ADP-like pattern. MKT-077 (200 μM) suppressed the ATP-bound form and favored band 2. Bands 1 and 2 were quantified in an NIH Image J densitometer and the ratio of these bands (*e.g.* relative formation of the ATP-bound state) is shown in the bottom panel. These results are representative of experiments performed in duplicate.

These observations lead us to formulate the following hypothesis of the mechanism of action of MKT-077 (see Figure 9). The figure summarizes a large body of structural, dynamical and interaction characteristics for the HSPA8, based on the work of our and other labs, especially those of L. Gierasch and M. Mayer/B.Bukau. Briefly, in the ADP-substrate-bound state, the nucleotide binding cleft is dynamically opening and closing, while the substrate binding domain is loosely tethered. The lid is docked to the substrate domain. In the ATP-apo state, the nucleotide binding cleft is closed, while the substrate binding domain is docked (through a

hydrophobic linker in an opened hydrophobic cleft on the NBD). In this state, the lid is dynamically tethered.

In the current work, we observed that MKT-077 selectively binds to the ADP-allosteric state. By doing so, it likely stalls the HSPA protein-refolding cycle in that state. As a consequence, the HSPA cannot release its substrate. In the context of tauopathies, one may hypothesize that the lifetime of the tau-HSPA8 complex becomes long enough to have an increased chance to engage in a triple complex with CHIP (C-terminal Hsp70 Interacting Protein). CHIP is an ubiquitin ligase[267], which promotes the ubiquitination of the HSPA8-MKT trapped tau, and clearance by the proteasome.

Interference of MKT-077 with HSPA's substrate binding and release cycle should also directly interfere with HSPA's abilities to promote survival of tumor cells.
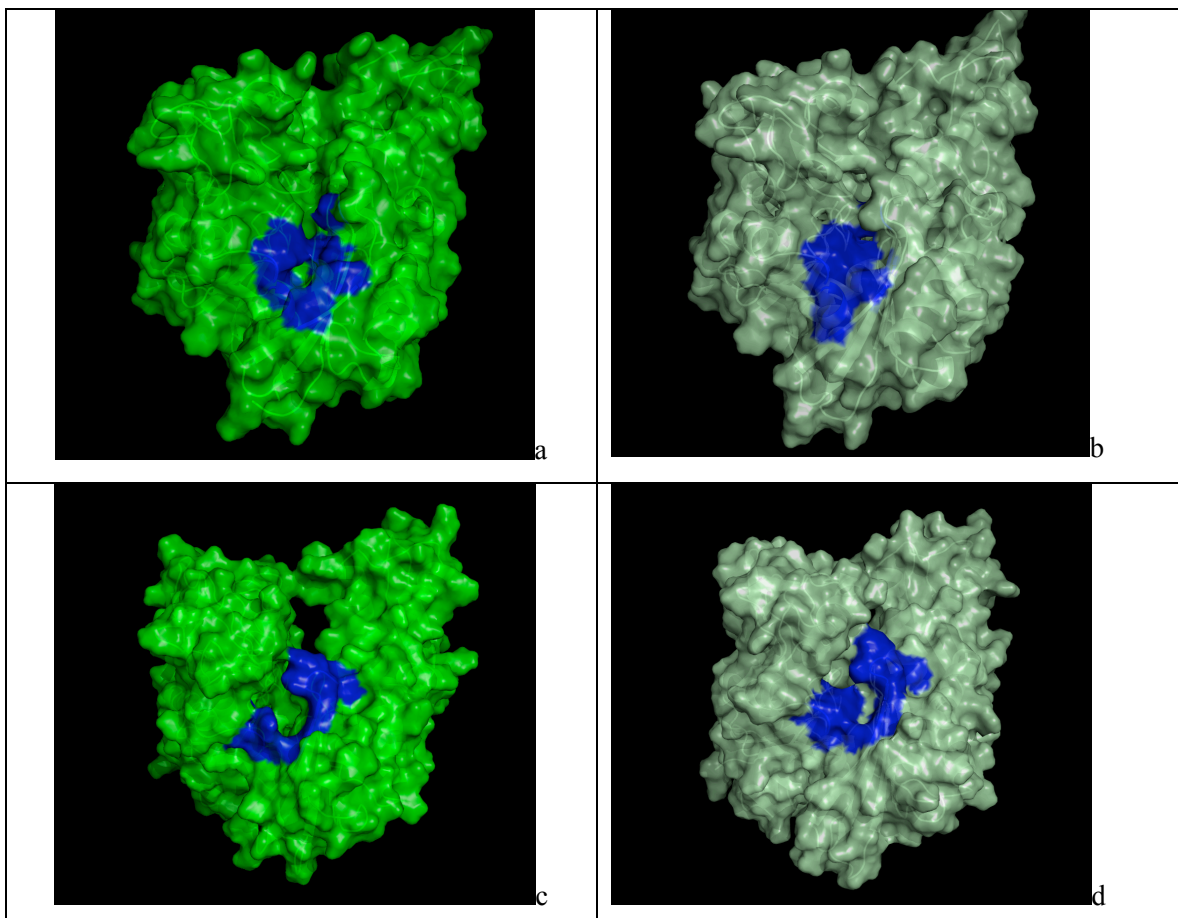
Figure VIII.8. ATP/ADP closed and open states respectively.Top: Changes in the overall architecture of the NBD of DnaK of Thermos Thermophilius in solution. A: The open ADP state; B: the closed AMPPNP (ATP) state. The MKT contact residues of Hsc70 NBD are projected on these conformations in blue. Based on Bhattacharya et al.

Bottom: Changes in the overall architecture of the NBD of human HSC70 in the crystal. C: The (equilibrated) crystal structure of Human Hsc70 NBD.ADP in complex with yeast Hsp110 (3C7N) resembles the solution open state. D: The (equilibrated) crystal structure of isolated Hsc70 NBD.ADP resembles the solution closed (ATP) state. The figure was generated in Pymol[398].

We used AUTODOCK[400] to obtain insight in the MKT-077 binding geometry at this pocket. Based on the information that MKT-077 only binds to the ADP state, we used the crystal structure of HSPA8 NBD[116] in complex with Hsp110 (3C7N) for the protein coordinates (see figure VIII.8c). The selection of this particular HSPA-NEF complex (there are 5 different ones in the Protein Data Bank) is based on the fact that it is the only one that contains ADP. The crystal coordinates of the NBD were minimized, equilibrated and relaxed to 300 K using a Amber11

[401] molecular dynamics protocol (see Methods).   The coordinates and degrees of freedom for MKT-077 were optimized and determined from quantum mechanical calculations.

Figure VIII.9. Cartoon showing the properties of HSPA in the ADP state (top) and ATP state (bottom). We hypothesize that MKT-077 stalls HSPA8 in the ADP state.
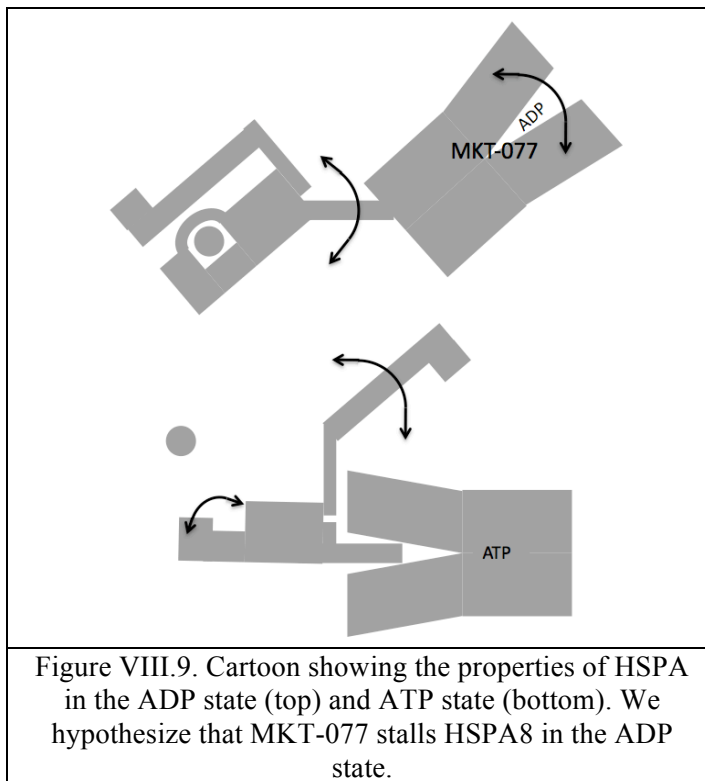
We used an AUTODOCK search box localized around the NMR-determined MKT-077 binding site. The results are shown in Figure VIII.10a. On the one hand, there is satisfactory agreement between the AUTODOCK results and the NMR data: all good docks are located in the area identified by NMR chemical shifts. On the other hand, the AUTODOCK computations yield a wide variety of possible binding poses with AUTODOCK energies ranging between 4 and 7 kCal/M. The electrostatic interaction does not exceed 0.4 kCal/M in any of these calculations, which we feel is at odds with the prominent role of electrostatics in MKT-077 action. After culling those dockings which have positive MKT charges contacting positive protein residues, we subdivide the dockings in four families as shown in Figures VIII.10 C-F.
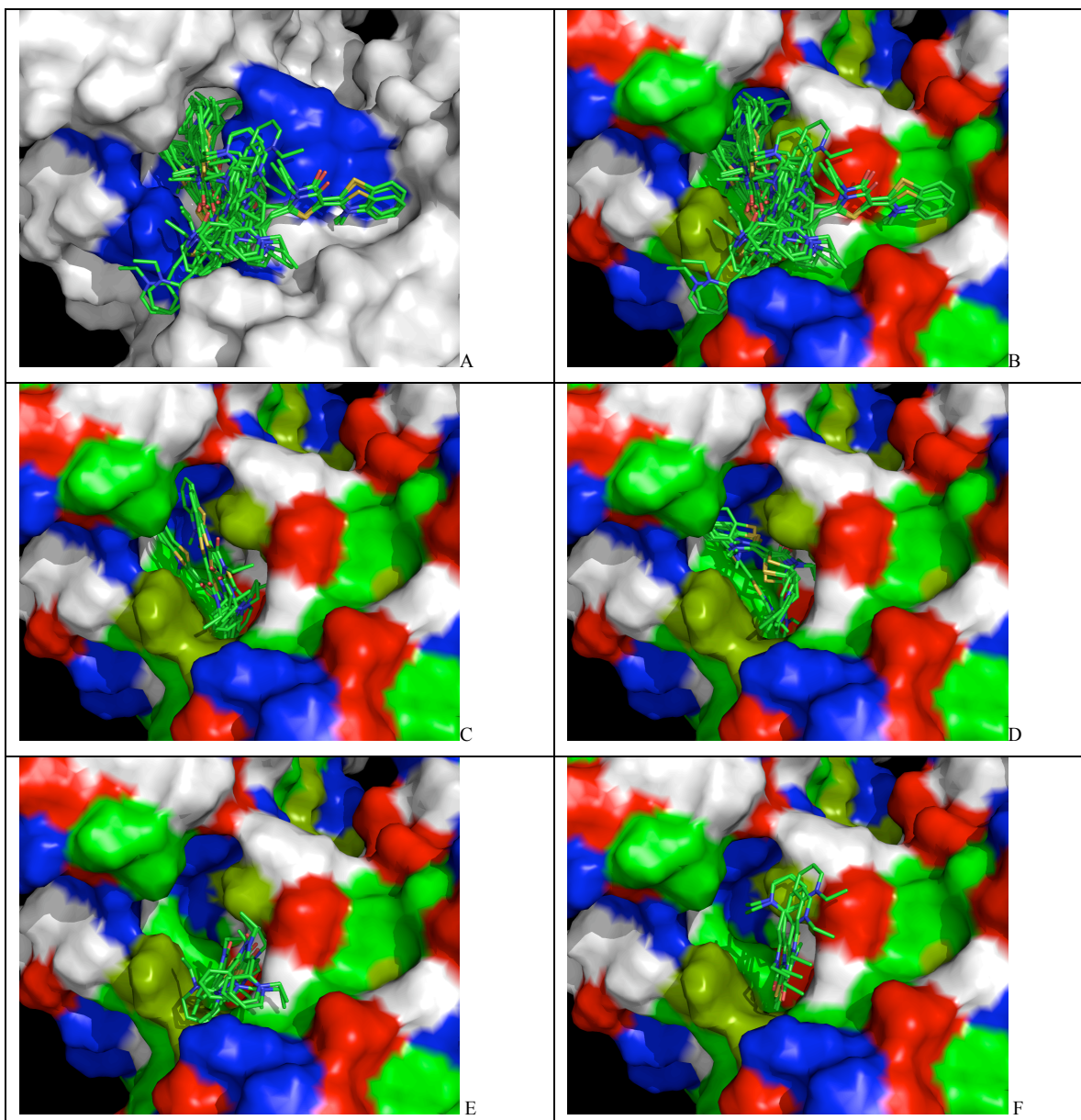
Figure VIII.10. Results of AUTODOCK. The search box was restricted to the binding area as determined by the NMR chemical shift perturbations. Panel A: all dockings ranging from 4.5 – 7.0 Kcal/mole in relation to the NMR shifts in blue. Panel B, the same ensemble in relation to the chemical properties of the protein (green: A,C,F,I,L,M,P,V,W; dark green: T,Y; blue: H,K,R; red:D,E; white:G,N,Q,S). Panel C, a family of feasible dockings with an energy of 7.03 kCal/M for its best member. Panel D, a family of feasible dockings with an energy of 6.32 kCal/M for its best member. Panel E, a family of feasible dockings with an energy of 5.36 kCal/M for its best member. Panel F, a family of feasible dockings with an energy of 5.25 kCal/M for its best member. Also see Table 2. The figures were generated in Pymol[398].

All docked families are in close vicinity / contact with the residues that show chemical shift perturbations. All of them are also close to Glu 175 and Asp 206 that reside deep within the pocket and contribute much to the negative electrostatic potential of the pocket. These residues,

as well as the other residues that are in contact with the MKT-077, are 100% conserved between the 13 human HSPA isoforms (see Table VIII.1). Hence, it is more than likely that MKT-077 also binds at this site in the mitochondrial protein, HSPA9, which was earlier identified as prime target of the drug[402, 403]. The binding site is mostly encompassed in the area 207-265 (human HSPA8 count), which was identified earlier as the binding area of MKT-077 to mouse HSPA9 [313].

One possible outcome of our studies could have been that MKT-077 binds to a site in HSPA8, which is not conserved amongst the HSPA chaperones. Such a finding would have been exciting, as it would have allowed a potential route for creating derivatives that are HSPA-isoform-specific inhibitors. As it stands, this is not the case, except for a possibility to modify MKT-077 to reach out to His 227, which is a Phe in HSPA9, the mitochondrial HSPA which is specifically implicated in breast cancer[404] (see table VIII.1 , Figure VIII.11 and below).

To be able to suggest where modifications should be made to improve MKT-077, one needs a detailed description of the interaction with HSPA. In the AUTODOCK results, in the family depicted in Fig VIII.10C, the positive pyridinium ring is reaching into the
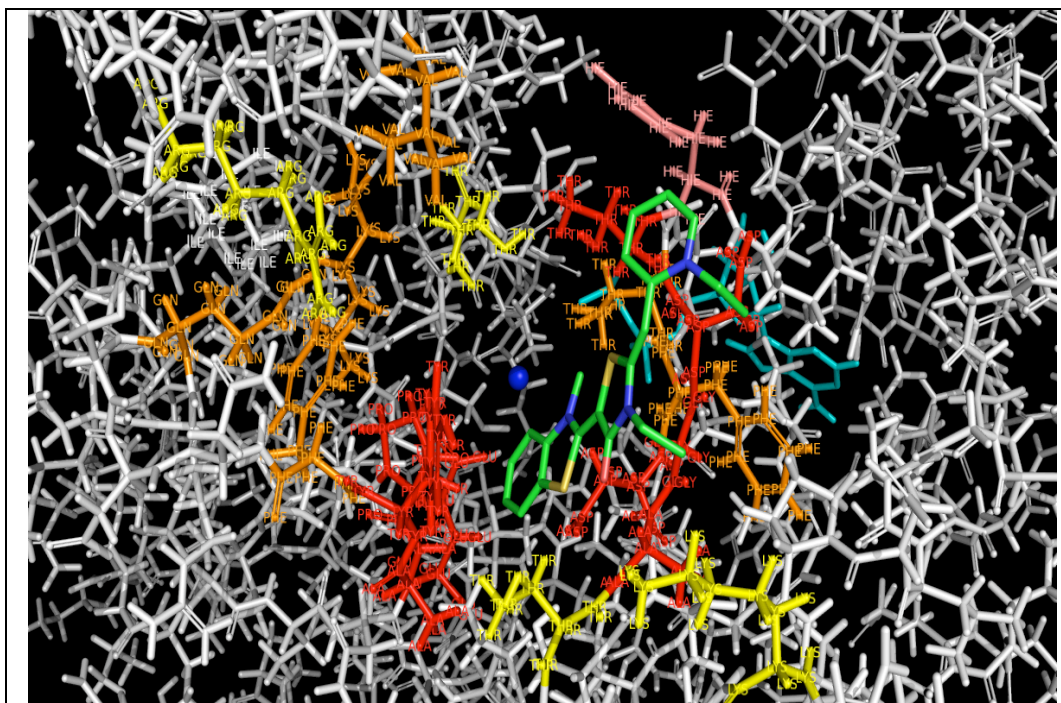
Figure VIII.11. HSPA8 residues in contact with the five MKT-077 docking families. Red, contacts with 4 or 5 families; orange, contacts with 2 families; yellow, contacts with 1 family. His 227 is shown in salmon (see text). Mg^{2+} is in blue, ADP in cyan. The docked MKT-077 structure of Fig 10 F is shown in green. Also compare Table 1. The figure was generated in Pymol[398].

pocket to contact Glu 175 and Asp 206. In the family depicted in Fig VIII.10D, partial contact occurs. In the other families, the positive pyridinium ring is solvent-exposed. In family 10F, it is in contact with Asp 225, which lines the rim of the pocket (at 2 o'clock in Figure VIII.10F). The AUTODOCK analysis cannot discriminate between these different orientations of MKT-077. Arguments for the pyridinium ring to stick into the pocket include that the AUTODOCK docking energies are best in this orientation (7.03 Kcal/M, corresponding to an K_D of 10 uM), and that it would most easily explain that an MKT-077 derivative with an uncharged pyridinium ring, does no show binding in the NMR assay (results not shown). An argument for the pyridinium ring to be solvent exposed and interact with Asp 225, is that the most dramatic chemical shifts occur for exactly that residue (see Fig VIII.3). In addition, MKT-077 derivatives with larger poly-aromatics in place of the pyridinium moiety are equally or more effective in biological assays[402]. Moreover, through derivitization of the pyridinium moiety, MKT-077 could be covalently linked to sepharose and be used to bind to HSPA9 [405]. This strongly

suggests that the pyridinium moiety is solvent-exposed in the complex. *Prima facie*, there is little reason for the methylbenzothiazolin moiety (left in Fig VIII.1) to seek the negatively charged pocket, since it does not carry a formal net charge. However, when using the AM1-BCC method[389] to compute the charge distribution on MKT-077, one obtains a sizeable positive charge on this moiety due to polarization (see Fig VIII.1). The AM1-BCC method is quoted to very representative of the "true" quantum mechanical charges. In addition, one may expect MKT-077 to become even more polarized when placed in the vicinity of negative charges.

Table 1

Section 1

	11	12	13	14	15				69	70	71	72	73	74	75	76		80	81	82	83	84
HSPA8	L	G	T	T	Y				D	A	K	R	L	I	G	*R*		D	A	V	V	Q
HspA1A	L	G	T	T	Y				D	A	K	R	L	I	G	*R*		D	P	V	V	Q
HspA1L	L	G	T	T	Y				D	A	K	R	L	I	G	*R*		D	P	V	V	Q
Hspa2	L	G	T	T	Y				D	A	K	R	L	I	G	*R*		D	A	T	V	Q
HSPA5	L	G	T	T	Y				D	A	K	R	L	I	G	*R*		D	P	S	V	Q
HSPA6	L	G	T	T	Y				D	A	K	R	L	I	G	*R*		D	T	T	V	Q
HSPA9	L	G	T	T	N				A	T	K	R	L	I	G	*R*		D	P	E	V	Q
HSP12A	F	G	T	T	S				Y	A	A	R	D	F	Y	*H*		P	N	E	A	K
HSPA12b	F	G	T	T	S				Y	T	A	R	D	Y	Y	*H*		P	E	E	A	R
HSPA13	L	G	T	T	Y				D	A	K	R	F	I	G	*K*		A	E	E	L	E
HSPA14	L	G	C	T	S				K	V	K	Q	I	L	G	*R*		D	P	Q	A	Q

Section 2

	145	146	147	148	149	150	151	152	153	154	155	156		173	174	175	176	177
HSPA8	T	V	P	*A*	*Y*	*F*	N	D	S	Q	R	Q		I	N	E	P	T
HspA1A	T	V	P	*A*	*Y*	*F*	N	D	S	Q	R	Q		I	N	E	P	T
HspA1L	T	V	P	*A*	*Y*	*F*	N	D	S	Q	R	Q		I	N	E	P	T
Hspa2	T	V	P	*A*	*Y*	*F*	N	D	S	Q	R	Q		I	N	E	P	T
HSPA5	T	V	P	*A*	*Y*	*F*	N	D	A	Q	R	Q		I	N	E	P	T
HSPA6	T	V	P	*A*	*Y*	*F*	N	D	S	Q	R	Q		I	N	E	P	T
HSPA9	T	V	P	*A*	*Y*	*F*	N	D	S	Q	R	Q		I	N	E	P	T
HSP12A	T	V	P	*A*	*I*	*W*	K	Q	P	A	K	Q		A	L	E	P	E
HSPA12b	T	V	P	*A*	*I*	*W*	K	Q	P	A	K	Q		A	L	E	P	E
HSPA13	S	V	P	*A*	*E*	*F*	D	L	K	Q	R	N		I	N	E	P	T
HSPA14	T	V	P	*F*	*D*	*F*	G	E	K	Q	K	N		I	H	E	P	S

Section 3

	202	203	204	205	206	207	208		220	221	222	223	224	225	226	227	228	229	230		318	319	320
HSPA8	G	G	T	F	D	V	S		K	S	*T*	*A*	*G*	*D*	*T*	H	L	G	G		E	K	A
HspA1A	G	G	T	F	D	V	S		K	A	*T*	*A*	*G*	*D*	*T*	H	L	G	G		E	K	A
HspA1L	G	G	T	F	D	V	S		K	A	*T*	*A*	*G*	*D*	*T*	H	L	G	G		E	K	A
Hspa2	G	G	T	F	D	V	S		K	S	*T*	*A*	*G*	*D*	*T*	H	L	G	G		E	K	A
HSPA5	G	G	T	F	D	V	S		V	A	*T*	*N*	*G*	*D*	*T*	H	L	G	G		Q	K	V
HSPA6	G	G	T	F	D	V	S		K	A	*T*	*A*	*G*	*D*	*T*	H	L	G	G		E	K	A
HSPA9	G	G	T	F	D	I	S		K	S	*T*	*N*	*G*	*D*	*T*	F	L	G	G		Q	K	A
HSP12A	G	G	T	V	D	L	T		K	A	*T*	*G*	*G*	*P*	*Y*	G	S	L	G		R	D	L
HSPA12b	G	G	T	V	D	L	T		K	A	*S*	*G*	*G*	*P*	*Y*	G	A	V	G		E	A	L
HSPA13	G	G	T	L	D	V	S		R	A	*M*	*S*	*G*	*N*	*N*	K	L	G	G		Q	Q	V
HSPA14	G	T	S	L	S	L	S		L	S	*T*	*N*	*T*	*D*	*D*	N	I	G	G		R	G	L

Table VIII.1. HSPA8 residues in contact with the five MKT-077 docking families, shown in the context of the human HSPA paralogs. The alignment was carried out in BLAST-P.
Red, contacts with 4 or 5 families; orange, contacts with 2 families; yellow, contacts with 1 family. These residues are also shown in Fig 11.
    The residues that showed chemical shifts are shown in italic. Numbering is for HSPA8.

We became interested if one would be able to distinguish between the different AUTODOCK poses by using the MMGB/PBSA solvation / desolvation computational protocol[406] on basis of snapshots of molecular dynamics simulations of the complex (see Materials). We first tested whether we could distinguish between pyridinium "in" and "out" conformations. As detailed in the Materials section, carefully equilibrated 250 ps molecular dynamics runs for the complexes as shown in Figure VIII.10, Panel C, with an energy of 7.03

Kcal/M (pyridinium "in") and in Figure VIII.10, Panel F, a with an energy of 5.25 Kcal/M (pyridinium "out") were obtained using Amber 11. We used the Generalized Born / Poisson Boltzmann protocol to estimate the solvation enthalpy of ligand, protein and complex (MMGB/PBSA).   For the pyridinium "in" conformation (7.03 Kcal/M binding energy by AUTODOCK) an total AMBER binding enthalpy of -12.1 +/- 4.1 Kcal was

Table VIII.2. MKT-HSPA8 docking energies				
Subfamily in Fig 10	AUTODOCK Energy	MM GB Energy	MM PBSA Energy	MM GB/PB average
	kCal/M	kCal/M	kCal/M	kCal/M
Panel C	7.03	-16.6 ± 1.8	-7.5 ± 3.7	-12.1 ± 4.1
Panel D	6.32	-18.6 ± 1.5	-14.0 ± 2.1	-16.3 ± 2.8
Panel E	5.36	-18.1 ± 1.2	-10.8 ± 2.0	-14.5 ± 2.3
Panel F	5.25	-22.8 ± 1.3	-13.8 ± 2.6	-18.3 ± 2.9

obtained, while for the pyridinium "out" conformation (5.25 Kcal/M binding energy by AUTODOCK) an AMBER binding enthalpy of -18.3 +/- 2.9 Kcal was obtained (Table VIII.2). This indicates a marked preference for the pyridinium "out" conformation. Moreover, since the pyridinium is the only freely rotatable moiety in MKT-077 which is still relatively free to move in the pyridinium "out" conformation (from checking the trajectories, see the supplemental information), the pyridinium "out" conformation should also have a substantial entropic advantage as compared to the pyridinium "in" conformation. Having passed this test, we proceeded to try to distinguish between the different pyridinium "out" poses as shown in Figs VIII.10 D, E and F, which have indistinguishable AUTODOCK energies of 6.32, 5.36 and 5.25 Kcal/M, respectively. As is shown in Table VIII.2, the results of the Amber calculations are too close to make this call, but the family shown in Fig VIII.10F has the best score.

The AMBER results may be used to guide MKT-077 modifications that would allow tighter binding. No modification should be made on non-pyridinium moieties of the molecule since these parts are buried in the pocket. An obvious modification is to add positive charge to the compound, as it binds to an area that has overall strong negative electric potential as is shown in Figure VIII.7. However, there is indication that positively charged compounds are more toxic to the kidneys than neutral compounds[407]. Hence, adding extra charge to MKT-077 is likely to exacerbate the toxic side-effects[408] which were cause for the termination of the Phase I trial[393]. MKT-077's renal toxicity may potentially be reduced by converting MKT-077 to a zwitter-ion, with a negative functionality on the pyridinium moiety to complement the sidechain

of His 227. His 227 is very close to the MKT pyridinium moiety in the best pose (see Tables VIII.1, 2 and Figure VIII.11). By trying to exploit such an interaction, the compound's affinity may be enhanced as well. However, the negative charge would likely interfere with MKT-077's ability to selectively target the strongly negatively charged mitochondria of tumor cells[409]. Hence, the suggested conversion of MKT-077 to a zwitter-ion will likely take MKT-077 out of contention as an anti-tumor drug, but may allow it to be used in the treatment of tauopathies such as Alzheimer's, potentially without the toxic renal side-effects found in the phase I trial. In fact, neutralization of the overall charge of MKT-077 could help enhance the compound's ability to cross the blood-brain barrier[410].

The pyridinium moiety is also close to an apolar surface area composed of residues V82 and T226. Modification of the pyridinium moiety to a larger poly-aromatic to exploit additional dispersion and hydrophobic interactions with these residues, may lead to a compound with a higher affinity. This may explain why the larger MKT-derivatives FJ-5744 and FJ-5826 are more potent HSPA inhibitors[402].

VIII.5 Conclusion.

We have determined that MKT-077 binds to a negatively charged pocket at the interface of the four HSPA8 NBD subdomains. All residues lining the pocket are conserved in all human HSPA isoforms. The compound binds selectively to the ADP state of the protein, and can hence be qualified as an allosteric drug. We suggest modifications that would potentially retain the compound's binding affinity but which likely diminish the compound's renal toxicity.

VIII.6 Materials and Methods.

VIII.6.1 Protein preparation:

The plasmid for the expression of bovine HSPA8 NBD domain (100% identical to the human protein) was a generous donation by D. B. McKay (Stanford School of Medicine, Stanford, CA). It was expressed in Escherichia coli strain BL21(DE3). In order to increase the yield of the induction, the cells were inoculated from a freshly transformed Petri dish a 2ml LB culture, were grown until OD(600)=0.4, transferred to a 100ml flask of M9 media and were grown until OD(600)=0.4. Subsequently the cells were centrifuged and transferred to a 1L M9 medium

containing 98% D_2O, 2gr/lt protonated [^{13}C glucose], and 1gr/lt $^{15}NH_4Cl$. The expression was induced by isopropylthio-B-galactoside to 0.5mM at OD(600)=0.8. Harvested cells were removed by centrifugation and disrupted mechanically by a French press. Cell debris was removed by centrifugation and the supernatant was loaded onto a DEAE52 column and eluted with 150mM KCl. The Hsc70 fractions were dialyzed against 20mM Hepes (pH 7.0)/25mM KCl/10mM EDTA. The EDTA was precipitated by the addition of 25mM $MgCl_2$ in the dialyzed protein pool yielding 5mM free Mg^{+2}. The precipitate of (Mg)EDTA was removed by centrifugation. The supernatant was loaded onto an ATP-agarose affinity column and was eluted with 3mM ADP. The protein was concentrated by using Amicon concentrators. The protein was at all times stabilized with protein inhibitors and was kept at 4C.

VIII.6.2 NMR Assignments.

For the assignment of the protein's NMR spectrum, we used a ^{15}N, ^{13}C, ^{2}H labeled 280 μM HSPA8-NBD sample that contained 5mM $MgCl_2$, 25mM KCl, 20mM Tris-HCl,10mM ADP, 5 mM K_3PO_4, 0.005% sodium azide and 10% (vol/vol) D_2O (pH 7.2). The experiments were performed at 26 ^{o}C on a Varian Inova 800 equipped with a triple-resonance cold probe. The protein spectra were assigned using 3D HNCA, HN(CO)CA, HNCO, HN(CA)CO, HNCACB, HN(CO)CACB TROSY. All spectra were processed with NMRPIPE[346] and converted into Sparky[347]. The Sparky program was used to peak-pick the spectra. The peak pick lists were manually curated to obtain consistent NH root labeling throughout the different spectra. Assignments were made from these curated lists using the automatic assignment program SAGA[345]. Alternative assignments as produced by SAGA were evaluated and further checked using SPARKY. Only assignments of stretches of more then 2 connected spin systems were retained. By enlarge, they corresponded to the previous manual assignments for this protein domain [93].

VIII.6.3 Synthesis of MKT-077.

The dye, originally manufactured by Fuji, Inc, is not longer commercially available. It was synthesized by us (Y.M. and J.E.G). The synthetic protocol will be described elsewhere. The ^{1}H spectrum of MKT-077 in H_2O was assigned using DQF-COSY and ROESY acquired on a 500

MHz Bruker Avance spectrometer. The ROESY spectra confirmed the *trans* configuration of the pyridinium ring and the nitrogen in the oxothiazolidin moiety over the double bond as shown in Fig 1.

VIII.6.4 NMR Titrations

HSPA8 NBD samples of 80 – 240 μM in 5mM $MgCl_2$, 25mM KCl,20mM Tris-HCl,10mM ADP, 5 mM K_3PO_4, 0.005% sodium azide and 10% (vol/vol) D_2O (pH 7.2) were used for the titrations, using 4 mM solutions of MKT-077 in water (neutral pH) as titrant. The results of two titrations are reported here. Using a sample of 80 μM ^{15}N-labeled HSPA8-NBD, MKT-077 was added to ratios of 1:1 and 2:1. Duplicate TROSY spectra of 8 hours each were recorded for each titration step. Using a triple-labeled 270 μM sample of HSPA8 NBD, MKT was titrated to ratios of 0.25:1, 0.5:1, 0.75:1 and 1:1. Duplicate TROSY spectra of 4 hours each were recorded for each titration step. The shifts upon the addition of the drugs were manually recorded in Sparky and were mapped on the crystal structure coordinates of HspA8 NBD (3HSC.pdb) using Pymol[398].

VIII.6.5 Partial Proteolysis:

The partial proteolysis protocol was adapted from a previously described method[88]. Briefly, HSPA8 (6 μM) in 40 mM HEPES buffer (20 mM NaCl, 8 mM $MgCl_2$, 20 mM KCl, 0.3 mM EDTA, pH 8.0) was incubated with 1 mM nucleotide (ADP or ATP), either a buffer control or MKT-077 (200 μM) and a J-domain (residues 2-108, 24 μM) when noted. Samples were incubated at room temperature for 30 minutes. The trypsin (SIGMA Ec 3.4.2.1.4) was added to a final concentration of 0.9 μM and the samples were incubated for another 30 minutes at room temperature. The reaction was then quenched with the addition of 25 μl of 3x SDS loading buffer (240 mM Tris, 6 % w/v SDS, 30 % v/v glycerol, and 16 % v/v β-mercaptoethanol, 0.6 mg/ml bromophenol blue, pH 6.8) and heated to 95 °C for 3 minutes. Bands were separated by 12 % SDS-PAGE and stained with Coomassie blue.

VIII.6.6 Docking computations:

AUTODOCK-4[411] was used for the docking of MKT-077 to HSPA8-NBD. The initial structure for MKT-077 was minimized in Jaguar (Schrödinger, LLC) at the B3LYP/6-31G* level. Standard charging methods within AUTODOCK leave MKT-077 uncharged. To obtain better charging models, we used the Antechamber[412] suite in AMBER[401]. In one round of computations, we use Gasteiger charging as afforded by Antechamber, and just added +1 to the charge of the pyridinium nitrogen. We also used AM1-BCC charges as computed in AMBER. AM1-BCC predicts considerable polarization over the remainder of the conjugated molecule (see Fig VIII.1) which also seems more realistic than the charge pattern in Gasteiger in which polarization is absent. The AMBER-charged models were hand-edited into the AUTODOCK . pdbqt files.

All available crystal structures for the NBD of HSPA8 conform to the closed (ATP) state[95]. These structures cannot be used for docking because MKT-077 does not bind to this state. In absence of a "true" high-resolution structure for the open ADP state, we chose one of the available crystal structures of HSPA8 in complex with a nucleotide exchange factor. According to the NMR analysis of a bacterial Hsp70 in the ADP and ATP state, HSPA8 in complex with a nucleotide exchange factor is a likely representation of the ADP state[95]. We chose HSPA8 in complex with yeast Hsp110 (3C7N.pdb[413]) as our model, because it is the only complex that contains ADP and Mg^{++}. We discarded the coordinates of Hsp110 in the docking computations. In order to relieve possible strain exerted by crystal and/or Hsp110, the extracted HSPA8-NBD coordinates were relaxed using restrained minimization and equilibration in AMBER (see below). The coordinates of the equilibrated protein, including ADP and Mg^{++} were used for the AUTODOCK runs.

The AUTODOCK gridbox was located on the interface of the four subdomains IA-IB-IIA-IIB with a 0.2 Å resolution. We used a Lamarckian genetic algorithm with the following parameters : the GA runs were set to 100, the size of the initial population to 1500, the maximum number of evaluations was set to long, the maximum number of top individuals that automatically survive was set to 1, the rate of gene mutation was set to 0.02, the rate of crossover was 0.8, the GA crossover mode was twopt, the mean of Cauchy distribution for gene mutation was set to 0, the variance of Cauchy distribution for gene mutation was set to 1 and the number of generations for picking worst individuals was set to 10. The calculations were performed on a MacIntosh

computer. The docked structures were clustered and evaluated by hand using Pymol[398].

VIII.6.7 Molecular dynamics:

The crystal structure coordinates of HSPA8 in complex with yeast Hsp110, ADP, SO_4^{2-} and Mg^{++} ions (3C7N.pdb) were used as a starting point. The coordinates of Hsp110 and SO_4^{2-} ions were removed. The NBD, ADP and Mg coordinates were minimized in 1000 steps using a hybrid forcefield (ff99SB for the protein, gaff for metal ions and a gaff-derived forcefield[414] for ADP) in the Amber 11 program suite[401]. The coordinates were restrained to the X-ray coordinates with a force constant of 5 Kcal/Mol/$Å^2$. Subsequently we carried out a molecular Langevin dynamics equilibration run in implicit generalized Born solvent with 0.1 M ionic strength, running from 0 - 300 K over 10 ps. The same hybrid forcefield was used. The dynamics equilibration was restrained by 940 CA-CA distances in the 2-5 Å range, 2952 CA-CA distances in the 10-20 Å range, and 742 restraints between protein CA atoms and all atoms of ADP and Mg^{++} in the 1-15 Å range. The restraints had as lower bounds the actual distances as computed from the PDB file, and as upper bounds the actual distance + 1 Å, enforced by a parabolic potential of 20 Kcal/Mol/$Å^2$. The calculations were performed on an Apple MacBookPro5.1 computer equipped with a 64-bit 2.4 GHz Inter Core 2 Duo processor, running MacOS X10.6.6.

VIII.6.8 Docking evaluation:

The AUTODOCK solutions with "energies" of 7.03, 6.32, 5.36 and 5.25 Kcal/M were evaluated using AMBER (vs. 11) in the following way. Hydrogen-atoms were re-attached to the coordinates of the docked MKT-077 molecules and the double and aromatic bonds were reassigned in the Pymol Builder module[398]. These coordinates were converted to AMBER .prepi and forcefield modification files using the Amber Antechamber suite. We used AM1-BCC charging for MKT-077 as shown in Fig VIII.1.

In order to carry out a proper MD-based binding energy evaluation, it is necessary to run the simulations using explicit solvation. For a molecule the size of HSPA8 NBD (380 residues) such computations become too time consuming for our labs, which do not have access to specialized super computers. Hence, we decided to carry out restrained MD simulations on a docking site consisting of HSPA8 residues 12-13+69-83+143-158+172-177+196-211+219-229+316-323 and the Mg^{++} ion, which was extracted from the equilibrated pdb files (see Figure S3). Four different docked MKT-077 poses, corresponding to the best members of each of the four families shown in Fig 10, were added the site (not simultaneously). Identical protocols were followed for the four computational series. The "complexes" were solvated with ~6500 TIP3P waters in a 12 $Å^3$ periodic box. After a minimization step, a molecular dynamics temperature ramp running from 0 - 300 K over 50 ps was carried out. The same hybrid force field was used as described above. This run was restrained by 3790 restraints between N, HN, CA, C' and O backbone atoms of the reduced binding site, 55 Mg^{++} - CA restraints, and ~2600 MKT - CA restraints based on the minimized structure (depending on family member). All restraints were defined within a 1.0 Å range and enforced with a 20 $Kcal/Mol/Å^2$ gradient. Subsequently, a density equilibration (for 50 ps, with pressure relaxation time of 1 ps) and general equilization (for 100 ps, with pressure relaxation time of 2 ps) with the same restraints followed. These equilibration steps were followed by a production run of 250 ps restrained MD computations at 300 K. In the production runs, the MKT restraints were removed, while all others remained.

The binding enthalpies were calculated using the MM-GB/PBSA protocol[406] as implemented in the Amber 11 release, using 100 frames of the last 50 ps of the molecular dynamics production runs. The calculations were performed on an Apple MacBookPro5.1 computer equipped with a 64-bit 2.4 GHz Inter Core 2 Duo processor, running MacOS X10.6.6.

VIII.7 Acknowledgements

VIII.8 Supplemental material

Supplemental Figure VIII.1.

800 MHz ^{1}H-^{15}N TROSY spectrum of 250 uM ^{15}N, ^{2}H, ^{13}C HSPA8 NBD in the ADP state (residues 1-387).

Supplemental Figure VIII.2. Compilation of chemical shift changes in the 15N-1H TROSY spectra. Top line: 80 uM 15N-labeled HSPA8 NBD in the presence of 10 mM ADP, with 80 uM MKT-077Middle line: 250 uM 15N-2H labeled HSPA8 NBD in the presence of 10 mM ADP, with 120 uM MKT-077.Bottom line: 120 uM 15N-labeled HSPA8 NBD in the presence of 2 mM AMPPNP, with 240 uM MKT-077Green, no changes; yellow, small changes; red, large changes; grey, no assignments; cyan, cannot tell because of overlap.

Supplemental Figure VIII.3. In cyan, the selection of residues of 3C7N.pdb used for the Amber MD docking evaluation by MMGB/PBSA (see Materials and Methods). ADP, not included in the evaluation, is shown in pale green. MKT-077 AUTODOCK-pose with 5.25 Kcal/M energy in magenta; 5.36 Kcal/M in yellow; 6.32 Kcal/M in blue; 7.03 Kcal/M in red.
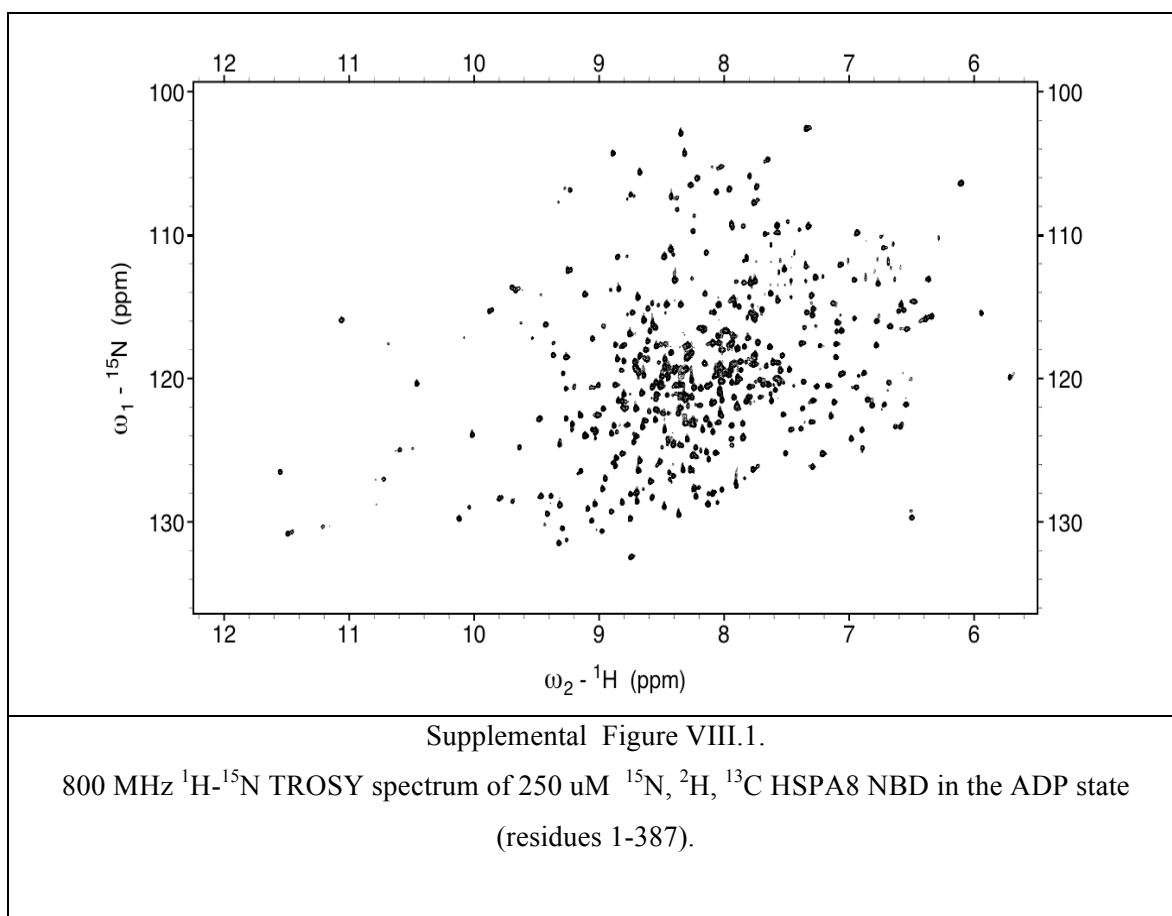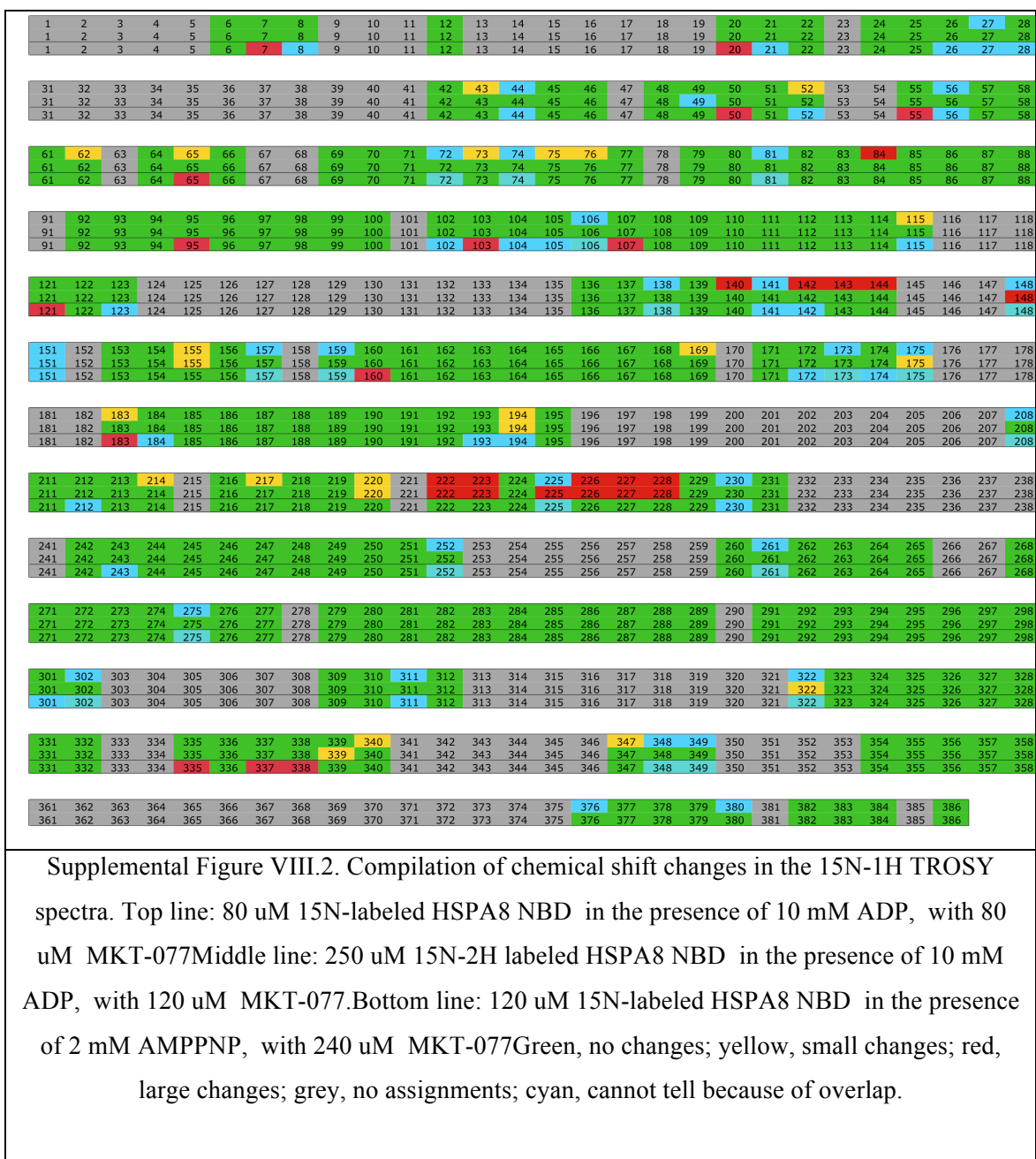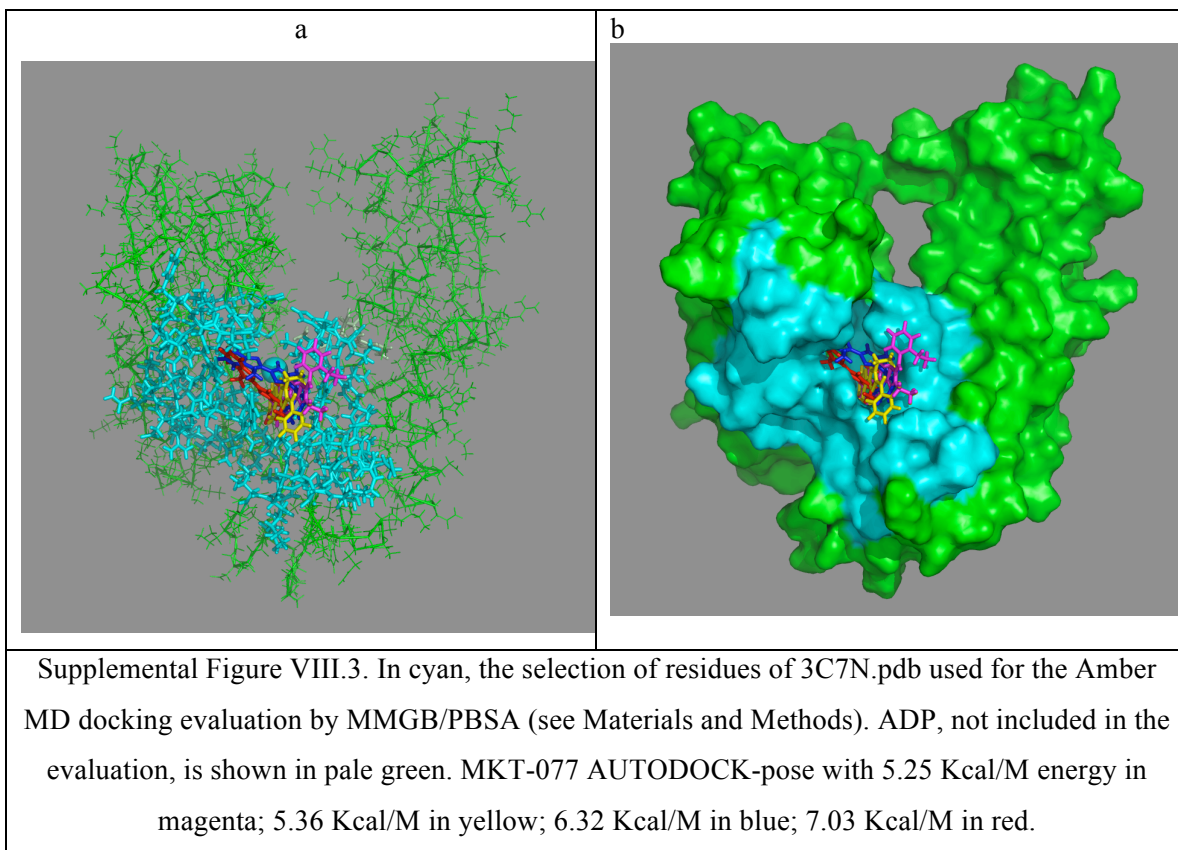
CHAPTER IX. Methylene blue and its binding to Hsc70.

IX.1 Abstract

Tau and Alzheimers are tightly tangled. Hsc70 interacts with tau and is thus tangled to Alzheimers disease too. Methylene blue is a promising anti-Alzheimers drug that interacts with the Hsc70 ATPase domain and reduces the levels of tau in HeLa cells. In this chapter we show that it binds to the Hsc70 ATPase domain and more specifically to its subdomain IB that contains Cysteine 17. The interaction causes a redox reaction to take place, that leads to color change of the solution that contains the protein.

IX.2 Introduction

Tau is a protein essential for the stability of microtubules. Its pathological form is hyperphoshorylated in which it tends to form intracellular tangles that contribute to neural cell death [399, 400]. HSPs (Heat Shock Proteins) on the other side are ubiquitous proteins that express under stress and non stress conditions, even through their name suggests that they only express upon stress. They interact with their cochaperones, the J domain protein and the nucleotide exchange factor, forming a cycle that can refold of recycle misfolded proteins [401]. Hsc70 is the constitutively expressed chaperone protein that exists in the cell cytosol under non stress conditions. As every Hsp70 it has two main domains[26], the ATPase domain and the substrate binding domain. The ATPase domain is composed of four subdomains called IA, IIA, IB, IIB. These subdomains move individually and contribute to the allostery of the protein [95]. Hsc70 is known to interact with tau proteins, and is therefore functionally linked to Alzeimer's disease [135, 312].

Methylene blue is an inexpensive drug available in hospital pharmacies. It was FDA approved in 2003 and it is generally used to treat emoglobinemia. It has been proposed that it destabilizes tau binding to the microtubules because the formation of a Hsc70-tau complex is energetically more favorable [219]. Experimental data have shown that methylene blue alters the structure of paired helical filaments isolated from the AD brain [308]. The structure of methylene blue is shown in Figure IX.1
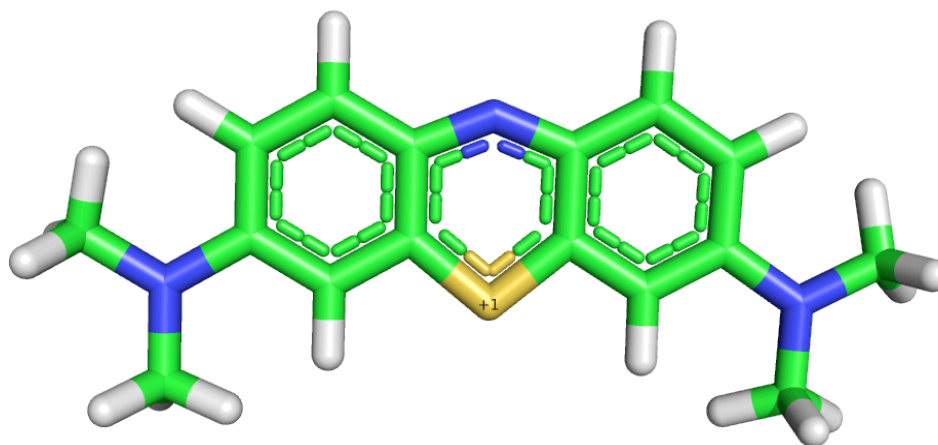
Figure IX.1: Structure of methylene blue.

A recent phase II clinical trial for AD indicated a positive therapeutic effect of this compound. The rate of decline of the patient's cognitive functions is lower when the patients take methylene blue orally. A larger phase III study is necessary to prove its efficacy. Along with this success, methylene blue has also been examined as an anticancer drug. Photodynamic therapy sensitized by intratumor administration of methylene blue was able to treat superficial tumors of the bladder, esophageal carcinomas, melanoma, and Kaposi's sarcoma with no reported toxicities. The mechanism underlying its success against cancer is related with the compound's complex redox chemistry [402].

IX.3 Materials and Methods

IX.3.1 Protein Preparation

The plasmid for the expression of bovine Hsc70 ATPase domain (100% identical to the human protein) was a generous donation by D. B. McKay (Stanford School of Medicine, Stanford, CA). It was expressed in Escherichia coli strain BL21(DE3). In order to increase the yield of the induction, the cells were inoculated from a freshly transformed Petri dish a 2ml LB culture, were grown until OD(600)=0.4, transferred to a 100ml flask of M9 media and were grown until OD(600)=0.4. Subsequently the cells were centrifuged and transferred to a 1L M9 medium containing 98% D_2O, 2gr/lt protonated [^{13}C glucose], and 1gr/lt $^{15}NH_4Cl$. The expression was induced by isopropylthio-B-galactoside to 0.5mM at OD(600)=0.8. Harvested cells were removed by centrifugation and disrupted mechanically by a French press. Cell debris was removed by centrifugation and the supernatant was loaded onto a DEAE52 column and eluted with 150mM KCl. The Hsc70 fractions were dialyzed against 20mM Hepes (pH 7.0)/25mM KCl/10mM EDTA. The EDTA was precipitated by the addition of 25mM $MgCl_2$ in the dialyzed protein pool yielding 5mM free Mg^{+2}. The precipitate of (Mg)EDTA was removed by centrifugation. The supernatant was loaded onto an ATP-agarose affinity column and was eluted with 3mM ADP. The protein was concentrated by using Amicon concentrators. The protein was at all times stabilized with protein inhibitors and was kept at 4C.

IX.4 Results

The ^{15}N-^{1}H HSQC-TROSY spectra [343] of 100 μM ^{15}Nlabeled human Hsc70(1–381) was collected as previously described[403]. Briefly, a 10mM MB stock solution was prepared in the same buffer as the NMR sample. Addition of 1 equivalent of MB caused several resonances corresponding to free Hsc70 to disappear. A second equivalent did not

cause additional changes; thus, MB is believed to bind in a 1:1 stoichiometry to Hsc70 with slow release kinetics.

Our collaborators Gestwicki and Dickey have established that Methylene blue is an Hsc70 inhibitor using ATP hydrolysis assays, and showed that Methylene blue causes reduction in tau levels in Hela transfectant cells (see Figure IX.2) . We have investigated the interaction of methylene blue and Hsc70 by NMR. We have found that MB binds to this protein, substantiating the linkage between Methylene blue – Hsc70 – tau.

Figure IX.2 :Inhibitors of Hsp70 decrease tau levels, and activators protect them. *A*, HeLa tau transfectants were treated for 24 hwith Hsp70 inhibitors (MB or AC) or activators (SW02 or 115-7c). *B*, Quantification plots of the Western blots after actin normalization illustrate significant decreases in total tau levels at higher doses of MB (OE) or AC (F), while treatment with either 115-7c or SW02 increased tau levels [312]
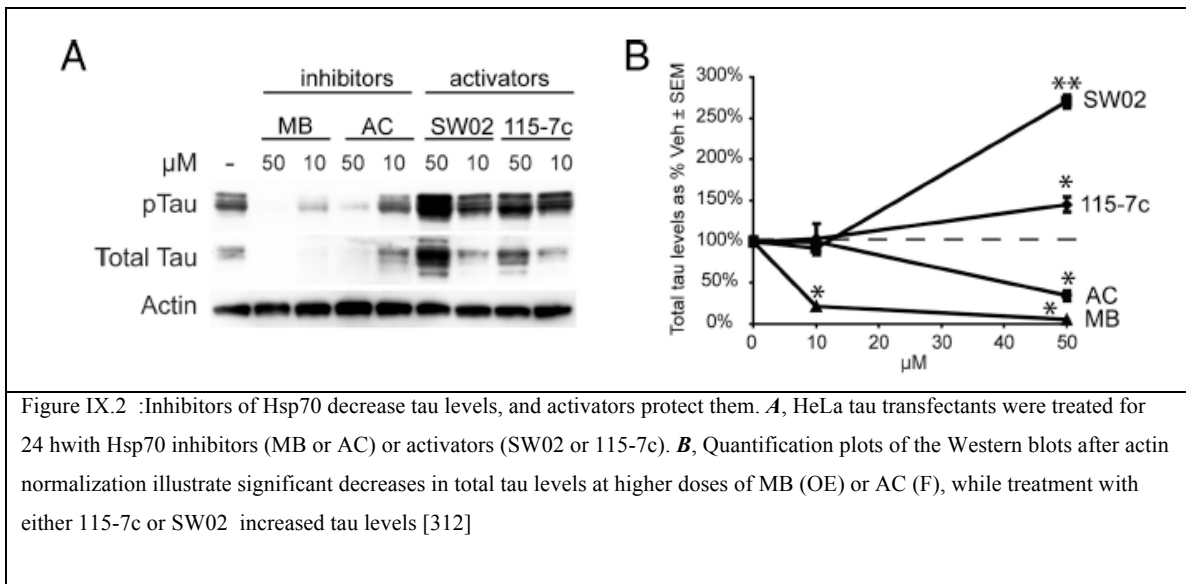
The spectrum upon titration of methylene blue to the Hsc70 ATPase domain has already been published [312]. In this paper we will show that methylene blue binds to the subdomain IB of the ATPase domain of Hsc70.

160
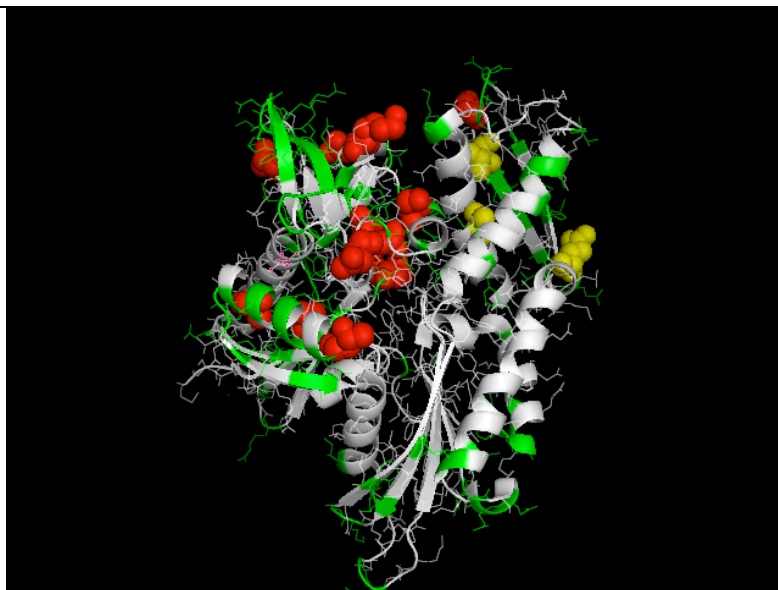
Figure IX.3 Chemical shift mapping upon addition of methylene blue to the Hsc70

ATPase domain (red-big shifts, yellow-small shifts, green- no shifts, grey-no data).

Chemical shift mapping of the chemical shifts on the existing 3HSC.pdb crystal structure of the Hsc70 protein revealed the binding site of the drug to the protein, which is in subdomain IB.

IX.5 Discussion

Previous publications [312] indicate that Hsc70 binds to methylene blue. Here, we show that MB interacts strongly with subdomain IB. A possible mechanism explaining the reduction of the tau levels by MB shown in Figure IX.2 is that MB interferes with the Hsc70 functional cycle so that the substrate tau is trapped in the binding cleft of Hsc70.

In such an event, tau is likely to be ubiquitinated and escorted to the proteosome for degradation.
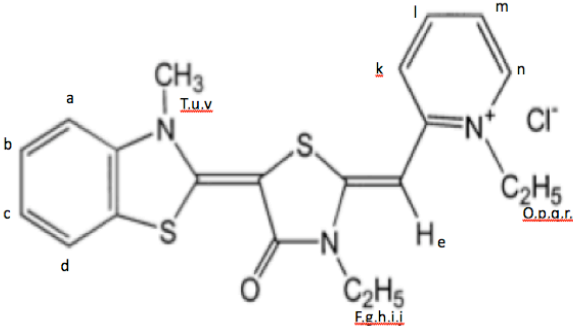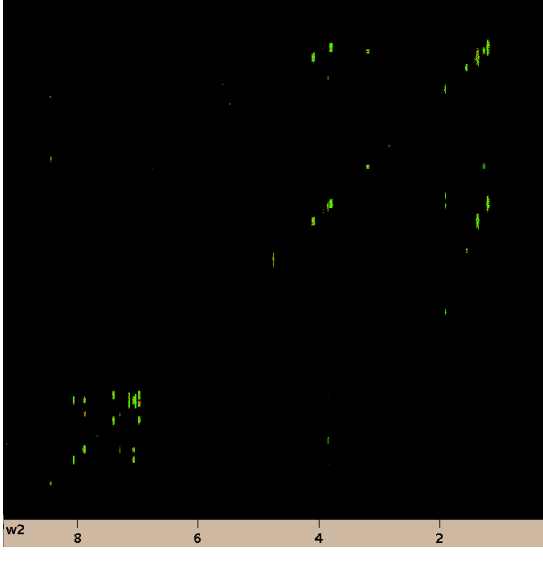
A concern is that we investigated just the interaction of MB with the Hsc70 ATPase domain and not the whole protein. Further studies need to be done on the whole protein in order to investigate the accuracy of our result.

APPENDIX I Binding of other drugs

Interaction of Hsc70 nucleotide binding domain with other drugs (drug structures available upon request to Pr Jason Gestwicki gestwick@umich.edu).

CE32	SW16
NDGA	YM1 (YM8 did not show any interactions)
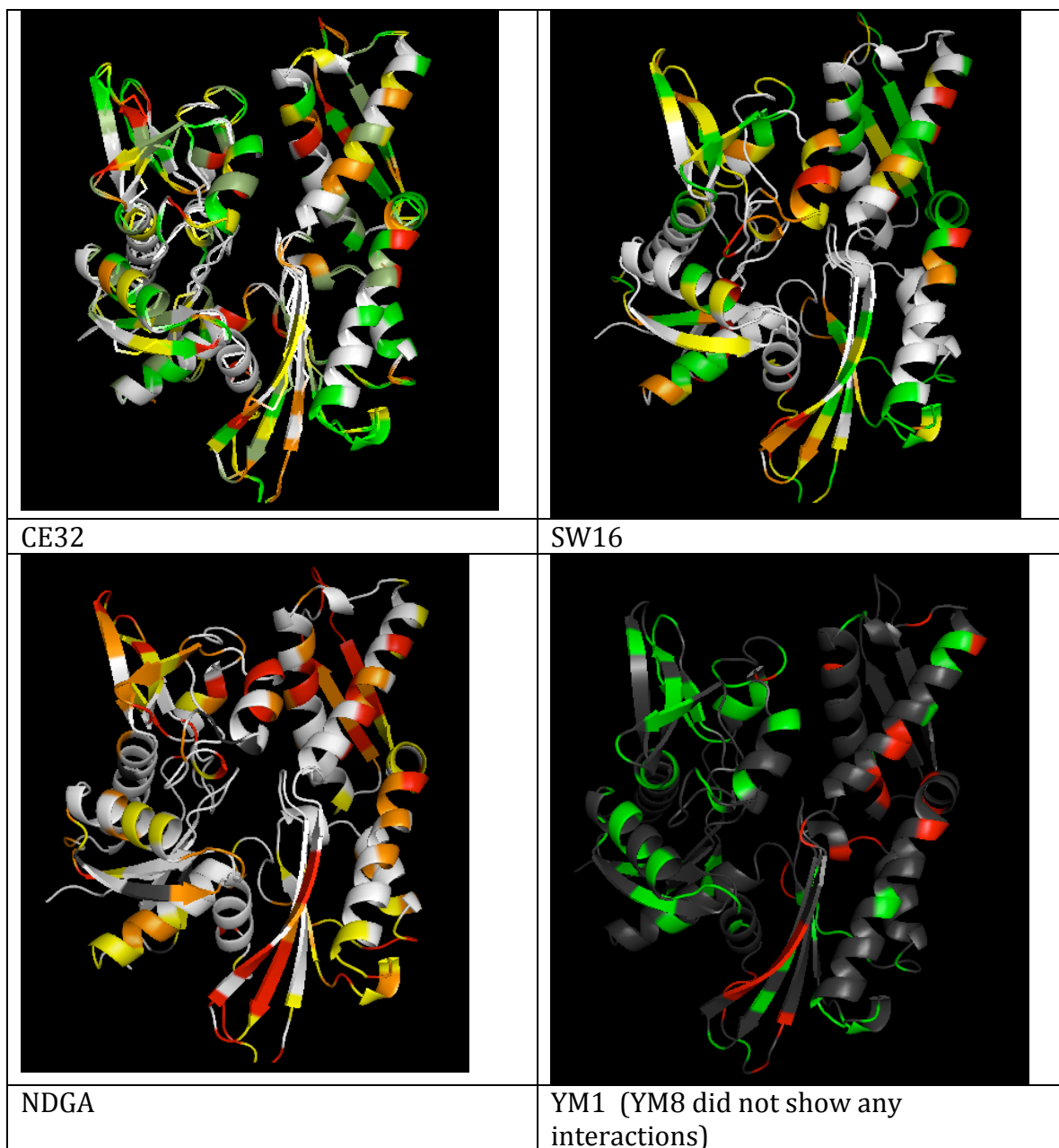
Structure of MKT-077 with nomenclature for assignments	DQF COSY of MKT-077 in H_2O.

The ^{1}H spectrum of MKT-077 in H_2O was assigned from presaturated DQF-COSY and ROESY acquired on a 500 MHz Bruker Avance spectrometer.
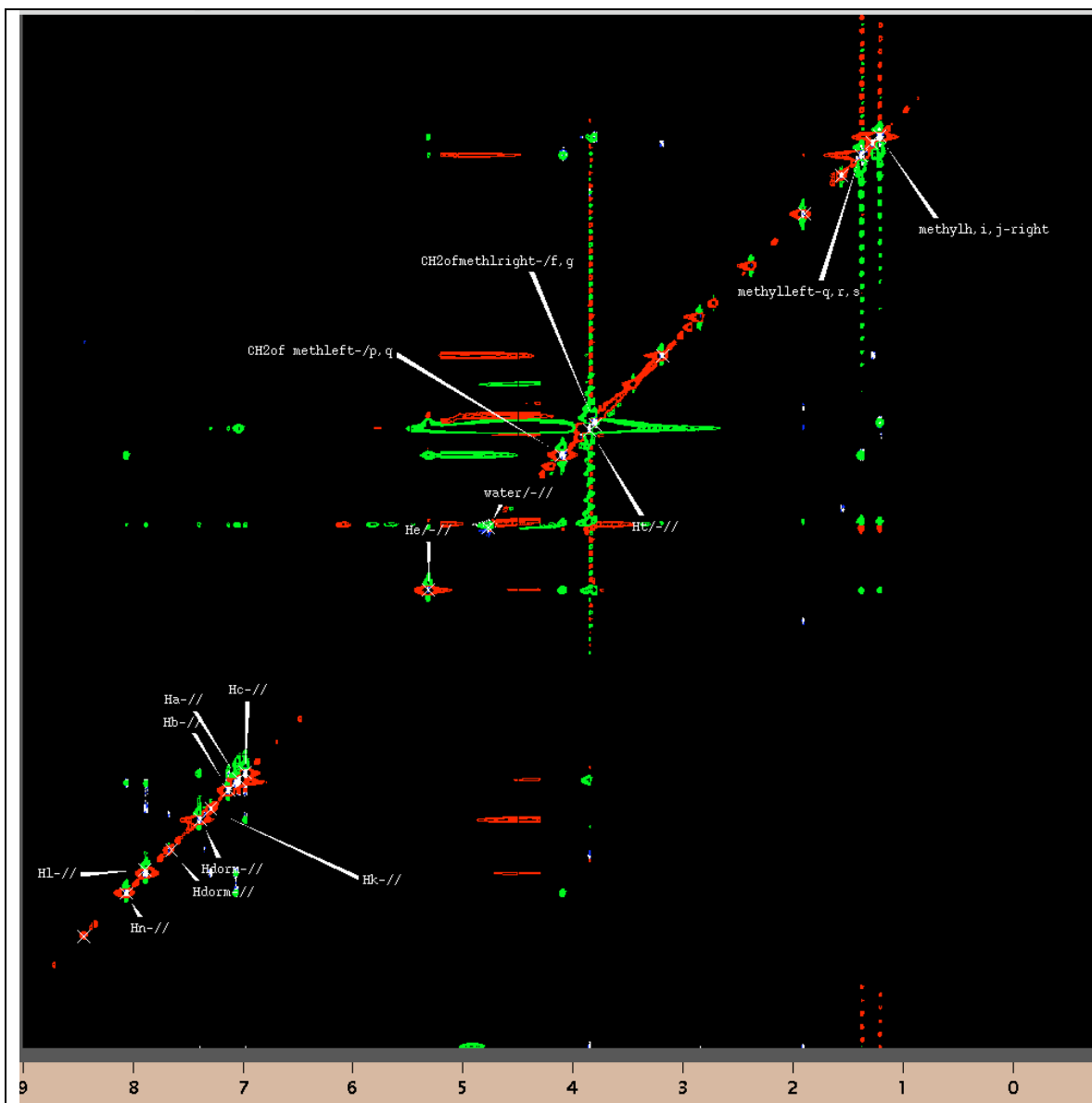
Fig VIII.16 ROESY spectrum of MKT077 with assignments following the nomenclature in
Of MKT-077 already shown.

Table VIII.1 Assignment for the 1H NMR lines of MKT077 (for nomenclature see Fig VIII.14)	
a	7.039
b	7.133
c	6.978
dorm	7.405
e	5.323
f,g	3.821
h,I,j	1.207
k	7.305
l	7.862
mord	7.305
n	8.072
o,p	4.104
q,r,s	1.382
t,u,v	3.875

APPENDIX III NOE of MKT-077 and Hsc70 NBD

Top a): MKT-077 b)MKT-077 and Hsc70 NBD c) Hsc70 Bottom Hsc70 NBD red-shifts, green-no shifts, blue- NOE, grey-no assignment/overlap/low intensity
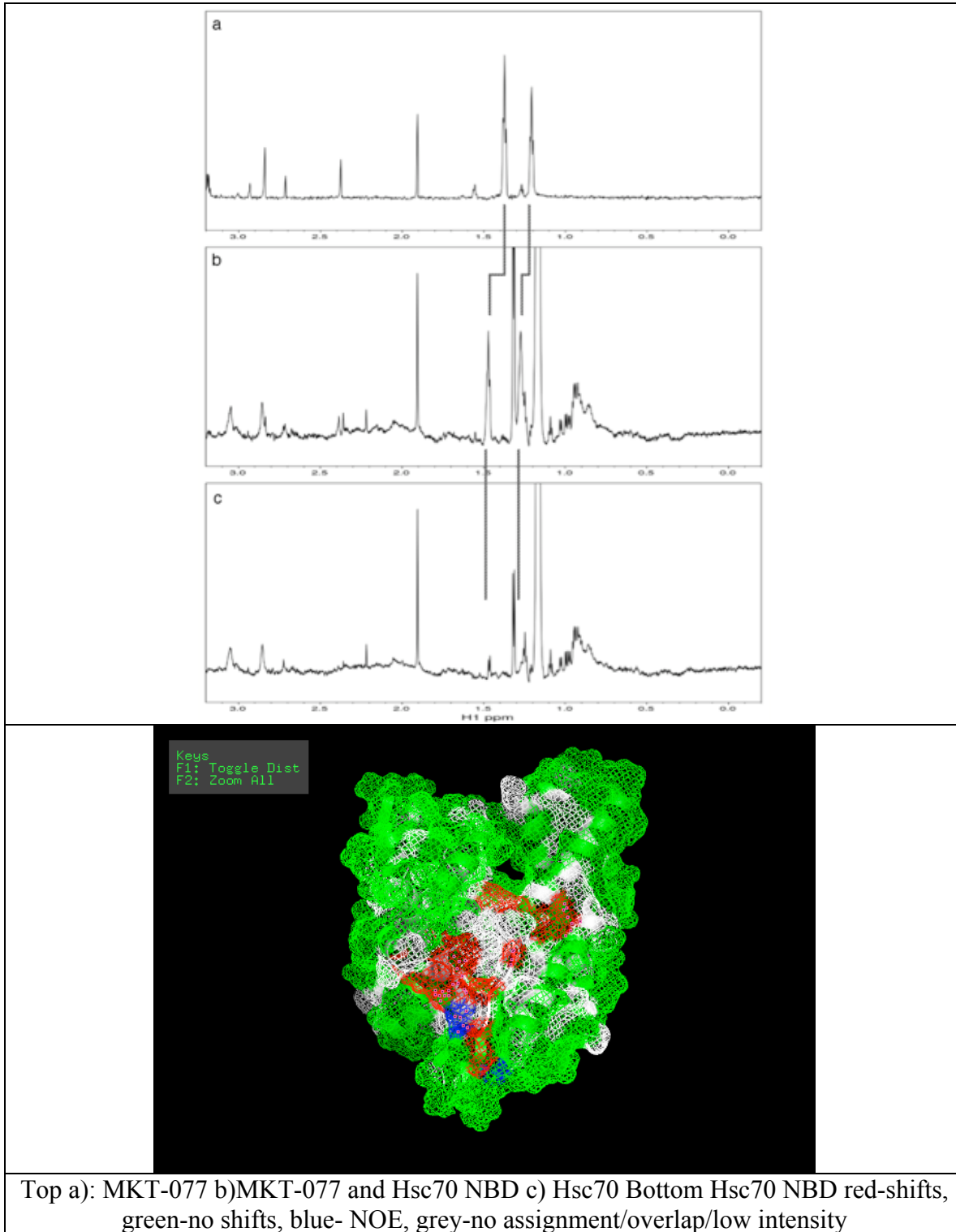
References

1. Ellis, R.J., *Proteins a Molecular Chaperones.* Nature, 1987. **328**: p. 378-379.
2. Hartl, F.U., *Molecular chaperones in cellular protein folding.* Nature, 1996. **381**(6583): p. 571-580.
3. Comartin, D.J. and E.D. Brown, *Non-ribosomal factors in ribosome subunit assembly are emerging targets for new antibacterial drugs.* Current Opinion in Pharmacology, 2006. **6**(5): p. 453-458.
4. Wang, Z.G. and S.H. Ackerman, *Identification of functional domains in Atp11p - Protein required for assembly of the mitochondrial F-1-ATPase in yeast.* Journal of Biological Chemistry, 1996. **271**(9): p. 4887-4894.
5. Rodriguez-Granillo, A., et al., *Copper-Transfer Mechanism from the Human Chaperone Atox1 to a Metal-Binding Domain of Wilson Disease Protein.* Journal of Physical Chemistry B, 2010. **114**(10): p. 3698-3706.
6. Pellecchia, M., et al., *NMR solution structure of the periplasmic chaperone FimC.* Nature Structural Biology, 1998. **5**(10): p. 885-890.
7. Bukau, B. and A.L. Horwich, *The Hsp70 and Hsp60 chaperone machines.* Cell, 1998. **92**(3): p. 351-366.
8. Ritossa, F., *NEW PUFFING PATTERN INDUCED BY TEMPERATURE SHOCK AND DNP IN DROSOPHILA.* Experientia, 1962. **18**(12): p. 571-&.
9. Georgopoulos, C.P., *NEW BACTERIAL GENE (GROPC) WHICH AFFECTS LAMBDA-DNA REPLICATION.* Molecular & General Genetics, 1977. **151**(1): p. 35-39.
10. Yochem, J., et al., *Genetic-Analysis of 2 Genes, DnaJ and DnaK, Necessary for Escherichia-Coli and Bacteriophage-Lambda DNA-Replication.* Mol. & Gen. Genet., 1978. **164**(1): p. 9-14.
11. Georgopoulos, C.P., et al., *IDENTIFICATION OF THE ESCHERICHIA-COLI DNAK (GROPC756) GENE-PRODUCT.* Molecular & General Genetics, 1979. **172**(2): p. 143-149.
12. Kelley, P.M. and M.J. Schlesinger, *EFFECT OF AMINO-ACID ANALOGS AND HEAT SHOCK ON GENE-EXPRESSION IN CHICKEN-EMBRYO FIBROBLASTS.* Cell, 1978. **15**(4): p. 1277-1286.
13. Li, G.C. and A. Laszlo, *AMINO-ACID ANALOGS WHILE INDUCING HEAT-SHOCK PROTEINS SENSITIZE CHO CELLS TO THERMAL-DAMAGE.* Journal of Cellular Physiology, 1985. **122**(1): p. 91-97.
14. Pouyssegur, J., R.P.C. Shiu, and I. Pastan, *INDUCTION OF 2 TRANSFORMATION-SENSITIVE MEMBRANE POLYPEPTIDES IN NORMAL FIBROBLASTS BY A BLOCK IN GLYCOPROTEIN SYNTHESIS OR GLUCOSE DEPRIVATION.* Cell, 1977. **11**(4): p. 941-947.
15. Levinson, W., H. Oppermann, and J. Jackson, *TRANSITION SERIES METALS AND SULFHYDRYL-REAGENTS INDUCE THE SYNTHESIS OF 4 PROTEINS IN EUKARYOTIC CELLS.* Biochimica Et Biophysica Acta, 1980. **606**(1): p. 170-180.

16. Ding, X.Z., et al., *Increases in HSF1 translocation and synthesis in human epidermoid A-431 cells: Role of protein kinase C and Ca2+ (i).* Journal of Investigative Medicine, 1996. **44**(4): p. 144-153.

17. Ciocca, D.R.a.C., S.K, *Heat shock proteins in cancer: diagnostic, prognostic, predictive, and treatment implications.* Cell Stress Chaperones, 2005. **10**: p. 86-103.

18. Bardwell, J.C. and E.A. Craig, *Major heat shock gene of Drosophila and the Escherichia coli heat-inducible dnaK gene are homologous.* Proc Natl Acad Sci U S A, 1984. **81**(3): p. 848-52.

19. Craig, E.A., *THE HEAT-SHOCK RESPONSE.* Crc Critical Reviews in Biochemistry, 1985. **18**(3): p. 239-280.

20. Lindquist, S., *The Heat-Shock Reponse.* Ann. Rev. Biochem., 1987. **55**: p. 1151-1191.

21. Caplan, A.J., D.M. Cyr, and M.G. Douglas, *Eukaryotic Homologs of Escherichia-Coli DnaJ - a Diverse Protein Family That Functions with Hsp70 Stress Proteins.* Mol. Biol. Cell, 1993. **4**(6): p. 555-563.

22. Hendrick, J.P. and F.U. Hartl, *Molecular Chaperone Functions of Heat-Shock Proteins.* Ann. Rev. Biochem., 1993. **62**: p. 349-384.

23. Craig, E.A. and C.A. Gross, *Is hsp70 the cellular thermometer?* Trends Biochem Sci, 1991. **16**(4): p. 135-40.

24. Craig, E.A., B.D. Gambill, and R.J. Nelson, *Heat-Shock Proteins - Molecular Chaperones of Protein Biogenesis.* Microbiol. Rev., 1993. **57**(2): p. 402-414.

25. Shi, L., M. Kataoka, and A.L. Fink, *Conformational characterization of DnaK and its complexes by small-angle X-ray scattering.* Biochemistry, 1996. **35**(10): p. 3297-3308.

26. Bertelsen, E.B. and E.R. Zuiderweg, *Solution conformation of E.Coli Hsp70 complexed with ADP and substrate.* Proceedings of the National Academy of Sceinces, USA, 2008.

27. Bork, P., C. Sander, and A. Valencia, *AN ATPASE DOMAIN COMMON TO PROKARYOTIC CELL-CYCLE PROTEINS, SUGAR KINASES, ACTIN, AND HSP70 HEAT-SHOCK PROTEINS.* Proceedings of the National Academy of Sciences of the United States of America, 1992. **89**(16): p. 7290-7294.

28. Harrison, C.J., et al., *Crystal structure of the nucleotide exchange factor GrpE bound to the ATPase domain of the molecular chaperone DnaK.* Science, 1997. **276**(5311): p. 431-5.

29. DeLuca-Flaherty, C., et al., *Crystals of an ATPase fragment of bovine clathrin uncoating ATPase.* J Mol Biol, 1988. **200**(4): p. 749-50.

30. Zhu, X.T., et al., *Structural analysis of substrate binding by the molecular chaperone DnaK.* Science, 1996. **272**(5268): p. 1606-1614.

31. Mayer, M.P., et al., *Multistep mechanism of substrate binding determines chaperone activity of Hsp70.* Nat Struct Biol, 2000. **7**(7): p. 586-93.

32. Rudiger, S., et al., *Modulation of substrate specificity of the DnaK chaperone by alteration of a hydrophobic arch.* J Mol Biol, 2000. **304**(3): p. 245-51.

33. Pellecchia, M., et al., *Structural insights into substrate binding by the molecular chaperone DnaK.* Nat Struct Biol, 2000. **7**(4): p. 298-303.

34.   Buczynski, G., et al., *Characterization of a lidless form of the molecular chaperone DnaK: deletion of the lid increases peptide on- and off-rate constants.* J Biol Chem, 2001. **276**(29): p. 27231-6.

35.   Morshauser, R.C., et al., *High-resolution solution structure of the 18 kDa substrate-binding domain of the mammalian chaperone protein Hsc70.* J Mol Biol, 1999. **289**(5): p. 1387-403.

36.   Stevens, S.Y., et al., *The solution structure of the bacterial HSP70 chaperone protein domain DnaK(393-507) in complex with the peptide NRLLLTG.* Protein Sci, 2003. **12**(11): p. 2588-96.

37.   Hartl, F.U., R. Hlodan, and T. Langer, *Molecular chaperones in protein folding: the art of avoiding sticky situations.* Trends Biochem. Sci., 1994. **19**(1): p. 20-25.

38.   Liberek, K., et al., *Escherichia-Coli Dnaj and Grpe Heat-Shock Proteins Jointly Stimulate Atpase Activity of Dnak.* Proc. Natl. Acad. Sci. USA, 1991. **88**(7): p. 2874-2878.

39.   McCarty, J.S., et al., *The role of ATP in the functional cycle of the DnaK chaperone system.* J. Mol. Biol., 1995. **249**(1): p. 126-137.

40.   Packschies, L., et al., *GrpE accelerates nucleotide exchange of the molecular chaperone DnaK with an associative displacement mechanism.* Biochemistry, 1997. **36**(12): p. 3417-3422.

41.   Laufen, T., et al., *Mechanism of regulation of hsp70 chaperones by DnaJ cochaperones.* Proc Natl Acad Sci U S A, 1999. **96**(10): p. 5452-7.

42.   Kelley, W.L., *The J-domain family and the recruitment of chaperone power.* Trends in Biochemical Sciences, 1998. **23**(6): p. 222-227.

43.   Mayer, M.P. and B. Bukau, *Hsp70 chaperone systems: diversity of cellular functions and mechanism of action.* Biol. Chem., 1998. **379**(3): p. 261-268.

44.   Caplan, A.J. and M.G. Douglas, *CHARACTERIZATION OF YDJ1 - A YEAST HOMOLOG OF THE BACTERIAL DNAJ PROTEIN.* Journal of Cell Biology, 1991. **114**(4): p. 609-621.

45.   Lu, Z. and D.M. Cyr, *The conserved carboxyl terminus and zinc finger-like domain of the co-chaperone Ydj1 assist Hsp70 in protein folding.* J. Biol. Chem., 1998. **273**(10): p. 5970-5978.

46.   Qiu, X.B., et al., *The diversity of the DnaJ/Hsp40 family, the crucial partners for Hsp70 chaperones.* Cellular and Molecular Life Sciences, 2006. **63**(22): p. 2560-2570.

47.   Tang, W. and C.C. Wang, *Zinc fingers and thiol-disulfide oxidoreductase activities of chaperone DnaJ.* Biochemistry, 2001. **40**(49): p. 14985-14994.

48.   Ahle, S. and E. Ungewickell, *AUXILIN, A NEWLY IDENTIFIED CLATHRIN-ASSOCIATED PROTEIN IN COATED VESICLES FROM BOVINE BRAIN.* Journal of Cell Biology, 1990. **111**(1): p. 19-29.

49.   Ungewickell, E., et al., *Role of auxilin in uncoating clathrin-coated vesicles.* Nature, 1995. **378**(6557): p. 632-635.

50.   Tobaben, S., et al., *A trimeric protein complex functions as a synaptic chaperone machine.* Neuron, 2001. **31**(6): p. 987-999.

51.   Mayer, M.P. and B. Bukau, *Hsp70 chaperones: cellular functions and molecular mechanism.* Cell Mol Life Sci, 2005. **62**(6): p. 670-84.

52.	Linke, K., et al., *The roles of the two zinc binding sites in DnaJ.* Journal of Biological Chemistry, 2003. **278**(45): p. 44457-44466.

53.	Hu, J., et al., *THE CRYSTAL STRUCTURE OF THE PUTATIVE PEPTIDE-BINDING FRAGMENT FROM THE HUMAN HSP40 PROTEIN HDJ1.*
. BMC Structural Biology, 2008. **8**.

54.	Pellecchia, M., et al., *NMR structure of the J-domain and the Gly/Phe-rich region of the Escherichia coli DnaJ chaperone.* J. Mol. Biol., 1996. **260**(2): p. 236-250.

55.	Sousa, M.C. and D.B. McKay, *The hydroxyl of threonine 13 of the bovine 70-kDa heat shock cognate protein is essential for transducing the ATP-induced conformational change.* Biochemistry, 1998. **37**(44): p. 15392-9.

56.	Genevaux, P., et al., *DjlA is a third DnaK co-chaperone of Escherichia coli, and DjlA-mediated induction of colanic acid capsule requires DjlA-DnaK interaction.* J Biol Chem, 2001. **276**(11): p. 7906-12.

57.	Greene, M.K., K. Maskos, and S.J. Landry, *Role of the J-domain in the cooperation of Hsp40 with Hsp70.* Proc. Natl. Acad. Sci. USA, 1998. **95**(11): p. 6108-6113.

58.	Karzai, A.W. and R. McMacken, *A bipartite signaling mechanism involved in DnaJ-mediated activation of the Escherichia coli DnaK protein.* Journal of Biological Chemistry, 1996. **271**(19): p. 11236-11246.

59.	Wall, D., M. Zylicz, and C. Georgopoulos, *The NH2-terminal 108 amino acids of the Escherichia coli DnaJ protein stimulate the ATPase activity of DnaK and are sufficient for lambda replication.* J Biol Chem, 1994. **269**(7): p. 5446-51.

60.	Sullivan, C.S. and J.M. Pipas, *T antigens of Simian virus 40: Molecular chaperones for viral replication and turnorigenesis.* Microbiology and Molecular Biology Reviews, 2002. **66**(2): p. 179-+.

61.	Zylicz, M., D. Ang, and C. Georgopoulos, *The grpE protein of Escherichia coli. Purification and properties.* J Biol Chem, 1987. **262**(36): p. 17437-42.

62.	Grimshaw, J.P.A., et al., *Thermosensor action of GrpE - The DnaK chaperone system at heat shock temperatures.* Journal of Biological Chemistry, 2003. **278**(21): p. 19048-19053.

63.	Takayama, S., et al., *BAG-1 modulates the chaperone activity of Hsp70/Hsc70.* Embo J., 1997. **16**(16): p. 4887-4896.

64.	Ang, D. and C. Georgopoulos, *THE HEAT-SHOCK-REGULATED GRPE GENE OF ESCHERICHIA-COLI IS REQUIRED FOR BACTERIAL-GROWTH AT ALL TEMPERATURES BUT IS DISPENSABLE IN CERTAIN MUTANT BACKGROUNDS.* Journal of Bacteriology, 1989. **171**(5): p. 2748-2755.

65.	Shomura, Y., et al., *Regulation of Hsp70 function by HspBP1: structural analysis reveals an alternate mechanism for Hsp70 nucleotide exchange.* Mol Cell, 2005. **17**(3): p. 367-79.

66.	Carrettiero, D.C., et al., *The Cochaperone BAG2 Sweeps Paired Helical Filament-Insoluble Tau from the Microtubule.* Journal of Neuroscience, 2009. **29**(7): p. 2151-2161.

67.	Lee-Yoon, D., et al., *Identification of a major subfamily of large hsp70-like proteins through the cloning of the mammalian 110-kDa heat shock protein.* J. Biol. Chem., 1995. **270**(26): p. 15725-15733.

68.   Buchberger, A., et al., *A conserved loop in the ATPase domain of the DnaK chaperone is essential for stable binding of GrpE.* Nat.. Struct. Biol., 1994. **1**(2): p. 95-101.

69.   Grimshaw, J.P.A., et al., *The heat-sensitive Escherichia coli grpE280 phenotype: Impaired interaction of GrpE(G122D) with DnaK.* Journal of Molecular Biology, 2005. **353**(4): p. 888-896.

70.   Mehl, A.F., L.D. Heskett, and K.M. Neal, *A GrpE mutant containing the NH2-terminal "tail" region is able to displace bound polypeptide substrate from DnaK.* Biochemical and Biophysical Research Communications, 2001. **282**(2): p. 562-569.

71.   Gassler, C.S., et al., *Bag-1M accelerates nucleotide release for human Hsc70 and Hsp70 and can act concentration-dependent as positive and negative cofactor.* J Biol Chem, 2001. **276**(35): p. 32538-44.

72.   Brehmer, D., et al., *Tuning of chaperone activity of Hsp70 proteins by modulation of nucleotide exchange.* Nat Struct Biol, 2001. **8**(5): p. 427-32.

73.   Takayama, S. and J.C. Reed, *Molecular chaperone targeting and regulation by BAG family proteins.* Nature Cell Biology, 2001. **3**(10): p. E237-E241.

74.   Sondermann, H., et al., *Structure of a Bag/Hsc70 complex: convergent functional evolution of Hsp70 nucleotide exchange factors.* Science, 2001. **291**(5508): p. 1553-7.

75.   Briknarova, K., et al., *Structural analysis of BAG1 cochaperone and its interactions with Hsc70 heat shock protein.* Nature Structural Biology, 2001. **8**(4): p. 349-352.

76.   Briknarova, K., et al., *BAG4/SODD protein contains a short BAG domain.* Journal of Biological Chemistry, 2002. **277**(34): p. 31172-31178.

77.   Buchberger, A., et al., *Functional defects of the DnaK756 mutant chaperone of Escherichia coli indicate distinct roles for amino- and carboxyl-terminal residues in substrate and co-chaperone interaction and interdomain communication.* J Biol Chem, 1999. **274**(53): p. 38017-26.

78.   Kabani, M., J.M. Beckerich, and J.L. Brodsky, *Nucleotide exchange factor for the yeast Hsp70 molecular chaperone Ssa1p.* Mol Cell Biol, 2002. **22**(13): p. 4677-89.

79.   Kabani, M., et al., *HspBP1, a homologue of the yeast Fes1 and Sls1 proteins, is an Hsc70 nucleotide exchange factor.* FEBS Lett, 2002. **531**(2): p. 339-42.

80.   Kampinga, H.H. and E.A. Craig, *The HSP70 chaperone machinery: J proteins as drivers of functional specificity.* Nat Rev Mol Cell Biol, 2010. **11**(8): p. 579-92.

81.   Schroder, H., et al., *Dnak, Dnaj and Grpe Form a Cellular Chaperone Machinery Capable of Repairing Heat-Induced Protein Damage.* Embo J., 1993. **12**(11): p. 4137-4144.

82.   Ben-Zvi, A., et al., *Active solubilization and refolding of stable protein aggregates by cooperative unfolding action of individual Hsp70 chaperones.* Journal of Biological Chemistry, 2004. **279**(36): p. 37298-37303.

83.   Frydman, J., *Folding of newly translated proteins in vivo: the role of molecular chaperones.* Annu Rev Biochem., 2000(70): p. 603-647.

84.   Hohfeld, J., Minami, Y., Hartl, F.-U. , *Hip, a novel cochaperone involved in the eukaryotic Hsc70/Hsp40 reaction cycle.* cell, 1995. **83**: p. 589-598.

85. Gross, M. and S. Hessefort, *Purification and characterization of a 66-kDa protein from rabbit reticulocyte lysate which promotes the recycling of Hsp 70.* Journal of Biological Chemistry, 1996. **271**(28): p. 16833-16841.

86. Szabo, A., et al., *The ATP hydrolysis-dependent reaction cycle of the Escherichia coli Hsp70 system DnaK, DnaJ, and GrpE.* Proc. Natl. Acad. Sci. USA, 1994. **91**(22): p. 10345-10349.

87. Buchberger, A., et al., *Nucleotide-induced conformational changes in the ATPase and substrate binding domains of the DnaK chaperone provide evidence for interdomain communication.* J. Biol. Chem., 1995. **270**(28): p. 16903-16910.

88. Chang, L., et al., *Mutagenesis Reveals the Complex Relationships between ATPase Rate and the Chaperone Activities of Escherichia coli Heat Shock Protein 70 (Hsp70/DnaK).* Journal of Biological Chemistry, 2010. **285**(28): p. 21282-21291.

89. Swain, J.F., et al., *Hsp70 chaperone ligands control domain association via an allosteric mechanism mediated by the interdomain linker.* Mol Cell, 2007. **26**(1): p. 27-39.

90. Swain, J.F., E.G. Schulz, and L.M. Gierasch, *Direct comparison of a stable isolated Hsp70 substrate-binding domain in the empty and substrate-bound states.* J Biol Chem, 2006. **281**(3): p. 1605-11.

91. Jiang, J., et al., *Structural basis of interdomain communication in the Hsc70 chaperone.* Mol. Cell, 2005. **20**: p. 513-524.

92. Liu, Q. and W.A. Hendrickson, *Insights into hsp70 chaperone activity from a crystal structure of the yeast Hsp110 Sse1.* Cell, 2007. **131**: p. 106-120.

93. Zhang, Y. and E.R. Zuiderweg, *The 70-kDa heat shock protein chaperone nucleotide-binding domain in solution unveiled as a molecular machine that can reorient its functional subdomains.* Proc Natl Acad Sci U S A, 2004. **101**(28): p. 10272-7.

94. Revington, M., et al., *NMR investigations of allosteric processes in a two-domain Thermus thermophilus Hsp70 molecular chaperone.* J Mol Biol, 2005. **349**(1): p. 163-83.

95. Bhattacharya, A., et al., *Allostery in Hsp70 chaperones is transduced by subdomain rotations.* J Mol Biol, 2009. **388**(3): p. 475-90.

96. Gassler, C.S., et al., *Mutations in the DnaK chaperone affecting interaction with the DnaJ cochaperone.* Proc Natl Acad Sci U S A, 1998. **95**(26): p. 15229-34.

97. Vogel, M., B. Bukau, and M.P. Mayer, *Allosteric regulation of Hsp70 chaperones by a proline switch.* Mol Cell, 2006. **21**(3): p. 359-67.

98. Vogel, M., M.P. Mayer, and B. Bukau, *Allosteric regulation of Hsp70 chaperones involves a conserved interdomain linker.* J Biol Chem, 2006. **281**(50): p. 38705-11.

99. Han, W. and P. Christen, *Mutations in the interdomain linker region of DnaK abolish the chaperone action of the DnaK/DnaJ/GrpE system.* FEBS letters, 2001. **497**: p. 55-58.

100. Montgomery, D.L., R.I. Morimoto, and L.M. Gierasch, *Mutations in the substrate binding domain of the Escherichia coli 70 kDa molecular chaperone, DnaK, which alter substrate affinity or interdomain coupling.* J. Mol. Biol., 1999. **286**(3): p. 915-932.

101. Burkholder, W.F., et al., *Mutations in the C-terminal fragment of DnaK affecting peptide binding.* Proc. Natl. Acad. Sci. USA, 1996. **93**(20): p. 10632-10637.

102. Voisine, C., et al., *The protein import motor of mitochondria: unfolding and trapping of preproteins are distinct and separable functions of matrix Hsp70.* Cell, 1999. **97**(5): p. 565-74.

103. Smock, R.G., et al., *An interdomain sector mediating allostery in Hsp70 molecular chaperones.* Molecular Systems Biology, 2010. **6**.

104. Wilbanks, S.M., et al., *Solution small-angle X-ray scattering study of the molecular chaperone Hsc70 and its subfragments.* Biochemistry, 1995. **34**(38): p. 12095-12106.

105. Rist, W., et al., *Amide hydrogen exchange reveals conformational changes in hsp70 chaperones important for allosteric regulation.* J Biol Chem, 2006. **281**(24): p. 16493-501.

106. Slepenkov, S.V. and S.N. Witt, *Kinetics of the reactions of the Escherichia coli molecular chaperone DnaK with ATP: evidence that a three-step reaction precedes ATP hydrolysis.* Biochemistry, 1998. **37**(4): p. 1015-1024.

107. Slepenkov, S.V. and S.N. Witt, *Peptide-induced conformational changes in the molecular chaperone DnaK.* Biochemistry, 1998. **37**(47): p. 16749-56.

108. Slepenkov, S.V. and S.N. Witt, *Kinetic analysis of interdomain coupling in a lidless variant of the molecular chaperone DnaK: DnaK's lid inhibits transition to the low affinity state.* Biochemistry, 2002. **41**(40): p. 12224-35.

109. Slepenkov, S.V. and S.N. Witt, *The unfolding story of the Escherichia coli Hsp70 DnaK: is DnaK a holdase or an unfoldase?* Mol Microbiol, 2002. **45**(5): p. 1197-206.

110. Slepenkov, S.V. and S.N. Witt, *Detection of a concerted conformational change in the ATPase domain of DnaK triggered by peptide binding.* FEBS Lett, 2003. **539**(1-3): p. 100-4.

111. Buchberger, A., et al., *The chaperone function of DnaK requires the coupling of ATPase activity with substrate binding through residue E171.* Embo J., 1994. **13**(7): p. 1687-1695.

112. Revington, M., T.M. Holder, and E.R. Zuiderweg, *NMR study of nucleotide-induced changes in the nucleotide binding domain of Thermus thermophilus Hsp70 chaperone DnaK: implications for the allosteric mechanism.* J Biol Chem, 2004. **279**(32): p. 33958-67.

113. Morshauser, R.C., et al., *The peptide-binding domain of the chaperone protein Hsc70 has an unusual secondary structure topology.* Biochemistry, 1995. **34**(19): p. 6261-6.

114. Swain, J.F., E.G. Schulz, and L.M. Gierasch, *Direct comparison of a stable isolated Hsp70 substrate-binding domain in the empty and substrate-bound states.* Journal of Biological Chemistry, 2006. **281**(3): p. 1605-1611.

115. Morshauser, R.C. and E.R.P. Zuiderweg, *High Resolution Four-Dimensional HMQC-NOESY-HSQC Spectroscopy.* J. Magn. Reson., 1999. **139**: p. 232-239.

116. Flaherty, K.M., C. Deluca-Flaherty, and D.B. McKay, *3-Dimensional Structure of the ATPase Fragment of a 70k Heat-Shock Cognate Protein.* Nature, 1990. **346**(6285): p. 623-628.

117. O'Brien, M.C. and D.B. McKay, *Threonine 204 of the chaperone protein Hsc70 influences the structure of the active site, but is not essential for ATP hydrolysis.* J Biol Chem, 1993. **268**(32): p. 24323-9.

118. Connell, P., et al., *The co-chaperone CHIP regulates protein triage decisions mediated by heat-shock proteins.* Nat Cell Biol, 2001. **3**(1): p. 93-6.

119. Meacham, G.C., et al., *The Hsc70 co-chaperone CHIP targets immature CFTR for proteasomal degradation.* Nat Cell Biol, 2001. **3**(1): p. 100-5.

120. Rocca, W.A., et al., *FREQUENCY AND DISTRIBUTION OF ALZHEIMERS-DISEASE IN EUROPE - A COLLABORATIVE STUDY OF 1980-1990 PREVALENCE FINDINGS.* Annals of Neurology, 1991. **30**(3): p. 381-390.

121. Ferri, C.P., et al., *Global prevalence of dementia: a Delphi consensus study.* Lancet, 2005. **366**(9503): p. 2112-2117.

122. Masters, C.L., et al., *AMYLOID PLAQUE CORE PROTEIN IN ALZHEIMER-DISEASE AND DOWN SYNDROME.* Proceedings of the National Academy of Sciences of the United States of America, 1985. **82**(12): p. 4245-4249.

123. Glenner, G.G. and C.W. Wong, *ALZHEIMERS-DISEASE - INITIAL REPORT OF THE PURIFICATION AND CHARACTERIZATION OF A NOVEL CEREBROVASCULAR AMYLOID PROTEIN.* Biochemical and Biophysical Research Communications, 1984. **120**(3): p. 885-890.

124. Kidd, M., *PAIRED HELICAL FILAMENTS IN ELECTRON MICROSCOPY OF ALZHEIMERS DISEASE.* Nature, 1963. **197**(486): p. 192-&.

125. Crowther, R.A. and C.M. Wischik, *IMAGE-RECONSTRUCTION OF THE ALZHEIMER PAIRED HELICAL FILAMENT.* Embo Journal, 1985. **4**(13B): p. 3661-3665.

126. Ohtsubo, K., et al., *3-DIMENSIONAL STRUCTURE OF ALZHEIMERS NEUROFIBRILLARY TANGLES OF THE AGED HUMAN BRAIN REVEALED BY THE QUICK-FREEZE, DEEP-ETCH AND REPLICA METHOD.* Acta Neuropathologica, 1990. **79**(5): p. 480-485.

127. Pollanen, M.S., et al., *TWISTED RIBBON STRUCTURE OF PAIRED HELICAL FILAMENTS REVEALED BY ATOMIC-FORCE MICROSCOPY.* American Journal of Pathology, 1994. **144**(5): p. 869-873.

128. Pollanen, M.S., P. Markiewicz, and M.C. Goh, *Paired helical filaments are twisted ribbons composed of two parallel and aligned components: Image reconstruction and modeling of filament structure using atomic force microscopy.* Journal of Neuropathology and Experimental Neurology, 1997. **56**(1): p. 79-85.

129. Schweers, O., et al., *STRUCTURAL STUDIES OF TAU-PROTEIN AND ALZHEIMER PAIRED HELICAL FILAMENTS SHOW NO EVIDENCE FOR BETA-STRUCTURE.* Journal of Biological Chemistry, 1994. **269**(39): p. 24290-24297.

130. Sadqi, M., et al., *alpha-helix structure in Alzheimer's disease aggregates of tau-protein.* Biochemistry, 2002. **41**(22): p. 7150-7155.

131. Spillantini, M.G., et al., *alpha-synuclein in Lewy bodies.* Nature, 1997. **388**(6645): p. 839-840.

132. Alonso, A.D., et al., *Interaction of tau isoforms with Alzheimer's disease abnormally hyperphosphorylated tau and in vitro phosphorylation into the*

disease-like protein. Journal of Biological Chemistry, 2001. **276**(41): p. 37967-37973.

133. Tolnay, M. and A. Probst, *REVIEW: tau protein pathology in Alzheimer's disease and related disorders.* Neuropathology and Applied Neurobiology, 1999. **25**(3): p. 171-187.

134. Friedhoff, P., et al., *Structure of tau protein and assembly into paired helical filaments.* Biochimica Et Biophysica Acta-Molecular Basis of Disease, 2000. **1502**(1): p. 122-132.

135. Braak, H. and E. Braak, *NEUROPATHOLOGICAL STAGING OF ALZHEIMER-RELATED CHANGES.* Acta Neuropathologica, 1991. **82**(4): p. 239-259.

136. Cleveland, D.W., S.Y. Hwo, and M.W. Kirschner, *PHYSICAL AND CHEMICAL PROPERTIES OF PURIFIED TAU FACTOR AND ROLE OF TAU IN MICROTUBULE ASSEMBLY.* Journal of Molecular Biology, 1977. **116**(2): p. 227-247.

137. Buee, L., et al., *Tau protein isoforms, phosphorylation and role in neurodegenerative disorders.* Brain Research Reviews, 2000. **33**(1): p. 95-130.

138. Hutton, M., et al., *Association of missense and 5 '-splice-site mutations in tau with the inherited dementia FTDP-17.* Nature, 1998. **393**(6686): p. 702-705.

139. Kosik, K.S., *THE MOLECULAR AND CELLULAR BIOLOGY OF TAU.* Brain Pathology, 1993. **3**(1): p. 39-43.

140. Spillantini, M.G. and M. Goedert, *Tau mutations in familial frontotemporal dementia.* Brain, 2000. **123**: p. 857-859.

141. Shahani, N. and R. Brandt, *Functions and malfunctions of the tau proteins.* Cellular and Molecular Life Sciences, 2002. **59**(10): p. 1668-1680.

142. Geschwind, D.H., *Tau phosphorylation, tangles, and neurodegeneration: The chicken or the egg?* Neuron, 2003. **40**(3): p. 457-460.

143. Dumanchin, C., et al., *Segregation of a missense mutation in the microtubule-associated protein tau gene with familial frontotemporal dementia and parkinsonism.* Human Molecular Genetics, 1998. **7**(11): p. 1825-1829.

144. Cleveland, D.W., S.Y. Hwo, and M.W. Kirschner, *PURIFICATION OF TAU, A MICROTUBULE-ASSOCIATED PROTEIN THAT INDUCES ASSEMBLY OF MICROTUBULES FROM PURIFIED TUBULIN.* Journal of Molecular Biology, 1977. **116**(2): p. 207-225.

145. Fellous, A., et al., *MICROTUBULE ASSEMBLY INVITRO - PURIFICATION OF ASSEMBLY-PROMOTING FACTORS.* European Journal of Biochemistry, 1977. **78**(1): p. 167-174.

146. Weingarten, M.D., et al., *PROTEIN FACTOR ESSENTIAL FOR MICROTUBULE ASSEMBLY.* Proceedings of the National Academy of Sciences of the United States of America, 1975. **72**(5): p. 1858-1862.

147. Hagestedt, T., et al., *TAU-PROTEIN BECOMES LONG AND STIFF UPON PHOSPHORYLATION - CORRELATION BETWEEN PARACRYSTALLINE STRUCTURE AND DEGREE OF PHOSPHORYLATION.* Journal of Cell Biology, 1989. **109**(4): p. 1643-1651.

148. Gong, C.X., I. Grundke-Iqbal, and K. Iqbal, *Targeting Tau Protein in Alzheimer's Disease.* Drugs & Aging, 2010. **27**(5): p. 351-365.

149. Butner, K.A. and M.W. Kirschner, *TAU-PROTEIN BINDS TO MICROTUBULES THROUGH A FLEXIBLE ARRAY OF DISTRIBUTED WEAK SITES.* Journal of Cell Biology, 1991. **115**(3): p. 717-730.

150. Feijoo, C., et al., *Evidence that phosphorylation of the microtubule-associated protein Tau by SAPK4/p38 delta at Thr50 promotes microtubule assembly.* Journal of Cell Science, 2005. **118**(2): p. 397-408.

151. Lindwall, G. and R.D. Cole, *PHOSPHORYLATION AFFECTS THE ABILITY OF TAU-PROTEIN TO PROMOTE MICROTUBULE ASSEMBLY.* Journal of Biological Chemistry, 1984. **259**(8): p. 5301-5305.

152. Biernat, J., et al., *PHOSPHORYLATION OF SER(262) STRONGLY REDUCES BINDING OF TAU-PROTEIN TO MICROTUBULES - DISTINCTION BETWEEN PHF-LIKE IMMUNOREACTIVITY AND MICROTUBULE-BINDING.* Neuron, 1993. **11**(1): p. 153-163.

153. Illenberger, S., et al., *Phosphorylation of microtubule-associated proteins MAP2 and MAP4 by the protein kinase p110(mark) - Phosphorylation sites and regulation of microtubule dynamics.* Journal of Biological Chemistry, 1996. **271**(18): p. 10834-10843.

154. Drewes, G., et al., *MARK, a novel family of protein kinases that phosphorylate microtubule-associated proteins and trigger microtubule disruption.* Cell, 1997. **89**(2): p. 297-308.

155. Illenberger, S., et al., *The endogenous and cell cycle-dependent phosphorylation of tau protein in living cells: Implications for Alzheimer's disease.* Molecular Biology of the Cell, 1998. **9**(6): p. 1495-1512.

156. Zheng-Fischhofer, Q.Y., et al., *Sequential phosphorylation of Tau by glycogen synthase kinase-3 beta and protein kinase A at Thr212 and Ser214 generates the Alzheimer-specific epitope of antibody AT100 and requires a paired-helical-filament-like conformation.* European Journal of Biochemistry, 1998. **252**(3): p. 542-552.

157. Drechsel, D.N., et al., *MODULATION OF THE DYNAMIC INSTABILITY OF TUBULIN ASSEMBLY BY THE MICROTUBULE-ASSOCIATED PROTEIN TAU.* Molecular Biology of the Cell, 1992. **3**(10): p. 1141-1154.

158. Brandt, R., et al., *DIFFERENTIAL EFFECT OF PHOSPHORYLATION AND SUBSTRATE MODULATION ON TAUS ABILITY TO PROMOTE MICROTUBULE GROWTH AND NUCLEATION.* Journal of Biological Chemistry, 1994. **269**(16): p. 11776-11782.

159. Yoshida, H. and Y. Ihara, *TAU IN PAIRED HELICAL FILAMENTS IS FUNCTIONALLY DISTINCT FROM FETAL TAU - ASSEMBLY INCOMPETENCE OF PAIRED HELICAL FILAMENT-TAU.* Journal of Neurochemistry, 1993. **61**(3): p. 1183-1186.

160. Bramblett, G.T., et al., *ABNORMAL TAU-PHOSPHORYLATION AT SER(396) IN ALZHEIMERS-DISEASE RECAPITULATES DEVELOPMENT AND CONTRIBUTES TO REDUCED MICROTUBULE-BINDING.* Neuron, 1993. **10**(6): p. 1089-1099.

161. Baudier, J., S.H. Lee, and R.D. Cole, *SEPARATION OF THE DIFFERENT MICROTUBULE-ASSOCIATED TAU-PROTEIN SPECIES FROM BOVINE BRAIN AND THEIR MODE-II PHOSPHORYLATION BY CA-2+*

PHOSPHOLIPID-DEPENDENT PROTEIN-KINASE-C. Journal of Biological Chemistry, 1987. **262**(36): p. 17584-17590.

162. Grundkeiqbal, I., et al., *ABNORMAL PHOSPHORYLATION OF THE MICROTUBULE-ASSOCIATED PROTEIN-TAU (TAU) IN ALZHEIMER CYTOSKELETAL PATHOLOGY.* Proceedings of the National Academy of Sciences of the United States of America, 1986. **83**(13): p. 4913-4917.

163. Hall, G.F., et al., *Staging of neurofibrillary degeneration caused by human tau overexpression in a unique cellular model of human tauopathy.* American Journal of Pathology, 2001. **158**(1): p. 235-246.

164. Williamson, R., et al., *Rapid tyrosine phosphorylation of neuronal proteins including tau and focal adhesion kinase in response to amyloid-beta peptide exposure: Involvement of src family protein kinases.* Journal of Neuroscience, 2002. **22**(1): p. 10-20.

165. Correas, I., J. Diaznido, and J. Avila, *MICROTUBULE-ASSOCIATED PROTEIN-TAU IS PHOSPHORYLATED BY PROTEIN-KINASE-C ON ITS TUBULIN BINDING DOMAIN.* Journal of Biological Chemistry, 1992. **267**(22): p. 15721-15728.

166. Drewes, G., et al., *MITOGEN ACTIVATED PROTEIN (MAP) KINASE TRANSFORMS TAU-PROTEIN INTO AN ALZHEIMER-LIKE STATE.* Embo Journal, 1992. **11**(6): p. 2131-2138.

167. Goedert, M., et al., *Phosphorylation of microtubule-associated protein tau by stress-activated protein kinases.* Febs Letters, 1997. **409**(1): p. 57-62.

168. Hanger, D.P., et al., *GLYCOGEN-SYNTHASE KINASE-3 INDUCES ALZHEIMERS DISEASE-LIKE PHOSPHORYLATION OF TAU - GENERATION OF PAIRED HELICAL FILAMENT EPITOPES AND NEURONAL LOCALIZATION OF THE KINASE.* Neuroscience Letters, 1992. **147**(1): p. 58-62.

169. Imahori, K. and T. Uchida, *Physiology and pathology of tau protein kinases in relation to Alzheimer's disease.* Journal of Biochemistry, 1997. **121**(2): p. 179-188.

170. Lucas, J.J., et al., *Decreased nuclear beta-catenin, tau hyperphosphorylation and neurodegeneration in GSK-3 beta conditional transgenic mice.* Embo Journal, 2001. **20**(1-2): p. 27-39.

171. Scott, C.W., et al., *PHOSPHORYLATION OF RECOMBINANT TAU BY CAMP-DEPENDENT PROTEIN-KINASE - IDENTIFICATION OF PHOSPHORYLATION SITES AND EFFECT ON MICROTUBULE ASSEMBLY.* Journal of Biological Chemistry, 1993. **268**(2): p. 1166-1173.

172. Geddes, J.F., et al., *PATHOLOGICAL OVERLAP IN CASES OF PARKINSONISM ASSOCIATED WITH NEUROFIBRILLARY TANGLES - A STUDY OF RECENT CASES OF POSTENCEPHALITIC PARKINSONISM AND COMPARISON WITH PROGRESSIVE SUPRANUCLEAR PALSY AND GUAMANIAN PARKINSONISM-DEMENTIA COMPLEX.* Brain, 1993. **116**: p. 281-302.

173. Goedert, M., et al., *P42 MAP KINASE PHOSPHORYLATION SITES IN MICROTUBULE-ASSOCIATED PROTEIN TAU ARE DEPHOSPHORYLATED BY PROTEIN PHOSPHATASE-2A1 - IMPLICATIONS FOR ALZHEIMERS-DISEASE.* Febs Letters, 1992. **312**(1): p. 95-99.

174.   Szucs, K., et al., *DEPHOSPHORYLATION OF TAU-PROTEIN FROM ALZHEIMERS-DISEASE PATIENTS.* Neuroscience Letters, 1994. **165**(1-2): p. 175-178.

175.   Yamamoto, H., et al., *DEPHOSPHORYLATION OF FETAL-TAU AND PAIRED HELICAL FILAMENTS-TAU BY PROTEIN PHOSPHATASE-1 AND PROTEIN PHOSPHATASE-2A AND CALCINEURIN.* Journal of Biochemistry, 1995. **118**(6): p. 1224-1231.

176.   Gong, C.X., I. Grundkeiqbal, and K. Iqbal, *DEPHOSPHORYLATION OF ALZHEIMERS-DISEASE ABNORMALLY PHOSPHORYLATED-TAU BY PROTEIN PHOSPHATASE-2A.* Neuroscience, 1994. **61**(4): p. 765-772.

177.   Gong, C.X., et al., *ALZHEIMERS-DISEASE ABNORMALLY PHOSPHORYLATED-TAU IS DEPHOSPHORYLATED BY PROTEIN PHOSPHATASE-2B (CALCINEURIN).* Journal of Neurochemistry, 1994. **62**(2): p. 803-806.

178.   Tucker, R.P., *THE ROLES OF MICROTUBULE-ASSOCIATED PROTEINS IN BRAIN MORPHOGENESIS - A REVIEW.* Brain Research Reviews, 1990. **15**(2): p. 101-120.

179.   Lannfelt, L., *Biochemical diagnostic markers to detect early Alzheimer's disease.* Neurobiology of Aging, 1998. **19**(2): p. 165-167.

180.   Drubin, D.G. and M.W. Kirschner, *TAU-PROTEIN FUNCTION IN LIVING CELLS.* Journal of Cell Biology, 1986. **103**(6): p. 2739-2746.

181.   Flanagan, L.A., et al., *The structure of divalent cation-induced aggregates of PIP2 and their alteration by gelsolin and tau.* Biophysical Journal, 1997. **73**(3): p. 1440-1447.

182.   Jenkins, S.M. and G.V.W. Johnson, *Tau complexes with phospholipase C-gamma in situ.* Neuroreport, 1998. **9**(1): p. 67-71.

183.   Cunningham, C.C., et al., *Microtubule-associated protein 2c reorganizes both microtubules and microfilaments into distinct cytological structures in an actin-binding protein-280-deficient melanoma cell line.* Journal of Cell Biology, 1997. **136**(4): p. 845-857.

184.   Mandell, J.W. and G.A. Banker, *A spatial gradient of tau protein phosphorylation in nascent axons.* Journal of Neuroscience, 1996. **16**(18): p. 5727-5740.

185.   Brandt, R., J. Leger, and G. Lee, *INTERACTION OF TAU WITH THE NEURAL PLASMA-MEMBRANE MEDIATED BY TAU AMINO-TERMINAL PROJECTION DOMAIN.* Journal of Cell Biology, 1995. **131**(5): p. 1327-1340.

186.   Lee, G., et al., *Tau interacts with src-family non-receptor tyrosine kinases.* Journal of Cell Science, 1998. **111**: p. 3167-3177.

187.   Ebneth, A., et al., *Overexpression of tau protein inhibits kinesin-dependent trafficking of vesicles, mitochondria, and endoplasmic reticulum: Implications for Alzheimer's disease.* Journal of Cell Biology, 1998. **143**(3): p. 777-794.

188.   Mandelkow, E.M. and E. Mandelkow, *Tau in Alzheimer's disease.* Trends in Cell Biology, 1998. **8**(11): p. 425-427.

189.   Brandt, R. and G. Lee, *FUNCTIONAL-ORGANIZATION OF MICROTUBULE-ASSOCIATED PROTEIN-TAU - IDENTIFICATION OF REGIONS WHICH AFFECT MICROTUBULE GROWTH, NUCLEATION, AND BUNDLE*

FORMATION INVITRO. Journal of Biological Chemistry, 1993. **268**(5): p. 3414-3419.

190. Trinczek, B., et al., *DOMAINS OF TAU-PROTEIN, DIFFERENTIAL PHOSPHORYLATION, AND DYNAMIC INSTABILITY OF MICROTUBULES.* Molecular Biology of the Cell, 1995. **6**(12): p. 1887-1902.

191. Kanai, Y., et al., *EXPRESSION OF MULTIPLE TAU ISOFORMS AND MICROTUBULE BUNDLE FORMATION IN FIBROBLASTS TRANSFECTED WITH A SINGLE TAU CDNA.* Journal of Cell Biology, 1989. **109**(3): p. 1173-1184.

192. Kanai, Y., J.G. Chen, and N. Hirokawa, *MICROTUBULE BUNDLING BY TAU PROTEINS INVIVO - ANALYSIS OF FUNCTIONAL DOMAINS.* Embo Journal, 1992. **11**(11): p. 3953-3961.

193. Lee, G. and S.L. Rook, *EXPRESSION OF TAU PROTEIN IN NONNEURONAL CELLS - MICROTUBULE BINDING AND STABILIZATION.* Journal of Cell Science, 1992. **102**: p. 227-237.

194. Gustke, N., et al., *DOMAINS OF TAU-PROTEIN AND INTERACTIONS WITH MICROTUBULES.* Biochemistry, 1994. **33**(32): p. 9511-9522.

195. Goode, B.L. and S.C. Feinstein, *IDENTIFICATION OF A NOVEL MICROTUBULE-BINDING AND ASSEMBLY DOMAIN IN THE DEVELOPMENTALLY-REGULATED INTER-REPEAT REGION OF TAU.* Journal of Cell Biology, 1994. **124**(5): p. 769-782.

196. Al-Bassam, J., et al., *MAP2 and tau bind longitudinally along the outer ridges of microtubule protofilaments.* Journal of Cell Biology, 2002. **157**(7): p. 1187-1196.

197. Chau, M.F., et al., *The microtubule-associated protein tau cross-links to two distinct sites on each alpha and beta tubulin monomer via separate domains.* Biochemistry, 1998. **37**(51): p. 17692-17703.

198. Kar, S., et al., *Repeat motifs of tau bind to the insides of microtubules in the absence of taxol.* Embo Journal, 2003. **22**(1): p. 70-77.

199. Drewes, G., et al., *MICROTUBULE-ASSOCIATED PROTEIN MICROTUBULE AFFINITY-REGULATING KINASE (P110(MARK)) - A NOVEL PROTEIN-KINASE THAT REGULATES TAU-MICROTUBULE INTERACTIONS AND DYNAMIC INSTABILITY BY PHOSPHORYLATION AT THE ALZHEIMER-SPECIFIC SITE SERINE-262.* Journal of Biological Chemistry, 1995. **270**(13): p. 7679-7688.

200. Carlier, M.F., et al., *INTERACTION BETWEEN MICROTUBULE-ASSOCIATED PROTEIN TAU AND SPECTRIN.* Biochimie, 1984. **66**(4): p. 305-311.

201. Griffith, L.M. and T.D. Pollard, *THE INTERACTION OF ACTIN-FILAMENTS WITH MICROTUBULES AND MICROTUBULE-ASSOCIATED PROTEINS.* Journal of Biological Chemistry, 1982. **257**(15): p. 9143-9151.

202. Henriquez, J.P., et al., *SUBPOPULATIONS OF TAU INTERACT WITH MICROTUBULES AND ACTIN-FILAMENTS IN VARIOUS CELL-TYPES.* Cell Biochemistry and Function, 1995. **13**(4): p. 239-250.

203. Sattilaro, R.F., W.L. Dentler, and E.L. Lecluyse, *MICROTUBULE-ASSOCIATED PROTEINS (MAPS) AND THE ORGANIZATION OF ACTIN-FILAMENTS INVITRO.* Journal of Cell Biology, 1981. **90**(2): p. 467-473.

204. Selden, S.C. and T.D. Pollard, *PHOSPHORYLATION OF MICROTUBULE-ASSOCIATED PROTEINS REGULATES THEIR INTERACTION WITH ACTIN-FILAMENTS.* Journal of Biological Chemistry, 1983. **258**(11): p. 7064-7071.

205. Aamodt, E.J. and R.C. Williams, *MICROTUBULE-ASSOCIATED PROTEINS CONNECT MICROTUBULES AND NEUROFILAMENTS INVITRO.* Biochemistry, 1984. **23**(25): p. 6023-6031.

206. Leterrier, J.F., R.K.H. Liem, and M.L. Shelanski, *INTERACTIONS BETWEEN NEUROFILAMENTS AND MICROTUBULE-ASSOCIATED PROTEINS - A POSSIBLE MECHANISM FOR INTRAORGANELLAR BRIDGING.* Journal of Cell Biology, 1982. **95**(3): p. 982-986.

207. Miyata, Y., et al., *BINDING OF MICROTUBULE-ASSOCIATED PROTEIN-2 AND TAU TO THE INTERMEDIATE FILAMENT REASSEMBLED FROM NEUROFILAMENT 70-KDA SUBUNIT PROTEIN - ITS REGULATION BY CALMODULIN.* Journal of Biological Chemistry, 1986. **261**(28): p. 3026-3030.

208. Matus, A., *STIFF MICROTUBULES AND NEURONAL MORPHOLOGY.* Trends in Neurosciences, 1994. **17**(1): p. 19-22.

209. Rendon, A., D. Jung, and V. Jancsik, *INTERACTION OF MICROTUBULES AND MICROTUBULE-ASSOCIATED PROTEINS (MAPS) WITH RAT-BRAIN MITOCHONDRIA.* Biochemical Journal, 1990. **269**(2): p. 555-556.

210. Muchowski, P.J. and J.L. Wacker, *Modulation of neurodegeneration by molecular chaperones.* Nature Reviews Neuroscience, 2005. **6**(1): p. 11-22.

211. Chen, S. and I.R. Brown, *Neuronal expression of constitutive heat shock proteins: implications for neurodegenerative diseases.* Cell Stress & Chaperones, 2007. **12**(1): p. 51-58.

212. Dou, F., et al., *Chaperones increase association of tau protein with microtubules.* Proceedings of the National Academy of Sciences of the United States of America, 2003. **100**(2): p. 721-726.

213. Shimura, H., et al., *CHIP-Hsc70 complex ubiquitinates phosphorylated tau and enhances cell survival.* Journal of Biological Chemistry, 2004. **279**(6): p. 4869-4876.

214. Sarkar, M., J. Kuret, and G. Lee, *Two motifs within the tau microtubule-binding domain mediate its association with the hsc70 molecular chaperone.* Journal of Neuroscience Research, 2008. **86**(12): p. 2763-2773.

215. Fourie, A.M., J.F. Sambrook, and M.J.H. Gething, *COMMON AND DIVERGENT PEPTIDE BINDING SPECIFICITIES OF HSP70 MOLECULAR CHAPERONES.* Journal of Biological Chemistry, 1994. **269**(48): p. 30470-30478.

216. Rudiger, S., et al., *Substrate specificity of the DnaK chaperone determined by screening cellulose-bound peptide libraries.* Embo Journal, 1997. **16**(7): p. 1501-1507.

217. Takenaka, I.M., et al., *HSC70-BINDING PEPTIDES SELECTED FROM A PHAGE DISPLAY PEPTIDE LIBRARY THAT RESEMBLE ORGANELLAR TARGETING SEQUENCES.* Journal of Biological Chemistry, 1995. **270**(34): p. 19839-19844.

218. Dickey, C.A., et al., *Akt and CHIP coregulate tau degradation through coordinated interactions.* Proceedings of the National Academy of Sciences of the United States of America, 2008. **105**(9): p. 3622-3627.

219.   Jinwal, U.K., et al., *Hsc70 Rapidly Engages Tau after Microtubule Destabilization.* Journal of Biological Chemistry, 2010. **285**(22): p. 16798-16805.

220.   Goedert, M., et al., *MULTIPLE ISOFORMS OF HUMAN MICROTUBULE-ASSOCIATED PROTEIN-TAU - SEQUENCES AND LOCALIZATION IN NEUROFIBRILLARY TANGLES OF ALZHEIMERS-DISEASE.* Neuron, 1989. **3**(4): p. 519-526.

221.   Goedert, M., et al., *CLONING AND SEQUENCING OF THE CDNA-ENCODING AN ISOFORM OF MICROTUBULE-ASSOCIATED PROTEIN TAU CONTAINING 4 TANDEM REPEATS - DIFFERENTIAL EXPRESSION OF TAU PROTEIN MESSENGER-RNAS IN HUMAN-BRAIN.* Embo Journal, 1989. **8**(2): p. 393-399.

222.   Himmler, A., et al., *TAU CONSISTS OF A SET OF PROTEINS WITH REPEATED C-TERMINAL MICROTUBULE-BINDING DOMAINS AND VARIABLE N-TERMINAL DOMAINS.* Molecular and Cellular Biology, 1989. **9**(4): p. 1381-1388.

223.   Kosik, K.S., N.W. Kowall, and A. McKee, *ALONG THE WAY TO A NEUROFIBRILLARY TANGLE - A LOOK AT THE STRUCTURE OF TAU.* Annals of Medicine, 1989. **21**(2): p. 109-112.

224.   Goedert, M. and R. Jakes, *EXPRESSION OF SEPARATE ISOFORMS OF HUMAN TAU-PROTEIN - CORRELATION WITH THE TAU-PATTERN IN BRAIN AND EFFECTS ON TUBULIN POLYMERIZATION.* Embo Journal, 1990. **9**(13): p. 4225-4230.

225.   Rosner, H., et al., *DEVELOPMENTAL EXPRESSION OF TAU PROTEINS IN THE CHICKEN AND RAT-BRAIN - RAPID DOWN-REGULATION OF A PAIRED HELICAL FILAMENT EPITOPE IN THE RAT CEREBRAL-CORTEX COINCIDES WITH THE TRANSITION FROM IMMATURE TO ADULT TAU-ISOFORMS.* International Journal of Developmental Neuroscience, 1995. **13**(6): p. 607-617.

226.   Lee, G., R.L. Neve, and K.S. Kosik, *THE MICROTUBULE BINDING DOMAIN OF TAU-PROTEIN.* Neuron, 1989. **2**(6): p. 1615-1624.

227.   Goedert, M., et al., *TAU-PROTEINS OF ALZHEIMER PAIRED HELICAL FILAMENTS - ABNORMAL PHOSPHORYLATION OF ALL 6 BRAIN ISOFORMS.* Neuron, 1992. **8**(1): p. 159-168.

228.   Hasegawa, M., et al., *PROTEIN-SEQUENCE AND MASS-SPECTROMETRIC ANALYSES OF TAU IN THE ALZHEIMERS-DISEASE BRAIN.* Journal of Biological Chemistry, 1992. **267**(24): p. 17047-17054.

229.   Lee, V.M.Y., *DISRUPTION OF THE CYTOSKELETON IN ALZHEIMERS-DISEASE.* Current Opinion in Neurobiology, 1995. **5**(5): p. 663-668.

230.   Morishimakawashima, M., et al., *PROLINE-DIRECTED AND NON-PROLINE-DIRECTED PHOSPHORYLATION OF PHF-TAU.* Journal of Biological Chemistry, 1995. **270**(2): p. 823-829.

231.   Nylandsted, J., K. Brand, and M. Jaattela, *Heat shock protein 70 is required for the survival of cancer cells.* Ann N Y Acad Sci, 2000. **926**: p. 122-5.

232.   Kaul, Z., et al., *Mortalin imaging in normal and cancer cells with quantum dot immuno-conjugates.* Cell Res, 2003. **13**(6): p. 503-7.

233. Kaul, S.C., et al., *Overexpressed mortalin (mot-2)/mthsp70/GRP75 and hTERT cooperate to extend the in vitro lifespan of human fibroblasts.* Exp Cell Res, 2003. **286**(1): p. 96-101.

234. Vargas-Roig, L.M., Fanelli, M.A., López, L.A., Gago, F.E., Tello, O., Aznar, J.C. and Ciocca, D.R., *Heat shock proteins and cell proliferation in human breast cancer biopsy samples.* . Cancer Detect Prev., 1997. **21**: p. 441-451.

235. Nylandsted, J., et al., *Eradication of glioblastoma, and breast and colon carcinoma xenografts by Hsp70 depletion.* Cancer Res, 2002. **62**(24): p. 7139-42.

236. Wadhwa, R., et al., *Reduction in mortalin level by its antisense expression causes senescence-like growth arrest in human immortalized cells.* J Gene Med, 2004. **6**(4): p. 439-44.

237. Modica-Napolitano, J.S., et al., *Selective damage to carcinoma mitochondria by the rhodacyanine MKT-077.* Cancer Res, 1996. **56**(3): p. 544-50.

238. Ciocca, D.R. and S.K. Calderwood, *Heat shock proteins in cancer: diagnostic, prognostic, predictive, and treatment implications.* Cell Stress Chaperones, 2005. **10**(2): p. 86-103.

239. Garrido, C., et al., *Heat shock proteins 27 and 70: anti-apoptotic proteins with tumorigenic properties.* Cell Cycle, 2006. **5**(22): p. 2592-601.

240. Nihei, T., et al., *Demonstration of selective protein complexes of p53 with 73 kDa heat shock cognate protein, but not with 72 kDa heat shock protein in human tumor cells.* Cancer Lett., 1993. **73**(2-3): p. 181-189.

241. Fourie, A.M., et al., *HSP70 binding sites in the tumor suppressor protein p53.* J. Biol. Chem., 1997. **272**(31): p. 19471-19479.

242. Zylicz, M., F.W. King, and A. Wawrzynow, *Hsp70 interactions with the p53 tumour suppressor protein.* Embo J, 2001. **20**(17): p. 4634-8.

243. Wadhwa, R., et al., *Hsp70 family member, mot-2/mthsp70/GRP75, binds to the cytoplasmic sequestration domain of the p53 protein.* Exp Cell Res, 2002. **274**(2): p. 246-53.

244. Walker, C., S. Bottger, and B. Low, *Mortalin-based cytoplasmic sequestration of p53 in a nonmammalian cancer model.* Am J Pathol, 2006. **168**(5): p. 1526-30.

245. Abarzua, F., et al., *Heat shock proteins play a crucial role in tumor-specific apoptosis by REIC/Dkk-3.* Int J Mol Med, 2007. **20**(1): p. 37-43.

246. Lanneau, D., et al., *Heat shock proteins: essential proteins for apoptosis regulation.* J Cell Mol Med, 2008. **12**(3): p. 743-61.

247. Calderwood, S.K. and D.R. Ciocca, *Heat shock proteins: stress proteins with Janus-like properties in cancer.* Int J Hyperthermia, 2008. **24**(1): p. 31-9.

248. Beere, H.M., et al., *Heat-shock protein 70 inhibits apoptosis by preventing recruitment of procaspase-9 to the Apaf-1 apoptosome.* Nat Cell Biol, 2000. **2**(8): p. 469-75.

249. Garrido, C., Schmitt, E., cande, C., Vahsen, N., Parcellier, A., Kroemer, G., *Hsp27 and Hsp70: potentially oncogenic apoptosis inhibitors.* Cell Cycle, 2003. **2**: p. 579-584.

250. Bienemann, A.S., et al., *Hsp70 suppresses apoptosis in sympathetic neurones by preventing the activation of c-Jun.* J Neurochem, 2008. **104**(1): p. 271-8.

251. Hui-Qing, X., et al., *HSP70 Inhibits Burn Serum-Induced Apoptosis of Cardiomyocytes via Mitochondrial and Membrane Death Receptor Pathways.* J Burn Care Res, 2008.

252. Guo, F., et al., *Mechanistic role of heat shock protein 70 in Bcr-Abl-mediated resistance to apoptosis in human acute leukemia cells.* Blood, 2005. **105**(3): p. 1246-55.

253. Gyrd-Hansen, M., J. Nylandsted, and M. Jaattela, *Heat shock protein 70 promotes cancer cell viability by safeguarding lysosomal integrity.* Cell Cycle, 2004. **3**(12): p. 1484-5.

254. Didelot, C., et al., *Anti-cancer therapeutic approaches based on intracellular and extracellular heat shock proteins.* Curr Med Chem, 2007. **14**(27): p. 2839-47.

255. Wadhwa, R., et al., *Inactivation of tumor suppressor p53 by mot-2, a hsp70 family member.* J Biol Chem, 1998. **273**(45): p. 29586-91.

256. Lehman, T.A., et al., *p53 mutations, ras mutations, and p53-heat shock 70 protein complexes in human lung carcinoma cell lines.* Cancer Res, 1991. **51**(15): p. 4090-6.

257. King, F.W., et al., *Co-chaperones Bag-1, Hop and Hsp40 regulate Hsc70 and Hsp90 interactions with wild-type or mutant p53.* Embo J, 2001. **20**(22): p. 6297-305.

258. Lane, D.P., C. Midgley, and T. Hupp, *Tumour suppressor genes and molecular chaperones.* Philos Trans R Soc Lond B Biol Sci, 1993. **339**(1289): p. 369-72; discussion 372-3.

259. Bagatell, R., et al., *Induction of a heat shock factor 1-dependent stress response alters the cytotoxic activity of hsp90-binding agents.* Clin Cancer Res, 2000. **6**(8): p. 3312-8.

260. Whitesell, L. and S. Lindquist, *Inhibiting the transcription factor HSF1 as an anticancer strategy.* Expert Opin Ther Targets, 2009. **13**(4): p. 469-78.

261. Wadhwa, R., K. Taira, and S.C. Kaul, *An Hsp70 family chaperone, mortalin/mthsp70/PBP74/Grp75: what, when, and where?* Cell Stress Chaperones, 2002. **7**(3): p. 309-16.

262. Henderson, B., E. Allan, and A.R. Coates, *Stress wars: the direct role of host and bacterial molecular chaperones in bacterial infection.* Infect Immun, 2006. **74**(7): p. 3693-706.

263. Wolska, K.I., et al., *Antibiotic susceptibility of Escherichia coli dnaK and dnaJ mutants.* Microb Drug Resist, 2000. **6**(2): p. 119-26.

264. Singh, V.K., et al., *Role for dnaK locus in tolerance of multiple stresses in Staphylococcus aureus.* Microbiology, 2007. **153**(Pt 9): p. 3162-73.

265. Patury, S., Y. Miyata, and J.E. Gestwicki, *Pharmacological targeting of the Hsp70 chaperone.* Curr Top Med Chem, 2009. **9**(15): p. 1337-51.

266. Hyman, B.T., et al., *ALZ-50 ANTIBODY RECOGNIZES ALZHEIMER-RELATED NEURONAL CHANGES.* Annals of Neurology, 1988. **23**(4): p. 371-379.

267. Petrucelli, L., et al., *CHIP and Hsp70 regulate tau ubiquitination, degradation and aggregation.* Human Molecular Genetics, 2004. **13**(7): p. 703-714.

268. Spillantini, M.G., et al., *Mutation in the tau gene in familial multiple system tauopathy with presenile dementia.* Proceedings of the National Academy of Sciences of the United States of America, 1998. **95**(13): p. 7737-7741.

269. Sun, L., et al., *Inhibition of protein phosphatase 2A- and protein phosphatase 1-induced tau hyperphosphorylation and impairment of spatial memory retention in rats.* Neuroscience, 2003. **118**(4): p. 1175-1182.

270. Dickey, C.A., et al., *HSP induction mediates selective clearance of tau phosphorylated at proline-directed Ser/Thr sites but not KXGS (MARK) sites.* Faseb Journal, 2006. **20**(2): p. 753-+.

271. Giese, K.P., *GSK-3: A Key Player in Neurodegeneration and Memory.* Iubmb Life, 2009. **61**(5): p. 516-521.

272. Phiel, C.J. and P.S. Klein, *Molecular targets of lithium action.* Annual Review of Pharmacology and Toxicology, 2001. **41**: p. 789-813.

273. Mazanetz, M.P. and P.M. Fischer, *Untangling tau hyperphosphorylation in drug design for neurodegenerative diseases.* Nature Reviews Drug Discovery, 2007. **6**(6): p. 464-479.

274. Churcher, I., *Tau therapeutic strategies for the treatment of Alzheimer's disease.* Current Topics in Medicinal Chemistry, 2006. **6**(6): p. 579-595.

275. DeAzevedo, W.F., et al., *Inhibition of cyclin-dependent kinases by purine analogues - Crystal structure of human cdk2 complexed with roscovitine.* European Journal of Biochemistry, 1997. **243**(1-2): p. 518-526.

276. Meijer, L., et al., *Biochemical and cellular effects of roscovitine, a potent and selective inhibitor of the cyclin-dependent kinases cdc2, cdk2 and cdk5.* European Journal of Biochemistry, 1997. **243**(1-2): p. 527-536.

277. Vita, M., et al., *Tissue distribution, pharmacokinetics and identification of roscovitine metabolites in rat.* European Journal of Pharmaceutical Sciences, 2005. **25**(1): p. 91-103.

278. Wen, Y., et al., *Interplay between cyclin-dependent kinase 5 and glycogen synthase kinase 3 beta mediated by neuregulin signaling leads to differential effects on tau phosphorylation and amyloid precursor protein processing.* Journal of Neuroscience, 2008. **28**(10): p. 2624-2632.

279. Goedert, M., et al., *PROTEIN PHOSPHATASE 2A IS THE MAJOR ENZYME IN BRAIN THAT DEPHOSPHORYLATES TAU-PROTEIN PHOSPHORYLATED BY PROLINE-DIRECTED PROTEIN-KINASES OR CYCLIC-AMP-DEPENDENT PROTEIN-KINASE.* Journal of Neurochemistry, 1995. **65**(6): p. 2804-2807.

280. Gong, C.X., et al., *Phosphorylation of microtubule-associated protein tau is regulated by protein phosphatase 2A in mammalian brain - Implications for neurofibrillary degeneration in Alzheimer's disease.* Journal of Biological Chemistry, 2000. **275**(8): p. 5535-5544.

281. Liu, F., et al., *Contributions of protein phosphatases PP1, PP2A, PP2B and PP5 to the regulation of tau phosphorylation.* European Journal of Neuroscience, 2005. **22**(8): p. 1942-1950.

282. Sontag, E., et al., *Regulation of the phosphorylation state and microtubule-binding activity of tau by protein phosphatase 2A.* Neuron, 1996. **17**(6): p. 1201-1207.

283. Gong, C.X., et al., *PHOSPHOPROTEIN PHOSPHATASE-ACTIVITIES IN ALZHEIMER-DISEASE BRAIN.* Journal of Neurochemistry, 1993. **61**(3): p. 921-927.

284.	Tanimukai, H., I. Grundke-Iqbal, and K. Iqbal, *Up-regulation of inhibitors of protein phosphatase-2A in Alzheimer's disease.* American Journal of Pathology, 2005. **166**(6): p. 1761-1771.

285.	Tsujio, I., et al., *Inhibitors of protein phosphatase-2A from human brain structures, immunocytological localization and activities towards dephosphorylation of the Alzheimer type hyperphosphorylated tau.* Febs Letters, 2005. **579**(2): p. 363-372.

286.	Arnold, C.S., et al., *The microtubule-associated protein tau is extensively modified with O-linked N-acetylglucosamine.* Journal of Biological Chemistry, 1996. **271**(46): p. 28741-28744.

287.	Lefebvre, T., et al., *Evidence of a balance between phosphorylation and O-GlcNAc glycosylation of Tau proteins - a role in nuclear localization.* Biochimica Et Biophysica Acta-General Subjects, 2003. **1619**(2): p. 167-176.

288.	Liu, F., et al., *O-GlcNAcylation regulates phosphorylation of tau: A mechanism involved in Alzheimer's disease.* Proceedings of the National Academy of Sciences of the United States of America, 2004. **101**(29): p. 10804-10809.

289.	d'Abramo, C., et al., *Troglitazone, a peroxisome proliferator-activated receptor-gamma agonist, decreases tau phosphorylation in CHOtau4R cells.* Journal of Neurochemistry, 2006. **98**(4): p. 1068-1077.

290.	Yuzwa, S.A., et al., *A potent mechanism-inspired O-GlcNAcase inhibitor that blocks phosphorylation of tau in vivo.* Nature Chemical Biology, 2008. **4**(8): p. 483-490.

291.	Pickhardt, M., et al., *Anthraquinones inhibit tau aggregation and dissolve Alzheimer's paired helical filaments in vitro and in cells.* Journal of Biological Chemistry, 2005. **280**(5): p. 3628-3635.

292.	Crowe, A., et al., *Identification of Aminothienopyridazine Inhibitors of Tau Assembly by Quantitative High-Throughput Screening.* Biochemistry, 2009. **48**(32): p. 7732-7745.

293.	Nixon, R.A., et al., *Extensive involvement of autophagy in Alzheimer disease: An immuno-electron microscopy study.* Journal of Neuropathology and Experimental Neurology, 2005. **64**(2): p. 113-122.

294.	Sarkar, S., et al., *Lithium induces autophagy by inhibiting inositol monophosphatase.* Journal of Cell Biology, 2005. **170**(7): p. 1101-1111.

295.	Zilka, N., E. Kontsekova, and M. Novak, *Chaperone-like Antibodies Targeting Misfolded Tau Protein: New Vistas in the Immunotherapy of Neurodegenerative Foldopathies.* Journal of Alzheimers Disease, 2008. **15**(2): p. 169-179.

296.	Morsch, R., W. Simon, and P.D. Coleman, *Neurons may live for decades with neurofibrillary tangles.* Journal of Neuropathology and Experimental Neurology, 1999. **58**(2): p. 188-197.

297.	Andorfer, C., et al., *Cell-cycle reentry and cell death in transgenic mice expressing nonmutant human tau isoforms.* Journal of Neuroscience, 2005. **25**(22): p. 5446-5454.

298.	Kieran, D., et al., *Treatment with arimoclomol, a coinducer of heat shock proteins, delays disease progression in ALS mice.* Nature Medicine, 2004. **10**(4): p. 402-405.

299. Westerheide, S.D. and R.I. Morimoto, *Heat shock response modulators as therapeutic tools for diseases of protein conformation.* Journal of Biological Chemistry, 2005. **280**(39): p. 33097-33100.

300. Shimura, H., Y. Miura-Shimura, and K.S. Kosik, *Binding of tau to heat shock protein 27 leads to decreased concentration of hyperphosphorylated tau and enhanced cell survival.* Journal of Biological Chemistry, 2004. **279**(17): p. 17957-17962.

301. Kosik, K.S. and H. Shimura, *Phosphorylated tau and the neurodegenerative foldopathies.* Biochimica Et Biophysica Acta-Molecular Basis of Disease, 2005. **1739**(2-3): p. 298-310.

302. Tseng, H.C., et al., *Phosphorylated tau can promote tubulin assembly.* Proceedings of the National Academy of Sciences of the United States of America, 1999. **96**(17): p. 9503-9508.

303. Lu, P.J., et al., *The prolyl isomerase Pin1 restores the function of Alzheimer-associated phosphorylated tau protein.* Nature, 1999. **399**(6738): p. 784-788.

304. Zhou, X.Z., et al., *Pin1-dependent prolyl isomerization regulates dephosphorylation of Cdc25C and tau proteins.* Molecular Cell, 2000. **6**(4): p. 873-883.

305. Gordon-Krajcer, W., L.S. Yang, and H. Ksiezak-Reding, *Conformation of paired helical filaments blocks dephosphorylation of epitopes shared with fetal tau except Ser199/202 and Ser202/Thr205.* Brain Research, 2000. **856**(1-2): p. 163-175.

306. Alonso, A.D., et al., *Hyperphosphorylation induces self-assembly of tau into tangles of paired helical filaments/straight filaments.* Proceedings of the National Academy of Sciences of the United States of America, 2001. **98**(12): p. 6923-6928.

307. Brunden, K.R., J.Q. Trojanowski, and V.M.Y. Lee, *Advances in tau-focused drug discovery for Alzheimer's disease and related tauopathies.* Nature Reviews Drug Discovery, 2009. **8**(10): p. 783-793.

308. Wischik, C.M., et al., *Selective inhibition of Alzheimer disease-like tau aggregation by phenothiazines.* Proceedings of the National Academy of Sciences of the United States of America, 1996. **93**(20): p. 11213-11218.

309. Williams, J.L., et al., *METHYLENE-BLUE AND THE PHOTODYNAMIC THERAPY OF SUPERFICIAL BLADDER-CANCER.* Journal of Photochemistry and Photobiology B-Biology, 1989. **4**(2): p. 229-232.

310. Orth, K., et al., *INTRALUMINAL TREATMENT OF INOPERABLE ESOPHAGEAL TUMORS BY INTRALESIONAL PHOTODYNAMIC THERAPY WITH METHYLENE-BLUE.* Lancet, 1995. **345**(8948): p. 519-520.

311. Tardivo, J.P., et al., *New photodynamic therapy protocol to treat AIDS-related Kaposi's sarcoma.* Photomedicine and Laser Surgery, 2006. **24**(4): p. 528-531.

312. Jinwal, U.K., et al., *Chemical Manipulation of Hsp70 ATPase Activity Regulates Tau Stability.* Journal of Neuroscience, 2009. **29**(39): p. 12079-12088.

313. Wadhwa, R., et al., *Selective toxicity of MKT-077 to cancer cells is mediated by its binding to the hsp70 family protein mot-2 and reactivation of p53 function.* Cancer Res, 2000. **60**(24): p. 6818-21.

314. Wadhwa, R., et al., *Rhodacyanine dye MKT-077 inhibits in vitro telomerase assay but has no detectable effects on telomerase activity in vivo.* Cancer Res, 2002. **62**(15): p. 4434-8.

315. Chen, L.B., *MITOCHONDRIAL-MEMBRANE POTENTIAL IN LIVING CELLS.* Annual Review of Cell Biology, 1988. **4**: p. 155-181.

316. Israel, B.A. and W.I. Schaeffer, *CYTOPLASMIC MEDIATION OF MALIGNANCY.* In Vitro Cellular & Developmental Biology, 1988. **24**(5): p. 487-490.

317. Hayashi, J.I., M. Takemitsu, and I. Nonaka, *RECOVERY OF THE MISSING TUMORIGENICITY IN MITOCHONDRIAL DNA-LESS HELA-CELLS BY INTRODUCTION OF MITOCHONDRIAL-DNA FROM NORMAL HUMAN-CELLS.* Somatic Cell and Molecular Genetics, 1992. **18**(2): p. 123-129.

318. Bernal, S.D., et al., *ANTICARCINOMA ACTIVITY INVIVO OF RHODAMINE-123, A MITOCHONDRIAL-SPECIFIC DYE.* Science, 1983. **222**(4620): p. 169-172.

319. Summerhayes, I.C., et al., *UNUSUAL RETENTION OF RHODAMINE-123 BY MITOCHONDRIA IN MUSCLE AND CARCINOMA-CELLS.* Proceedings of the National Academy of Sciences of the United States of America-Biological Sciences, 1982. **79**(17): p. 5292-5296.

320. Bax, A., R.H. Griffey, and B.L. Hawkins, *Correlation of Proton and ^{15}N Chemical-Shifts by Multiple Quantum Nmr.* J. Magn. Reson., 1983. **55**(2): p. 301-315.

321. Bodenhausen, G. and D.J. Ruben, *Natural Abundance ^{15}N NMR by Enhanced Heteronuclear Spectroscopy.* Chem. Phys. Lett., 1980. **69**(1): p. 185-189.

322. Bax, A., et al., *COMPARISON OF DIFFERENT MODES OF 2-DIMENSIONAL REVERSE-CORRELATION NMR FOR THE STUDY OF PROTEINS.* Journal of Magnetic Resonance, 1990. **86**(2): p. 304-318.

323. Cavanagh, J., et al., *Protein NMR Spectroscopy, Principles and Practice.* 1996, Academic Press: London. p. 279.

324. Mori, S., et al., *Improved sensitivity of HSQC spectra of exchanging protons at short interscan delays using a new fast HSQC (FHSQC) detection scheme that avoids water saturation.* J. Magn. Reson. B, 1995. **108**(1): p. 94-98.

325. Pervushin, K., et al., *Attenuated T2 relaxation by mutual cancellation of dipole-dipole coupling and chemical shift anisotropy indicates an avenue to NMR structures of very large biological macromolecules in solution.* Proc Natl Acad Sci U S A, 1997. **94**(23): p. 12366-71.

326. Pervushin, K., et al., *Transverse Relaxation-Optimized Spectroscopy (TROSY) for NMR Studies of Aromatic Spin Systems in ^{13}C-Labeled Proteins.* J. Am. Chem. Soc., 1998. **120**(25): p. 6394-6400.

327. Sanders, n., C. R.2nd and J.P. Schwonek, *Characterization of magnetically orientable bilayers in mixtures of dihexanoylphosphatidylcholine and dimyristoylphosphatidylcholine by solid-state NMR.* Biochemistry, 1992. **31**(37): p. 8898-8905.

328. Pervushin, K., *Impact of transverse relaxation optimized spectroscopy (TROSY) on NMR as a technique in structural biology.* Q Rev Biophys, 2000. **33**(2): p. 161-97.

329.   Rance, M., J.P. Loria, and A.G.r. Palmer, *Sensitivity improvement of transverse relaxation-optimized spectroscopy.* J Magn Reson, 1999. **136**(1): p. 92-101.

330.   van de Ven, F. and C. Hilbers, J. Magn. Reson, 1983. **54**: p. 512-520.

331.   Sorensen, O.W., et al., *PRODUCT OPERATOR-FORMALISM FOR THE DESCRIPTION OF NMR PULSE EXPERIMENTS.* Progress in Nuclear Magnetic Resonance Spectroscopy, 1983. **16**: p. 163-192.

332.   Schulte-Herbruggen, T. and O.W. Sorensen, *Clean TROSY: compensation for relaxation-induced artifacts.* J Magn Reson, 2000. **144**(1): p. 123-8.

333.   Aue, W.P., E. Bartholdi, and R.R. Ernst, *2-DIMENSIONAL SPECTROSCOPY - APPLICATION TO NUCLEAR MAGNETIC-RESONANCE.* Journal of Chemical Physics, 1976. **64**(5): p. 2229-2246.

334.   Rance, M., et al., *Improved spectral resolution in cosy 1H NMR spectra of proteins via double quantum filtering.* Biochem Biophys Res Commun, 1983. **117**(2): p. 479-85.

335.   Rance, M., et al., *IMPROVED SPECTRAL RESOLUTION IN COSY H-1-NMR SPECTRA OF PROTEINS VIA DOUBLE QUANTUM FILTERING.* Biochemical and Biophysical Research Communications, 1983. **117**(2): p. 479-485.

336.   Solomon, I., *RELAXATION PROCESSES IN A SYSTEM OF 2 SPINS.* Physical Review, 1955. **99**(2): p. 559-565.

337.   Kumar, A., R.R. Ernst, and K. Wuthrich, *A two-dimensional nuclear Overhauser enhancement (2D NOE) experiment for the elucidation of complete proton-proton cross-relaxation networks in biological macromolecules.* Biochem Biophys Res Commun, 1980. **95**(1): p. 1-6.

338.   Lee, J.M., et al., *CAMELSPIN - TRANSVERSE NUCLEAR OVERHAUSER EFFECT STUDY OF ERYTHRONOLIDE A AND OF LYSOZYME.* Federation Proceedings, 1986. **45**(6): p. 1606-1606.

339.   Clore, G.M., et al., *IDENTIFICATION AND LOCALIZATION OF BOUND INTERNAL WATER IN THE SOLUTION STRUCTURE OF INTERLEUKIN-1-BETA BY HETERONUCLEAR 3-DIMENSIONAL H-1 ROTATING-FRAME OVERHAUSER N-15-H-1 MULTIPLE QUANTUM COHERENCE NMR-SPECTROSCOPY.* Biochemistry, 1990. **29**(24): p. 5671-5676.

340.   Kay, L.E., et al., *3-Dimensional Triple-Resonance NMR-Spectroscopy of Isotopically Enriched Proteins.* J. Magn. Reson., 1990. **89**(3): p. 496-514.

341.   Cavanagh, J., et al., *Protein NMR Spectroscopy: principles and practice.* 2nd ed. 2007, Amsterdam: Elsevier Academic Press.

342.   Yamazaki, T., et al., *Assignment of Backbone Resonances for Larger Proteins Using the ^{13}C-^{1}Ha Coherence of a ^{1}H-, ^{2}H-, ^{13}C-, and ^{15}N-Labeled Sample.* J. Am. Chem. Soc., 1997. **119**(5): p. 872-880.

343.   Salzmann, M., et al., *TROSY in triple-resonance experiments: new perspectives for sequential NMR assignment of large proteins.* Proc Natl Acad Sci U S A, 1998. **95**(23): p. 13585-90.

344.   Loria, J.P., M. Rance, and A.G. Palmer, 3rd, *Transverse-relaxation-optimized (TROSY) gradient-enhanced triple-resonance NMR spectroscopy.* J Magn Reson, 1999. **141**(1): p. 180-4.

345.   Crippen, G.M., et al., *SAGA: rapid automatic mainchain NMR assignment for large proteins.* J Biomol NMR, 2010. **46**(4): p. 281-98.

346. Delaglio, F., et al., *NMRPipe: a multidimensional spectral processing system based on UNIX pipes.* J. Biomol. NMR, 1995. **6**: p. 277-293.

347. Goddard, T.D. and D.G. Kneller, *SPARKY 3.* University of California, San Francisco, 2000.

348. Moseley, H.N., D. Monleon, and G.T. Montelione, *Automatic determination of protein backbone resonance assignments from triple resonance nuclear magnetic resonance data.* Methods Enzymol, 2001. **339**: p. 91-108.

349. Kellenberger, E., et al., *Comparative evaluation of eight docking tools for docking and virtual screening accuracy.* Proteins-Structure Function and Bioinformatics, 2004. **57**(2): p. 225-242.

350. Radestock, S., M. Bohm, and H. Gohlke, *Improving binding mode predictions by docking into protein-specifically adapted potential fields.* Journal of Medicinal Chemistry, 2005. **48**(17): p. 5466-5479.

351. Stoddard, B.L. and D.E. Koshland, *PREDICTION OF THE STRUCTURE OF A RECEPTOR PROTEIN COMPLEX USING A BINARY DOCKING METHOD.* Nature, 1992. **358**(6389): p. 774-776.

352. Myshkin, E., N.B. Leontis, and G.S. Bullerjahn, *Computational simulation of the docking of Prochlorothrix hollandica plastocyanin to photosystem I: Modeling the electron transfer complex.* Biophysical Journal, 2002. **82**(6): p. 3305-3313.

353. Sousa, S.F., P.A. Fernandes, and M.J. Ramos, *Protein-ligand docking: Current status and future challenges.* Proteins-Structure Function and Bioinformatics, 2006. **65**(1): p. 15-26.

354. Morris, G.M., et al., *Automated docking using a Lamarckian genetic algorithm and an empirical binding free energy function.* Journal of Computational Chemistry, 1998. **19**(14): p. 1639-1662.

355. Goodford, P.J., *A COMPUTATIONAL-PROCEDURE FOR DETERMINING ENERGETICALLY FAVORABLE BINDING-SITES ON BIOLOGICALLY IMPORTANT MACROMOLECULES.* Journal of Medicinal Chemistry, 1985. **28**(7): p. 849-857.

356. Morris, G., et al., *AutoDock Version 4.2.* 2010.

357. Kirkpatrick, S., *OPTIMIZATION BY SIMULATED ANNEALING - QUANTITATIVE STUDIES.* Journal of Statistical Physics, 1984. **34**(5-6): p. 975-986.

358. Goodsell, D.S., G.M. Morris, and A.J. Olson, *Automated docking of flexible ligands: Applications of AutoDock.* Journal of Molecular Recognition, 1996. **9**(1): p. 1-5.

359. Dominguez, C., R. Boelens, and A.M. Bonvin, *HADDOCK: a protein-protein docking approach based on biochemical or biophysical information.* J Am Chem Soc, 2003. **125**(7): p. 1731-7.

360. Mercier, K.A., et al., *FAST-NMR: Functional annotation screening technology using NMR spectroscopy.* Journal of the American Chemical Society, 2006. **128**(47): p. 15292-15299.

361. Park, H., J. Lee, and S. Lee, *Critical assessment of the automated AutoDock as a new docking tool for virtual screening.* Proteins-Structure Function and Bioinformatics, 2006. **65**(3): p. 549-554.

362. Bursulaya, B.D., et al., *Comparative study of several algorithms for flexible ligand docking.* Journal of Computer-Aided Molecular Design, 2003. **17**(11): p. 755-763.

363. Morris, G.M., et al., *AutoDock4 and AutoDockTools4: Automated Docking with Selective Receptor Flexibility.* Journal of Computational Chemistry, 2009. **30**(16): p. 2785-2791.

364. Koya, K., et al., *MKT-077, a novel rhodacyanine dye in clinical trials, exhibits anticarcinoma activity in preclinical studies based on selective mitochondrial accumulation.* Cancer Res, 1996. **56**(3): p. 538-43.

365. Kampinga, H., et al., *Guidelines for the nomenclature of the human heat shock proteins.* Cell Stress Chap, 2009. **14**: p. 105-111.

366. Flaherty, K.M., et al., *Structural basis of the 70-kilodalton heat shock cognate protein ATP hydrolytic activity. II. Structure of the active site with ADP or ATP bound to wild type and mutant ATPase fragment.* J Biol Chem, 1994. **269**(17): p. 12899-907.

367. Shin, B.K., et al., *Global profiling of the cell surface proteome of cancer cells uncovers an abundance of proteins with chaperone function.* J Biol Chem, 2003. **278**(9): p. 7607-16.

368. Garg, M., et al., *Heat-shock protein 70-2 (HSP70-2) expression in bladder urothelial carcinoma is associated with tumour progression and promotes migration and invasion.* Eur J Cancer, 2010. **46**(1): p. 207-15.

369. Aghdassi, A., et al., *Heat shock protein 70 increases tumorigenicity and inhibits apoptosis in pancreatic adenocarcinoma.* Cancer Res, 2007. **67**(2): p. 616-25.

370. Soti, C. and P. Csermely, *Chaperones and aging: role in neurodegeneration and in other civilizational diseases.* Neurochem Int, 2002. **41**(6): p. 383-9.

371. Soti, C. and P. Csermely, *Chaperones come of age.* Cell Stress Chaperones, 2002. **7**(2): p. 186-90.

372. Kaul, S.C., et al., *Malignant transformation of NIH3T3 cells by overexpression of mot-2 protein.* Oncogene, 1998. **17**(7): p. 907-11.

373. Propper, D., et al., *Phase I trial of the selective mitochondrial toxin MKT 077 in chemo-resistant solid tumours.* Annal of Oncology, 1999. **10**: p. 923-927.

374. Pilzer, D., et al., *Mortalin inhibitors sensitize K562 leukemia cells to complement-dependent cytotoxicity.* Int J Cancer, 2010. **126**(6): p. 1428-35.

375. Modica-Napolitano, J.S., et al., *The selective in vitro cytotoxicity of carcinoma cells by AZT is enhanced by concurrent treatment with delocalized lipophilic cations.* Cancer Lett, 2003. **198**(1): p. 59-68.

376. Abdul, M. and N. Hoosein, *Potentiation of the antiproliferative activity of MKT-077 by loperamide, diltiazem and tamoxifen.* Oncol Rep, 2003. **10**(6): p. 2023-6.

377. Jinwal, U.K., et al., *Chemical manipulation of hsp70 ATPase activity regulates tau stability.* J Neurosci, 2009. **29**(39): p. 12079-88.

378. Opar, A., *Mixed results for disease-modification strategies for Alzheimer's disease.* Nat Rev Drug Discov, 2008. **7**(9): p. 717-8.

379. Medina, D.X., A. Caccamo, and S. Oddo, *Methylene Blue Reduces Abeta Levels and Rescues Early Cognitive Deficit by Increasing Proteasome Activity.* Brain Pathol, 2010.

380. Trapp, S. and R.W. Horobin, *A predictive model for the selective accumulation of chemicals in tumor cells.* Eur Biophys J, 2005. **34**(7): p. 959-66.

381. Lo, S., et al., *Assessment of the significance of mitochondrial DNA damage by chemotherapeutic agents.* Int J Oncol, 2005. **27**(2): p. 337-44.

382. Kaul, S.C., et al., *An N-terminal region of mot-2 binds to p53 in vitro.* Neoplasia, 2001. **3**(2): p. 110-4.

383. Deocaris, C.C., et al., *Mortalin sensitizes human cancer cells to MKT-077-induced senescence.* Cancer Lett, 2007. **252**(2): p. 259-69.

384. Gupta, R.S., *Protein phylogenies and signature sequences: A reappraisal of evolutionary relationships among archaebacteria, eubacteria, and eukaryotes.* Microbiol Mol Biol Review, 1998. **62**: p. 1435-1491.

385. DeLano, W., *The PyMOL Molecular Graphics System* 2002, DeLano Scientific, San Carlos, CA, USA.

386. Lerner, M. and H. Carlson, *Pymol APBS Tools*. 2009.

387. Morris, G., et al., *Automated docking using a Lamarckian genetic algorithm and an empirical binding free energy function.* J. Comput. Chem., 1998. **19**: p. 1639 - 1662.

388. Case, D.A., et al., *The Amber biomolecular simulation programs.* J Comput Chem, 2005. **26**(16): p. 1668-88.

389. Vegt, E., et al., *Renal toxicity of radiolabeled peptides and antibody fragments: mechanisms, impact on radionuclide therapy, and strategies for prevention.* J Nucl Med, 2010. **51**(7): p. 1049-58.

390. Somogyi, A., *Renal transport of drugs: specificity and molecular mechanisms.* Clin Exp Pharmacol Physiol, 1996. **23**(10-11): p. 986-9.

391. Huang, S., et al., *Aspartyl residue 10 is essential for ATPase activity of rat hsc70.* Journal of Biological Chemistry, 1993. **268**: p. 2063-2068.

392. Chang, L., et al., *High-throughput screen for small molecules that modulate the ATPase activity of the molecular chaperone DnaK.* Anal Biochem, 2008. **372**(2): p. 167-76.

393. Bertelsen, E.B., et al., *Solution conformation of wild-type E. coli Hsp70 (DnaK) chaperone complexed with ADP and substrate.* Proc Natl Acad Sci U S A, 2009. **106**(21): p. 8471-6.

394. Liberek, K., et al., *Escherichia coli DnaJ and GrpE heat shock proteins jointly stimulate ATPase activity of DnaK.* Proc Natl Acad Sci U S A, 1991. **88**(7): p. 2874-8.

395. Russell, R., R. Jordan, and R. McMacken, *Kinetic characterization of the ATPase cycle of the DnaK molecular chaperone.* Biochemistry, 1998. **37**(2): p. 596-607.

396. Schroder, H., et al., *DnaK, DnaJ and GrpE form a cellular chaperone machinery capable of repairing heat-induced protein damage.* Embo J, 1993. **12**(11): p. 4137-44.

397. Meagher, K., L. Redman, and H. Carlson, *Development of polyphosphate parameters for use with the AMBER force field.* Journal of Computational Chemistry, 2003. **24**: p. 1016-1025.

398. Morris, G., et al., *Automated Docking Using a Lamarckian Genetic Algorithm and and Empirical Binding Free Energy Function.* J. Computational Chemistry, 1998. **19**: p. 1639-1662.

399.   Oddo, S., et al., *Triple-transgenic model of Alzheimer's disease with plaques and tangles: Intracellular A beta and synaptic dysfunction.* Neuron, 2003. **39**(3): p. 409-421.

400.   Frautschy, S.A., A. Baird, and G.M. Cole, *EFFECTS OF INJECTED ALZHEIMER BETA-AMYLOID CORES IN RAT-BRAIN.* Proceedings of the National Academy of Sciences of the United States of America, 1991. **88**(19): p. 8362-8366.

401.   Bukau, B., *Regulation of the Escherichia coli heat-shock response.* Mol Microbiol, 1993. **9**(4): p. 671-80.

402.   Oz, M., D.E. Lorke, and G.A. Petroianu, *Methylene blue and Alzheimer's disease.* Biochemical Pharmacology, 2009. **78**(8): p. 927-932.

403.   Zuiderweg, E.R., *Mapping protein-protein interactions in solution by NMR spectroscopy.* Biochemistry, 2002. **41**(1): p. 1-7.